AD-A069 748 MASSACHUSETTS INST OF TECH CAMBRIDGE AEROELASTIC AND--ETC F/G 20/11
HYBRID CRACK ELEMENTS FOR THREE-DIMENSIONAL SOLIDS AND PLATE BE--ETC(U)
SEP 77 K MORIYA F49620-77-C-0084
UNCLASSIFIED ASRL-TR-191-1 AFOSR-TR-79-0619 NL

1 OF 3
AD
A069748

UNCLASSIFIED

SECURITY CLASSIFICATION OF THIS PAGE (When Data Entered)

REPORT DOCUMENTATION PAGE	READ INSTRUCTIONS BEFORE COMPLETING FORM
1. REPORT NUMBER (18) (19) AFOSR-TR- 79-0619 / 2. GOVT ACCESSION NO.	3. RECIPIENT'S CATALOG NUMBER
4. TITLE (and Subtitle) (6) Hybrid Crack Elements for Three-Dimensional Solids and Plate Bending.	5. TYPE OF REPORT & PERIOD COVERED (9) INTERIM rept. 15 Mar 77-30 Sept. 77,
	6. PERFORMING ORG. REPORT NUMBER (14) ASRL-TR-191-1
7. AUTHOR(s) (10) Kazumasa Moriya	8. CONTRACT OR GRANT NUMBER(s) (15) F49620-77-C-0084
9. PERFORMING ORGANIZATION NAME AND ADDRESS Massachusetts Institute of Technology Aeroelastic and Structures Research Laboratory Cambridge, MA 02139	10. PROGRAM ELEMENT, PROJECT, TASK AREA & WORK UNIT NUMBERS 2307B1 61102F
11. CONTROLLING OFFICE NAME AND ADDRESS Air Force Office of Scientific Research/NA Bldg. 410 Bolling Air Force Base, D.C. 20332	12. REPORT DATE (11) September 1977
	13. NUMBER OF PAGES 263
14. MONITORING AGENCY NAME & ADDRESS(if different from Controlling Office) (16) 2307 (17) B1	15. SECURITY CLASS. (of this report) UNCLASSIFIED
	15a. DECLASSIFICATION/DOWNGRADING SCHEDULE

16. DISTRIBUTION STATEMENT (of this Report)

Approved for public release; distribution unlimited

(12) 265 p.

17. DISTRIBUTION STATEMENT (of the abstract entered in Block 20, if different from Report)

18. SUPPLEMENTARY NOTES

19. KEY WORDS (Continue on reverse side if necessary and identify by block number)

Finite Element Method
Hybrid Stress Elements
Fracture Mechanics
Stress Analysis
Stress Intensity Factors
Three-Dimensional Solids
Plate Bending
Bi-Material Plates
Anisotropic Materials

20. ABSTRACT (Continue on reverse side if necessary and identify by block number)

Special crack front elements have been developed and have been assembled into superelements for direct evaluation of stress intensity factors K_{I}, K_{II} and K_{III} of arbitrarily shaped three-dimensional cracks. The formulation is based on the assumed stress hybrid finite element model. The assumption of stresses and boundary displacements contains asymptotically exact terms. The stress-free condition over the crack surface and the displacement compatibility across interelement boundaries are completely →

DD FORM 1 JAN 73 1473 EDITION OF 1 NOV 65 IS OBSOLETE

UNCLASSIFIED

SECURITY CLASSIFICATION OF THIS PAGE (When Data Entered)

006 850

satisfied. The superelements are compatible with most existing finite element computer programs.

Numerical results for commonly used fracture test specimens (single edge crack specimen, center crack specimen, double edge crack specimen and compact tension specimen), an embedded penny-shaped crack, a semi-circular surface flaw, and a quarter-circular corner flaw are presented.

A superelement has been developed directly for the analysis of bending and shearing stress intensity factors, $K_{(B)}$ and $K_{(S)}$, of thin plates with a through-the-thickness crack subjected to out of plane bending. The particular approach is also based on the hybrid element concept, for which the assumed stresses satisfy both equilibrium and compatibility conditions. Poisson-Kirchhoff's thin plate theory and the complex variable technique are used. Numerical example includes the problem of pure cylindrical bending of a thin plate with finite width and centrally located through-the-thickness crack. Extensions of the formulation have been made to bending analyses of an anisotropic plate with through-the-thickness crack, an isotropic plate with wedge shaped notch, and a bi-material plate with through-the-thickness crack located parallel or normal to the interface.

Accession For	
NTIS GRA&I	☑
DDC TAB	☐
Unannounced	☐
Justification	
By	
Distribution/	
Availability Codes	
Dist	Avail and/or special
A	

[redacted]

ASRL TR 191-1

HYBRID CRACK ELEMENTS FOR THREE-DIMENSIONAL SOLIDS AND PLATE BENDING

KAZUMASA MORIYA

AEROELASTIC AND STRUCTURES RESEARCH LABORATORY
DEPARTMENT OF AERONAUTICS AND ASTRONAUTICS
MASSACHUSETTS INSTITUTE OF TECHNOLOGY
CAMBRIDGE, MASSACHUSETTS 02139

SEPTEMBER 1977

PREPARED FOR

AIR FORCE OFFICE OF SCIENTIFIC RESEARCH
UNITED STATES AIR FORCE

UNDER

CONTRACT NO. F49620-77-C-0084

FOREWORD

This research was conducted by the Aeroelastic and Structures Research Laboratory, Department of Aeronautics and Astronautics, Massachusetts Institute of Technology, Cambridge, Massachusetts. The author would like to thank the National Defense Academy of Japan for the financial support to the author's tuition and living expenses. A part of the computations was supported under Contract No. F49620-77-C-0084 with the Air Force Office of Scientific Research, Bolling A.F.B., D.C. Mr. William Walker is the Technical Monitor.

The author wishes to express his sincere appreciation to Professor Theodore H.H. Pian for his guidance and supervision during the course of this study. The author is also very grateful to Professors James W. Mar and John Dugundji for their guidance and for serving as thesis readers. To Professor E.A. Witmer and Dr. O. Orringer the author wishes to extend his appreciation for their guidance.

The computations were performed at the Information Processing Center of the Massachusetts Institute of Technology.

TABLE OF CONTENTS

TABLE OF CONTENTS (Continued)

TABLE OF CONTENTS (Concluded)

LIST OF ILLUSTRATIONS

LIST OF ILLUSTRATIONS (Continued)

LIST OF ILLUSTRATIONS (Concluded)

LIST OF TABLES

LIST OF TABLES (Continued)

LIST OF TABLES (Concluded)

SECTION 1

INTRODUCTION

Linear fracture mechanics has gained a substantial acceptance in industries and has become one of the most important design considerations. It is now well recognized that many engineering structures such as airplanes, rockets, pressure vessels, bridges, etc. may contain preexisting flaws and that crack propagation emanating from such flaws occupies a major fraction of useful fatigue life of structures. These structures are being designed for fracture prevention and for limited service life. The basic parameters in linear fracture mechanics are the elastic stress intensity factors K_I, K_{II} and K_{III} for the opening mode, the in-plane shear mode and the anti-plane shear mode, respectively. Numerous methods are now available for determining these factors.

One of the most powerful methods which can be used to determine the stress intensity factors in structures of complicated geometry is the finite element method. A large number of papers, most of which have appeared since 1970, discuss the application of the finite element methods to fracture mechanics. The survey on the finite element analyses of two-dimensional fracture problems has been made by several authors [1-7].

When applying the finite element method to analyze fracture problems which contain regions of stress singularities,

it is necessary to increase the detail of the finite element model in the vicinity of the singularity to obtain reasonably accurate results. However, most attempts to model a crack front by a profusion of tiny conventional elements have been unsuccessful due to the limited storage capacity of the present-generation computer and to the resulting malconditioned global stiffness matrix. In reference 8, it has been shown that the convergence rate for the finite element solution in the presence of singularities is controlled by the nature of singularities and that the conventional high accuracy element obtained by using polynomials of high order as interpolation functions cannot improve the rate of convergence and they are either inadequate or inefficient.

During the last five years, to overcome such difficulty, there have been many investigators who developed special crack elements which incorporate the singular behavior. These special elements are used to model the region near the crack front, while the remaining region, in general, is modelled with conventional elements. Owing to these special crack elements, the linear elastic, two-dimensional fracture problems seem to be well in hand for application of the finite element methods.

Although there has been a notable increase in interest in the application of the linear fracture mechanics to realistic engineering problems which are inherently three-dimensional, only a few studies in finite element analysis of such problems

have been published to date [56,58,59,63-70,72,75,76]. Particularly, for the problem of surface flaw which is the most common type of realistic crack no analytical solution has been reported to date. Numerical-analytical method such as an alternating technique has been limited to problems of simple geometries [39,40,42,43,45]. Huge amount of computation time and storage requirement of matrices of large bandwidths farther restrict the use of the conventional finite element analysis.

In three-dimensional solid, the stress in the plane normal to and near the crack front has the same angular distribution as that of a two-dimensional crack problem under the action of in-plane stretching and shear and out-of-plane shear [38]. It has an inverse square root r singularity. In the last few years several authors have developed three-dimensional crack front elements, taking such kind of singularity at the crack front into consideration [58,59,66,67,72,75]. However, effort is still needed to seek for efficient methods to obtain reliable stress intensity factor solutions.

Another important crack problem is to determine the plate bending and shearing stress intensity factors, K_B and K_S, for a sharp notch in a plate subjected to out of plane bending. There have been several analytical studies dealing with the bending of a cracked plate. Most recently, Ishida analyzed the interference effect of cracks located randomly in an infinite plate subjected to out of plane bending based on the

Poisson-Kirchhoff thin plate theory.

The assumed stress hybrid finite element method pioneered by Pian [85], has been successfully applied to problems in which conventional finite element model finds difficulties. Notable examples are bending of thin plates and/or thick plates, problems with prescribed boundary conditions, shell problems and singularity problems.

There exist two assumed stress hybrid finite element models for the development of special crack elements for linear fracture mechanics: (1) Scheme I is based on the complete expansion of the exact near-field solution each term of which satisfies both equilibrium and compatibility conditions inside the element. (2) Scheme II is based on assumed equilibrating stress field including the singular term and on independently assumed boundary displacements. The singular stress term also satisfies the compatibility condition.

In the first part of this thesis, special crack front elements are developed for direct evaluation of stress intensity factors K_I, K_{II} and K_{III} of arbitrarily shaped three-dimensional cracks based on the second scheme of the hybrid stress finite element model described above. The elements have been utilized to analyze several fracture test specimens of typical geometries, i.e., a center crack tension specimen, a single edge crack tension specimen, a double edge crack tension specimen and a compact tension specimen. Other numerical examples include an axisymmetrically located penny-shaped

crack in a cylindrical rod, an embedded penny-shaped crack in a cube, a semi-circular surface crack in a rectangular prism and a quarter-circular corner crack in a rectangular prism under uniform tension loading.

In the second part of this thesis, a superelement is developed for the analysis of plate bending and plate shearing stress intensity factors, K_B and K_S, of thin plates with a through-the-thickness crack subjected to out of plane bending. The particular approach is based on the first scheme of the hybrid finite element model, Poisson-Kirchhoff thin plate theory and the complex variable technique. Numerical example includes the problem of pure cylindrical bending of a thin plate with finite width W and a centrally located through-the-thickness crack of length 2a for a number of cases with different ratios of 2a/W. This method of approach is extended to bending analysis of a bi-material plate with through-the-thickness cracks located along and/or normal to the interface, an isotropic plate with a wedge-shaped notch and an anisotropic plate with through-the-thickness cracks.

SECTION 2

ON LINEAR FRACTURE MECHANICS

2.1 Introduction

By considering the configuration of an isolated slit crack which minimizes the total free energy of the system, Griffith first formulated a basic criterion for crack extension in terms of the fundamental energy-balance concept of classical mechanics and thermodynamics [29]. The principles laid down in his pioneering work and implications drawn from them have played a vital part in the development of present day fracture mechanics theory. The Griffith's criterion can be written as

$\sigma_{cr} = (2E\gamma/\pi a)^{1/2}$ for plane stress condition

and

$\sigma_{cr} = \{2E\gamma/\pi a(1 - \nu^2)\}^{1/2}$ for plane strain condition

where σ_{cr} is the critical applied stress, E is the Young's modulus, γ is the free surface energy per unit area, a is the half length of the crack and ν is the Poisson's ratio. If the applied stress exceeds the critical value of σ_{cr}, a brittle crack is free to propagate spontaneously without limit.

Irwin gave the Griffith's concept a more general theoretical framework [31]. In his theory the concept of the elastic stress intensity factor K which is the magnitude of the local stress field is introduced in place of the Griffith's free surface energy γ. It can be shown that both the energy ap-

proach and the stress intensity factor approach are equivalent and the stress intensity factor is related to the free surface energy through the strain energy release rate $G = (\partial U/\partial a)$ as $K = (EG)^{1/2}$ for plane stress problems and as $K = \{EG/(1 - \nu^2)\}^{1/2}$ for plane strain problems. The Griffith-Irwin fracture criterion states that the fast fracture occurs when K or G exceeds a critical value K_c or G_c. K_c and G_c are material constants and are refered to as the fracture toughness of the material. They have the dimension of stress$\cdot$(length)$^{1/2}$ and stress$\cdot$length respectively.

2.2 Modes of Fracture

Irwin also proposed three basic modes of crack surface displacement as in Figure 1. Mode I (opening mode) corresponds to normal separation of the crack surfaces under the action of tensile stresses; mode II (sliding mode) corresponds to mutual shearing of the crack surfaces in a direction normal to the crack front; mode III (tearing mode) corresponds to mutual shearing parallel to the crack front. Any crack problems can be considered to be a combination of these modes for various loading situations. However, since there is always a tendency for a brittle crack to propagate in the direction which minimizes the shear loading, the first mode is by far the most pertinent to crack growth in brittle materials. In fact, to the author's knowledge, the experimental value of G_c or K_c for mode II and mode III crack extensions has not been reported to date.

2.3 Asymptotic Field in the Vicinity of the Crack Front

Sneddon first obtained the local stress field in the vicinity of the crack front for a penny-shaped crack [32]. Recognizing the general applicability of this stress field, Williams extended the inverse square root r character of the local stresses of Sneddon's solution to the most general case of two-dimensional isotropic crack problems [30]. Later, Irwin reformulated the local stress and displacement field based on his characterization of three basic fracture modes [31]. In their simplified crack model, it is assumed that the crack front is perfectly sharp and that the crack surface remains stress free at all stages of loading. The stress and displacement fields thus obtained take a simple analytic form and are given below for each of the three modes of fracture under plane-strain condition:

Mode I:

$$\sigma_x \simeq \{K_I/(2\pi r)^{1/2}\}\cos\tfrac{\theta}{2}(1 - \sin\tfrac{\theta}{2}\sin\tfrac{3\theta}{2})$$

$$\sigma_y = \nu(\sigma_x + \sigma_z)$$

$$\sigma_z \simeq \{K_I/(2\pi r)^{1/2}\}\cos\tfrac{\theta}{2}(1 + \sin\tfrac{\theta}{2}\sin\tfrac{3\theta}{2})$$

$$\tau_{zx} \simeq \{K_I/(2\pi r)^{1/2}\}\sin\tfrac{\theta}{2}\cos\tfrac{\theta}{2}\cos\tfrac{3\theta}{2}$$

$$\tau_{xy} \simeq \tau_{yz} \simeq 0$$

$$u \simeq (K_I/G)(r/2\pi)^{1/2}\cos\tfrac{\theta}{2}(1 - 2\nu + \sin^2\tfrac{\theta}{2})$$

$$v \simeq 0$$

$$w \simeq (K_I/G)(r/2\pi)^{1/2}\sin\tfrac{\theta}{2}(2 - 2\nu - \cos^2\tfrac{\theta}{2})$$

Mode II:

$$\sigma_x \simeq -\{K_{II}/(2\pi r)^{1/2}\}\sin\frac{\theta}{2}(2 + \cos\frac{\theta}{2}\cos\frac{3\theta}{2})$$

$$\sigma_y = \nu(\sigma_x + \sigma_z)$$

$$\sigma_z \simeq \{K_{II}/(2\pi r)^{1/2}\}\sin\frac{\theta}{2}\cos\frac{\theta}{2}\cos\frac{3\theta}{2}$$

$$\tau_{zx} \simeq \{K_{II}/(2\pi r)^{1/2}\}\cos\frac{\theta}{2}(1 - \sin\frac{\theta}{2}\sin\frac{3\theta}{2})$$

$$\tau_{xy} \simeq \tau_{yz} \simeq 0$$

$$u \simeq (K_{II}/G)(r/2\pi)^{1/2}\sin\frac{\theta}{2}(2 - 2\nu + \cos^2\frac{\theta}{2})$$

$$v \simeq 0$$

$$w \simeq (K_{II}/G)(r/2\pi)^{1/2}\cos\frac{\theta}{2}(-1 + 2\nu + \sin^2\frac{\theta}{2})$$

Mode III:

$$\sigma_x \simeq \sigma_y \simeq \sigma_z \simeq \tau_{zx} \simeq 0$$

$$\tau_{xy} \simeq -\{K_{III}/(2\pi r)^{1/2}\}\sin\frac{\theta}{2}$$

$$\tau_{yz} \simeq \{K_{III}/(2\pi r)^{1/2}\}\cos\frac{\theta}{2}$$

$$u \simeq w \simeq 0$$

$$v \simeq (K_{III}/G)(2r/\pi)^{1/2}\sin\frac{\theta}{2}$$

where the crack lies along the x-axis in the y-plane and the polar coordinates (r,θ) are measured from a crack front [Figure 2], G is the elastic shear modulus, ν is the Poisson's ratio and the K_I, K_{II} and K_{III} are stress intensity factors corresponding to mode I, mode II and mode III type of fracture respectively. In the asymptotic stress and displacement field described above, the stress intensity factors which specify the magnitude of the local field depend only on the applied load and the geometry of the cracked body. The remaining terms, which are divided further into a radial component and an angular component, depend only on spatial coordinates about

the crack front. Since only the dominant terms are included in the above expressions, they are valid only in the region where r is small compared to other planer (y-plane) dimensions.

Considering an embedded elliptical crack in a combined stress stress field, Kassir and Sih [38] found that the three-dimensional asymptotic stress fields near the crack front can be expressed explicitly in terms of a local coordinate system (r,θ) defined in a plane normal to the crack front and that they have the same functional form as those in a two-dimensional crack under plane strain condition, i.e.,

$$\sigma_x \simeq (1/\sqrt{2\pi r})\{K_I\cos\tfrac{\theta}{2}(1 - \sin\tfrac{\theta}{2}\sin\tfrac{3\theta}{2}) - K_{II}\sin\tfrac{\theta}{2}(2 + \cos\tfrac{\theta}{2}\cos\tfrac{3\theta}{2})\}$$

$$\sigma_y \simeq (2\nu/\sqrt{2\pi r})\{K_I\cos\tfrac{\theta}{2} - K_{II}\sin\tfrac{\theta}{2}\}$$

$$\sigma_z \simeq (1/\sqrt{2\pi r})\{K_I\cos\tfrac{\theta}{2}(1 + \sin\tfrac{\theta}{2}\sin\tfrac{3\theta}{2}) - K_{II}\sin\tfrac{\theta}{2}\cos\tfrac{\theta}{2}\cos\tfrac{3\theta}{2}\}$$

$$\tau_{xz} \simeq (1/\sqrt{2\pi r})\{K_I\sin\tfrac{\theta}{2}\cos\tfrac{\theta}{2}\cos\tfrac{3\theta}{2} + K_{II}\cos\tfrac{\theta}{2}(1 - \sin\tfrac{\theta}{2}\sin\tfrac{3\theta}{2})\}$$

$$\tau_{yz} \simeq (1/\sqrt{2\pi r})K_{III}\cos\tfrac{\theta}{2}$$

$$\tau_{xy} \simeq -(1/\sqrt{2\pi r})K_{III}\sin\tfrac{\theta}{2}$$

$$u \simeq (1/8G)(2r/\pi)^{\frac{1}{2}}\{K_I[(5 - 8\nu)\cos\tfrac{\theta}{2} - \cos\tfrac{3\theta}{2}] + K_{II}[(9 - 8\nu)\sin\tfrac{\theta}{2} + \sin\tfrac{3\theta}{2}]\}$$

$$v \simeq (1/G)(2r/\pi)^{\frac{1}{2}}K_{III}\sin\tfrac{\theta}{2}$$

$$w \simeq (1/8G)(2r/\pi)^{\frac{1}{2}}\{K_I[(7 - 8\nu)\sin\tfrac{\theta}{2} - \sin\tfrac{3\theta}{2}] - K_{II}[(3 - 8\nu)\cos\tfrac{\theta}{2} + \cos\tfrac{3\theta}{2}]\}$$

where the x-axis is on the plane of the crack and normal to the crack front, the y-axis is tangent to the crack front and the z-axis is normal to the crack plane.

2.4 Numerical Techniques for Three-Dimensional Linear Fracture Analysis

In this section, a brief review is given of numerical techniques other than finite element method that are readily applied to three-dimensional linear fracture problems. The finite difference method is omitted because its application to three-dimensional crack problems has been limited to elastic-perfectly plastic analysis [41].

(1) Schwartz-Newmann Alternating Technique

The Schwartz-Newmann alternating technique is an iterative method [42]. In using this method stresses are first applied to the crack surface and using the known analytical solution for an embedded crack stresses can be computed in a semi-infinite solid at the locations of the surfaces of the solid in which the crack is assumed to reside. Then, the opposite of these stresses is applied to the surface of the body in question. The resulting stresses at the location of the crack surface are computed by using the known analytical solution of a semi-infinite solid subjected to variable surface traction over its flat surface. The crack surface stresses are again removed as before and the process is repeated until further contributions are negligible. The results of all iteration are superimposed to obtain stress intensity factors.

This method requires an analytical solution for an infinite solid with the crack subjected to variable pressure. Since such solution is not available for cracks of complex geometries, the alternating technique can be applied only to cracks of simple geometry.

(2) Boundary Integral Equation Method

Boundary integral equation method has been used extensively to solve practical three-dimensional crack problems by Cruse et al. [46,47,50]. This method also uses the known singular solution to the Navier-Cauchy elasticity equations and this gives rise to a vector identity similar to that of Green's formula for Laplace's equation. Taking the reference area to lie on the boundary of the body in question, a set of simultaneous integral equations which relates boundary displacements to corresponding boundary tractions is generated. Since either of these boundary quantities determines the other the unknown displacements or tractions of each boundary reference area are obtained by solving the resulting simultaneous equations. The boundary quantities are assumed to be constant or linear over each reference area.

2.5 Finite Element Methods for Three-Dimensional crack Problems

2.5.1 Introduction

Finite element methods have been used in linear fracture mechanics quite extensively. The survey on the finite element analyses for two-dimensional fracture problems has been made

by several authors [1-7].

The application of finite element methods to three-dimensional linear fracture problems can be classified into the following three categories:

(1) Conventional finite element

(2) Special singular element

(3) Superposition of analytical and finite element solutions

2.5.2 Conventional Finite Element Model

The assumed displacement approach, in general, cannot provide the stress intensity factor solution directly. However, various quantities, such as displacements, stresses, strain energy release rate and local strain energy are related to the stress intensity factors. Therefore, once one of these quantities is obtained by the finite element analysis, the stress intensity factor can be calculated. Various procedures have been developed to translate the finite element solutions to the stress intensity factors. Basically, they are divided into the following three categories.

(1) Based on a crack opening displacement (C.O.D.)

The mode I stress intensity factor can be represented in terms of local coordinates (x,y,z) and (r,θ) as in Equation (2.2). Thus knowing w at some point on the crack surface, the stress intensity factor K_I is obtained by substituting w into Equation (2.2). More accurate K_I solution can be obtained by extrapolating the solutions of several reference points to the crack front.

(2) Based on a stress value

Normal stress σ_z is related to the mode I stress intensity factor K_I by Equation (2.1). Thus, if the value of σ_z at some point near the crack front is obtained from the finite element analysis, K_I is calculated readily. In this case, extrapolation technique can also be used to obtain accurate K_I solution.

(3) Based on a strain energy release rate

The stress intensity factor K_I is related to the strain energy release rate by the following equation.

$$G = K_I^2(1-\nu^2)/E$$

First the total strain energy for a given crack geometry is computed and then the total strain energy for a small crack extension is recomputed. The resulting total strain energy difference ΔU divided by the difference in surface areas of the two crack lengths ΔA yields the strain energy release rate G as

$$G = \lim_{\Delta a \to o} \frac{\Delta U}{\Delta A} \quad .$$

However, this procedure cannot be used effectively in three-dimensional analysis because of the variability of K_I along the crack front.

Miyamoto and Miyoshi [55-57] analyzed a semi-elliptical surface crack in a plate of finite thickness subjected to tension by conventional finite element method. They used six

node-pentahedron elements built-up from three four-node tetrahedron elements. The crack opening displacement necessary for the determination of stress intensity factor K_I was obtained through a two step computation involving coarse mesh (2332 d.o.f.) analysis for the entire plate and fine mesh (1722 d.o.f.) analysis for the small region near the crack front. The reported CPU time is 1814 seconds for the step 1 and 1457 seconds for the step 2 analysis.

Bergan and Aamodt [62] employed a conventional twenty node isoparametric hexahedron elements to study the crack propagation of a semi-elliptical surface crack in a thick plate. For increasing the computational efficiency, they utilized certain techniques such as multilevel subdivision of the structure (substructure) and condensation of the unnecessary degrees of freedom. The stress intensity factor was calculated based on the strain energy release rate G. Three levels substructures contained 3360 nodal degrees of freedom. For obtaining the condensed stiffness matrix associated with 360 nodal degrees of freedom, a computing time of one and a half hours were required, while only 1.6 seconds of CPU time were required to solve the condensed matrix equation.

Miyata, Shida and Kusumoto [64] developed a simple method for estimating stress intensity factors by using only four-node constant strain tetrahedron elements near the crack

front. They obtained a simple formula to relate the stress intensity factors to the average stresses in a given area around the crack front. Initially this basic approach was developed for two-dimensional crack analysis by using constant strain triangular elements at the crack tip and later extended to three-dimensional analysis. However, even the mesh subdivision for the two-dimensional analysis of the center crack specimen contained as many as several thousand degrees of freedom.

Parks presented a technique to obtain stress intensity factors by a single conventional finite element analysis based on the energy release rate [61]. In his method, the energy release rate is expressed as

$$-\frac{\partial \pi_p}{\partial a} = K_I^2 \frac{1-\nu^2}{E} = \frac{1}{2} \underset{\sim}{q}^T \frac{\partial \underset{\sim}{K}}{\partial a} \underset{\sim}{q}$$

If the displacement $\underset{\sim}{q}$ and the rate of changing stiffness matrix $\underset{\sim}{K}$ are determined, the stress intensity factor is readily obtained from above equation. This procedure was extended by Parks [61] to general three-dimensional crack configurations and was applied to a three-dimensional formulation of an axisymmetric penny shape crack problem.

2.5.3 Special Singularity Element

Although the complexities of formulating three-dimensional singularity element are multiplied manyfold over those of analogous two-dimensional element, several authors

developed three-dimensional crack front elements, taking the singularity at the crack front into consideration.

Based on assumed displacement finite element model, Tracey [58,59] developed six-node pentahedron elements for the three-dimensional analysis of combined mode I - mode II crack. Special interpolation functions for element displacements are chosen so that the displacement in planes normal to the front depends on the square root of distance from the front and this results in the inverse square root stress mode in these planes. Since the angular variations of displacements can not follow those of the corresponding asymptotic terms, twelve special elements encircle each segment of the crack front. For the analysis of a compact tension specimen, the finite element mesh representation contained 522 elements and 1980 degrees of freedom. Stress intensity factors were calculated by C.O.D. at nodes closest to the crack front. He gaged the candidate degree of error on the stress intensity factor solution as 6 per cent of the exact solution.

Blackburn and Hellen [72] presented a fifteen-node pentahedron element in which the displacement includes terms varying linearly and as the square root of the distance from the crack front. The stress intensity factors were determined by C.O.D. and/or by the method of virtual crack extensions which is similar to the technique developed by Parks. With meshes containing between 50 and 100 quadratic isoparametric elements

and with 5 minutes of CPU time on an IBM 370/165 computer, results accurate to within a range of 1 per cent to 4 per cent of known solutions were obtained.

Raju and Newman [75,76] used eight-node hexahedron square root elements which contain the square root terms in their assumed displacement field in addition to the pentahedron singularity elements which are similar to those of Tracey's. In their approach, 8 singularity elements encircle each segment of the crack front, while 32 square-root elements surround these singular elements. Their typical finite element model for the analysis of the surface flaw contains 4317 degrees of freedom. Mode I stress intensity factor was extrapolated from SIF determined by stress values at several reference points away from the crack front.

It is well known that an inverse square root r singularity occurs in isoparametric finite elements if the mid-side nodes are displaced to the quarter point from their usual position of any side. Barsoum [67] extended the idea of the distorted isoparametric element to three-dimensional crack analysis. He constructed 20-node pentahedron and 20-node hexahedron special elements. However, later Hibbit [71] pointed out that the strain energy in the distorted hexahedron element is unbounded and he recommended to use only the pentahedron element.

Bloom [69] studied the convergence of twenty-node

distorted hexahedron elements by analyzing a compact tension specimen. Three mesh representations of 1200, 3528 and 4965 degrees of freedom were used to model a quadrant of the specimen. The resulting stress intensity factors at the midsurface were respectively 3.5, 6.3 and 7.3 per cent higher than the accepted two-dimensional plane strain solution. Both Barsoum and Bloom utilized the C.O.D. method to obtain stress intensity factor solutions.

Recently Atluri and Kathiresan [66,120,121] developed a three-dimensional crack element based on the assumed displacement hybrid model. The geometry of the crack element is a twenty-node isoparametric hexahedron element with six quadratically curved surfaces. Since the stress intensity factor K_I, K_{II} and K_{III} were assumed to be quadratic functions of the crack front coordinates, the strain energy corresponding to the singular strains had to be evaluated by volume integrals with strong $1/r$ and $1/\sqrt{r}$ singularities. In their initial attempt [66] this integration was done by product Gaussian quadrature using as many as 340 integral points. However, in their later development [120] refined integration schemes were employed to remove the singularities in the volume integrals. Also, it appears that a curved crack front element will require the two profile faces to be flat and normal to the curved crack front. In that case there will, in general, be gaps or overlaps in the resulting finite element mesh. It is realized, however, that errors due to

such finite element approximations will be reduced when the element size is reduced.

2.5.4 Superposition of Analytical and Finite Element Solutions

Yamamoto and Tokuda [20] proposed a method for the stress analysis of two-dimensional cracks on the basis of the superposition of analytical and finite element solutions. Later, Yamamoto and Sumi [60] extended the superposition method to three-dimensional crack problems. Basically, the method consists of arranging three solutions, i.e. an analytical solution for an infinite domain, a finite element solution which, when added to the analytical solution, satisfies the prescribed external boundary condition, and a finite element solution for a given boundary condition so as to meet the internal boundary condition (stress free condition on some collocation points on the crack surface). The superposition method is similar to the Schwartz alternating technique commonly used in solving two-dimensional boundary value problems for a doubly connected region. Instead of an analytical solution for semi-infinite domain required in the alternating technique, a finite element solution is utilized. Therefore, this method has the same drawbacks as those of the alternating technique. The result is very sensitive to the location of the collocation points where the stress-free conditions are enforced as well as the analytical solution

chosen. Since it requires an analytical solution, it can be applied only to cracks of simple geometry.

A survey of existing finite element approaches for three-dimensional crack analyses is given in Table 1.

SECTION 3

HYBRID STRESS CRACK FRONT ELEMENT FOR THREE-DIMENSIONAL LINEAR FRACTURE PROBLEMS

3.1 Introduction

There exist two assumed stress hybrid finite element models for the development of special crack front elements for linear fracture mechanics. The basic schemes for these models are as follows:

(1) Scheme I is based on the complete expansion of the exact near field solution each term of which satisfies both equilibrium and compatibility conditions inside the element and the stress free condition over the crack surface. Independently assumed boundary displacements are assumed to satisfy the compatibility condition with neighboring elements.

(2) Scheme II is based on assumed equilibrating stress field including the dominant singular term as well as regular polynomial basis term and on independently assumed boundary displacements. The dominant singular term also satisfies the compatibility condition and independently assumed boundary displacements are assumed to satisfy the interelement compatibility condition with neighboring elements.

The application of these two schemes to two-dimensional crack elements have been reported by Tong, Pian and Lasry [19],

by Pian, Tong and Luk [12], respectively. It appears that for two-dimensional problems the most desirable element is one formulated by the first scheme for which only one crack element is needed and an embedded crack is included in the element. In implementing such element, only boundary integrations are called for. Since the element boundary does not contain the crack tip, the integration does not involve any singular term.

For a three-dimensional crack front element, it is not possible to obtain the complete expansion of the exact solution in the vicinity of a crack front. The only available singular solution is the asymptotically exact term which is derived from the well known solution along the plane normal to the front of an embedded elliptical crack. Hence, only the second scheme described above is applicable to develop three-dimensional crack front element.

In this section, three-dimensional crack front elements are developed based on the second scheme of the hybrid stress finite element method. The basic concern in the present development is to construct a relatively simple finite element model so that it can be used conveniently to solve everyday engineering problems in fracture mechanics.

3.2 Outline of the Three-Dimensional Crack Element

The geometrical shape of the presently derived crack front element is an arbitrarily oriented hexahedron with

straight edges shown in Figure 3. In order to conveniently identify element faces, we call the face 1485 and 1265 which contain the crack front line "frontal face", the face 1234 and 5678 which intersect the front line "profile face" and the face 4378 and 2376 which are remote from the crack boundary "remote face". Two remote faces can be warped surfaces but other faces should be flat. Since the edges are all made straight lines, if in a problem the crack front is curved it must be approximated by an assemblage of straight segments. Each segment of the crack front, then serves as the common edge of a group of crack front elements that surround it. An example arrangement is shown in Figure 3. These elements are classified as type A element which contains the crack surface and type B element which does not contain the crack surface. Elements labelled as A' and B' are those with the crack front located at the upper corners of the block elements.

Three types of crack front elements, i.e., 8-node, 12-node and 16-node elements are constructed (Figure 6). The 16-node element has mid-side nodes on all edges on the profile face that intersects the crack front, whereas the 12-node element has mid-side nodes only on edges which are not connected with the crack front. Figure 6 indicates typical assemblages of crack front elements. The 12-node, 20-node and 26-node half elements are for problems which are symmetric about the plane of the crack, while the 20-node, 36-node and

46-node superelements are for general asymmetric problems.

It is seen that since only the two-dimensional behavior of the singular term is introduced, the elements are necessarily narrow in the direction along the crack front. The stress intensity factors K_I, K_{II} and K_{III} associated with each crack front element are assumed to be constant and hence to determine the distribution of K_I, K_{II} and K_{III} a number of special elements should be used along the crack front.

3.3 Variational Formulation

The modified complementary energy functional π_{mc} can be written as follows [87],

$$\pi_{mc} (\sigma_{ij}, \tilde{u}_i) = \sum_{n=1}^{N} [\int_{V_n} \frac{1}{2} C_{ijk\ell}\, \sigma_{ij}\, \sigma_{k\ell}\, dV - \int_{\partial V_n} T_i\, \tilde{u}_i\, dS + \int_{S_{\sigma_n}} \bar{T}_i\, \tilde{u}_i\, dS \tag{3.1}$$

In the above expression,

σ_{ij} - Stress component

$C_{ijk\ell}$ - Elastic compliance tensor

$\tilde{u}_i$ - Boundary displacement component

$\bar{T}_i$ - Prescribed surface traction on S_{σ_n}

V_n - Volume of the nth element (n = 1,2,3, ..., N)

∂V_n - Entire boundary of the nth element

S_{σ_n} - Portion of the element boundary where surface traction $\bar{T}_i$ is prescribed

N - Total number of finite elements

dV - Elemental volume

dS - Elemental surface

T_i - Surface traction component

The independent field variables are the equilibrating stresses σ_{ij} and the boundary displacements $\tilde{u}_i$. In the crack front elements which are directly adjacent to the crack front, the assumed stresses include not only the simple polynomial expansion along the three coordinate axes, but also the asymptotically exact terms which are derived from the well known classical near-field solutions of an embedded elliptical crack in an infinite domain and are given in Equation (2.1). In the far-field elements where the effect of stress singularity is of little importance, only regular polynomial basis terms are incorporated in the stress assumption.

In a crack front element, the assumed stresses are expressed as follows:

$$\sigma_{ij} = \sigma_{s_{ij}}(1/\sqrt{r},\ \theta) + \sigma_{r_{ij}}(x,y,z) \tag{3.2}$$

where $\sigma_{s_{ij}}$ corresponds to the singular stress solution, Equation (2.1), and $\sigma_{r_{ij}}$ contains only regular polynomials. The subscript s and r refer to "singular" and "regular" respectively. The singular stress term satisfies both the homogeneous equations of equilibrium and the stress free boundary conditions over the crack surface, i.e.,

$$\begin{aligned} \sigma_{s_{ij,j}} &= 0 \qquad && \text{in } V_n \\ \sigma_{s_{ij}} \nu_j &= 0 \qquad && \text{on the crack surface} \end{aligned} \tag{3.3}$$

where ν_j's are the components of the unit normal vector to the element surface. The regular stress terms are selected so as to satisfy the complete equations of equilibrium with prescribed body forces, i.e.

$$\sigma_{r_{ij,j}} + \bar{F}_i = 0 \tag{3.4}$$

where $\bar{F}_i$ is a component of the prescribed body forces and a known function of coordinates. The surface tractions for crack front elements are also divided into two parts and are related to the interior stresses by

$$\begin{aligned} T_i &= T_{s_i} + T_{r_i} \\ T_{s_i} &= \sigma_{s_{ij}} \nu_j \\ T_{r_i} &= \sigma_{r_{ij}} \nu_j \end{aligned} \tag{3.5}$$

The regular stress term $\sigma_{r_{ij}}$ is further divided into two parts as

$$\sigma_{r_{ij}} = \sigma_{h_{ij}} + \sigma_{p_{ij}} \tag{3.6}$$

where $\sigma_{h_{ij}}$ satisfy the homogeneous equilibrium equations while $\sigma_{p_{ij}}$ is a particular solution of the equations of equilibrium with the prescribed body forces. The subscript h denotes "homogeneous" while p denotes "particular".

Substituting Equation (3.2) into the first term of the right hand side of Equation (3.1), the complementary strain

energy in the crack front element is written as

$$\int_{V_n} \frac{1}{2} C_{ijk\ell} \, \sigma_{ij} \, \sigma_{k\ell} \, dV$$

$$= \int_{V_n} \frac{1}{2} C_{ijk\ell} \, \sigma_{s_{ij}} \, \sigma_{s_{k\ell}} \, dV + \int_{V_n} C_{ijk\ell} \, \sigma_{r_{ij}} \, \sigma_{s_{k\ell}} \, dV$$

$$+ \int_{V_n} \frac{1}{2} C_{ijk\ell} \, \sigma_{r_{ij}} \, \sigma_{r_{k\ell}} \, dV \qquad (3.7)$$

Since the singular stress field $\sigma_{s_{ij}}$ is the exact asymptotic solution of an embedded elliptical crack, it satisfies compatibility conditions as well as homogeneous equations of equilibrium. Hence, the volume integral of the first term of Equation (3.7) can be replaced by the surface integral through the application of divergence theorem.

$$\int_{V_n} C_{ijk\ell} \, \sigma_{s_{ij}} \, \sigma_{s_{ij}} \, dV = \int_{\partial V_n} \sigma_{s_{ij}} \, u_{s_i} \, \nu_j \, dS$$

$$= \int_{\partial V_n} T_{s_i} \, u_{s_i} \, dS \qquad (3.8)$$

where u_{s_i} is an asymptotically exact displacement field which corresponds to the singular stress field $\sigma_{s_{ij}}$. The explicit form of u_{s_i} is given in Equation (2.2). The regular stress term $\sigma_{r_{ij}}$ satisfies the equations of equilibrium with prescribed body forces and hence the second term in Equation (3.7) can be converted to

$$\int_{V_n} C_{ijk\ell}\, \sigma_{r_{ij}}\, \sigma_{s_{k\ell}}\, dV = \int_{\partial V_n} \sigma_{r_{ij}}\, u_{s_i}\, \nu_j\, dS$$

$$- \int_{V_n} \sigma_{r_{ij,j}}\, u_{s_i}\, dV = \int_{\partial V_n} T_{r_i}\, u_{s_i}\, dS + \int_{V_n} \bar{F}_i\, u_{s_i}\, dV \qquad (3.9)$$

Upon substitution of Equations (3.7), (3.8) and (3.9) into Equation (3.1), the hybrid variational functional π_{mc} can be written in the form

$$\pi_{mc} = \sum_{n=1}^{N_c} [\int_{V_n} \frac{1}{2} C_{ijk\ell}\, \sigma_{r_{ij}}\, \sigma_{r_{k\ell}}\, dV + \int_{\partial V_n} \frac{1}{2} T_{s_i}\, u_{s_i}\, dS$$

$$+ \int_{\partial V_n} T_{r_i}\, u_{s_i}\, dS + \int_{V_n} \bar{F}_i\, u_{s_i}\, dV - \int_{\partial V_n} T_i\, \tilde{u}_i\, dS$$

$$+ \int_{S_{\sigma_n}} \bar{T}_i\, \tilde{u}_i\, dS] + \sum_{m=1}^{N_f} [\int_{V_m} \frac{1}{2} C_{ijk\ell}\, \sigma_{ij}\, \sigma_{k\ell}\, dV$$

$$- \int_{\partial V_m} T_i\, \tilde{u}_i\, dS + \int_{S_{\sigma_m}} \bar{T}_i\, \tilde{u}_i\, dS] \qquad (3.10)$$

where N_f is the total number of far field elements and N_c is the number of crack front elements.

3.4 Matrix Formulation

For each crack front element V_n ($n = 1,2, \ldots N_c$), the assumed stresses are written in the matrix form as:

$$\underset{\sim}{\sigma} = \underset{\sim}{P}_s \underset{\sim}{\beta}_s + \underset{\sim}{P}\, \underset{\sim}{\beta} + \underset{\sim}{P}_p \underset{\sim}{\beta}_p \qquad (3.11)$$

where $\underset{\sim}{P}_s \underset{\sim}{\beta}_s$ is the asymptotically exact singular solution function given in Equation (2.1) in terms of r and θ, β_s represents the vector of undetermined stress intensity factors as

$$\beta_s = \{K_I, K_{II}, K_{III}\} \tag{3.12}$$

In the present formulation, $\underset{\sim}{\beta}_s$ is assumed to be constant within each crack front element. $\underset{\sim}{P}$ is the regular polynomial basis function of spatial coordinates, $\underset{\sim}{\beta}$ is unknown stress parameters and $\underset{\sim}{P}\underset{\sim}{\beta}$ satisfies the homogeneous equations of equilibrium. $\underset{\sim}{P}_p\underset{\sim}{\beta}_p$ is a known particular solution of the non-homogeneous equations of equilibrium and in case any non-zero tractions are prescribed on the boundary of the element, appropriate terms should be added to $\underset{\sim}{P}_p\underset{\sim}{\beta}_p$.

The surface tractions on the element boundary ∂V_n ($n = 1,2, \ldots N_c$), which relates to the assumed stress distribution, can be expressed in terms of the generalized stresses by equation of the form:

$$\underset{\sim}{T} = \underset{\sim}{R}_s\underset{\sim}{\beta}_s + \underset{\sim}{R}\,\underset{\sim}{\beta} + \underset{\sim}{R}_p\underset{\sim}{\beta}_p \tag{3.13}$$

in which $\underset{\sim}{R}_s$, $\underset{\sim}{R}$ and $\underset{\sim}{R}_p$ are obtained from $\underset{\sim}{P}_s$, $\underset{\sim}{P}$ and $\underset{\sim}{P}_p$, respectively. On the other hand, in the far field elements V_m($m = 1,2, \ldots N_f$) only the polynomial basis terms are included in the stress and traction assumption, i.e.,

$$\begin{aligned} \underset{\sim}{\sigma} &= \underset{\sim}{P}\,\underset{\sim}{\beta} + \underset{\sim}{P}_p\underset{\sim}{\beta}_p \\ \underset{\sim}{T} &= \underset{\sim}{R}\,\underset{\sim}{\beta} + \underset{\sim}{R}_p\underset{\sim}{\beta}_p \end{aligned} \tag{3.14}$$

The asymptotically exact displacement matrix which corresponds to the singular stress matrix $\underset{\sim}{P}_s\underset{\sim}{\beta}_s$ can be written as:

$$u_s = L_s \beta_s \tag{3.15}$$

where u_s is the asymptotic solution matrix of displacements defined by

$$u_s = \{u_{s_1}, u_{s_2}, u_{s_3}\} \tag{3.16}$$

L_s is the exact displacement solution function given in Equation (2.2).

The assumed displacement on the element boundary ∂V_n can be expressed as:

$$\tilde{u} = L\, q \tag{3.17}$$

where

$$\tilde{u} = \{u_1, u_2, u_3\} \tag{3.18}$$

q is the generalized nodal displacement vector and L is the interpolation function matrix. In crack front elements, L contains asymptotically correct variation of displacements on the faces that meet or intersect the crack front line. For the other part of the boundary of singular elements and for the entire boundary of far-field elements, L consists only of conventional polynomial basis interpolation functions. Inserting Equations (3.11), (3.13), (3.14), (3.15) and (3.17) into Equation (3.10) gives

$$\pi_{mc} = \sum_{n=1}^{N_c} [\frac{1}{2} \underset{\sim}{\beta}^T \underset{\sim}{H}_{hh} \underset{\sim}{\beta} + \underset{\sim}{\beta}^T \underset{\sim}{H}_{hp} \underset{\sim}{\beta}_p + \frac{1}{2} \underset{\sim}{\beta}_s^T \underset{\sim}{H}_{ss} \underset{\sim}{\beta}_s$$

$$+ \underset{\sim}{B}^T \underset{\sim}{\beta}_s + \underset{\sim}{\beta}^T \underset{\sim}{H}_{hs} \underset{\sim}{\beta}_s - \underset{\sim}{\beta}_s^T \underset{\sim}{G}_s \underset{\sim}{q} - \underset{\sim}{\beta}^T \underset{\sim}{G} \underset{\sim}{q} + \underset{\sim}{S}^T \underset{\sim}{q} + A]$$

$$+ \sum_{n=1}^{N_f} [\frac{1}{2} \underset{\sim}{\beta}^T \underset{\sim}{H}_{hh} \underset{\sim}{\beta} + \underset{\sim}{\beta}^T \underset{\sim}{H}_{hp} \underset{\sim}{\beta}_p - \underset{\sim}{\beta}^T \underset{\sim}{G} \underset{\sim}{q} + \underset{\sim}{S}^T \underset{\sim}{q} + A] \tag{3.19}$$

where

$$\underset{\sim}{H}_{hh} = \int_{V_n} \underset{\sim}{P}^T \underset{\sim}{C} \underset{\sim}{P} \, dV$$

$$\underset{\sim}{H}_{hp} = \int_{V_n} \underset{\sim}{P}^T \underset{\sim}{C} \underset{\sim}{P}_p \, dV$$

$$\underset{\sim}{H}_{ss} = \int_{\partial V_n} \underset{\sim}{R}_s^T \underset{\sim}{L}_s \, dS$$

$$\underset{\sim}{H}_{ps} = \int_{\partial V_n} \underset{\sim}{R}_p^T \underset{\sim}{L}_s \, dS$$

$$\underset{\sim}{H}_{hs} = \int_{\partial V_n} \underset{\sim}{R}^T \underset{\sim}{L}_s \, dS$$

$$\underset{\sim}{G}_s = \int_{\partial V_n} \underset{\sim}{R}_s^T \underset{\sim}{L} \, dS$$

$$\underset{\sim}{G} = \int_{\partial V_n} \underset{\sim}{R}^T L \, dS$$

$$\underset{\sim}{G}_p = \int_{\partial V_n} \underset{\sim}{R}_p^T \underset{\sim}{L} \, dS$$

$$A = \frac{1}{2} \underset{\sim}{\beta}_p^T \left(\int_{V_n} \underset{\sim}{P}_p^T C \underset{\sim}{P}_p \, dV\right) \underset{\sim}{\beta}_p$$

$$\underset{\sim}{B}^T = \int_{V_n} \underset{\sim}{\bar{F}}^T \underset{\sim}{L}_s \, dV + \underset{\sim}{\beta}_p^T \underset{\sim}{H}_{ps}$$

$$\underset{\sim}{S}^T = - \underset{\sim}{\beta}_p^T \underset{\sim}{G}_p + \int_{S_{\sigma_n}} \underset{\sim}{\bar{T}}^T \underset{\sim}{L} \, dS \tag{3.20}$$

The stationary condition of the above functional π_{mc} with respect to variations of stress parameters $\underset{\sim}{\beta}$ which are independent from one element to the other gives

$$\underset{\sim}{H}_{hh}\,\underset{\sim}{\beta} + \underset{\sim}{H}_{hp}\underset{\sim}{\beta}_p + \underset{\sim}{H}_{hs}\underset{\sim}{\beta}_s - \underset{\sim}{G}\,\underset{\sim}{q} = 0 \quad \text{for crack front elements} \tag{3.21}$$

and

$$\underset{\sim}{H}_{hh}\,\underset{\sim}{\beta} + \underset{\sim}{H}_{hp}\underset{\sim}{\beta}_p - \underset{\sim}{G}\,\underset{\sim}{q} = 0 \quad \text{for far field elements} \tag{3.22}$$

Equations (3.21) and (3.22) can be solved for $\underset{\sim}{\beta}$ as follows.

$$\underset{\sim}{\beta} = H_{hh}^{-1}\,(\underset{\sim}{G}\,\underset{\sim}{q} - \underset{\sim}{H}_{hs}\underset{\sim}{\beta}_s - \underset{\sim}{H}_{hp}\underset{\sim}{\beta}_p) \quad \text{for crack front elements} \tag{3.23}$$

$$\underset{\sim}{\beta} = H_{hh}^{-1}\,(\underset{\sim}{G}\,\underset{\sim}{q} - \underset{\sim}{H}_{hp}\underset{\sim}{\beta}_p) \quad \text{for far field elements} \tag{3.24}$$

Substituting Equations (3.23) and (3.24) back into the functional Equation (3.19), we obtain the modified complementary energy functional π_{mc} expressed in terms of generalized nodal displacements $\underset{\sim}{q}$ and the stress intensity factor vector $\underset{\sim}{\beta}_s$ as:

$$\pi_{mc} = \sum_{n=1}^{N_c} [-\frac{1}{2}\,\underset{\sim}{q}^T\,\underset{\sim}{K}\,\underset{\sim}{q} + \frac{1}{2}\,\underset{\sim}{\beta}_s^T\underset{\sim}{K}_{ss}\,\underset{\sim}{\beta}_s + \underset{\sim}{\beta}_s^T\underset{\sim}{K}_{rs}\,\underset{\sim}{q} + \underset{\sim}{B}'^T\underset{\sim}{\beta}_s$$

$$+ \bar{\underset{\sim}{Q}}^T\underset{\sim}{q} + A'] + \sum_{m=1}^{N_f} [-\frac{1}{2}\,\underset{\sim}{q}^T\underset{\sim}{K}\,\underset{\sim}{q} + \bar{\underset{\sim}{Q}}^T\underset{\sim}{q} + A'] \tag{3.25}$$

where

$$\underset{\sim}{K} = \underset{\sim}{G}^T\,\underset{\sim}{H}_{hh}^{-1}\,\underset{\sim}{G},$$

$$\underset{\sim}{K}_{ss} = \underset{\sim}{H}_{ss} - \underset{\sim}{H}_{hs}^T\,\underset{\sim}{H}_{hh}^{-1}\,\underset{\sim}{H}_{hs},$$

$$K_{rs} = H_{hs}^T H_{hn}^{-1} G - G_s,$$

$$B' = B - H_{hs}^T H_{hh}^{-1} H_{hp} \beta_p$$

$$\bar{Q} = S + G^T H_{hh}^{-1} H_{hp} \beta_p$$

$$A' = A - \frac{1}{2} \beta_p^T H_{hp}^T H_{hh}^{-1} H_{hp} \beta_p \quad (3.26)$$

In the above, the matrix H_{hh} is a symmetric matrix. The stress intensity factor β_s is not completely independent, but is common to a group of crack front elements which have one crack front segment as a common edge. This group of crack front elements can be conveniently treated as a "superelement". Element matrices K, K_{ss}, K_{rs}, B' and $\bar{Q}$ for a superelement are constructed by summing the overlapping terms of the corresponding element matrices for the group of crack front elements. Since the constant term A' has no effect on the variation, it may be dropped from the functional representation. Hence, the variational function in Equation (3.25) is rewritten as:

$$\pi_{mc} = \sum_{n=1}^{N_s} [-\frac{1}{2} q^T K q + \frac{1}{2} \beta_s^T K_{ss} \beta_s + \beta_s^T K_{rs} q + B'^T \beta_s + \bar{Q}^T q]$$

$$+ \sum_{n=1}^{N_f} [-\frac{1}{2} q^T K q + \bar{Q}^T q] \quad (3.27)$$

where N_s is the total number of the superelements and the matrices K, K_{ss}, K_{rs}, B' and $\bar{Q}$ denotes their assembled element matrices.

Since the stress intensity factor vector $\underset{\sim}{\beta}_s$ is independent for different superelements, the vanish of the variation of the functional in Equation (3.27) with respect to $\underset{\sim}{\beta}_s$ gives

$$\underset{\sim}{K}_{ss} \underset{\sim}{\beta}_s + \underset{\sim}{K}_{rs} \underset{\sim}{q} + \underset{\sim}{B}' = 0 \tag{3.28}$$

The stress intensity factor vector $\underset{\sim}{\beta}_s$ can now be expressed in terms of the generalized nodal displacement vector $\underset{\sim}{q}$ as follows.

$$\underset{\sim}{\beta}_s = - \underset{\sim}{K}_{ss}^{-1} (\underset{\sim}{K}_{rs} \underset{\sim}{q} + \underset{\sim}{B}') \tag{3.29}$$

Substituting Equation (3.29) back into Equation (3.27) and neglecting constant terms, the modified complementary energy functional π_{mc} can thus be written as:

$$\pi_{mc} = \sum_{n=1}^{N_s} [- \frac{1}{2} \underset{\sim}{q}^T \underset{\sim}{K}_s \underset{\sim}{q} + \underset{\sim}{\bar{Q}}_s^T \underset{\sim}{q}]$$

$$+ \sum_{m=1}^{N_f} [- \frac{1}{2} \underset{\sim}{q}^T \underset{\sim}{K} \underset{\sim}{q} + \underset{\sim}{\bar{Q}}^T \underset{\sim}{q}] \tag{3.30}$$

where

$$\underset{\sim}{K}_s = \underset{\sim}{K} + \underset{\sim}{K}_{rs}^T \underset{\sim}{K}_{ss}^{-1} \underset{\sim}{K}_{rs}$$

$$\underset{\sim}{Q}_s^T = \underset{\sim}{\bar{Q}}^T - \underset{\sim}{B}'^T \underset{\sim}{K}_{ss}^{-1} \underset{\sim}{K}_{rs} \tag{3.31}$$

In the above expression, all the stress parameters are formally eliminated from the functional and it contains only generalized nodal displacements $\underset{\sim}{q}$ as unknown parameters. $\underset{\sim}{K}_s$ gives the

element stiffness matrix of a crack front superelement which is compatible with those of both assumed displacement and hybrid stress elements.

The assemblage process of the element matrices to the global matrices also follows completely that of conventional method. For the purpose of completeness, the assemblage and solution procedure is briefly sketched.

The element nodal displacements $\underset{\sim}{q}$ are not completely independent of those in other elements because of the requirement of interelement compatibility. They are expressed as a function of the independent generalized global displacements. Expressing all element nodal displacements $\underset{\sim}{q}$ in terms of a global set $\underset{\sim}{q}^*$, the functional π_{mc} yields

$$\pi_{mc} = \frac{1}{2} \underset{\sim}{q}^{*T} \underset{\sim}{K}^* \underset{\sim}{q}^* + \bar{\underset{\sim}{Q}}^{*T} \underset{\sim}{q}^* \tag{3.32}$$

where $\underset{\sim}{K}^*$ is the global stiffness matrix obtained by assembling the element stiffness matrices associated with the same generalized displacements for the entire domain. $\bar{\underset{\sim}{Q}}^*$ is the vector of global generalized nodal forces.

The stationary condition $\delta\pi_{mc} = 0$ with respect to the variation of $\underset{\sim}{q}^*$ yields the global equation

$$\underset{\sim}{K}^* \underset{\sim}{q}^* = \bar{\underset{\sim}{Q}}^* \tag{3.33}$$

The above equation is solved for the global displacements $\underset{\sim}{q}^*$, thus determining the generalized displacements $\underset{\sim}{q}$ for each

element. Then as a final step in the solution procedure, the stress intensity factor vector $\underset{\sim}{\beta}_s$ is calculated for each crack front superelement by substituting the corresponding displacement solutions into Equation (3.29).

Instead of condensing the stress parameter (stress intensity factor vector) $\underset{\sim}{\beta}_s$ a priori, we may carry it into the global system of equations. This approach leads to a dual hybrid method with generalized displacements $\underset{\sim}{q}$ and stress parameters $\underset{\sim}{\beta}_s$ as unknowns. After assembling the element matrices $\underset{\sim}{K}$, $\underset{\sim}{K}_{rs}$, $\underset{\sim}{K}_{ss}$ and $\underset{\sim}{\bar{Q}}$, the variation of π_{mc} $(\underset{\sim}{q}^*, \underset{\sim}{\beta}_s^*)$ leads to the final algebraic equation of the form,

$$\begin{bmatrix} \underset{\sim}{K}^* & \underset{\sim}{K}_{rs}^* \\ \underset{\sim}{K}_{rs}^{*T} & \underset{\sim}{K}_{ss}^* \end{bmatrix} \begin{Bmatrix} \underset{\sim}{q}^* \\ \underset{\sim}{\beta}_s^* \end{Bmatrix} = \begin{Bmatrix} \underset{\sim}{\bar{Q}}^* \\ \underset{\sim}{0} \end{Bmatrix} \tag{3.34}$$

The above matrix equation can be solved directly for the generalized nodal displacements q* and the stress intensity factors $\underset{\sim}{\beta}_s^*$. Since the global matrix

$$\begin{bmatrix} \underset{\sim}{K}^* & \underset{\sim}{K}_{rs}^* \\ \underset{\sim}{K}_{rs}^{*T} & \underset{\sim}{K}_{ss}^* \end{bmatrix}$$

is not always positive definite, but positive semi-definite, this formulation may not be compatible with the conventional general purpose finite element program for the assumed displacement method.

3.5 Local Coordinate System

In the derivation of element matrices, the local Cartesian coordinate system (x,y,z) with its origin being at one end of the crack front edge is taken as shown in Figure 7. The y-axis is taken to coincide with the crack front edge, while the x-axis is taken to be normal to the crack front edge so that the crack surface lies on the x-y plane. The z-axis is normal to both the x- and y-axes. There is no loss of generality in defining the local coordinate system in the above manner. The coordinates (r, θ) are defined on the plane which is perpendicular to the crack front and are related to the local Cartesian coordinates as:

$$x = r \cos\theta$$
$$z = r \sin\theta$$

The isoparametric non-dimensional coordinate system (ξ,η,ζ) is also utilized to specify a point within the element. This coordinate system also facilitates the numerical integration of element matrices. The relationship between the non-dimensional coordinate (ξ,η,ζ) at any point P and the local Cartesian coordinate (x,y,z) can be written as

$$x = \sum_{i=1}^{8} \phi_i(\xi,\eta,\zeta)x_i$$
$$y = \sum_{i=1}^{8} \phi_i(\xi,\eta,\zeta)y_i$$
$$z = \sum_{i=1}^{8} \phi_i(\xi,\eta,\zeta)z_i \quad (3.35)$$

where

$$\phi_i = \frac{1}{8}(1+\xi_i\xi)(1+\eta_i\eta)(1+\zeta_i\zeta)$$

(x_i, y_i, z_i) and (ξ_i, η_i, ζ_i) are the Cartesian coordinate and the non-dimensional coordinate of the ith corner node of the crack front element. The non-dimensional coordinate system (ξ,η,ζ) are scaled so that six element faces are defined by $\xi = \pm 1$, $\eta = \pm 1$, $\zeta = \pm 1$. For example, for a type B element in Figure 3, the profile faces determine $\eta = \pm 1$, the frontal faces define $\xi = -1$, $\zeta = -1$ and the remote faces are $\xi = 1$, $\zeta = 1$.

For the twelve-node and sixteen-node crack front elements, whose geometrical shape is a hexahedron with straight edges, the mid-side nodes do not affect the original element shape, i.e., the mid-side nodes do not affect the relation between the non-dimensional and the Cartesian coordinates. Therefore, for the twelve-node and sixteen-node element, the same relationship as that in Equation (3.35) holds between these two coordinate systems.

3.6 Assumed Stress Field

The stresses to be assumed inside the element, which are σ_x, σ_y, σ_z, τ_{yz}, τ_{zx} and τ_{xy}, should satisfy the following homogeneous equations of equilibrium.

$$\frac{\partial \sigma_x}{\partial x} + \frac{\partial \tau_{xy}}{\partial y} + \frac{\partial \tau_{zx}}{\partial z} = 0$$

$$\frac{\partial \tau_{xy}}{\partial x} + \frac{\partial \sigma_y}{\partial y} + \frac{\partial \tau_{yz}}{\partial z} = 0$$

$$\frac{\partial \tau_{zx}}{\partial x} + \frac{\partial \tau_{yz}}{\partial y} + \frac{\partial \sigma_z}{\partial z} = 0 \qquad (3.36)$$

Since the prescribed boundary stresses do not constitute a restrained boundary condition in the hybrid stress finite element model, it is not necessary to select the stress field so as to satisfy the natural boundary conditions. However, in the type A and type A' crack front elements which contain the crack surface, the assumed stresses are chosen to satisfy the stress free condition over the crack surface for obtaining more accurate stress intensity factor solutions.

The magnitude of the stress intensity factor K_I, K_{II} and K_{III} will vary from point to point along the crack front. However, in this case, it is impossible to construct the self equilibrating singular stress field with K_I, K_{II} and K_{III} being simple functions of the crack front coordinate y, and hence, in the present formulation, the stress intensity factors are assumed to be constant within each crack front element. The singular part of the assumed stresses with constant K_I, K_{II} and K_{III} is listed in Table 10. Since it is the exact asymptotic solution for a line crack embedded in an

infinite domain, it satisfies both the homogeneous equations of equilibrium in the element interior and the stress free condition over the crack surface.

Although no method has been reported to date to determine the sufficient and/or optimum number of stress parameters a priori, the number of stress parameters cannot be chosen freely. The following necessary condition should always be met to avoid kinematic deformation modes which involve zero strain energy.

$$m \geq n - \ell \tag{3.37}$$

where m is the total number of stress parameters β and β_s, n is the total number of generalized nodal displacements and ℓ is the number of rigid body modes. For a general three-dimensional problem $\ell = 6$.

The regular polynomial-based self-equilibrating stress field is derived from the three-dimensional stress functions. First, Maxwell's stress functions χ_1, χ_2 and χ_3 are assumed in the polynomial form in terms of Cartesian coordinates x, y and z. Then, all stress components are computed algebraically based on the following stress representations.

$$\sigma_x = \frac{\partial^2 \chi_3}{\partial y^2} + \frac{\partial^2 \chi_2}{\partial z^2}$$

$$\sigma_y = \frac{\partial^2 \chi_1}{\partial z^2} + \frac{\partial^2 \chi_3}{\partial x^2}$$

$$\sigma_z = \frac{\partial^2 \chi_2}{\partial x^2} + \frac{\partial^2 \chi_1}{\partial y^2}$$

$$\tau_{yz} = - \frac{\partial^2 \chi_1}{\partial y \partial z}$$

$$\tau_{zx} = - \frac{\partial^2 \chi_2}{\partial z \partial x}$$

$$\tau_{xy} = - \frac{\partial^2 \chi_3}{\partial x \partial y} \tag{3.38}$$

In type A and type A' crack front elements, the stress field derived in the above mentioned manner should be modified so as to satisfy the stress free condition over the crack surface ($z = 0$).

Within type B and type B' 8-node crack front element, the stress field is assumed as

$$\begin{aligned}
\sigma_x &= \beta_1 + \beta_7 y + \beta_8 z + \beta_9 x + \beta_{10} yz \\
\sigma_y &= \beta_2 + \beta_{11} x + \beta_{12} z + \beta_{13} y + \beta_{14} zx \\
\sigma_z &= \beta_3 + \beta_{15} x + \beta_{16} y + \beta_{17} z + \beta_{18} xy \\
\tau_{yz} &= \beta_4 - (\beta_{17} + \beta_{20}) y + \beta_{19} z + \beta_{22} x \\
\tau_{zx} &= \beta_5 - (\beta_9 + \beta_{21}) z + \beta_{20} x + \beta_{23} y \\
\tau_{xy} &= \beta_6 - (\beta_{13} + \beta_{19}) x + \beta_{21} y + \beta_{24} z
\end{aligned} \tag{3.39}$$

Within type A and type A' 8-node element, the stresses are assumed as

$$\sigma_x = \beta_1 + \beta_4 y + \beta_5 z + \beta_6 x + \beta_{13} xy + \beta_{14} yz + \beta_{15} zx$$
$$+ (\beta_{19} + \beta_{20}) x^2 + \beta_{22} x^2 y + \beta_{24} x^2 z$$

$$\sigma_y = \beta_2 + \beta_7 z + \beta_8 x + \beta_9 y + \beta_{16} yz + \beta_{17} zx + \beta_{18} xy$$
$$+ (\beta_{20} + \beta_{21}) y^2 + \beta_{23} xy^2 + \beta_{24} y^2 z$$

$$\sigma_z = (\beta_{19} + \beta_{21}) z^2 + \beta_{22} yz^2 + \beta_{23} z^2 x$$

$$\sigma_{yz} = - (\beta_9 - \beta_{10}) z - \beta_{18} zx - 2\beta_{21} yz - 2\beta_{23} xyz$$

$$\sigma_{zx} = - (\beta_6 - \beta_{11}) z - \beta_{13} yz - 2\beta_{19} zx - 2\beta_{22} xyz$$

$$\sigma_{xy} = \beta_3 - \beta_{10} x - \beta_{11} y + \beta_{12} z - \beta_{15} yz - \beta_{16} zx - 2\beta_{20} xy$$
$$- 2\beta_{24} xyz \qquad (3.40)$$

The above stress field satisfies the stress free condition over the crack surface as well as the homogeneous equations of equilibrium.

Regular polynomial-based assumed stress field used in the present study are listed in matrix form in Tables 2, 4, 6 and 8. Table 14 also lists the number of β's used in the various crack front elements.

3.7 Body Forces

Body forces may be caused by gravity, acceleration, magnetic field and so on. The equivalent nodal force vector associated with the prescribed body forces is obtained as follows.

For a far field element

$$\bar{\underset{\sim}{Q}}_B = - \underset{\sim}{G}_p^T \underset{\sim}{\beta}_p + \underset{\sim}{G}^T \underset{\sim}{H}_{hh}^{-1} \underset{\sim}{H}_{hp} \underset{\sim}{\beta}_p \tag{3.41}$$

For a crack front element

$$\underset{\sim}{Q}_B = - \underset{\sim}{G}_p^T \underset{\sim}{\beta}_p + \underset{\sim}{G}^T \underset{\sim}{H}_{hh}^{-1} \underset{\sim}{H}_{hp} \underset{\sim}{\beta}_p - \underset{\sim}{K}_{rs}^T \underset{\sim}{K}_{ss}^{-1} (\underset{\sim}{B} - \underset{\sim}{H}_{hs}^T \underset{\sim}{H}_{hh}^{-1} \underset{\sim}{H}_{hp} \underset{\sim}{\beta}_p) \tag{3.42}$$

To insure a unique finite element solution, there is a requirement for the given particular solution that the order of the polynomials in the particular solution should be equal to or lower than that of the highest complete polynomials in the homogeneous stress field [87]. For type B and B' crack elements and far-field elements, the following particular solution can be used for constant body forces

$$\sigma_x = - \bar{F}_x \, x$$

$$\sigma_y = - \bar{F}_y \, y$$

$$\sigma_z = - \bar{F}_z \, z$$

$$\tau_{yz} = \tau_{zx} = \tau_{xy} = 0 \tag{3.43}$$

However, for type A and A' crack front elements, if the stress assumption given in Equation (3.40) is used, the assumed stress σ_z, σ_{yz} and σ_{zx} lacks the constant term and hence a unique solution is not guaranteed for the particular solution of any order. In this case, the equivalent nodal forces may be calculated in the inconsistent manner.

3.8 Assumed Boundary Displacement Field

A crack front element is connected to conventional solid elements on its remote faces, while it joins to other singular elements through the frontal and profile faces. For a successful implementation of this crack front element, displacements must be compatible along those interelement boundaries. This condition is normally satisfied in the hybrid model by assuming boundary displacements in terms of interpolation functions and generalized nodal displacements on each element interface. For far-field (regular) elements, a single interpolation function can be used for the assumptions of all displacement components over all element faces if each face consists of the same number of nodes and same geometrical shape. However, in a crack front element, one has to work with a different displacement interpolation for each face to simulate the correct asymptotic behavior of displacements in the neighborhood of the crack front. In the present study the boundary displacements adopted follow the approach used by Atluri and Kathiresan [66,120], in connection with their crack element by the assumed displacement hybrid model.

Assumed Boundary Displacements for 8-Node Element

Figure 7 shows the typical 8-node crack front element and its relative node numbering scheme.

Frontal Face (1, 4, 8, 5, - 1, 2, 6, 5)

On the frontal face, which contains the crack front edge, the asymptotic behavior of displacements in Equation (2.2) indicates square root r variation. Displacement component u, v, w can use the same interpolation polynomials. For example, on face 1, 4, 8, 5 ($\xi = -1$), the x-direction displacement $\tilde{u}$ is assumed as

$$\tilde{u} = a_1 + a_2\sqrt{r} + a_3\eta + a_4\sqrt{r}\,\eta$$

where all a's are constants.

Prescribing the nodal displacement in terms of the nodal values of coordinates r and η, one obtains a set of simultaneous equations as

$$\tilde{u}_i = a_1 + a_2\sqrt{r_i} + a_3\eta_i + a_4\sqrt{r_i}\,\eta_i \qquad (i = 1,4,8,5)$$

where r_i, η_i are the coordinates r and η of the ith node. Solving these equations, the parameters $a_i (i = 1,2,3,4)$ are uniquely expressed in terms of the corresponding generalized nodal displacements, viz, q_1, q_{10}, q_{22}, q_{13}. The y and z-direction displacement $\tilde{v}$ and $\tilde{w}$ are assumed in a similar fashion.

Profile Face (1, 2, 3, 4, - 5, 6, 7, 8)

On the profile face which intersects the crack front edge, the asymptotic behavior of displacements takes the form of a trigonometric function of θ bounded by square root r as shown in Equation (2.2). To simulate this correct angular and radial variation of displacement, the boundary displacements over this face are assumed as

$$\tilde{u} = a_1 + a_2\sqrt{r}\ [(2\kappa-1)\cos\frac{\theta}{2} - \cos\frac{3\theta}{2}]$$

$$+ a_3\sqrt{r}\ [(2\kappa+3)\sin\frac{\theta}{2} + \sin\frac{3\theta}{2}] + a_4 r$$

$$\tilde{v} = b_1 + b_2\sqrt{r}\sin\frac{\theta}{2} + b_3\sqrt{r}\cos\frac{\theta}{2} + b_4 r$$

$$\tilde{w} = c_1 + c_2\sqrt{r}\ [(2\kappa+1)\sin\frac{\theta}{2} - \sin\frac{3\theta}{2}]$$

$$+ c_3\sqrt{r}\ [(2\kappa-3)\cos\frac{\theta}{2} + \cos\frac{3\theta}{2}] + c_4 r$$

where the coordinates r and θ are measured on the plane perpendicular to the crack front line, κ is related to the Poisson's ratio by $\kappa = 3-4\nu$.

Inserting nodal values of r and θ into the above equations and equating them to appropriate generalized nodal displacements, we obtain three sets of simultaneous equations. Upon solving these equations, all coefficients (a_1,a_2,a_3,a_4), (b_1,b_2,b_3,b_4) and (c_1,c_2,c_3,c_4) are evaluated uniquely in terms of their respective generalized nodal displacements.

For example, on face 1, 2, 3, 4 (a_1, a_2, a_3, a_4) are determined in terms of (q_1, q_4, q_7, q_{10}), (b_1, b_2, b_3, b_4) are determined by (q_2, q_5, q_8, q_{11}), and (c_1, c_2, c_3, c_4) are determined by (q_3, q_6, q_9, q_{12}).

When the crack front is straight, boundary displacement is compatible with that of the adjoining crack front element on this face. However, when the crack front is curved, the hypothetically rectilinear crack front line should be symmetrical across the profile face to maintain the interelement displacement compatibility on this face.

<u>Remote Face (2, 3, 7, 6, - 4, 3, 7, 8)</u>

On the remote face which is distant from the crack front, the well known interpolation function of polynomial form can be used for boundary displacements assumption.

For example on face 2, 3, 7, 6, boundary displacements are interpolated as

$$\tilde{u} = \phi_1 q_4 + \phi_2 q_7 + \phi_3 q_{19} + \phi_4 q_{16}$$

$$\tilde{v} = \phi_1 q_5 + \phi_2 q_8 + \phi_3 q_{20} + \phi_4 q_{17}$$

$$\tilde{w} = \phi_1 q_6 + \phi_2 q_9 + \phi_3 q_{21} + \phi_4 q_{18}$$

where

$$\phi_1 = \frac{1}{4} (1-\zeta)(1-\eta)$$

$$\phi_1 = \frac{1}{4} (1+\zeta)(1-\eta)$$

$$\phi_3 = \frac{1}{4}(1+\zeta)(1+\eta)$$

$$\phi_4 = \frac{1}{4}(1-\zeta)(1+\eta)$$

It is obvious that when a 8-node far-field element based on the assumed displacement model is connected at this face, interelement compatibility of displacements is preserved. However, strictly speaking, the assumed boundary displacement is discontinuous across the element edge 2-3, 3-4, 6-7 and 7-8. A number of performance tests which will be described later shows that this slight inconsistency has no appreciable effect on the finite element solution.

Assumed Boundary Displacements for 12-Node Element

A typical 12-node crack front element and its relative node numbering scheme are shown in Figure 8.

Frontal Face (1, 4, 8, 5, - 1, 2, 6, 5)

Since there is no intermediate side node on this face, the same interpolates are used as those on the frontal face of 8-node element.

Profile Face (1, 2, 9, 3, 10, 4, - 5, 6, 11, 7, 12, 8)

Since there are two additional mid-side nodes on this face, displacements are assumed as

$$\tilde{u} = a_1 + a_2\sqrt{r}\,[(2\kappa-1)\cos\frac{\theta}{2} - \cos\frac{3\theta}{2}]$$

$$+ a_3\sqrt{r}\,[(2\kappa+1)\sin\frac{\theta}{2} - \sin\frac{3\theta}{2}]$$

$$+ a_4\sqrt{r}\ [(2\kappa+3)\sin\frac{\theta}{2} + \sin\frac{3\theta}{2}]$$

$$+ a_5\sqrt{r}\ [(2\kappa-3)\cos\frac{\theta}{2} + \cos\frac{3\theta}{2}] + a_6 r$$

$\tilde{v}$ and $\tilde{w}$ are given by identical expression with $(a_1, a_2, \ldots a_6)$ above, being replaced by $(b_1, b_2, \ldots b_6)$ and $(c_1, c_2, \ldots c_6)$, respectively.

<u>Remote Face (4, 10, 3, 7, 12, 8, - 2, 9, 3, 7, 11, 6)</u>

For example on face 4, 10, 3, 7, 12, 8, displacements are interpolated as

$$\tilde{u} = \phi_1\, q_{10} + \phi_2\, q_7 + \phi_3\, q_{19} + \phi_4\, q_{22} + \phi_5\, q_{28} + \phi_6\, q_{34}$$

$$\tilde{v} = \phi_1\, q_{11} + \phi_2\, q_8 + \phi_3\, q_{20} + \phi_4\, q_{23} + \phi_5\, q_{29} + \phi_6\, q_{35}$$

$$\tilde{w} = \phi_1\, q_{12} + \phi_2\, q_9 + \phi_3\, q_{21} + \phi_4\, q_{24} + \phi_5\, q_{30} + \phi_6\, q_{36}$$

where

$$\phi_1 = -\frac{1}{4}(1-\xi)(1-\eta)\xi$$

$$\phi_2 = \frac{1}{4}(1+\xi)(1-\eta)\xi$$

$$\phi_3 = \frac{1}{4}(1+\xi)(1+\eta)\xi$$

$$\phi_4 = -\frac{1}{4}(1-\xi)(1+\eta)\xi$$

$$\phi_5 = \frac{1}{2}(1-\xi^2)(1-\eta)$$

$$\phi_6 = \frac{1}{2}(1-\xi^2)(1+\eta)$$

Assumed Boundary Displacement for 16-Node Element

A typical 16-node crack front element and its relative node numbering scheme are shown in Figure 9.

Frontal Face (1, 12, 4, 8, 16, 5, - 1, 9, 2, 6, 13, 5)

There is one mid-side node on each edge that intersects the crack front line. For example, on face 1, 12, 4, 8, 16, 5, the displacements are assumed as

$$\tilde{u} = a_1 + a_2\sqrt{r} + a_3 r + a_4 \eta + a_5\sqrt{r}\eta + a_6 r\eta$$

Identical assumptions are made for $\tilde{v}$ and $\tilde{w}$ with $(a_1, a_2, \ldots a_6)$ being replaced by $(b_1, b_2, \ldots b_6)$ $(c_1, c_2, \ldots c_6)$, respectively.

Profile Face (1, 9, 2, 10, 3, 11, 4, 12, - 5, 13, 6, 14, 7, 15, 8, 16)

Since every edge has a mid-side node on this face, displacements are assumed as

$$\tilde{u} = a_1 + a_2\xi + a_3\zeta + a_4\xi\zeta$$

$$+ a_5\sqrt{r}\ [(2\kappa-1)\cos\frac{\theta}{2} - \cos\frac{3\theta}{2}]$$

$$+ a_6\sqrt{r}\ [(2\kappa+1)\sin\frac{\theta}{2} - \sin\frac{3\theta}{2}]$$

$$+ a_7\sqrt{r}\ [(2\kappa+3)\sin\frac{\theta}{2} + \sin\frac{3\theta}{2}]$$

$$+ a_8\sqrt{r}\ [(2\kappa-3)\cos\frac{\theta}{2} + \cos\frac{3\theta}{2}]$$

$\tilde{v}$ and $\tilde{w}$ are assumed in the identical form with $(a_1, a_2, \ldots a_8)$ above, being replaced by $(b_1, b_2 \ldots b_8)$ and $(c_1, c_2, \ldots c_8)$, respectively.

Remote Face (4, 11, 3, 7, 15, 8, - 2, 10, 3, 7, 14, 6)

Displacement interpolates are the same with those on the remote face of 12-node element.

3.9 Integration of Element Matrices

In the present formulation, the evaluation of element matrices entails the integration of both surface integrals and volume integrals. Some of these surface integrals contain singularities at the crack front. This section gives a brief comment on the integration techniques utilized in the present study.

Any face of the crack front element is conveniently represented by a set of three parametric equations. For example, the element face $\eta = 1$ in Figure 7 is expressed in the form of

$$x = x\ (\xi, \zeta)$$

$$y = y\ (\xi, \zeta)$$

$$z = z\ (\xi, \zeta)$$

The differential surface dS on this face is expressed in terms of $d\xi$ and $d\zeta$ as

$$dS = \left| \frac{d\bar{r}}{d\xi} \times \frac{d\bar{r}}{d\zeta} \right|_{\eta=1} d\xi d\zeta = \sqrt{a(\xi,\zeta)}\ d\xi d\zeta$$

where $\quad r = x\bar{i} + y\bar{j} + z\bar{k}$

Expanding the vector cross product leads to

$$\sqrt{a(\xi,\zeta)} = (a_1^2 + a_2^2 + a_3^2)^{1/2}$$

where

$$a_1 = \left[\frac{\partial(y,z)}{\partial(\xi\ \zeta)}\right]_{\eta=1} = \left[\frac{\partial y}{\partial\xi}\frac{\partial z}{\partial\zeta} - \frac{\partial y}{\partial\zeta}\frac{\partial z}{\partial\xi}\right]_{\eta=1}$$

$$a_2 = \left[\frac{\partial(z,x)}{\partial(\xi,\zeta)}\right]_{\eta=1} = \left[\frac{\partial z}{\partial\xi}\frac{\partial x}{\partial\zeta} - \frac{\partial z}{\partial\zeta}\frac{\partial x}{\partial\xi}\right]_{\eta=1}$$

$$a_3 = \left[\frac{\partial(x,y)}{\partial(\xi,\zeta)}\right]_{\eta=1} = \left[\frac{\partial x}{\partial\xi}\frac{\partial y}{\partial\zeta} - \frac{\partial x}{\partial\zeta}\frac{\partial y}{\partial\xi}\right]_{\eta=1}$$

Thus, the surface integral of an arbitrary function $f(\xi,\zeta)$ over the face $\eta = 1$ can be written as

$$\iint_{\eta=1} f(\xi,\zeta)dS = \int_{-1}^{1}\int_{-1}^{1} f(\xi,\zeta)\ \sqrt{a(\xi,\zeta)}\ d\xi d\zeta$$

This idea of evaluating surface integral is similar to the idea used by Atluri et al. [66,120].

In the evaluation of the strain energy due to the exact asymptotic stress and displacement field, the matrix $\underset{\sim}{R}_s$ in Equation (3.13) contains a $1/\sqrt{r}$ variation over the surface while $\underset{\sim}{L}_s$ contains a $\sqrt{r}$ variation. Therefore, the matrix $\underset{\sim}{H}_{ss}$ in Equation (3.20) is completely free from singularity and the aforementioned surface integration technique can immediately be applied to its numerical integration. On the other hand, the integrand of $\underset{\sim}{G}_s$ in Equation (3.20) still involves a $1/\sqrt{r}$ singularity at the crack front. When $\underset{\sim}{G}_s$ is evaluated on both the frontal and profile faces which include the crack

front and the singularities, proper changes of the integration variables are necessary in order to improve the numerical accuracy.

On the frontal face, for example, on the face $\xi = -1$, only the variable ζ is transformed into a new variable t by

$$\zeta = \frac{1}{2}(t+1)^2 - 1$$

The surface integral can be rewritten as

$$\int_{-1}^{1}\int_{-1}^{1} f(\eta,\zeta)\ \sqrt{a(\eta,\zeta)}\ d\eta d\zeta$$

$$= \int_{-1}^{1}\int_{-1}^{1} f(\eta,\zeta(t))\ \sqrt{a(\eta,\zeta(t))}\ (t+1)\ d\eta dt$$

In the numerical integration of $\underset{\sim}{G}_s$ over this frontal face, 3-point Gaussian quadrature was used for η while 5-point quadrature was used for the new variable t.

On the profile face $\eta = \pm 1$, both ξ and ζ are transformed into new variables s and t by

$$\xi = \frac{1}{2}(s+1)^2 - 1$$

$$\zeta = \frac{1}{2}(t+1)^2 - 1$$

The surface integral over this face is written as

$$\int_{-1}^{1}\int_{-1}^{1} f(\xi,\zeta)\ \sqrt{a(\xi,\zeta)}\ d\xi d\zeta$$

$$= \int_{-1}^{1}\int_{-1}^{1} f(\xi(s),\zeta(t))\ \sqrt{a(\xi(s),\zeta(t))}\ (s+1)(t+1)\ dsdt$$

On this face, numerical integration was performed in terms of s and t by using 5x5 point Gaussian quadrature.

On the remote face, any integrand does not contain singularity and hence 3x3 point Gaussian quadrature was used for the evaluation of surface integrals over this face.

The volume integrals in the present model are completely free from singularities. The differential volume dV is expressed in terms of $d\xi$, $d\eta$ and $d\zeta$ as

$$dV = |J|_{abs}\, d\xi d\eta d\zeta$$

where $|J|$ is the Jacobian defined by

$$|J| = \begin{vmatrix} \frac{\partial x}{\partial \xi} & \frac{\partial y}{\partial \xi} & \frac{\partial z}{\partial \xi} \\ \frac{\partial x}{\partial \eta} & \frac{\partial y}{\partial \eta} & \frac{\partial z}{\partial \eta} \\ \frac{\partial x}{\partial \zeta} & \frac{\partial y}{\partial \zeta} & \frac{\partial z}{\partial \zeta} \end{vmatrix}$$

The volume integral is written as

$$\iiint_{V_n} f(x,y,z)\, dV$$

$$= \int_{-1}^{1}\int_{-1}^{1}\int_{-1}^{1} f(x(\xi,\eta,\zeta), y(\xi,\eta,\zeta), z(\xi,\eta,\zeta))\, |J|\, d\xi d\eta d\zeta$$

For the evaluation of the matrix $\underset{\sim}{H}_{hh}$ in Equation (3.20), one can reduce the computation time in the following manner. Every element of $\underset{\sim}{H}_{hh}$, which consists of an integral of a linear combination of a small number of distinct terms such

as $x, y, z, x^2, y^2, z^2, xy$ and so on, is expressed algebraically a priori. Numerical integration needs be carried out only for these distinct terms. For example, in an 8-node type B element, only 159 entires of the upper or lower triangular part of $\underset{\sim}{H}_{hh}$ are not identically zero. In these nonzero elements, there are only 23 distinct terms, i.e., $1, x, y, z, xy, yz, zx, x^2, y^2, z^2, xy^2, x^2y, yz^2, y^2z, zx^2, z^2x, xyz, x^2y^2, y^2z^2, z^2x^2, xyz^2, xy^2z, x^2yz$. In an 8-node type A element, the upper or lower triangular matrix of $\underset{\sim}{H}_{hh}$ has 244 nonzero entries, which consists of a linear combination of 72 distinct terms. These terms are $1, x, y, z, xy, yz, zx, x^2, y^2, z^2, xy^2, x^2y, yz^2, y^2z, zx^2, z^2x, x^3, y^3, z^3, x^2yz, xy^2z, xyz^2, xy^3, x^3y, yz^3, y^3z, zx^3, z^3x, x^2y^2, y^2z^2, z^2x^2, x^4, y^4, z^4, x^4y, xy^4, y^4z, yz^4, z^4x, zx^4, xyz^3, x^3yz, xy^3z, xy^2z^2, x^2yz^2, x^2y^2z, x^2y^3, x^3y^2, y^3z^2, y^2z^3, z^3x^2, z^2x^3, x^4yz, xy^4z, xyz^4, xy^2z^3, xy^3z^2, x^2y^3z, x^3y^2z, x^2yz^3, x^3yz^2, x^2y^2z^2, x^4y^2, x^2y^4, y^4z^2, y^2z^4, z^4x^2, z^2x^4, x^3y^3, y^3z^3, z^3x^3$.

3.10 On the Crack Front Element with Curved Boundaries

One of the most desirable geometrical shape for three-dimensional crack front elements will be a general hexhahedron with arbitrarily curved boundaries. Figure 4 shows such a general "brick" element located at the crack front. A certain group of practical brick elements with curved boundaries can easily be constructed by using the well-known isoparametric transformation technique. However, because of the necessity of incorporating the two-dimensional asymptotic behavior

in the finite element formulation, the actual shapes of the hexagonal elements must be somewhat restricted. The only available asymptotic solution near a crack front is a two-dimensional behavior in terms of r and θ, where r and θ are the polar coordinates with the crack tip as their origin.

Let A and B be the two arbitrary points on the profile face which intersects the crack front line. If the face is warped, the two points are, in general, on two different normal planes perpendicular to the crack front line. This indicates that there is no one to one (unique) correspondence between the two-dimensional coordinates (r,θ) and an arbitrary point on the warped profile face. Hence, on these element faces, it is impossible to construct a reasonable boundary displacement interpolation function which contains asymptotically correct variation of displacement. Therefore, profile faces are required to be flat. In addition to that, if the front edge of the crack element is curved and the profile face is flat but not normal to the front line, the normal to the crack front which passes through an arbitrary point A on the profile face may intersect the crack front line outside the element. Asymptotic behavior of displacements and stresses at point A can be expressed only in terms of the coordinates r and θ and their origin lies on the curved front outside the element. It is not practical to calculate element matrices by using the structural geometries outside the element. Hence, if the crack front edge is curved, the

element profile faces should be flat and normal to the crack front. However, there arises another inconsistency. The higher order elements with curved boundaries are, in general, derived by the nonlinear coordinate transformation. For twenty-node general brick element, the edge line is made of quasi-quadratic (parabolic) curve. Thus, if we analyze a curved crack, for example a penny shape crack, by using twenty-node and/or other higher order elements, the circular crack front is approximated by the assemblage of parabolic and/or other incomplete polynomial basis segments which do not provide a complete fit to the actual circular crack front. However, the profile face of such elements should be flat and normal to the element front edge, so the overlapping or gapping is unavoidable between two neighboring crack front elements (Figure 5). It is realized that errors due to such approximations in finite element formulations will become small when the element size becomes small. The main reason for the choice of element with a straight crack front is the ease of satisfying the equilibrium conditions for the singular stress terms.

3.11 Evaluation of Crack Front Elements

To assess the accuracy of the crack front elements developed in the present study, a simple test, following that given by Refs. 66 and 120 has been performed. In this and all the following numerical computations, the IBM 370/165 at the Information Processing Center of M.I.T. has been used. For each crack front element, the nodal displacements are calculated from the known analytical solution viz., Equation (2.2) that corresponds to the mixed mode

condition of $K_I = K_{II} = K_{III} = 1.00$. Using these displacements as input data, the values of K_I, K_{II} and K_{III} are then computed from the numerically generated element matrices by using Equation (3.29). The results obtained for different types of crack front elements and for different half elements and superelements are listed in Table 14. It is seen that they all compare favorably with the correct values. Obviously elements with more nodes yield more accurate solutions.

3.12 Numerical Examples of Three-Dimensional Cracks

3.12.1 Rectangular Prism with a Single Edge Crack

Figure 10 shows a rectangular prism of width b thickness 2t and length 2L containing a single edge crack of depth a. A uniformly distributed normal traction is applied over the upper and lower surfaces which are parallel to the crack plane. The orientation of the global coordinate axes are drawn in Figure 10 with the origin at the center of the crack front; the Y-axis is taken along the crack front, the X-Y plane lies on the crack surface, and the Z-axis is normal to the crack surface. Theoretical value of the stress intensity factor K_I for a single edge crack in a rectangular plate has been obtained by Bowie and Gross based on two-dimensional plane strain assumption and is found in Reference 33.

Since the geometry and the loading is symmetric across the plane Y=0 and Z=0, only a quadrant of the prism is required for finite element analysis. Figure 11 shows two

different finite element mesh representations. In both mesh representations, a quadrant of the prism is divided into five equal layers by planes perpendicular to the crack front. Each layer contains one upper half superelement. The mesh in Figure 11(1) is constructed from 30 regular elements and 5 superelements or a total of 35 elements. The nodes are arranged at the following locations.

$X/b = -0.5, -0.0625, 0, 0.0625, 0.5$

$Z/L = 0, 0.0125, 1$

The mesh in Figure 11(2) is constructed from 80 regular elements and 5 superelements or a total of 85 elements. The nodes are placed at the following locations.

$X/b = -0.5, -0.28125, -0.0625, 0, 0.0625, 0.28125, 0.5$

$Z/L = 0, 0.125, 0.5625, 1$

12-node upper half superelement is used for two different finite element meshes, while 20-node superelement is used only for the coarse mesh model. For the remaining elements, 8-node hexahedron elements based on the hybrid stress model are used. However, when 20-node superelements are used, special 10-node hybrid stress hexahedron elements encircle each superelement to connect 8-node far-field elements to 20-node superelements. When 12-node superelements are used, the finite element model of coarse mesh contains 90 nodes, 270 degrees of freedom,

while it contains 114 nodes, 342 degrees of freedom when 20-node superelements are used. In the fine mesh subdivision there are 168 nodes, 504 degrees of freedom. To simulate the effects of the adhacent prism quadrants, symmetric boundary conditions are imposed on the plane Y=0 and Z=0. The Poisson's ratio ν = 0.3 is used in this case.

The numerical values of the stress intensity factor K_I thus obtained are listed in Table 15. The variation of K_I solution along the crack front and its comparison with the two-dimensional plane strain solution are shown in Figure 12. The values of K_I in Table 15 and in Figure 12 are normalized by the exact two-dimensional plane strain solution $K_I = \sigma a^{1/2}$ for a crack of length 2a in an infinite plate. The K_I solution takes the highest value in the superelement closest to the center of the prism and gradually decreases as the surface is approached. Two-dimensional plane strain solutions obtained by Bowie and Gross for crack length a, total width b and total length 2L are expressed in the form of $K_I = \sigma(a\pi)^{1/2} F(a/b)$, where σ is the applied stress. For a/b = 0.5, L/6 = 1, the numerical values of F(a/b) obtained by Bowie and Gross are 2.86 and 2.82, respectively. When the fine (85 elements) esh subdivision is used, in the superelement adjacent to the center plane, the 12-node superelement gives a value of F(a/b) of 2.89 which is 1% higher than Bowie's plane strain solution and is 2.5% higher than Gross's solution. When the

20-node superelement is used, the coarse (35 elements) mesh representation yields a value of $F(a/b)$ of 2.76 which is 3.5% lower than that of Bowie and 2.1% lower than that of Gross. It is seen that the value of $F(a/b)$ obtained by the combination of 12-node superelement and the coarse mesh subdivision is still within the needed engineering accuracy.

3.12.2 Rectangular Prism with a Center Crack

Figure 10 shows a rectangular prism of width 2b, thickness 2t and length 2L containing a center crack of length 2a. The origin of the global Cartesian coordinates (X,Y,Z) is taken at the center of the prism. A uniformly distributed tension load is applied on both upper and lower surfaces of the prism. A two-dimensional plane strain solution of the stress intensity factor K_I for a center crack in a rectangular plate has been obtained by Ishida by extensively developing the mapping functions and his results are found in Reference 33.

Since the geometry and the loading are symmetric across the plane X=0, Y=0 and Z=0, only one eighth of the prism needs be modelled for finite element analysis. The same mesh representations as those in the preceding example are again used in this problem. Symmetric boundary conditions are imposed on the plane X=0, Y=0 and Z=0.

The stress intensity factor K_I solution thus obtained are shown in the normalized form $Y = K_I/\sigma a^{1/2}$ in Table 16 and

in Figure 13. Ishida's two-dimensional solutions which are considered to be accurate within 1 or 2 per cent are expressed in the form of $K_I = \sigma(a\pi)^{1/2} F(a/b)$, where σ is the applied stress, a is the half crack length, b is the half plate width. The a/b ratios used by Ishida do not exactly match that of the present example. His F(a/b) values are 1.18 for a/b = 0.466, 1.25 for a/b = 0.535 and 1.33 for a/b = 0.592. When the fine (85 elements) mesh representation is used, the use of the 12-node superelements gives a F(a/b) value of 1.18 in the element adjacent to the center plane for a/b = 0.5. In case of the coarse (35 elements) mesh representation, the F(a/b) value obtained by using the 20-node superelement is 1.21. These F(a/b) values correlates very well with those of Ishida's two-dimensional analysis. The worst combination, i.e., the combination of the coarse mesh representation and the 12-node superelement yields the F(a/b) value of 1.05 which is about 10% lower than Ishida's solution.

3.12.3 Rectangular Prism with a Double Edge Crack

Figure 10 shows a rectangular prism of width 2b, thickness 2t and length 2L containing a double edge crack of depth a. The origin of the global coordinates (X,Y,Z) is taken at the center of the prism. The loading condition is the uniformly distributed tension load applied on both the upper and lower surfaces of the prism. Two-dimensional plane strain solution of the stress intensity factor K_I for a double edge

crack in a rectangular plate has been obtained by Bowie and is found in Reference 33.

Since the geometry and the loading are symmetric with respect to the plane X=0, Y=0 and Z=0, it is necessary to consider only one eighth of the prism for finite element analysis. The mesh representations used in this analysis are the same as those in the preceding two examples. Symmetric boundary conditions are imposed on the plane X=0, Y=0 and Z=0. The resulting K_I solution are shown in the normalized form of $Y = K_I/\sigma a^{1/2}$ in Table 17 and in Figure 14. Two-dimensional solutions of Bowie are expressed as $K_I = \sigma(\pi a)^{1/2} F(a/b)$, where σ is the applied stress, a is the crack length and b is the half plate width. For the geometry of $a/b = 0.5$, $L/b \rightarrow \infty$, his computed value of F(a/b) is 1.15, where L is the half length of the plate. When the fine mesh representation is used, the 12-node superelement adjacent to the center plane gives the F(a/b) value of 1.20 which is 4.3% higher than Bowie's solution. When the coarse mesh representation is used, the resulting F(a/b) value in the 20-node superelement adjacent to the center plane is 1.18 which is 2.6% higher than that of Bowie's analysis. The value of F(a/b) obtained by the combination of the 12-node superelement and the coarse mesh representation is 1.06 and is 7.8% lower than Bowie's value.

The above-mentioned three examples, i.e., single edge crack, center crack, double edge crack specimens have been

analyzed not to pursue the accurate solutions for individual problems but only to confirm the possibility of the three-dimensional crack element based on the assumed stress hybrid stress finite element model. The 35 and 85 elements mesh representations used in these analyses are both extremely coarse. However, the resulting stress intensity factor solutions show the sufficient engineering accuracy.

3.12.4 Compact Tension Specimen

Compact tension specimen, as the name implies, can be made more compact than any other specimens that could be used for fracture toughness K_{I_c} testing. Due to its compactness the specimen has become widely used especially in the fields where economy or space for exposure of material is of particular interest. Therefore, the analysis of compact test specimen is significant to the application and development of fracture mechanics.

Figure 15 shows the standard compact tension specimen (ASTM E-399-72). The geometry is a plate of thickness t, width W and height h with a through the thickness single edge crack of uniform depth a. Uniformly distributed line load of magnitude T (force/length) which is normal to the crack surfaces is applied at the pin holes throughout the thickness. Test results obtained by using compact tension specimen are usually analyzed with the aid of the two-dimensional plane strain solution for the stress intensity factor. However,

since the thickness of this specimen is not negligibly small and the interior points are not remote from the outer surfaces, the stress field in the interior is highly three-dimensional and hence the magnitude of the stress intensity factor appears to vary considerably along the crack front. Therefore, three-dimensional analysis is essential for the detailed estimation of the specimen behavior. Several authors, Cruse [46], Tracey [59], Barsoum [67] and Yamamoto and Sumi [70] have carried out three-dimensional analyses of this specimen. Because of the complexity of three-dimensional crack analysis, numerical methods have been used by such authors. Cruse used singular integral method (direct potential method), Tracey and Barsoum performed finite element analyses based on assumed displacement model. Yamamoto and Sumi applied the method of superposition of analytical and finite element solution to determine the detailed stress field of this specimen.

The orientation of the axes of global coordinates (X,Y,Z) are shown in Figure 15 with the origin at the center of the crack front. Since the geometry of the specimen and loading are symmetric across the plane Y=0 and Z=0, only one quarter of the specimen is needed in the finite element analysis. In the present study, the pin holes are removed and the loading is represented by a distributed line load applied along the contact lines of pins and pin holes. Twelve-node upper half superelement which consists of two 8-node crack front elements

is used for near-field element, while 8-node hexahedron element based on hybrid stress model occupies the rest of the domain. Two different specimen geometries, $a/W = 3/8$ and $a/W = 5/8$ are considered. In both cases, the Poisson's ratio $\nu = 0.3$ is used. The finite element mesh subdivisions for two different specimen geometries are drawn in Figure 16 and both models have 85 elements, 168 nodal points and 504 degrees of freedom. In these finite element representations, a quadrant of the specimen is divided into five layers at equal intervals by planes normal to the crack front. Each layer contains one superelement.

For the specimen of $a/W = 3/8$, the depth of the crack contained in each superelement is one third of the total crack depth a. Along the X-axis, the nodal points are arranged at

$X/W = -0.625, -0.375, -0.125, 0, 0.125, 0.375, 0.625$

Along the Z-axis, the nodes are located at

$Z/W = 0.125, 0.4, 0.6$

For the specimen of $a/W = 5/8$, the depth of the crack in each superelement is one fifth of the total crack depth a. The nodes are arranged at the following locations along the X-axis

$X/W = -0.875, -0.625, -0.375, -0.125, 0, 0.125, 0.375$

Along the Z-axis

$Z/W = 0.125, 0.4, 0.6$

Symmetrical boundary conditions are imposed on the plane Y=0 and Z=0.

Figures 17 and 18 show the variation of the magnitude of the stress intensity factor K_I thus obtained for the specimen of a/W = 3/8 and a/W = 5/8, respectively. They are also listed in Table 18. The corresponding two dimensional plane strain solutions are drawn in the above figures for convenience. These solutions are normalized in the form of

$$Y = K_I / \frac{T(2W+a)}{t(W-a)}$$

where T is the total applied load.

The resulting solution takes the maximum value in the superelement closest to the center of the specimen and gradually decreases as the free surface is approached. The solutions obtained by Yamamoto and Sumi are plotted in Figures 17 and 18 for the purpose of comparison. For the geometry of a/W = 3/8, the correlation between these two solutions is indeed excellent. For a/W = 5/8, the correlation is less good than that of a/W = 3/8. In this case the present K_I solution in the superelement closest to the center of the specimen is only 1% above the plane strain solution, while Yamamoto's solution is 5% above the plane strain solution at the center of the specimen. It is seen that for both solutions the value of K_I at the center of the specimen of a/W = 3/8 deviates more from the plane strain solution than that of the specimen of a/W = 5/8.

It should be noted that for the present solution only one set of matrix equations of 504 unknowns is solved while in the method by Yamamoto and Sumi, computation of finite element solutions should be performed (2m + 1) times where m is the number of finite element layers across the thickness of the plate. For each solution they considered a mesh pattern with 2106 degrees of freedom. As indicated in Table 19, by using a mesh subdivision with fewer degrees of freedom than that by Tracey and Barsoum, the present hybrid stress superelements provide results which are closer to the solution by Yamamoto and Sumi. The latter are used here as reference because they were obtained by finer meshes and also contain a complete treatment of the singular behavior at the crack front.

3.12.5 Cylindrical Rod with an Axisymmetrically Located Penny Shape Crack under Uniform Tension Loading

A cylinder of radius R, length 2L containing a penny-shaped crack of radius a with the axis of symmetry being normal to the crack plane is shown in Figure 19. Cylindrical coordinates (r,θ,Z) are also drawn in the same figure. With reference to this coordinates system, the crack occupies the region $Z = 0^{\pm}$, $0 \leq r \leq a$. The Z direction is the longitudinal axis of the cylinder through the center of the crack. Uniformly distributed tension load is applied on both upper and lower end surfaces of the cylinder. The semi-analytical solution for this problem has been obtained by Benthem and can be found in Reference 36.

Since the geometry and loading are not only axisymmetric with respect to the Z-axis, but also symmetric across the plane Z=0, only one narrow sector of the cylinder in the region $Z \geq 0$ needs to be modelled for finite element analysis. Analysis has been carried out for two different included angles $\theta = 10^\circ$ and $\theta = 5^\circ$, and for two different finite element mesh representations, 396 degrees of freedom and 810 degrees of freedom. The 396 d.o.f. finite element model is shown in Figure 20(a). It has 132 nodal points and is constructed from a twelve-node upper half superelement, 5 six-node pentahedron elements and 46 eight-node hexahedron elements or a total of 52 finite elements. The nodal points are arranged at the following locations along the r-axis

r/R = 0, 0.05, 0.1, 0.125, 0.15, 0.175, 0.2, 0.225, 0.25, 0.275, 0.3, 0.35, 0.55, 1.0

Along the Z-axis, they are located at

Z/L = 0, 0.05, 0.1, 0.2, 0.6, 1.0

The 810 d.o.f. finite element model is drawn in Figure 20(b). This model has 270 nodal points and a twelve-node upper half superelement, 8 six-node pentahedron elements and 107 eight-node hexahedron elements or a total of 116 finite elements. The nodes are arranged at the following locations along the r-axis

r/R = 0, 0.05, 0.1, 0.125, 0.15, 0.175, 0.2, 0.225, 0.25, 0.275, 0.3, 0.4, 0.7, 1.0

On the Z-axis, they are at

Z/L = 0, 0.025, 0.05, 0.075, 0.1, 0.2, 0.4, 0.7, 1.0

In both finite element representations, one-eighth of the total crack radius a is included in the superelement. The far-field elements, i.e., 6-node pentahedron and 8-node hexahedron regular elements are based on assumed displacement finite element model and are generated by using isoparametric transformation techniques. To simulate the axisymmetric behavior of the cylinder, all nodes are fixed in the circumferential direction. The nodes which are ahead of the crack plane are also restrained from moving in the Z-direction.

The stress intensity factor K_I thus obtained are listed in Table 20. For both included angles the fine (116 elements) mesh subdivision yields the solution within 1% of Benthem's result. The error of the solution obtained by using the coarse (52 elements) mesh representation is 1.2% for $\theta = 10^o$ and 2.9% for $\theta = 5^o$.

In order to check the influence of the element size upon the stress intensity factor solution, computation has been carried out for the finite element model of the included angle $\theta = 5^o$ by using the crack front element with profile edges two times larger than those of the aforementioned crack front element. The fine mesh representation (810 d.o.f.) is used. The resulting solution is $K_I = 1.617$. It seems that the effect of the element size is not severe if it is between one-third and one-tenth of the crack size a.

3.12.6 Embedded Penny-Shaped Crack in a Cube in Tension

Figure 21 shows a cube of dimension $2b \times 2b \times 2b$ containing a penny-shaped crack of radius $a (= b/5)$. The global Cartesian coordinates (X,Y,Z) and cylindrical coordinates (r,θ,Z) are drawn in the same figure. Uniformly distributed tension load is applied on both top and bottom surfaces which are parallel to the crack plane. For a penny-shaped crack of radius a in an infinite solid under a uniform normal applied stress σ at infinity, Sneddon has obtained an exact stress intensity factor solution $K_I = 2\sigma\sqrt{a/\pi}$ [32].

Since the geometry and loading is symmetric across the planes X=0, Y=0 and Z=0, it suffices to model only one-eighth of the cube for finite element analysis. The finite element mesh subdivision, which is shown in Figure 24, consists of seven planes of nodes at 15° intervals about the Z-axis. On these planes, the nodes are arranged at the following distances from the Z-axis.

$r/b = 0, 0.05, 0.1, 0.15, 0.175, 0.2, 0.225, 0.25, 0.3, 0.5, 1.0$

Along the line drawn from the crack front parallel to the Z-axis, the nodes are arranged at

$Z/b = 0, 0.025, 0.05, 0.1, 0.4, 1.0$

The above finite element representation contains 284 nodes, 852 degrees of freedom, 6 twelve-node upper half superelements, 78 six-node pentahedron elements and 138 eight-node hexahedron

elements or a total of 222 finite elements. The depth of the crack included in each superelement is one-eighth of the crack radius. All far-field elements, i.e., 6-node pentahedron and 8-node hexahedron elements are based on the assumed displacement finite element model. Symmetric boundary conditions are imposed on the plane X=0, Y=0 and Z=0.

The resulting stress intensity factor solution is $K_I = 1.58$ or $Y = 0.990$ for all crack front elements, where $Y = K_I/2\sigma(a/\pi)^{1/2}$. Since the Sneddon's solution for a penny-shaped crack of radius a in an infinite solid is $K_I = 2\sigma(a/\pi)^{1/2}$, the above result shows 1% deviation from the Sneddon's solution. Tracey's solution for a penny-shaped crack in a cylindrical rod is shown in Figure 25 for comparison purposes.

3.12.7 Semi-Circular Surface Crack in a Rectangular Prism

Surface crack problems occur frequently in service conditions. Figure 22 shows a semi-circular surface crack of radius a which lies normal to the surface of a rectangular prism of height 2b, width 2b and thickness b. Radius a of the crack is one-fifth of the half width b of the prism. The global Cartesian coordinates (X,Y,Z) and cylindrical coordinates (r,θ,Z) are also drawn in the above figure. The problem is to obtain the variation of the stress intensity factor K_I along the semi-circular crack front under uniform

tension loading applied at both upper and lower surfaces of the prism.

Since the geometry and loading is symmetric across the plane X=0 and Z=0, only a quadrant of the prism is needed for finite element analysis. The finite element mesh representation shown in Figure 24, which has been used for the preceding example, is used again in the present example. Symmetric boundary conditions are imposed on the plane X=0 and Z=0.

Figure 26 presents the variation of the stress intensity factor K_I thus obtained along the crack front. They are normalized by Sneddon's solution. It is seen that K_I takes the minimum value in the superelement of the deepest penetration while the maximum stress intensity factor occurs in the element adjacent to the free surface. Smith [42] obtained the stress intensity factor for a semi-circular surface flaw in a semi-infinite solid subjected to uniaxial tension by using the alternating technique. Tracey solved the semi-circular surface crack in a rod of semi-circular cross section. Their results are also shown in Figure 26 for comparison purposes. The present solution correlates well with their results.

3.12.8 Quarter-Circular Corner Crack in a Rectangular Prism in Tension

Figure 23 shows a quarter circular corner crack of radius a in a rectangular prism of height 2b, width b and thickness b. Crack radius a is one-fifth of the width of the

prism. Uniformly distributed tension loading is applied on both top and bottom surfaces of the prism. The global coordinates (X,Y,Z) and (r,θ,Z) are drawn in Figure 23.

Since the geometry and loading is symmetric across the plane Z=0, one-half of the prism is modelled for finite element analysis. The same mesh subdivision as that in the preceding two examples is used in the present problem.

The variation of the normalized stress intensity factor solution along the crack front is presented in Figure 27. Also shown for comparison purposes is the finite element solution obtained by Tracey for a quarter-circular corner crack in a rod of quarter-circular cross section.

3.13 Concluding Remarks

A special crack front element has been developed based on the hybrid stress finite element model for the analyses of arbitrarily shaped three-dimensional crack problems. The superelement is compatible with most of the existing general purpose finite element computer programs. The CPU time for generating a 12-node crack front superelement is 5.4 seconds on an IBM S-370/165.

For obtaining stress intensity factor solutions it is not necessary to use any interpolation techniques such as C.O.D. method, virtual crack extension method, etc., which are troublesome particularly for a three-dimensional crack problems due to the variability of stress intensity factors

along the crack front. In the present crack front elements three stress intensity factors K_I, K_{II} and K_{III} are unknown stress parameters and hence can be calculated directly.

The displacement compatibility with adjoing far-field elements is completely satisfied across interelement boundaries whether they are based on an assumed displacement finite element model or a hybrid model. However, if the crack front is curved, the crack front elements should be arranged so that the crack front is symmetrical across the profile face which is common to two neighboring crack elements in order to maintain the displacement compatibility on this face.

The stress intensity factors are assumed to be constant within each crack front element. To determine the distributions of K_I, K_{II} and K_{III} along the crack front, a number of special elements should be used along the crack front.

In a special element model based on the assumed displacement method a number of elements must be used around each segment of the crack front to simulate the rapid variation of local fields with θ. However, in the present method, only a single superelement is needed around each segment of the crack front and thus the crack front region can be modelled with much fewer degrees of freedom compared to other displacement-based crack elements. In the analysis of fracture test specimens, the finite element mesh representations used in the present study contain only 270 ~ 504 degrees of freedom

which are less than those required in two-dimensional analyses by using the displacement-based special elements.

For three-dimensional crack problems available analytical solution is limited only to that for an embedded crack in an infinite solid. Due to this lack of the analytical solution of finite domain which can be served as a basis for comparison, accuracy of the present method is still an open question in the true sense of the word. However, the solutions of the stress intensity factors for the present example problems are found to be in good agreement with those obtained by other semi-analytical methods and/or two-dimensional analyses.

As the present crack front element incorporates a inverse square root r stress singularity at the crack front a priori, it appears to provide no additional insight into the nature of singularity at the intersection point between the crack front and the free surface. Unfortunately, at the present state of knowledge, the order of the stress singularity at this intersection point has not yet been known and no numerical technique can be expected to provide any meaningful solution for this fundamental problem. Therefore, in the present study, no attempt has been done to deal with the details of the variation of the stress intensity factor solution in the thin boundary layer near the surface. Even for the variation of the stress intensity factor K_I approaching

a free surface, there exist quite contradictory solutions. In one solution, the magnitude of K_I increases as the free surface is approached, in another it increases and rapidly decreases, and in the third it decreases. However, except in a thin boundary layer near a free surface, the present crack front element appears to provide highly accurate stress intensity factor solutions all along the crack front.

For body force problems, the inconsistent approach for obtaining equivalent nodal forces is adequate. This approach eliminates the non-uniqueness problem of the finite element solution for the type A crack front element.

The present method can be easily applied to thermal stress problems. The temperature variation within each element can be expressed in terms of its nodal value by using interpolation technique. In this case the use of a 16-node crack front element is desirable because it contains constant strain terms in the boundary displacement assumption. Present 8-node and 12-node crack front elements do not have complete constant strain terms and so may provide erroneous results in thermal gradients.

The present method can also be easily extended to the determination of stress intensity factors for a crack in an anisotropic material.

SECTION 4

HYBRID CRACK ELEMENT FOR ANALYZING THROUGH FLAWS IN PLATES IN BENDING

4.1 Introduction

The characteristics of the local stress and displacement field at the base of a through-the-thickness stationary crack in a plate has been analytically investigated for both symmetrical and antisymmetrical out of plane loadings by several researchers. Williams [101] first analyzed this problem by using the technique of Fadle eigenfunction expansions based on the fourth order thin plate theory of Poisson and Kirchhoff and found that the elastic bending stresses near the tip of a semi-infinite straight line crack vary as the inverse square root of the radial distance from the crack tip. His results were incomplete in that the magnitude of the local stresses were left undetermined. Later, Sih and Rice [103] cleared the way of finding the coefficients in the eigenfunction expansion through an application of the theory of complex functions. Sih, Paris and Erdogan [102] modified William's results to define stress intensity factors in bending in a manner consistent with Irwin's definitions for extensional problems in plates.

However, the above solution based on the classical plate theory satisfies the stress free condition along a crack surface only in an approximate manner. The three physically

natural boundary conditions of vanishing bending moment, twisting moment and transverse shear stress at the edge of the crack are contracted into two conditions. To overcome this shortcoming, Knowls and Wang [106] formulated the problem in terms of Reissner's six order plate theory in which all three boundary conditions on the crack surfaces can be satisfied. They reduced the formulation to singular integral equations and obtained the form of the bending stress distribution in the vicinity of a crack tip of a vanishingly thin infinite plate subjected to constant bending moment at infinity. They found that the bending stresses of primary importance possess singularities at a crack tip of the same order as in the classical theory, but the angular distribution of these stresses around the crack tip has slight discrepancies. Furthermore, the stress resultants Q_x and Q_y become infinite like $r^{-3/2}$ in the classical theory, while they remain finite as $r \to 0$ in the Reissner theory. Their work was later extended by Hartranft and Sih [107] to study the thickness effect on the stress distribution around the crack. Recently, in the framework of Reissner's theory Wang [108] obtained the asymptotic stress field for a crack in an infinite plate subjected to constant twisting moment at infinity by using the Fourier integral transform techniques to reduce the problem to a system of dual integral equations. Accoring to his analysis, the singularity of the stress resultants is of the

order of $r^{-1/2}$ in case of twisting, while it is of the order of $r^{-3/2}$ in the classical theory.

However, it is noted that the solutions obtained by the aforementioned methods are based on some approximations to a fully three-dimensional theory, viz, the theory of bending of a plate, whether it is a fourth order Kirchhoff theory or a sixth order Reissner theory. The above methods assume linear distribution of the in-plane stresses σ_x, σ_y and τ_{xy} through the thickness of the plate and thus cannot account for the nonlinear disturbances of these stresses near the crack edges and the surfaces of the plate which are important for cracks in very thick plate. For these cases, the use of fully three-dimensional theory is necessary. In the analytical study to examine the effect of plate thickness on the stress distribution around the crack in a plate subjected to out of plane bending, Sih [119] obtained the qualitative features of the exact solution by using a three-dimensional asymptotic expansion of stresses and displacements.

As described above, numerous analytical and/or numerical investigations have been worked out for the flexural problems of plate containing a crack. However, very few reports for the application of finite element method to bending problems of cracked plate have been published to date, though a great number of plate bending finite element models have been developed over the past ten years.

AD-A069 748 MASSACHUSETTS INST OF TECH CAMBRIDGE AEROELASTIC AND--ETC F/G 20/11

HYBRID CRACK ELEMENTS FOR THREE-DIMENSIONAL SOLIDS AND PLATE BE--ETC(U)

SEP 77 K MORIYA F49620-77-C-0084

UNCLASSIFIED ASRL-TR-191-1 AFOSR-TR-79-0619 NL

2 OF 3

AD A069748

Wilson and Thompson [109] determined the bending stress intensity factor K_1 for a through thickness crack in a plate subject to purely cylindrical bending by using conventional assumed displacement bending elements of triangular shape. Estimate of K_1 was obtained by substituting the resulting values of displacements at different points near the crack tip into the known classical solution along with the respective coordinates of the reference point and solving for K_1. The resulting K_1 values appear to be smooth curves when plotted against the distance of the reference point from the crack tip. But they break down as the reference point approaches to the crack tip. The break down is due to the inability of the assumed displacement function to represent the singular behavior at the crack tip. The best estimate of K_1 was obtained by extrapolating back to the crack tip from the results calculated at several points just beyond the break down point near the crack tip.

Luk formulated the hybrid stress crack element based on Reissner-type plate theory without implementation. He adopted the second scheme described in Subsection 3.1 so that in the vicinity of the crack tip the dominant part of asymptotic solution for stress couples and stress resultants obtained by Hartranft, Sih [107] and Wang [108], is included in elements surrounding the crack tip. In Luk's formulation the crack tip superelement consists of four 4-node rectangular basic

singular elements which encircle the crack tip. The assumed stress field in the interior of the special element includes self-equilibrating stress terms of regular polynomials as well as the known singular stress solutions. The stress assumption satisfies a priori the traction free boundary condition over the crack surface. In the boundary displacement assumption, both the transverse deflection w and the total rotation vary as $r^{1/2}$ along the edges which adjoin the other basic singular elements. However, it is easy to point out the inconsistency in this displacement assumption. Since the exact asymptotic solution for the displacement field is not readily available, none of the surface integrals in element matrices can be converted to line integrals. In constructing a single basic special element, 16 surface integrals and 5 line integrals or a total of 21 distinct integrals must be evaluated for generating element matrices. Some of the integrand involve either inverse r singularity or inverse square root r singularity. For the evaluation of such integrals, special treatment is required to obtain accurate solutions. Rhee and Atluri [111] used the hybrid stress model and corrected this inconsistency. They solved several pure bending problems of cracked plates. Before everything, one has to make clear the asymptotic behavior of the displacement field in the vicinity of the crack tip in order to create a crack tip element model for practical

use based on the 2nd scheme of the hybrid element model using Reissner's 6th order plate theory.

In the present report, a hybrid crack element model for bending problems is developed based on the first scheme, using Poisson-Kirchhoff's 4th order plate theory. It is realized, however, that this theory is only applicable to thin plates. Stress and displacement fields in the element interior are derived by the complex variable method and conformal mapping technique and they satisfy equilibrium as well as compatibility conditions in the general boundary value problem of cracked plate. The procedure to obtain the superelement follows closely that in the plane-element given in Reference 19. In later chapters, extension to bending analysis of an isotropic plate with wedge-shaped notch, an anisotropic plate with through-the-thickness crack, and bi-material plate with through-the-thickness crack located parallel or normal to the interface will be discussed.

4.2 Stress and Displacement Field Equations

The asymptotic behavior of the Kirchhoff stress-field in the vicinity of the crack tip in a plate subject to out-of-plane bending, which has been obtained by Williams [101] and later modified by Sih, takes the following form when expressed in terms of stress couples in Cartesian coordinates in Figure 28:

$$M_x \sim -\frac{1-\nu}{24(3+\nu)} \frac{K_1}{\sqrt{2r}} h^2 [3 \cos\frac{\theta}{2} + \cos\frac{5\theta}{2}]$$

$$+ \frac{1-\nu}{24(3+\nu)} \frac{K_2}{\sqrt{2r}} h^2 [\sin\frac{5\theta}{2} - (\frac{9+7\nu}{1-\nu}) \sin\frac{\theta}{2}] + O(r^o)$$

$$M_y \sim \frac{1-\nu}{24(3+\nu)} \frac{K_1}{\sqrt{2r}} h^2 [\cos\frac{5\theta}{2} + (\frac{11+5\nu}{1-\nu}) \cos\frac{\theta}{2}]$$

$$+ \frac{1+\nu}{24(3+\nu)} \frac{K_2}{\sqrt{2r}} h^2 [\sin\frac{\theta}{2} - \sin\frac{5\theta}{2}] + O(r^o)$$

$$M_{xy} \sim -\frac{1-\nu}{24(3+\nu)} \frac{K_1}{\sqrt{2r}} h^2 [\sin\frac{5\theta}{2} + (\frac{7+\nu}{1-\nu}) \sin\frac{\theta}{2}]$$

$$+ \frac{1-\nu}{24(3+\nu)} \frac{K_2}{\sqrt{2r}} h^2 [(\frac{5+3\nu}{1-\nu}) \cos\frac{\theta}{2} - \cos\frac{5\theta}{2}] + O(r^o) \quad (r \to 0+)$$

$$Q_x \sim \frac{1}{3(3+\nu)} \frac{h^2}{(2r)^{3/2}} [-K_1 \cos\frac{3\theta}{2} + K_2 \sin\frac{3\theta}{2}] + O(r^{-1}) (r \to 0+)$$

$$Q_y \sim -\frac{1}{3(3+\nu)} \frac{h^2}{(2r)^{3/2}} [K_1 \sin\frac{3\theta}{2} + K_2 \cos\frac{3\theta}{2}] + O(r^{-1}) \quad (4.1)$$

where K_1 and K_2 are the stress intensity factor for plate bending and plate shearing respectively (Figure 29). The two coordinate system (r,θ,z), (x,y,z) are defined in Figure 28, h is the plate thickness and ν is Poisson's ratio.

The corresponding displacement field takes the following form:

$$W \sim \frac{(7+\nu) r^{3/2} K_1}{3\sqrt{2}\ (3+\nu) Gh} [\cos\frac{3\theta}{2} - \frac{3(1-\nu)}{7+\nu} \cos\frac{\theta}{2}]$$

$$- \frac{(5+3\nu) K_2}{3\sqrt{2}\ (3+\nu) Gh} [\sin\frac{3\theta}{2} - \frac{3(1-\nu)}{5+3\nu} \sin\frac{\theta}{2}] \qquad (4.2)$$

where G is the shear modulus.

4.3 Variational Formulation

The following notations are used in this section.

σ_{ij} - stress tensor

u_i - displacement component

$\bar{u}_i$ - prescribed displacement

$\bar{F}_i$ - component of body force

T_i - surface traction

$\bar{T}_i$ - prescribed surface traction over S_σ

V - volume

$B(\sigma_{ij})$, $B(M_{\alpha\beta})$ - complementary energy density

$M_{\alpha\beta}$ - stress couples per unit length

Q_α - transverse shear stress resultant

w - transverse displacement normal to the midplane of the plate

$\tilde{w}$ - deflection along ∂A_n

$\bar{w}$ - prescribed deflection

ν_α - direction cosine of the normal to the boundary

A_n - area of nth element

∂A_n - entire boundary of nth element

S_σ, C_σ - portion of boundary over which the surface traction is prescribed

S_u, C_u - portion of boundary over which the displacement is prescribed

C_n - interelement boundary

$\overline{M_{\alpha\beta}}$ - prescribed stress couple over C_σ

$\bar{Q}_\alpha$ - prescribed transverse shear stress resultant over C_σ

S - boundary of V

s - arc length along boundary

In Hellinger-Reissner variational principle, the functional π_R takes the form,

$$\pi_R = \sum_n \{\iiint_{V_n} [- B(\sigma_{ij}) + \frac{1}{2} \sigma_{ij} (u_{i,j} + u_{j,i}) - \bar{F}_i u_i] dV$$

$$- \iint_{S_{\sigma_n}} \bar{T}_i u_i ds - \iint_{S_{u_n}} T_i (u_i - \bar{u}_i) ds\} \tag{4.3}$$

The independent quantities subject to variation in π_R are both displacements u_i and stresses σ_{ij}. These field variables should be continuous and single-valued in each

element and compatible along interelement boundaries. Specializing above functional for flexural problem of plate and excluding body force for simplicity gives

$$\pi_R = \sum_n \{\iint_{A_n} [- B(M_{\alpha\beta}) - M_{\alpha\beta}w_{,\alpha\beta}]dA$$

$$+ \int_{C_{\sigma_n}} (\bar{M}_{\alpha\beta}\nu_\beta w_{,\alpha} - \bar{Q}_\alpha\nu_\alpha w)ds$$

$$+ \int_{C_u} [M_{\alpha\beta}\nu_\beta(w_{,\alpha} - \bar{w}_{,\alpha}) - Q_\alpha\nu_\alpha(w - \bar{w})]ds\} \qquad (4.4)$$

where α and β range from 1 to 2.

Introducing the displacement compatibility conditions along the interelement boundaries as conditions of constraints through the Lagrange multiplier technique, the variational functional is modified as

$$\pi_{mR} = \sum_n \{\iint_{A_n} [- B(M_{\alpha\beta}) - M_{\alpha\beta}w_{,\alpha\beta}]dA$$

$$+ \int_{C_{\sigma_n}} (\bar{M}_{\alpha\beta}\nu_\beta w_{,\alpha} - \bar{Q}_\alpha\nu_\alpha w)ds$$

$$+ \int_{C_{u_n}} [M_{\alpha\beta}\nu_\beta(w_{,\alpha} - \bar{w}_{,\alpha}) - Q_\alpha\nu_\alpha(w - \bar{w})]ds$$

$$+ \int_{C_n} [M_{\alpha\beta}\nu_\beta(w_{,\alpha} - \tilde{w}_{,\alpha}) - Q_\alpha\nu_\alpha(w - \tilde{w})]ds\} \qquad (4.5)$$

If the boundary displacements $\tilde{w}$ and $\tilde{w}_{,\alpha}$ are so chosen that the geometrical boundary conditions are satisfied,

$\tilde{w}_{,\alpha} = \bar{w}_{,\alpha}$ and $\tilde{w} = \bar{w}$ along S_{u_n}, the functional π_{mR} is rewritten as

$$\pi_{mR} = \sum_n \{\iint_{A_n} [- B(M_{\alpha\beta}) - M_{\alpha\beta} w_{,\alpha\beta}] dA$$

$$+ \int_{C_{\sigma_n}} (\bar{M}_{\alpha\beta} \nu_\beta \tilde{w}_{,\alpha} - \bar{Q}_\alpha \nu_\alpha \tilde{w}) ds$$

$$+ \int_{\partial A_n} [M_{\alpha\beta} \nu_\beta (w_{,\alpha} - \tilde{w}_{,\alpha}) - Q_\alpha \nu_\alpha (w - \tilde{w})] ds\} \quad (4.6)$$

The vanishing of $\delta\pi_{mR}$ with respect to variations of $M_{\alpha\beta}$, w and $\tilde{w}$ can be shown to give the following Euler equations

(1) Stress-strain relation

$$w_{,\alpha\beta} = - \frac{\partial B(M_{\alpha\beta})}{\partial M_{\alpha\beta}} \qquad \text{in } An$$

(2) Homogeneous equilibrium equation

$$M_{\alpha\beta,\alpha\beta} = 0 \qquad \text{in } An$$

(3) Compatibility condition

$$w = \tilde{w}, \quad w_{,\alpha} = \tilde{w}_{,\alpha} \qquad \text{on } \partial An$$

(4) Traction boundary condition (4.7)

$$M_{\alpha\beta} = \bar{M}_{\alpha\beta}, \quad Q_\alpha = \bar{Q}_\alpha \qquad \text{on } C_{\sigma_n}$$

(5) Traction equilibrium condition

$$M_{\alpha\beta}^+ = M_{\alpha\beta}^-, \quad Q_\alpha^+ = Q_\alpha^- \qquad \text{on } C_n$$

where the superscripts (+) and (-) denote, arbitrarily, the left and right sides of C_n as C_n is approached.

4.4 Complex Variable Formulation

It is recognized that the complete solution of plate bending problem can be obtained from the equations of equilibrium in terms of displacements, which takes the form of a biharmonic equation,

$$\nabla^2\nabla^2 w = 0 \tag{4.8}$$

The moments and the Kirchhoff's shear forces are related to the displacement in the following manner.

$$M_x = -D\left(\frac{\partial^2 w}{\partial x^2} + \nu\frac{\partial^2 w}{\partial y^2}\right)$$

$$M_y = -D\left(\nu\frac{\partial^2 w}{\partial x^2} + \frac{\partial^2 w}{\partial y^2}\right)$$

$$M_{xy} = -D(1 - \nu)\frac{\partial^2 w}{\partial x \partial y}$$

$$Q_x = -D\left(\frac{\partial^3 w}{\partial x^3} + \frac{\partial^3 w}{\partial x \partial y^2}\right)$$

$$Q_y = -D\left(\frac{\partial^3 w}{\partial x^2 \partial y} + \frac{\partial^3 w}{\partial y^3}\right)$$

By applying the method of complex potential originated by Muskhelishvili [112], the general solution to the Equation (4.8) can be represented in terms of two analytic functions of the complex variable z(z = x+iy).

$$w(r, \theta) = \mathrm{Re}[\bar{z}\Phi(z) + \chi(z)] \tag{4.9}$$

where $\bar{z}$ is the complex conjugate of z.

The moments and Kirchhoff's shear forces corresponding to this displacement field are expressed in terms of complex potential $\Phi(z)$ and $\chi(z)$ by

$$M_x = -D\mathrm{Re}[2(1+\nu)\Phi'(z) + (1-\nu)\{\bar{z}\Phi''(z) + \chi''(z)\}]$$

$$M_y = -D\mathrm{Re}[2(1+\nu)\Phi'(z) - (1-\nu)\{\bar{z}\Phi''(z) + \chi''(z)\}]$$

$$M_{xy} = D(1-\nu)\mathrm{Im}[\bar{z}\Phi''(z) + \chi''(z)]$$

$$Q_x = -4D\mathrm{Re}[\Phi''(z)]$$

$$Q_y = 4D\mathrm{Im}[\Phi''(z)] \tag{4.10}$$

or in combined form

$$M_x + M_y = -4D(1+\nu)\mathrm{Re}[\Phi'(z)]$$

$$M_y - M_x + 2iM_{xy} = 2D(1-\nu)\{\bar{z}\Phi''(z) + \chi''(z)\}$$

$$Q_x - iQ_y = -4D\Phi''(z) \tag{4.11}$$

where D is the flexural rigidity of the plate.

$$D = Eh^3/12(1-\nu^2)$$

ν is Poisson's ratio. ( )' denotes differentiation.

The derivatives of the transverse displacement are written in the form.

$$\frac{\partial w}{\partial x} = \mathrm{Re}[\Phi(z) + \bar{z}\Phi'(z) + \chi'(z)]$$

$$\frac{\partial w}{\partial y} = \mathrm{Im}[\Phi(z) - \bar{z}\Phi'(z) - \chi'(z)] \tag{4.12}$$

or in the form

$$\frac{\partial w}{\partial x} + i\frac{\partial w}{\partial y} = \Phi(z) + z\overline{\Phi'(z)} + \overline{\chi'(z)} \tag{4.13}$$

where ($\bar{\ }$) denotes the complex conjugate.

The stresses and displacements given in Equations (4.10), (4.9) and (4.12) satisfy exactly the compatibility condition as well as the equation of equilibrium.

4.5 Conformal Mapping

To express the singularities of all order, the following conformal mapping function is selected.

$$z = \omega(\zeta) = \zeta^2 \tag{4.14}$$

The arguments of z and ζ are limited to the range $-\pi \leq \arg z \leq \pi$, and $-\frac{\pi}{2} \leq \arg \zeta \leq \frac{\pi}{2}$. If, for a superelement containing embedded crack, the origin of the coordinate system is placed at the crack tip and the two crack surfaces which are on the negative real axis of the z plane are mapped to the imaginary axis of the ζ plane and the element then lies on the region where the real part of ζ is positive [Figure 30].

Introducing the mapping function $\omega(\zeta)$ into Equations (4.10), (4.9) and (4.12) the field variables are given by

$$M_x = -D\mathrm{Re}[2(1+\nu)\Phi'(\zeta)/\omega'(\zeta) + (1-\nu)\{\overline{\omega(\zeta)}(\Phi'(\zeta)/\omega'(\zeta))'$$

$$+ (\chi'(\zeta)/\omega'(\zeta))'\}/\omega'(\zeta)]$$

$$M_y = -D\mathrm{Re}[2(1+\nu)\Phi'(\zeta)/\omega'(\zeta) - (1-\nu)\{\overline{\omega(\zeta)}(\Phi'(\zeta)/\omega'(\zeta))'$$

$$+ (\chi'(\zeta)/\omega'(\zeta))'\}/\omega'(\zeta)]$$

$$M_{xy} = D(1-\nu)\mathrm{Im}[\{\overline{\omega(\zeta)}(\Phi'(\zeta)/\omega'(\zeta))'$$

$$+ (\chi'(\zeta)/\omega'(\zeta))'\}/\omega'(\zeta)]$$

$$Q_x = -4D\mathrm{Re}[\{\Phi'(\zeta)/\omega'(\zeta)\}'/\omega'(\zeta)]$$

$$Q_y = 4D\mathrm{Im}[\{\Phi'(\zeta)/\omega'(\zeta)\}'/\omega'(\zeta)] \tag{4.15}$$

$$w = \mathrm{Re}[\overline{\omega(\zeta)}\Phi(\zeta) + \chi(\zeta)] \tag{4.16}$$

$$\frac{\partial w}{\partial x} = \mathrm{Re}[\Phi(\zeta) + \{\overline{\omega(\zeta)}\Phi'(\zeta) + \chi'(\zeta)\}/\omega'(\zeta)]$$

$$\frac{\partial w}{\partial y} = \mathrm{Im}[\Phi(\zeta) - \{\overline{\omega(\zeta)}\Phi'(\zeta) + \chi'(\zeta)\}/\omega'(\zeta)] \tag{4.17}$$

The Equations (4.15) and (4.17) may be combined into the form

$$M_x + M_y = -4D(1+\nu)\mathrm{Re}[\Phi'(\zeta)/\omega'(\zeta)]$$

$$M_y - M_x + 2iM_{xy} = 2D(1-\nu)[\overline{\omega(\zeta)}\{\Phi'(\zeta)/\omega'(\zeta)\}'$$

$$+\{\chi'(\zeta)/\omega'(\zeta)\}']/\omega'(\zeta)$$

$$Q_x - iQ_y = -4D\{\Phi'(\zeta)/\omega'(\zeta)\}'/\omega'(\zeta) \tag{4.18}$$

$$\frac{\partial w}{\partial x} + i\frac{\partial w}{\partial y} = \Phi(\zeta) + \omega(\zeta)\overline{\Phi'(\zeta)/\omega'(\zeta)} + \overline{\chi'(\zeta)/\omega'(\zeta)} \tag{4.19}$$

The complex potential Φ and χ which are analytic functions of z are then also analytic functions of ζ and can always be represented by polynomials consisting of only positive powers of ζ. There are two alternative approaches to the derivation of the stress and displacement fields that satisfy the stress free boundary condition over the crack surface.

Approach 1

In the first approach, $\Phi(\zeta)$ and $\chi(\zeta)$ are assumed independently and all the field variables M_x, M_y, M_{xy}, Q_x, Q_y, W, $W_{,x}$ and $W_{,y}$ are expressed in terms of ζ. Then they are substituted into the stress free boundary condition over the crack surface to obtain the relations between the coefficients of $\Phi(\zeta)$ and $\chi(\zeta)$. The potential functions $\Phi(\zeta)$ and $\chi(\zeta)$ are assumed as

$$\Phi(\zeta) = \sum_{j=1}^{2N} b_j \zeta^j$$
$$= \sum_{j=1}^{2N} (\beta_j + i\beta_{2N+j})\zeta^j$$

$$= \sum_{j=1}^{N} [(\beta_{2j-1} + i\beta_{2N+2j-1})\zeta^{2j-1} + (\beta_{2j} + i\beta_{2N+2j})\zeta^{2j}]$$

$$\chi(\zeta) = \sum_{j=3}^{2N+2} c_j \zeta^j$$

$$= \sum_{j=3}^{2N+2} (\gamma_j + i\gamma_{2N+j})\zeta^j$$

$$= \sum_{j=1}^{N} [(\gamma_{2j+1} + i\gamma_{2N+2j+1})\zeta^{2j+1} + (\gamma_{2j+2} + i\gamma_{2N+2j+2})\zeta^{2j+2}] \quad (4.20)$$

in which N is a finite integer and β's and γ's are real constants.

Taking as boundary conditions along the crack surface ($\zeta = i\eta$), the usual Kirchhoff condition for a free edge; viz.,

$$M_y \equiv 0 \quad (4.21)$$

$$V_y \equiv 0 \quad (4.22)$$

where $V_y = Q_y + \frac{\partial M_{xy}}{\partial x}$

Over the crack surface, M_y and V_y are expressed as

$$M_y = -D \sum_{j=1}^{N} (-1)^{j-1} [[\{(1+\nu)(2j-1) - \tfrac{1}{4}(1-\nu)(2j-1)(2j-3)\}\beta_{2N+2j}$$

$$- \tfrac{1}{4}(1-\nu)(2j+1)(2j-1)\gamma_{2N+2j+1}]\eta^{2j-3}$$

$$+ [\{(1+\nu)2j - \tfrac{1}{4}(1-\nu)2j(2j-2)\}\beta_{2j}$$

$$- \tfrac{1}{4}(1-\nu)(2j+2)2j\gamma_{2j+2}]\eta^{2j-2}] \quad (4.23)$$

$$V_y = \frac{D}{8}\sum_{j=1}^{N} (-1)^{j-1} [[\{2(5-\nu)(2j-1)(2j-3)$$

$$+ (1-\nu)(2j-1)(2j-3)(2j-5)\}\beta_{2j-1}$$

$$+ (1-\nu)(2j+1)(2j-1)(2j-3)\gamma_{2j+1}]\eta^{2j-5}$$

$$- [\{2(5-\nu)2j(2j-2) + (1-\nu)2j(2j-2)(2j-4)\}\beta_{2N+2j}$$

$$+ (1-\nu)(2j+2)2j(2j-2)\gamma_{2N+2j+2}]\eta^{2j-4}] \qquad (4.24)$$

Substituting Equation (4.23) and (4.24) into Kirchhoff stress free condition (4.21) and (4.22), all γ's can be expressed in terms of β's.

$$\gamma_{2j+1} = p(2j-1)\beta_{2j-1}$$

$$\gamma_{2j+2} = q(2j)\beta_{2j}$$

$$\gamma_{2N+2j+1} = q(2j-1)\beta_{2N+2j-1}$$

$$\gamma_{2N+2j+2} = p(2j)\beta_{2N+2j} \qquad (4.25)$$

where

$$p(j) = -\{\frac{4}{j+2}(\frac{1+\nu}{1-\nu}) + 1\}$$

$$q(j) = 8/(j+2)(1-\nu) - 1$$

Hence, all the field variables M_x, M_y, M_{xy}, Q_x, Q_y, w, $w_{,x}$ and $w_{,y}$ can be expressed in terms of β's only.

The moments are

$$M_x = \sum_{i=1}^{4N} a_i \beta_i$$

$$M_y = \sum_{i=1}^{4N} b_i \beta_i \qquad (4.26)$$

$$M_{xy} = \sum_{i=1}^{4N} c_i \beta_i$$

where

$$a_{2j-1} = -D[\{(1+\nu) + \tfrac{1}{4}(1-\nu)(2j+1)p(2j-1)\}(2j-1)\mathrm{Re}(\zeta^{2j-3})$$
$$+ \tfrac{1}{4}(1-\nu)(2j-1)(2j-3)\mathrm{Re}(\bar{\zeta}^2\zeta^{2j-5})]$$

$$a_{2j} = -D[\{(1+\nu) + \tfrac{1}{4}(1-\nu)(2j+2)q(2j)\}\mathrm{Re}(\zeta^{2j-2})$$
$$+ \tfrac{1}{4}(1-\nu)2j(2j-2)\mathrm{Re}(\bar{\zeta}^2\zeta^{2j-4})]$$

$$a_{2N+2j-1} = D[\{(1+\nu) + \tfrac{1}{4}(1-\nu)(2j+1)q(2j-1)\}(2j-1)\mathrm{Im}(\zeta^{2j-3})$$
$$+ \tfrac{1}{4}(1-\nu)(2j-1)(2j-3)\mathrm{Im}(\bar{\zeta}^2\zeta^{2j-5})]$$

$$a_{2N+2j} = D[\{(1+\nu) + \tfrac{1}{4}(1-\nu)(2j+2)p(2j)\}2j\mathrm{Im}(\zeta^{2j-2})$$
$$+ \tfrac{1}{4}(1-\nu)2j(2j-2)\mathrm{Im}(\bar{\zeta}^2\zeta^{2j-4})]$$

$$b_{2j-1} = -D[\{(1+\nu) - \tfrac{1}{4}(1-\nu)(2j+1)p(2j-1)\}(2j-1)\mathrm{Re}(\zeta^{2j-3})$$
$$- \tfrac{1}{4}(1-\nu)(2j-1)(2j-3)\mathrm{Re}(\bar{\zeta}^2\zeta^{2j-5})]$$

$$b_{2j} = -D[\{(1+\nu) - \tfrac{1}{4}(1-\nu)(2j+2)q(2j)\}2j\mathrm{Re}(\zeta^{2j-2})$$
$$- \tfrac{1}{4}(1-\nu)2j(2j-2)\mathrm{Re}(\bar{\zeta}^2\zeta^{2j-4})]$$

$$b_{2N+2j-1} = D[\{(1+\nu) - \tfrac{1}{4}(1-\nu)(2j+1)q(2j-1)\}(2j-1)\mathrm{Im}(\zeta^{2j-3})$$

$$- \frac{1}{4}(1-\nu)(2j-1)(2j-3)\mathrm{Im}(\bar{\zeta}^2\zeta^{2j-5})]$$

$$b_{2N+2j} = D[\{(1+\nu) - \frac{1}{4}(1-\nu)(2j+2)p(2j)\}2j\mathrm{Im}(\zeta^{2j-2})$$

$$+ \frac{1}{4}(1-\nu)2j(2j-2)\mathrm{Im}(\bar{\zeta}^2\zeta^{2j-4})]$$

$$c_{2j-1} = \frac{1}{4}D(1-\nu)(2j-1)[(2j-3)\mathrm{Im}(\bar{\zeta}^2\zeta^{2j-5}) + (2j+1)p(2j-1)\mathrm{Im}(\zeta^{2j-3})]$$

$$c_{2j} = \frac{1}{4}D(1-\nu)2j[(2j-2)\mathrm{Im}(\bar{\zeta}^2\zeta^{2j-4}) + (2j+2)q(2j)\mathrm{Im}(\zeta^{2j-2})]$$

$$c_{2N+2j-1} = \frac{1}{4}D(1-\nu)(2j-1)[(2j-3)\mathrm{Re}(\bar{\zeta}^2\zeta^{2j-5}) + (2j+1)q(2j-1)\mathrm{Re}(\zeta^{2j-3})]$$

$$c_{2N+2j} = \frac{1}{4}D(1-\nu)2j[(2j-2)\mathrm{Re}(\bar{\zeta}^2\zeta^{2j-4}) + (2j+2)p(2j)\mathrm{Re}(\zeta^{2j-2})]$$

$$(j = 1, 2, 3, \cdots\cdots\cdots, N-1, N)$$

The Kirchhoff's shear stresses are

$$Q_x = \sum_{j=1}^{2N} (d_{1j}\beta_j + d_{2j}\beta_{2N+j})$$

$$Q_y = \sum_{j=1}^{2N} (d_{2j}\beta_j - d_{1j}\beta_{2N+j}) \tag{4.27}$$

where

$$d_{1j} = -Dj(j-2)\mathrm{Re}(\zeta^{j-4})$$

$$d_{2j} = Dj(j-2)\mathrm{Im}(\zeta^{j-4})$$

The displacement w is

$$w = \sum_{i=1}^{4N} f_i\beta_i \tag{4.28}$$

where

$$f_{2j-1} = \mathrm{Re}(\bar{\zeta}^2\zeta^{2j-1}) + p(2j-1)\mathrm{Re}(\zeta^{2j+1})$$

$$f_{2j} = \mathrm{Re}(\bar{\zeta}^2\zeta^{2j}) + q(2j)\mathrm{Re}(\zeta^{2j+2})$$

$$f_{2N+2j-1} = -\mathrm{Im}(\bar{\zeta}^2\zeta^{2j-1}) - q(2j-1)\mathrm{Im}(\zeta^{2j+1})$$

$$f_{2N+2j} = -\mathrm{Im}(\bar{\zeta}^2\zeta^{2j}) - p(2j)\mathrm{Im}(\zeta^{2j+2})$$

$$(j = 1, 2, \cdots\cdots, N)$$

The slopes $w_{,x}$ and $w_{,y}$ are

$$w_{,x} = \sum_{i=1}^{4N} g_i\beta_i$$

$$w_{,y} = \sum_{i=1}^{4N} h_i\beta_i \tag{4.29}$$

where

$$g_{2j-1} = [1 + \tfrac{1}{2}(2j+1)p(2j-1)]\mathrm{Re}(\zeta^{2j-1}) + \tfrac{1}{2}(2j-1)\mathrm{Re}(\bar{\zeta}^2\zeta^{2j-3})$$

$$g_{2j} = [1 + (j+1)q(2j)]\mathrm{Re}(\zeta^{2j}) + j\mathrm{Re}(\bar{\zeta}^2\zeta^{2j-2})$$

$$g_{2N+2j-1} = -[1 + \tfrac{1}{2}(2j+1)q(2j-1)]\mathrm{Im}(\zeta^{2j-1}) - \tfrac{1}{2}(2j-1)\mathrm{Im}(\bar{\zeta}^2\zeta^{2j-3})$$

$$g_{2N+2j} = -[1 + (j+1)p(2j)]\mathrm{Im}(\zeta^{2j}) - j\mathrm{Im}(\bar{\zeta}^2\zeta^{2j-2})$$

$$h_{2j-1} = [1 - \tfrac{1}{2}(2j+1)p(2j-1)]\mathrm{Im}(\zeta^{2j-1}) - \tfrac{1}{2}(2j-1)\mathrm{Im}(\bar{\zeta}^2\zeta^{2j-3})$$

$$h_{2j} = [1 - (j+1)q(2j)]\mathrm{Im}(\zeta^{2j}) - j\mathrm{Im}(\bar{\zeta}^2\zeta^{2j-2})$$

$$h_{2N+2j-1} = [1 - \tfrac{1}{2}(2j+1)q(2j-1)]\mathrm{Re}(\zeta^{2j-1}) - \tfrac{1}{2}(2j-1)\mathrm{Re}(\bar{\zeta}^2\zeta^{2j-3})$$

$$h_{2N+2j} = [1 - (j+1)p(2j)]\mathrm{Re}(\zeta^{2j}) - j\mathrm{Re}(\bar{\zeta}^2\zeta^{2j-2})$$

$$(j = 1, 2, \cdots, N)$$

Approach 2

In the second approach, first only $\Phi(\zeta)$ is assumed in terms of ζ. The stress free boundary condition is expressed in an integral form by using the Lechnitzky's extension of Muschelisvili's method and $\chi'(\zeta)$ is related to $\Phi(\zeta)$.

The stress free boundary condition over the crack surface can be written in an integral form as

$$n\Phi(z) + z\overline{\Phi'(z)} + \overline{\chi'(z)} = 0 \tag{4.30}$$

where

$$n = -(3+\nu)/(1-\nu) \tag{4.31}$$

For the following derivation, it is expedient to introduce a new variable $\psi(z)$ such that

$$\psi(z) = \frac{d\chi(z)}{dz} \tag{4.32}$$

Using the mapping $z = \omega(\zeta) = \zeta^2$ and the new variable $\psi(z)$, Equation (4.30) is written as

$$n\Phi(\zeta) + \omega(\zeta)\overline{\Phi'(\zeta)/\omega'(\zeta)} + \overline{\psi(\zeta)} = 0 \tag{4.33}$$

Equation (4.33) is satisfied by taking the complex potential $\psi(\zeta)$ in the form

$$\psi(\zeta) = -n\overline{\Phi(-\overline{\zeta})} - \overline{w(-\overline{\zeta})}\Phi'(\zeta)/\omega'(\zeta) \tag{4.34}$$

The potential $\Phi(\zeta)$ can be assumed in the form of a polynomial ζ as

$$\Phi(\zeta) = \sum_{j=1}^{N} b_j \zeta^j \tag{4.35}$$

where $b_j = \beta_j + i\beta_{N+j}$, N is a finite integer and β's are real constants. In case of in-plane elasticity, β_{N+2} are zero, because the corresponding terms of $\Phi(\zeta)$ and $\psi(\zeta)$ contribute no contribution to stresses. However, in flexural problem, β_{N+2} is not necessarily zero and cannot be eliminated a priori. Inserting Equation (4.35) into Equation (4.34) gives

$$\psi(\zeta) = -\sum_{j=1}^{N} [n\overline{b_j}(-1)^j + \frac{j}{2}b_j]\zeta^j \tag{4.36}$$

From Equation (4.18), (4.16), (4.19), (4.35) and (4.36), one can write

$$M_x + M_y = 2D(1+\nu)\sum_{j=1}^{2N} A_j(\zeta, \overline{\zeta})\beta_j$$

$$M_y - M_x + 2iM_{xy} = 2D(1-\nu)\sum_{j=1}^{2N} B_j(\zeta, \overline{\zeta})\beta_j$$

$$Q_x - iQ_y = D\sum_{j=1}^{2N} C_j(\zeta, \overline{\zeta})\beta_j = C(\zeta, \overline{\zeta}; \beta_j) \tag{4.37}$$

$$w = \sum_{j=1}^{2N} f_j\beta_j = f(\zeta, \overline{\zeta}, \beta_j) \tag{4.38}$$

$$\frac{\partial w}{\partial x} + i\frac{\partial w}{\partial y} = \sum_{j=1}^{2N} g_j\beta_j = g(\zeta, \overline{\zeta}, \beta_j) \tag{4.39}$$

where

$$A_j = -\mathrm{Re}(j\zeta^{j-2})$$

$$A_{N+j} = \mathrm{Im}(j\zeta^{j-2})$$

$$B_j = [\frac{j-2}{4}\frac{\bar{\zeta}^2}{\zeta^2} - n\frac{(-1)^j}{2} - \frac{j}{4}]j\zeta^{j-2}$$

$$B_{N+j} = i[\frac{j-2}{4}\frac{\bar{\zeta}^2}{\zeta^2} + n\frac{(-1)^j}{2} - \frac{j}{4}]j\zeta^{j-2}$$

$$C_j = -j(j-2)\zeta^{j-4}$$

$$C_{N+j} = -ij(j-2)\zeta^{j-4}$$

$$f_j = \mathrm{Re}[\bar{\zeta}^2\zeta^j] - \frac{1}{j+2}[2n(-1)^j - j]\mathrm{Re}[\zeta^{j+2}]$$

$$f_{N+j} = -\mathrm{Im}[\bar{\zeta}^2\zeta^j] - \frac{1}{j+2}[2n(-1)^j + j]\mathrm{Im}[\zeta^{j+2}]$$

$$g_j = \zeta^j - n(-1)^j\bar{\zeta}^j + ij\bar{\zeta}^{j-2}\mathrm{Im}[\zeta^2]$$

$$g_{N+j} = i\{\zeta^j - n(-1)^j\bar{\zeta}^j + j\bar{\zeta}^{j-2}\mathrm{Re}[\zeta^2]\}$$

for $j = 1, 2, 3, \cdots\cdots, N-1, N$

It is obvious that these two approaches will yield identical results. The latter appears to be expressed in simpler form but the first one is more straightforward. From the computational point of view, however, the first approach is more efficient and convenient than the second approach especially for the construction of the superelement for flexural problems.

4.6 Finite Element Formulation

The stresses and displacements given in Equations (4.26), (4.27), (4.28) and (4.29) or Equations (4.37), (4.38) and (4.39) satisfy equations of equilibrium and compatibility and kinematic boundary conditions in the general boundary value problem of a plate containing a crack. These solutions for the stresses and displacements are used to construct around the crack tip a superelement which accounts for singularities of all order under Poisson-Kirchhoff theory. For elements far away from the crack front, the regular hybrid and/or conventional assumed displacement elements can be used. Compatibility of displacements and equilibrium of tractions between the crack tip superelement and the surrounding regular elements is maintained through a Lagrange multiplier technique based on the modified Hellinger-Reissner variational principle [Eq. (4.6)].

Since some of the Euler equations, i.e., $w_{,\alpha\beta} = -\dfrac{\partial B(M_{\alpha\beta})}{\partial M_{\alpha\beta}}$ and $M_{\alpha\beta,\alpha\beta} = 0$ are satisfied a priori in the crack tip superelement, they can be removed from the modified Hellinger-

Reissner functional [Eq. (4.6)]. Thus, the functional corresponding to the superelement which is designated as A_1 becomes

$$\pi^C_{mR} = \int_{\partial A_1} (-M_{\alpha\beta}\nu_\beta \tilde{w}_{,\alpha} + Q_\alpha \nu_\alpha \tilde{w})\, dS$$

$$- \frac{1}{2} \int_{\partial A_1} (-M_{\alpha\beta}\nu_\beta w_{,\alpha} + Q_\alpha \nu_\alpha w)\, dS$$

$$+ \int_{C_{\sigma_1}} (\bar{M}_{\alpha\beta}\nu_\beta \tilde{w}_{,\alpha} - \bar{Q}_\alpha \nu_\alpha \tilde{w})\, dS \qquad (4.40)$$

When the assumed stress hybrid elements are used for far-field elements, the homogeneous equilibrium equation $M_{\alpha\beta,\alpha\beta} = 0$ is satisfied a priori in these elements. Thus, the functional for far-field elements is written as

$$\pi^R_{mR} = \sum_{n=2}^{m} [\int_{A_n} -B(M_{\alpha\beta})\, dA + \int_{\partial A_n} (-M_{\alpha\beta}\nu_\beta \tilde{w}_{,\alpha} + Q_\alpha \nu_\alpha \tilde{w})\, dS$$

$$+ \int_{C_{\sigma_n}} (\bar{M}_{\alpha\beta}\nu_\beta \tilde{w}_{,\alpha} - \bar{Q}_\alpha \nu_\alpha \tilde{w})\, dS \qquad (4.41)$$

Therefore, the total hybrid function π_{mR} becomes

$$\pi_{mR} = \pi^C_{mR} + \pi^R_{mR} \qquad (4.42)$$

As mentioned before, the far-field elements, n = 2, ... m, can be simply generated through the conventional assumed

displacement finite element model provided the displacement field is the same along the interface between these elements and the crack tip superelement.

4.7 Derivation of Element Stiffness Matrix

The above functional π can be expressed in a matrix form as

$$\pi = \int_{\partial A_1} \underset{\sim}{T}^T \underset{\sim}{\tilde{u}} \, dS - \frac{1}{2} \int_{\partial A_1} \underset{\sim}{T}^T \underset{\sim}{u} \, dS - \int_{C_{\sigma_1}} \underset{\sim}{\bar{T}}^T \underset{\sim}{\tilde{u}} \, dS$$

$$+ \sum_{n=2}^{NE} \left[\frac{1}{2} \int_{A_n} \underset{\sim}{\sigma}^T \underset{\sim}{C} \underset{\sim}{\sigma} \, dA + \int_{\partial A_n} \underset{\sim}{T}^T \underset{\sim}{\tilde{u}} \, dS - \int_{C_{\sigma_n}} \underset{\sim}{\bar{T}}^T \underset{\sim}{\tilde{u}} \, dS \right] \tag{4.43}$$

where

$$\underset{\sim}{T} = \begin{Bmatrix} Q \\ M_{x\nu} \\ M_{y\nu} \end{Bmatrix} = \begin{Bmatrix} Q_x \nu_x + Q_y \nu_y \\ M_x \nu_x + M_{xy} \nu_y \\ M_{xy} \nu_x + M_y \nu_y \end{Bmatrix}$$

$$\underset{\sim}{u} = \begin{Bmatrix} w \\ -w_{,x} \\ -w_{,y} \end{Bmatrix}$$

$$\underset{\sim}{\tilde{u}} = \begin{Bmatrix} \tilde{w} \\ -\tilde{w}_{,x} \\ -\tilde{w}_{,y} \end{Bmatrix} = \begin{Bmatrix} \tilde{w} \\ -\tilde{w}_{,\nu} \nu_x + \tilde{w}_{,s} \nu_y \\ -\tilde{w}_{,\nu} \nu_y - \tilde{w}_{,s} \nu_x \end{Bmatrix}$$

$$\underset{\sim}{\sigma} = \begin{Bmatrix} M_x \\ M_y \\ M_{xy} \end{Bmatrix}$$

$$\underset{\sim}{C} = \frac{12}{Eh^3} \begin{bmatrix} 1 & -\nu & 0 \\ -\nu & 1 & 0 \\ 0 & 0 & 2(1+\nu) \end{bmatrix}$$

This functional is analogous to that used by Tong, et al. [19] who treated the plane stress crack problem in two dimensional elasticity. In the following derivations of the crack tip superelement, it is necessary to consider only the first three integrals in Equation (4.43).

Using Equations (4.26), (4.27), (4.28) and (4.29) or Equations (4.37), (4.38) and (4.39) the assumed stress and displacement modes can be expressed in terms of undetermined real parameter β's as

$$\underset{\sim}{T} = \underset{\sim}{R}\underset{\sim}{\beta} \tag{4.44}$$

$$\underset{\sim}{u} = \underset{\sim}{U}\underset{\sim}{\beta} \tag{4.45}$$

where $\underset{\sim}{\beta} = \{\beta_1, \beta_2 \ldots, \beta_{NB}\}$, NB is a total number of β's.

The assumed boundary displacements $\tilde{\underset{\sim}{u}}$ can be expressed in terms of the generalized nodal displacements as

$$\tilde{\underset{\sim}{u}} = \underset{\sim}{L}\underset{\sim}{q} \tag{4.46}$$

where $\underset{\sim}{L}$ is the one-dimensional interpolation function matrix defined on the element boundaries excluding the crack surface. The generalized nodal displacement $\underset{\sim}{q}$ can be selected in the form

$$\underset{\sim}{q}_i = \{w,\ w_{,x},\ w_{,y}\}_i \tag{4.47}$$

The interpolation function must be chosen such that when the nodal displacements for the neighboring elements are matched, the displacements along the corresponding interelement boundary are the same. We can use the osculatory Hermite polynomials $H_{ik}^{(1)}(s)$ to represent the assumed boundary displacement $\tilde{w}$ in terms of generalized nodal displacement $\underset{\sim}{q}$. For instance along the edge AB in Figure 32, $\tilde{w}$ is expressed as follows

$$\begin{aligned} w &= H_{01}^{(1)}(s)w_A + H_{02}^{(1)}(s)w_B + H_{11}^{(1)}(s)w_{,s_A} + H_{12}^{(1)}(s)w_{,s_B} \\ &= H_{01}^{(1)}(s)w_A + H_{02}^{(1)}(s)w_B + H_{11}^{(1)}(s)(-\nu_y w_{,x_A} + \nu_x w_{,y_A}) \\ &+ H_{12}^{(1)}(s)(-\nu_y w_{,x_B} + \nu_x w_{,y_B}) \end{aligned} \tag{4.48}$$

where

$$H_{01}^{(1)}(s) = 1 - 3(\frac{s}{\ell})^2 + 2(\frac{s}{\ell})^3$$

$$H_{02}^{(1)}(s) = 3(\frac{s}{\ell})^2 - 2(\frac{s}{\ell})^3$$

$$H_{11}^{(1)}(s) = \ell[\frac{s}{\ell} - 2(\frac{s}{\ell})^2 + (\frac{s}{\ell})^3] \tag{4.49}$$

$$H_{12}^{(1)}(s) = -\ell[(\frac{s}{\ell})^2 - (\frac{s}{\ell})^3]$$

ℓ is the distance between nodes A and B, and s is measured from A.

From Equation (4.48), we obtain

$$\begin{aligned} w_{,s} = {} & \frac{dH_{01}^{(1)}}{ds} w_A + \frac{dH_{02}^{(1)}}{ds} w_B + \frac{dH_{11}^{(1)}}{ds}(-\nu_y w_{,x_A} + \nu_x w_{,y_A}) \\ & + \frac{dH_{12}^{(1)}}{ds}(-\nu_y w_{,x_B} + \nu_x w_{,y_B}) \end{aligned} \tag{4.50}$$

The normal slope along the edge AB must be linear in s to maintain normal slope compatibility along the entire edge. Hence, we may use a linear interpolation function to represent it as

$$w_{,\nu} = (1 - \frac{s}{\ell}) w_{,\nu_A} + (\frac{s}{\ell}) w_{,\nu_B} \tag{4.51}$$

The assumed boundary displacement $\tilde{u}$ can thus be expressed in terms of the generalized nodal displacement $\underset{\sim}{q}$. This leads to

to a cubic variation for w and a linear variation for the normal slope on the boundary. The displacement interpolation function matrix $\underset{\sim}{L}$ is given in Table 24. It is noted that the boundary displacement $\underset{\sim}{\tilde{u}}$ are assumed only on interelement boundaries and it is not necessary to assume those over the crack surfaces.

Substitution of Equations (4.44), (4.45) and (4.46) into the first three terms of Equation (4.43) yields equation of the form

$$\pi = \underset{\sim}{\beta}^T \underset{\sim}{G} \underset{\sim}{q} - \frac{1}{2} \underset{\sim}{\beta}^T \underset{\sim}{H} \underset{\sim}{\beta} \tag{4.52}$$

The matrices $\underset{\sim}{G}$ and $\underset{\sim}{H}$ are given by

$$\underset{\sim}{G} = \int_{\partial A_1} \underset{\sim}{R}^T \underset{\sim}{L} \, ds \tag{4.53}$$

$$\underset{\sim}{H} = \frac{1}{2} \int_{\partial A_1} (\underset{\sim}{R}^T \underset{\sim}{U} + \underset{\sim}{U}^T \underset{\sim}{R}) ds \tag{4.54}$$

The stationary condition of the functional π with respect to variations of β yields

$$\underset{\sim}{G} \underset{\sim}{q} - \underset{\sim}{H} \underset{\sim}{\beta} = 0 \tag{4.55}$$

By solving for $\underset{\sim}{\beta}$ from Equation (4.55) and substituting back into Equation (4.52), the functional π can be expressed in terms of the generalized nodal displacements $\underset{\sim}{q}$ only, i.e.

$$\pi = \frac{1}{2}\underset{\sim}{q}^T \underset{\sim}{K}\underset{\sim}{q} \tag{4.56}$$

where $$\underset{\sim}{K} = \underset{\sim}{G}^T \underset{\sim}{H}^{-1} \underset{\sim}{G} \tag{4.57}$$

$\underset{\sim}{K}$ is the stiffness matrix of the crack tip superelement.

It is well known that for a successful implementation of this finite element model the number of β's should be greater than or at least equal to the number of degrees of freedom minus the number of rigid body modes for each element. This condition is understood either as the necessary condition to make the element kinematically stable or as the solvability condition of q's in terms of β's.

4.8 Geometry of the Crack Tip Superelement

The superelement can be of arbitrarily polygonal shape except that it needs to contain a crack [Figure 31]. The vertices of the polygon are chosen as the nodal points. If the outer boundary of the superelement is selected as a regular polygon, the integration of element matrices $\underset{\sim}{G}$ and $\underset{\sim}{H}$ is simplified. A further numerical simplification can be achieved if the superelement contains a crack along an axis of symmetry of the polygon, since certain symmetrical and antisymmetrical properties can be used in the computation of element matrices. It should be pointed out that the nodal point may not be located on the crack tip, since any terms which involve the displacement at the crack tip are cancelled

in the integrations of the element matrices $\underset{\sim}{G}$ and $\underset{\sim}{H}$ which are taken all around the element boundary.

For the present formulation, the superelement generated is a nine-node rectangular shape element with 27 degrees of freedom as shown in Figure 32. In this case at least 24 β's must be used in the representation of stress and displacement field to fulfill the condition described in the previous section.

4.9 The Integration of the Matrix $\underset{\sim}{G}$ and $\underset{\sim}{H}$

It is seen that in constructing the crack tip superelement only two line integrals along the element boundary need be evaluated. On the basis of the Poisson-Kirchhoff theory of thin plates, the stress and displacement field given in Equations (4.44) and (4.45) satisfies the stress-free condition along the crack surface only in an approximate manner. The three physically natural boundary conditions of prescribing bending moment, twisting moment and transverse shear stress are replaced by the following two conditions:

$$\left.\begin{aligned} M_\nu &= 0 \\ Q + \frac{\partial M_{\nu s}}{\partial s} &= 0 \end{aligned}\right\} \quad \text{on crack surface}$$

Therefore, neither the shear stress Q nor the twisting moment $M_{\nu s}$ is identically zero on the crack surface. The line integral of $\underset{\sim}{T}^T\underset{\sim}{u}$ over the crack surface can thus be written

$$\int \underset{\sim}{T}^T \underset{\sim}{u}\, ds = \int_{FO} (-Qw + M_{xy} w_{,x}) dx + \int_{AO} (Qw - M_{xy} w_{,x}) dx$$

$$= -\int_{FO} (Q + \frac{\partial M_{xy}}{\partial x}) w dx + M_{xy} w \Big|_F^O$$

$$+ \int_{AO} (Q + \frac{\partial M_{xy}}{\partial x}) w dx - M_{xy} w \Big|_A^O = M_{xy} w \Big|_F^A \tag{4.58}$$

in which O denotes the crack tip and A and F are the nodes at the intersection of the crack surface and the side of the crack tip superelement. It should be noted that in the above expression the values of M_{xy} are those on the crack surface side of these nodes.

In a similar manner, the line integral of $\underset{\sim}{T}^T \underset{\sim}{u}$ over the crack surface becomes

$$\int_{FOA} \underset{\sim}{T}^T \underset{\sim}{\tilde{u}}\, ds = M_{xy} \tilde{w} \Big|_F^A \tag{4.59}$$

These terms are represented by concentrated loads at the nodes and should be added to the matrices $\underset{\sim}{G}$ and $\underset{\sim}{H}$. Thus, it is seen that the boundary displacements $\tilde{w}$ and $\tilde{w}_{,\nu}$ need not be assumed over the crack surface. The process for integrating the $\underset{\sim}{G}$ and $\underset{\sim}{H}$ matrices does not involve any singular terms, hence, can be carried out numerically without any special treatment.

When the first approach is adopted to obtain stress and

displacement fields, all field variables M_x, M_y, M_{xy}, Q_x, Q_y, w, $w_{,x}$ and $w_{,y}$ are expressed explicitly in terms of β's. Therefore, it is a straightforward procedure to calculate all the terms of the matrices $\underset{\sim}{R}$ and $\underset{\sim}{U}$ and then matrices $\underset{\sim}{G}$ and $\underset{\sim}{H}$ are computed according to Equations (4.53) and (4.54) by standard numerical integration technique. However, if the second approach is adopted the field variables are not expressed distinctly in terms of β's but are given in the form of complex stress and complex displacement. In this case, the computation of the matrices $\underset{\sim}{G}$ and $\underset{\sim}{H}$ are accelerated in the following manner. From the first two equations of Equations (4.37), one can easily obtain

$$M_x - iM_{xy} = D \sum_{j=1}^{2N} p_j(\zeta,\overline{\zeta})\beta_j = p(\zeta,\ \overline{\zeta};\ \beta_j) \tag{4.60}$$

$$M_y + iM_{xy} = D \sum_{j=1}^{2N} h_j(\zeta,\overline{\zeta})\beta_j = h(\zeta,\ \overline{\zeta};\ \beta_j) \tag{4.61}$$

where

$$p_j = (1+\nu)A_j - (1-\nu)B_j$$

$$h_j = (1+\nu)A_j + (1-\nu)B_j$$

One can then express $\underset{\sim}{T}^T\underset{\sim}{u}$ and $\underset{\sim}{T}^T\underset{\sim}{\tilde{u}}$ in the form

$$\underset{\sim}{T}^T\underset{\sim}{u} = -\mathrm{Im}[(ip\nu_x + h\nu_y)g - ic\nu f] \tag{4.62}$$

$$\underset{\sim}{T}^T \underset{\sim}{u} = -\mathrm{Im}[(ip\nu_x + h\nu_y)(w_{,x} + iw_{,y}) - ic\nu\tilde{w}] \tag{4.63}$$

where ν is the complex direction cosine defined by

$$\nu = \nu_x + i\nu_y$$

p, h, g, c, and f are complex functions of x and y defined in Equations (4.60), (4.61), (4.39), (4.37) and (4.38). $\tilde{w}$, $\tilde{w}_{,x}$, $\tilde{w}_{,y}$ are assumed boundary displacements given in Table 24.

The integration for the matrices $\underset{\sim}{H}$ and $\underset{\sim}{G}$ can now be can now be carried out by standard numerical schemes. For instance, the integrations of $\underset{\sim}{H}$ and $\underset{\sim}{G}$ for the particular geometry of Figure 31 become

$$\underset{\sim}{\beta}^T \underset{\sim}{H} \underset{\sim}{\beta} = \int_{\partial A_1} \underset{\sim}{T}^T \underset{\sim}{u} \, ds$$

$$= -\mathrm{Re}[\int_{AB} + \int_{CD} + \int_{EF} \nu_x (pg - cf) ds]$$

$$- \mathrm{Im}[\int_{BC} + \int_{DE} \nu_y (hg + cf) ds] + \mathrm{Im}[hf]\Big|_F^A \tag{4.64}$$

$$\underset{\sim}{\beta}^T \underset{\sim}{G} \underset{\sim}{q} = \int_{\partial A_1} \underset{\sim}{T}^T \underset{\sim}{\tilde{u}} \, ds$$

$$= -\mathrm{Re}[\int_{AB} + \int_{CD} + \int_{EF} \nu_x \{p(w_{,x} + iw_{,y}) - c\tilde{w}\} ds]$$

$$- \mathrm{Im}[\int_{BC} + \int_{DE} \nu_y \{h(w_{,x} + iw_{,y}) + c\tilde{w}\} ds] + \mathrm{Im}[h\tilde{w}]\Big|_F^A \tag{4.65}$$

in which pg, hg, cf and hf are expressed in the form

$$pg = D \sum_{m=1}^{2N} \sum_{n=1}^{2N} \beta_m \beta_n (p_m g_n + p_n g_m)/2$$

$$hg = D \sum_{m=1}^{2N} \sum_{n=1}^{2N} \beta_m \beta_n (h_m g_n + h_n g_m)/2$$

$$cf = D \sum_{m=1}^{2N} \sum_{n=1}^{2N} \beta_m \beta_n (c_m f_n + c_n f_m)/2$$

$$hf = D \sum_{m=1}^{2N} \sum_{n=1}^{2N} \beta_m \beta_n (h_m f_n + h_n f_m)/2 \qquad (4.66)$$

When the crack lies along the x-axis, the first 2N (for approach 1) or N (for approach 2) terms correspond to a symmetrical solution and the last 2N or N terms correspond to antisymmetrical solution with respect to the x-axis. Therefore, the matrix $\underset{\sim}{H}$ has the property

$$H_{j,M+j} = H_{M+j,j} = 0 \qquad (4.67)$$

where M = 2N for approach 1

M = N for approach 2

Thus, $\underset{\sim}{H}$ takes the form

$$\underset{2M\times 2M}{\underset{\sim}{H}} = \begin{bmatrix} \underset{M\times M}{\underset{\sim}{H}_1} & \\ & \underset{M\times M}{\underset{\sim}{H}_2} \end{bmatrix} \qquad (4.68)$$

This property reduces the effort for the computation of $\underset{\sim}{H}$ matrix and its inverse.

In plane stress crack problems, the $\underset{\sim}{H}$ matrix is reduced to (M-1) $\times$ (M-1) matrix by eliminating β_{M+2}, but in flexural problems, the size of the $\underset{\sim}{H}$ matrix can not be reduced.

For the crack tip superelement in Figure 32, the stiffness matrix is given in Table 29. In this example, the material constants E=1, ν=0.3 are used. For the assumption of field variables 24 β's are used and five-point Gaussian quadrature is chosen for the integration of the $\underset{\sim}{G}$ and $\underset{\sim}{H}$ matrices.

4.10 Stress Intensity Factor

The bending stress intensity factors K_1 and K_2 on the basis of the Kirchhoff's hypothesis are originally defined by Williams [101]. But later Sih et al. redefined them considering the similarity between out of plane bending and in plane stretching problems. However, the physical meaning of the bending stress intensity factors K_1 and K_2 under Sih's definition has not, to the author's knowledge, been clarified yet. First, we briefly describe the process of Sih's definition and redefine them to make their physical meaning clear.

The sum of the normal stresses is,

for stretching:

$$\sigma_x + \sigma_y = k_1\left(\frac{2}{r}\right)^{\frac{1}{2}}\cos\frac{\theta}{2} - k_2\left(\frac{2}{r}\right)^{\frac{1}{2}}\sin\frac{\theta}{2} \qquad (4.69)$$

and for bending

$$\sigma_r + \sigma_\theta = \frac{12(M_x + M_y)z}{h^3}$$

$$= \frac{2\sqrt{2}(1+\nu)z}{(3+\nu)h}\left[\frac{K_1}{\sqrt{r}}\cos\frac{\theta}{2} - \frac{K_2}{\sqrt{r}}\sin\frac{\theta}{2}\right] \quad (4.70)$$

where k_1 and k_2 are stress intensity factors for plate extension and K_1 and K_2 are bending stress intensity factors defined by Sih such that both bending and stretching stress intensity factors have the identical character. These stress intensity factors are represented as the real and negative imaginary parts of a complex constant as:

$$k = k_1 - ik_2 \quad (4.71)$$

$$K = K_1 - iK_2 \quad (4.72)$$

Introducing the complex variable $z = re^{i\theta}$, Equations (4.69) and (4.70) can be rewritten as,

for stretching:

$$\sigma_x + \sigma_y = \mathrm{Re}\{k(\frac{2}{z})^{\frac{1}{2}}\} \quad (4.73)$$

and for bending

$$M_x + M_y = \frac{(1+\nu)h^2}{3\sqrt{2}(3+\nu)}\mathrm{Re}\{K(\frac{1}{z})^{\frac{1}{2}}\} \quad (4.74)$$

The relationship between the stress functions and the left-hand members of Equations (4.73) and (4.74) are

for extension:

$$\sigma_x + \sigma_y = 4\mathrm{Re}\{\Phi_s'(z)\} \tag{4.75}$$

and for bending

$$M_x + M_y = -4D(1 + \nu)\mathrm{Re}\{\Phi_b'(z)\} \tag{4.76}$$

where $\Phi_s(z)$ and $\Phi_b(z)$ are stress function for plate stretching and for plate bending, respectively. In the vicinity of a crack tip, the dominant behavior of $\Phi'(z)$ takes the form of a complex constant divided by $z^{1/2}$. Therefore, equating the results of Equations (4.73) and (4.75), the stress intensity factors can be written, for *stretching:*

$$k = 2\sqrt{2} \lim_{z\to 0} z^{\frac{1}{2}}\Phi_s'(z) \tag{4.77}$$

and for bending

$$K = -\frac{12\sqrt{2}D(3 + \nu)}{h^2} \lim_{z\to 0} z^{\frac{1}{2}}\Phi_b'(z) \tag{4.78}$$

Equation (4.78) is the definition of the bending stress intensity factors proposed by Sih et al. K_1 and K_2 are called the bending stress intensity factor and the shearing stress intensity factor, respectively.

The Equation (4.78) involves the material constant ν explicitly and so the above definition can be applied only

for the plate of isotropic material. The present author defines the stress intensity factors for flexural problems in the following manner.

$$K_1 = \lim_{r \to 0} \frac{6\sqrt{2}}{h^2} r^{\frac{1}{2}} M_y(r, 0)$$

$$K_2 = \lim_{r \to 0} \frac{6\sqrt{2}}{h^2} r^{3/2} V_y(r, 0) \tag{4.79}$$

where $V_y = Q_y + \frac{\partial M_{xy}}{\partial x}$

The stress intensity factors thus defined can be shown to coincide with those defined by Sih in isotropic problems. Their physical meaning is apparent i.e., K_1 represents the intensity of bending moments, whereas K_2 corresponds to statically equivalent stress resultants in the Kirchhoff's sense. This definition can be immediately applied to the flexural problem of the plate made of anisotropic materials. From the definition (4.79), together with equations (4.26) and (4.27), the bending and vertical force stress intensity factor K_1 and K_2 can be written in terms of β's as

$$K_1 = -\frac{6\sqrt{2}D(3 + \nu)}{h^2}\beta_1$$

$$K_2 = \frac{6\sqrt{2}D(3 + \nu)}{h^2}\beta_{2N+1} \tag{4.80}$$

Since the field parameters β's are derived from the generalized nodal displacement vector $\underset{\sim}{q}$ using Equation (4.55), K_1 and K_2 are expressed in the form

$$\begin{Bmatrix} K_1 \\ K_2 \end{Bmatrix} = \underset{\sim}{B}\,\underset{\sim}{q} \tag{4.81}$$

For the crack tip superelement shown in Figure 32, the matrix $\underset{\sim}{B}$ is given in Table 30 for E=1, ν=0.3.

4.11 Numerical Examples

Several performance tests have been carried out in order to investigate the accuracy of the stress intensity factor solution and the effect of the size of the crack tip superelement. In the first example, the crack tip superelement has been applied to the problems for which exact solutions exist. As the second example an analysis has been made of the bending of the center cracked plate of finite dimension, for which the finite element solution was obtained by Wilson and Thompson [109] by using the conventional elements.

Example 1

The plate geometry is a certain cracked plate of infinite dimensions. The through-the-thickness crack of a total length of 2a lies along the x-axis. Utilizing the symmetries in the problem, one half of the plate is concerned. A nine-node square shape superelement occupies a crack tip region as shown in Figure 33. The total length of the crack is varied from 2ε to 20ε where ε is the length of the crack within the superelement and the side of the element is equal to 2ε.

Three different loading conditions, i.e. purely cylindrical bending, pure bending and twisting are considered. The closed form analytical solution for the infinite plate with an elliptical hole is readily available [113] in the form of a stress function under above loading conditions. The through-the-thickness crack problem is a limiting case of this problem. Using these analytical solutions of closed form, the deflections w, $w_{,x}$, $w_{,y}$ are calculated at all points on which the nodal points of the superelement are located. With these corresponding values as prescribed displacements, the stress intensity factor solutions are computed from Equation (4.81) for several ratios a/ε and compared with the exact stress intensity factor solutions given in the handbook [33].

Case 1 Pure Cylindrical Bending of an Infinite Plate Containing a Finite Crack

This problem is illustrated in Figure 33(a). The uniform bending moment M_o per unit length is applied at infinity along the edges which are parallel to the x-axis on which the crack is located

$$M_y = M_0$$

$$M_x = M_{xy} = 0$$

The exact stress intensity factor solutions for this problem are

$$K_1 = \frac{6M_0}{h^2} a^{\frac{1}{2}}$$

$$K_2 = 0$$

where h is the plate thickness.

The computational results are tabulated in Table 25 for several ratios a/ε. It is observed that the best estimation for the K_1 value is obtained when the superelement contains the entire crack. In that case the element gives an error of only 0.18 percent. However, when the superelement is taken as small as one-tenth of the size of the length of the crack the K_1 solution still shows an excellent accuracy. The error is 1.22%. The values of K_2 solution are negligibly small for the entire range of a/ε.

Case 2 Pure Bending of an Infinite Plate Containing a Finite Crack

Figure 33(b) illustates this example. Uniform bending moment of M_o per unit length is applied all around the boundary of the plate at infinity

$$M_x = M_y = M_0$$

$$M_{xy} = 0$$

The exact stress intensity factor solutions are the same as those in the previous case.

$$K_1 = \frac{6M_0}{h^2} a^{\frac{1}{2}} \quad , \qquad K_2 = 0$$

The results are independent of the moment M_x. The finite element solutions are shown in Table 25. The nature of the K_1 solutions are completely the same as that in the case of cylindrical bending. The accuracy of the K_2 solutions appears to be slightly worse but it is still of the same order.

Case 3 Pure Twisting of an Infinite Plate Containing a Finite Crack

Uniform pure twisting moment of M_o per unit length is applied all around the contour of the plate at infinity as shown in Figure 33(c).

$$M_x = M_y = 0$$

$$M_{xy} = M_0$$

The exact stress intensity factor solutions are

$$K_1 = 0$$

$$K_2 = \frac{6M_0}{h^2} a^{\frac{1}{2}}$$

The stress intensity factor solutions are given in Table 25. It is seen that the error of K_2 solution is only 0.61% when the size of the superelement is one-tenth of the crack length while it has 2.28 percent error when the superelement contains the entire crack. This result is opposite to those in the previous two cases. The values of the K_1 solution is negligibly small in every a/ε.

It can be seen from the above results that the accuracy of the stress intensity factor solution is excellent and it is not so much affected by the size of that crack tip superelement. The size of the superelement may be of the same order as that of the crack length. This is due to the accuracy of the stress and displacement field in the interior of the superelement. Further improvement of the solution will be achieved by increasing both the number of the parameter β's and the number of nodes.

Example 2

Consider the problem of pure cylindrical bending of a thin plate made of isotropic materials with a finite width and centrally located through-the-thickness crack, whose geometry is shown in Figure 35. Due to symmetry, one-half of the plate was considered in the finite element analysis. A number of cases were studied with different ratios of 2a/W, where 2a was the total crack length as in the previous example and W, the width of the plate. In each case only a single nine-node superelement with 27 degrees of freedom was used [Figure 36]. Figure 37 presents the results of stress intensity factor K_1 versus 2a/W. The solid line in this figure represents the results obtained by Wilson and Thompson which were computed using more than five-hundred conventional 3-node triangular plate elements based on assumed displacement finite element model. The results indicated by circles are those obtained by the present superelement.

It is seen that results obtained by a single crack tip superelement already correlate very well with the other results which were estimated to be accurate to within 2 percent according to their paper. In this simple example problem, it is shown that the use of the hybrid superelement will give result of sufficient accuracy for this kind of problem even when only a single element is used.

4.12 Conclusions and Recommendations

A hybrid finite element model has been presented for the computation of bending and stress resultant stress intensity factors K_1 and K_2 respectively in the flexural problem of a plate containing a crack. From the results of several numerical examples the following conclusions can be made:

(1) The computation time required for the generation of a crack element stiffness matrix is a fraction of one second on current generation large computers. The CPU time needed for the entire process to solve the second example is still around one second.

(2) The use of this hybrid crack element model gives the stress intensity factor solutions with excellent accuracy.

(3) The accuracy of the stress intensity factor solution is not considerably affected by the size of the crack tip superelement. The size may be of the

same order as that of the crack length. This indicates that the very crude structure models can be used for finite element analysis.

(4) It is to be noted that strickly speaking the solution to the flexural problem is valid only when sufficient extension is superimposed such that the occurrence of the overlapping of the crack faces on the compression side of the plate can be avoided.

The first three conclusions are valid only in the framework of Poisson-Kirchhoff plate theory. A further refinement of this superelement is possible by adopting Reissner's sixth order plate theory. In his theory, the deflection w of the plate takes the form of a biharmonic function in the absence of lateral loads and can be represented in terms of two analytic functions of complex variable z ($z = x+iy$) in exactly the same form as that in the classical plate theory.

$$w = \mathrm{Re}[\bar{z}\Phi(z) + \chi(z)] \tag{4.82}$$

The average rotations β_x and β_y about y- and x-axes respectively are given by

$$\beta_x + i\beta_y = -[\Phi(z) + z\overline{\Phi'(z)} - 2(n-1)\varepsilon^2\overline{\Phi''(z)} + \overline{\chi'(z)}] + i(n-1)\varepsilon^2\frac{\partial\psi}{\partial\bar{z}} \tag{4.83}$$

where $n = -\frac{3+\nu}{1-\nu}$, $\varepsilon = h/\sqrt{10}$

and h is the plate thickness. ψ is the stress function and satisfies the Helmholtz equation.

$$\psi - \varepsilon^2\nabla^2\psi = 0$$

The bending moments M_x, M_y, twisting moment M_{xy} and shear forces Q_x and Q_y can be expressed in terms of $\Phi(z)$, $\chi(z)$ and $\psi(z,\bar{z})$ in the form

$$M_x + M_y = -\frac{8(n+1)}{\kappa - 1} D\,\mathrm{Re}[\Phi'(z)]$$

$$M_x - M_y - 2iM_{xy} = \frac{8}{n-1} D\,[\chi''(z) + \bar{z}\Phi''(z) - 2(n-1)\varepsilon^2\Phi''''(z)] + 8i\varepsilon^2\frac{\partial^2\psi}{\partial z^2}$$

$$Q_x - iQ_y = -D[4\Phi''(z) - 2i\frac{\partial\psi}{\partial z}] \tag{4.84}$$

The functional forms of the complex potential $\Phi(z)$ and $\chi(z)$ and the stress function $\psi(z,\bar{z})$ are determined from the boundary conditions of the problem. The procedure to obtain the crack element stiffness matrix follows completely that in the classical fourth order plate theory.

SECTION 5

BENDING ANALYSIS OF BI-MATERIAL PLATE WITH THROUGH-THE-THICKNESS CRACK LOCATED ALONG OR NORMAL TO THE INTERFACE, ISOTROPIC PLATE WITH WEDGE-SHAPED NOTCH AND ANISOTROPIC PLATE WITH THROUGH-THE-THICKNESS CRACK

5.1 Introduction

In this section, stress and displacement fields are obtained for bending analyses of bi-material plates with a crack located along or normal to the interface, an isotropic plate with a wedge-shaped notch and an anisotropic plate with a through-the-thickness crack. The procedure to construct a superelement for above cases follows completely that given in Section 4.

5.2 Bi-Material Plate with a Through-the-Thickness Crack Lying along the Interface

Figure 38 shows a through-the-thickness crack lying along the interface of two dissimilar materials. The origin of the coordinates is placed at the crack tip. The positive real axis lies along the line of bonding, while the negative real axis lies along the crack. All quantities referred to the region $y > 0$ and $y < 0$ are designated by subscript 1 and 2, respectively.

On the basis of the Poisson-Kirchhoff theory of thin

plates and the complex variable approach, the boundary conditions can be stated as follows.

(1) Stress free condition along the crack surfaces $\theta = \pm\pi$

$$\begin{aligned} (M_y)_1 &= 0, \quad (V_y)_1 = 0 \quad \text{at } \theta = +\pi \\ (M_y)_2 &= 0, \quad (V_y)_2 = 0 \quad \text{at } \theta = -\pi \end{aligned} \tag{5.1}$$

(2) Continuity condition of the bending moment M_y and the Kirchhoff shearing force V_y across the bonded portion of the interface

$$\begin{aligned} (M_y)_1 &= (M_y)_2 \quad \text{at } \theta = 0 \\ (V_y)_1 &= (V_y)_2 \quad \text{at } \theta = 0 \end{aligned} \tag{5.2}$$

(3) Continuity condition of the deflection w and the slope $\partial w/\partial y$ across the bonded portion of the interface

$$\begin{aligned} (w)_1 &= (w)_2 \quad \text{at } \theta = 0 \\ (\partial w/\partial y)_1 &= (\partial w/\partial y)_2 \quad \text{at } \theta = 0 \end{aligned} \tag{5.3}$$

All field variables are expressed in terms of a set of analytic functions of z, i.e., $\Phi(z)$ and $\chi(z)$. $\Phi(z)$ and $\chi(z)$ in both materials are assumed as

$$\begin{aligned} \Phi_1(z) &= \sum_i a_1^{(i)} z^{\lambda_i} \qquad \chi_1(z) = \sum_i c_1^{(i)} z^{\lambda_i+1} \\ \Phi_2(z) &= \sum_i a_2^{(i)} z^{\lambda_i} \qquad \chi_2(z) = \sum_i c_2^{(i)} z^{\lambda_i+1} \end{aligned} \tag{5.4}$$

where $a_1^{(i)}$, $c_1^{(i)}$, $a_2^{(i)}$ and $c_2^{(i)}$ are unknown real or complex coefficients and can be evaluated from the above boundary conditions. λ_i are real or complex eigenparameters which are taken to be the same in both regions.

Inserting Equation (5.4) into the boundary conditions gives

$$
\begin{aligned}
&(\lambda - \mu_1)(a_1 e^{i\lambda\pi} + \bar{a}_1 e^{-i\lambda\pi}) + (\lambda + 1)(c_1 e^{i\lambda\pi} + \bar{c}_1 e^{-i\lambda\pi}) = 0 \\
&(\lambda - \mu_2)(a_2 e^{-i\lambda\pi} + \bar{a}_2 e^{i\lambda\pi}) + (\lambda + 1)(c_2 e^{-i\lambda\pi} + \bar{c}_2 e^{i\lambda\pi}) = 0 \\
&(\lambda + \mu_1)(a_1 e^{i\lambda\pi} - \bar{a}_1 e^{-i\lambda\pi}) + (\lambda + 1)(c_1 e^{i\lambda\pi} - \bar{c}_1 e^{-i\lambda\pi}) = 0 \\
&(\lambda + \mu_2)(a_2 e^{-i\lambda\pi} - \bar{a}_2 e^{i\lambda\pi}) + (\lambda + 1)(c_2 e^{-i\lambda\pi} - \bar{c}_2 e^{i\lambda\pi}) = 0 \\
&\gamma\{(\lambda - \mu_1)(a_1 + \bar{a}_1) + (\lambda + 1)(c_1 + \bar{c}_1)\} \\
&\qquad\qquad = (\lambda - \mu_2)(a_2 + \bar{a}_2) + (\lambda + 1)(c_2 + \bar{c}_2) \\
&\gamma\{(\lambda + \mu_1)(a_1 - \bar{a}_1) + (\lambda + 1)(c_1 - \bar{c}_1)\} \\
&\qquad\qquad = (\lambda + \mu_2)(a_2 - \bar{a}_2) + (\lambda + 1)(c_2 - \bar{c}_2) \\
&a_1 + \bar{a}_1 + c_1 + \bar{c}_1 = a_2 + \bar{a}_2 + c_2 + \bar{c}_2 \\
&(\lambda - 1)(a_1 - \bar{a}_1 - a_2 + \bar{a}_2) + (\lambda + 1)(c_1 - \bar{c}_1 - c_2 + \bar{c}_2) = 0
\end{aligned}
\tag{5.5}
$$

where the superscripts are omitted and γ, μ_1 and μ_2 are defined as

$$
\gamma = \frac{D_1(1 - \nu_1)}{D_2(1 - \nu_2)} \quad , \qquad \mu_i = \frac{3 + \nu_i}{1 - \nu_i} \qquad (i = 1, 2) \tag{5.6}
$$

Equation (5.5) consists of eight equations with eight unknown constants a_i, $\bar{a}_i$, c_i, $\bar{c}_i$ $(i = 1, 2)$. By eliminating c_1, $\bar{c}_1$, c_2 and $\bar{c}_2$ from Equation (5.5), one obtains the following equation.

$$
\begin{bmatrix}
1 + \mu_1 e^{i2\lambda\pi} & -1 - \mu_2 e^{-i2\lambda\pi} & 0 & 0 \\
\gamma\mu_1(1 - e^{i2\lambda\pi}) & -\mu_2(1 - e^{-i2\lambda\pi}) & 0 & 0 \\
0 & 0 & 1 + \mu_1 e^{-i2\lambda\pi} & -1 - \mu_2 e^{i2\lambda\pi} \\
0 & 0 & \gamma\mu_1(1 - e^{-i2\lambda\pi}) & -\mu_2(1 - e^{i2\lambda\pi})
\end{bmatrix}
$$

$$\times \begin{Bmatrix} a_1 \\ a_2 \\ \bar{a}_1 \\ \bar{a}_2 \end{Bmatrix} = \begin{Bmatrix} 0 \\ 0 \\ 0 \\ 0 \end{Bmatrix} \tag{5.7}$$

The above equation has nontrivial solutions if and only if the coefficient determinant vanishes, i.e.

$$\lambda = n \qquad (n = 1, 2, \ldots.) \tag{5.8}$$

or

$$e^{-i2\lambda\pi} = - \frac{\mu_1(\mu_2 + \gamma)}{\mu_2(\gamma\mu_1 + 1)} \quad (= p) \tag{5.9}$$

It is observed that the eigenvalues corresponding to Equation (5.9) are complex and are expressed in the form of

$$\lambda_n = (n - \tfrac{1}{2}) \pm i\kappa \qquad (n = 1, 2, \ldots..) \tag{5.10}$$

where

$$\kappa = -(1/2\pi)\log\{\mu_1(\mu_2 + \gamma)/\mu_2(\gamma\mu_1 + 1)\} \tag{5.11}$$

The deflection and stress couples are expressed as follows.

<u>For $\lambda = 1, 2, \ldots\ldots$</u>

in material 1

$$w = \sum_{n=1}^{N} b_n r^{\lambda_n + 1}\left[\cos(\lambda_n - 1)\theta - \frac{\lambda_n - \mu_1}{\lambda_n + 1}\cos(\lambda_n + 1)\theta\right]$$

$$M_x = -D_1 \sum_{n=1}^{N} b_n \lambda_n r^{\lambda_n - 1}[2(1 + \nu_1)\cos(\lambda_n - 1)\theta$$
$$+ (1 - \nu_1)\{(\lambda_n - 1)\cos(\lambda_n - 3)\theta - (\lambda_n - \mu_1)\cos(\lambda_n - 1)\theta\}]$$

$$M_y = -D_1 \sum_{n=1}^{N} b_n \lambda_n r^{\lambda_n - 1}[2(1 + \nu_1)\cos(\lambda_n - 1)\theta$$
$$- (1 - \nu_1)\{(\lambda_n - 1)\cos(\lambda_n - 3)\theta - (\lambda_n - \mu_1)\cos(\lambda_n - 1)\theta\}]$$

$$Q_x = -4D_1 \sum_{n=1}^{N} b_n \lambda_n (\lambda_n - 1) r^{\lambda_n - 2} \cos(\lambda_n - 2)\theta$$

$$Q_y = 4D_1 \sum_{n=1}^{N} b_n \lambda_n (\lambda_n - 1) r^{\lambda_n - 2} \sin(\lambda_n - 2)\theta$$

and in material 2

$$w = \alpha \sum_{n=1}^{N} b_n r^{\lambda_n + 1} [\cos(\lambda_n - 1)\theta - \{(\lambda_n - \mu_2)/(\lambda_n + 1)\}\cos(\lambda_n + 1)\theta]$$

$$M_x = -\alpha D_2 \sum_{n=1}^{N} b_n \lambda_n r^{\lambda_n - 1} [2(1 + \nu_2)\cos(\lambda_n - 1)\theta$$

$$+ (1 - \nu_2)\{(\lambda_n - 1)\cos(\lambda_n - 3)\theta - (\lambda_n - \mu_2)\cos(\lambda_n - 1)\theta\}]$$

$$M_y = -\alpha D_2 \sum_{n=1}^{N} b_n \lambda_n r^{\lambda_n - 1} [2(1 + \nu_2)\cos(\lambda_n - 1)\theta$$

$$-(1 - \nu_2)\{(\lambda_n - 1)\cos(\lambda_n - 3)\theta - (\lambda_n - \mu_1)\cos(\lambda_n - 1)\theta\}]$$

$$M_{xy} = \alpha D_2 (1 - \nu_2) \sum_{n=1}^{N} b_n \lambda_n r^{\lambda_n - 1} [(\lambda_n - 1)\sin(\lambda_n - 3)\theta$$

$$- (\lambda_n - \mu_2)\sin(\lambda_n - 1)\theta]$$

$$Q_x = -4\alpha D_2 \sum_{n=1}^{N} b_n \lambda_n (\lambda_n - 1) r^{\lambda_n - 2} \cos(\lambda_n - 2)\theta$$

$$Q_y = 4\alpha D_2 \sum_{n=1}^{N} b_n \lambda_n (\lambda_n - 1) r^{\lambda_n - 2} \sin(\lambda_n - 2)\theta$$

where

$$\alpha = (1 + \mu_1)/(1 + \mu_2)$$

<u>For $\lambda = (n - \frac{1}{2}) \pm i\kappa \quad (n = 1, 2, \ldots.)$</u>

in material 1

$$w = \mathrm{Re} \sum_{n=1}^{N} b_n r^{\lambda_n + 1} [e^{i(\lambda_n - 1)\theta} - \{(\lambda_n - t)/(\lambda_n + 1)\} e^{i(\lambda_n + 1)\theta}]$$

$$M_x = -D_1 \mathrm{Re} \sum_{n=1}^{N} b_n \lambda_n r^{\lambda_n - 1} [2(1+\nu_1) e^{i(\lambda_n - 1)\theta}$$

$$+ (1-\nu_1)\{(\lambda_n - 1) e^{i(\lambda_n - 3)\theta} - (\lambda_n - t) e^{i(\lambda_n - 1)\theta}\}]$$

$$M_y = -D_1 R_e \sum_{n=1}^{N} b_n \lambda_n r^{\lambda_n - 1} [2(1+\nu_1) e^{i(\lambda_n - 1)\theta}$$

$$- (1-\nu_1)\{(\lambda_n - 1) e^{i(\lambda_n - 3)\theta} - (\lambda_n - t) e^{i(\lambda_n - 1)\theta}\}]$$

$$M_{xy} = D_1 (1-\nu_1) \mathrm{Im} \sum_{n=1}^{N} b_n \lambda_n r^{\lambda_n - 1} [(\lambda_n - 1) e^{i(\lambda_n - 3)\theta}$$

$$- (\lambda_n - t) e^{i(\lambda_n - 1)\theta}]$$

$$Q_x = -4D_1 \mathrm{Re} \sum_{n=1}^{N} b_n \lambda_n (\lambda_n - 1) r^{\lambda_n - 2} e^{i(\lambda_n - 2)\theta}$$

$$Q_y = 4D_1 \mathrm{Im} \sum_{n=1}^{N} b_n \lambda_n (\lambda_n - 1) r^{\lambda_n - 2} e^{i(\lambda_n - 2)\theta}$$

and in material 2

$$w = -\gamma\omega \mathrm{Re} \sum_{n=1}^{N} p b_n r^{\lambda_n + 1} [e^{i(\lambda_n - 1)\theta} - \{(\lambda_n - \mu_2 p)/(\lambda_n + 1)\} e^{i(\lambda_n + 1)\theta}]$$

$$M_x = \gamma\omega D_1 \mathrm{Re} \sum_{n=1}^{N} p b_n \lambda_n r^{\lambda_n - 1} [2(1+\nu_2) e^{i(\lambda_n - 1)\theta}$$

$$+ (1-\nu_2)\{(\lambda_n - 1) e^{i(\lambda_n - 3)\theta} - (\lambda_n - \mu_2 p) e^{i(\lambda_n - 1)\theta}\}]$$

$$M_y = \gamma\omega D_2 \mathrm{Re} \sum_{n=1}^{N} p b_n \lambda_n r^{\lambda_n - 1} [2(1+\nu_2) e^{i(\lambda_n - 1)\theta}$$

$$- (1-\nu_2)\{(\lambda_n - 1) e^{i(\lambda_n - 3)\theta} - (\lambda_n - \mu_2 p) e^{i(\lambda_n - 1)\theta}\}]$$

$$M_{xy} = -\gamma\omega D_2 (1-\nu_2) \mathrm{Im} \sum_{n=1}^{N} p b_n \lambda_n [(\lambda_n - 1) e^{i(\lambda_n - 3)\theta}$$

$$- (\lambda_n - \mu_2 p) e^{i(\lambda_n - 1)\theta}]$$

$$Q_x = 4\gamma\omega D_2 \mathrm{Re} \sum_{n=1}^{N} p b_n \lambda_n (\lambda_n - 1) r^{\lambda_n - 2} e^{i(\lambda_n - 2)\theta}$$

$$Q_y = -4\gamma\omega D_2 \mathrm{Im} \sum_{n=1}^{N} pb_n\lambda_n(\lambda_n - 1)r^{\lambda_n-2} e^{i(\lambda_n-2)\theta} \tag{5.12}$$

where

$$\omega = \mu_1/\mu_2 \quad , \qquad t = \mu_1/p$$

5.3 Bi-Material Plate with a Through-the-Thickness Crack Lying Normal to the Interface

Figure 39 shows a through-the-thickness crack lying normal to the interface of two dissimilar materials. The origin of the coordinates is placed at the crack tip. The negative real axis lies along the crack, while the imaginary axis lies along the line of bonding. All quantities referred to the region $x < 0$ and $x > 0$ are designated by subscript 1 and 2, respectively.

On the basis of the Poisson-Kirchhoff theory of thin plates and the complex variable approach, the boundary conditions can be stated as follows.

(1) Stress free condition along the crack surfaces $\theta = \pm\pi$

$$\left.\begin{aligned} (M_y)_1 &= 0 \\ (V_y)_1 &= 0 \end{aligned}\right\} \quad \text{at } \theta = \pm\pi \tag{5.13}$$

(2) Continuity condition of the bending moment M_x and the Kirchhoff shearing force V_x across the bonded portion of the interface

$$\left.\begin{aligned} (M_x)_1 &= (M_x)_2 \\ (V_x)_1 &= (V_x)_2 \end{aligned}\right\} \quad \text{at } \theta = \pm\frac{\pi}{2} \tag{5.14}$$

(3) Continuity condition of the deflection w and the slope $\partial w/\partial x$ across the bonded portion of the interface

$$(w)_1 = (w)_2 \qquad \text{at } \theta = \pm\frac{\pi}{2} \tag{5.15}$$
$$(\partial w/\partial x)_1 = (\partial w/\partial x)_2$$

All field variables are expressed in terms of a set of analytic functions of z, i.e., $\Phi(z)$ and $\chi(z)$. $\Phi(z)$ and $\chi(z)$ in both materials are assumed as

$$\Phi_1(z) = \sum_i^N a_1^{(i)} z^{\lambda_i} \qquad \chi_1(z) = \sum_i^N c_1^{(i)} z^{\lambda_i+1}$$
$$\Phi_2(z) = \sum_i^N a_2^{(i)} z^{\lambda_i} \qquad \chi_2(z) = \sum_i^N c_2^{(i)} z^{\lambda_i+1} \tag{5.16}$$

where $a_1^{(i)}$, $c_1^{(i)}$, $a_2^{(i)}$ and $c_2^{(i)}$ are unknown real or complex coefficients and can be evaluated from the above boundary conditions. λ_i are real or complex eigenparameters which are taken to be the same in both regions.

Symmetric Loading with Respect to the x-Axis

In this case $a_2^{(i)}$ and $c_2^{(i)}$ are real constants if λ_i are considered to be real. Substituting Equation (5.16) into the boundary conditions and omitting the superscripts yield the following equations.

$$(e^{i\lambda\pi} + \mu_1 e^{2i\lambda\pi})a_1 - 2\lambda\bar{a}_1 - (e^{i\lambda\pi} - \lambda)a_2 - (\lambda+1)c_2 = 0$$

$$2\lambda a_1 - (e^{-i\lambda\pi} + \mu_1 e^{-2i\lambda\pi})\bar{a}_1 - (\lambda - e^{-i\lambda\pi})a_2 + (\lambda+1)c_2 = 0$$

$$[(\gamma\mu_1 + 1)e^{i\lambda\pi} - (\gamma-1)\mu_1 e^{2i\lambda\pi}]a_1 + 2(\gamma-1)\lambda\bar{a}_1 - (\mu_2+1)e^{i\lambda\pi}a_2 = 0 \tag{5.17}$$

$$2(\gamma-1)\lambda a_1 + [(\gamma\mu_1+1)e^{-i\lambda\pi} - (\gamma-1)\mu_1 e^{-2i\lambda\pi}]\bar{a}_1 - (\mu_2+1)e^{-i\lambda\pi}a_2$$
$$= 0$$

The above equations have nontrivial solutions if and only if the coefficient determinant vanishes, i.e.,

$$\sin\lambda\pi = 0$$

or (5.18)

$$4\lambda^2(\gamma - 1)(\gamma + \mu_2) + 2\mu_1(\gamma + \mu_2)(\gamma\mu_1 + 1)\cos\lambda\pi - \mu_1^2(\gamma - 1)(\gamma + \mu_2) + (\gamma\mu_1 + 1)(\mu_2 - \gamma\mu_1) = 0$$

All unknown constants are expressed in terms of $a_2 (= b)$ in the form of

$$a_1 = f(\lambda)b$$
$$c_1 = g(\lambda)b \qquad (5.19)$$
$$c_2 = h(\lambda)b$$

where b is real if λ is considered as real and

$$f(\lambda) = (\mu_2 + 1)[(\gamma\mu_1 + 1) - (\gamma - 1)(\mu_1 + 2\lambda)e^{-i\lambda\pi}]/S(\lambda)$$

$$g(\lambda) = -(\mu_2 + 1)[(\gamma\mu_1 + 1)(\lambda - \mu_1 e^{-2i\lambda\pi}) + (\gamma - 1)(2\lambda - \mu_1)(\lambda - \mu_1 e^{-i\lambda\pi})]/(\lambda + 1)S(\lambda)$$

$$h(\lambda) = (\lambda - e^{-i\lambda\pi})/(\lambda + 1) - (\mu_2 + 1)\{2\lambda\gamma(\mu_1 + 1) + \mu_1(\gamma - 1) - [(\gamma - 1)(4\lambda^2 - \mu_1^2) + (\gamma\mu_1 + 1)]e^{-i\lambda\pi} + \mu_1(\gamma\mu_1 + 1)e^{-2i\lambda\pi}\}/(\lambda + 1)S(\lambda) \qquad (5.20)$$

$$S(\lambda) = (\gamma\mu_1 + 1)^2 - 2\mu_1(\gamma - 1)(\gamma\mu_1 + 1)\cos\lambda\pi + (\gamma - 1)^2(\mu_1^2 - 4\lambda^2)$$

The resulting displacement and stress couples are in material 1:

$$w = \mathrm{Re}\sum_{n=1}^{N} b_n r^{\lambda_n + 1}[f_R\cos(\lambda_n - 1)\theta - f_I\sin(\lambda_n - 1)\theta + g_R\cos(\lambda_n + 1)\theta - g_I\sin(\lambda_n + 1)\theta]$$

$$M_x = -D_1 \mathrm{Re} \sum_{n=1}^{N} \lambda_n b_n r^{\lambda_n - 1} \{[2(1+\nu_1) f_R$$

$$+ (1-\nu_1)(\lambda_n + 1) g_R] \cos(\lambda_n - 1)\theta - [2(1+\nu_1) f_I$$

$$+ (1-\nu_1)(\lambda_n + 1) g_I] \sin(\lambda_n - 1)\theta$$

$$+ (1-\nu_1)(\lambda_n - 1)[f_R \cos(\lambda_n - 3)\theta - f_I \sin(\lambda_n - 3)\theta]\}$$

$$M_y = -D_1 \mathrm{Re} \sum_{n=1}^{N} \lambda_n b_n r^{\lambda_n - 1} \{[2(1+\nu_1) f_R$$

$$- (1-\nu_1)(\lambda_n + 1) g_R] \cos(\lambda_n - 1)\theta - [2(1+\nu_1) f_I$$

$$- (1-\nu_1)(\lambda_n + 1) g_I] \sin(\lambda_n - 1)\theta$$

$$- (1-\nu_1)(\lambda_n - 1)[f_R \cos(\lambda_n - 3)\theta - f_I \sin(\lambda_n - 3)\theta]\}$$

$$M_{xy} = D_1 (1-\nu_1) \mathrm{Im} \sum_{n=1}^{N} b_n \lambda_n r^{\lambda_n - 1} \{(\lambda_n - 1)[f_R \sin(\lambda_n - 3)\theta$$

$$+ f_I \cos(\lambda_n - 3)\theta] + (\lambda_n + 1)[g_R \sin(\lambda_n - 1)\theta + g_I \cos(\lambda_n - 1)\theta]\}$$

$$Q_x = -4D_1 \mathrm{Re} \sum_{n=1}^{N} b_n \lambda_n (\lambda_n - 1)[f_R \cos(\lambda_n - 2)\theta - f_I \sin(\lambda_n - 2)\theta]$$

$$Q_y = 4D_1 \mathrm{Re} \sum_{n=1}^{N} b_n \lambda_n (\lambda_n - 1)[f_R \sin(\lambda_n - 2)\theta + f_I \cos(\lambda_n - 2)\theta]$$

and in material 2:

$$w = \mathrm{Re} \sum_{n=1}^{N} b_n r^{\lambda_n + 1} [\cos(\lambda_n - 1)\theta + h_R \cos(\lambda_n + 1)\theta]$$

$$M_x = -D_2 \mathrm{Re} \sum_{n=1}^{N} \lambda_n b_n r^{\lambda_n - 1} \{2(1+\nu_2)\cos(\lambda_n - 1)\theta$$

$$+ (1-\nu_2)[(\lambda_n - 1)\cos(\lambda_n - 3)\theta + h_R(\lambda_n + 1)\cos(\lambda_n - 1)\theta]\}$$

$$M_y = -D_2 \mathrm{Re} \sum_{n=1}^{N} \lambda_n b_n r^{\lambda_n - 1} \{2(1+\nu_2)\cos(\lambda_n - 1)\theta$$

$$-(1-\nu_2)[(\lambda_n - 1)\cos(\lambda_n - 3)\theta + h_R(\lambda_n + 1)\cos(\lambda_n - 1)\theta]\}$$

$$M_{xy} = D_2(1-\nu_2)\mathrm{Re} \sum_{n=1}^{N} \lambda_n b_n r^{\lambda_n - 1} [(\lambda_n - 1)\sin(\lambda_n - 3)\theta$$

$$+ h_R(\lambda_n + 1)\sin(\lambda_n - 1)\theta]$$

$$Q_x = -4D_2 \mathrm{Re} \sum_{n=1}^{N} b_n \lambda_n (\lambda_n - 1) r^{\lambda_n - 2} \cos(\lambda_n - 2)\theta$$

$$Q_y = 4D_2 \mathrm{Re} \sum_{n=1}^{N} b_n \lambda_n (\lambda_n - 1) r^{\lambda_n - 2} \sin(\lambda_n - 2)\theta \qquad (5.21)$$

where

$$f_R(\lambda) = (\mu_2 + 1)[(\gamma\mu_1 + 1) - (\gamma - 1)(\mu_1 + 2\lambda)\cos\lambda\pi]/S(\lambda)$$

$$f_I(\lambda) = (\mu_2 + 1)(\gamma - 1)(\mu_1 + 2\lambda)\sin\lambda\pi/S(\lambda)$$

$$g_R(\lambda) = -(\mu_2 + 1)[(\gamma\mu_1 + 1)(\lambda - \mu_1\cos 2\lambda\pi)$$

$$+ (\gamma - 1)(2\lambda - \mu_1)(\lambda - \mu_1\cos\lambda\pi)]/(\lambda + 1)S(\lambda)$$

$$g_I(\lambda) = -\mu_1(\mu_2 + 1)[(\gamma\mu_1 + 1)\sin 2\lambda\pi$$

$$+ (\gamma - 1)(2\lambda - \mu_1)\sin\lambda\pi]/(\lambda + 1)S(\lambda)$$

$$h_R(\lambda) = (\lambda - \cos\lambda\pi)/(\lambda + 1) - (\mu_2 + 1)\{2\lambda\gamma(\mu_1 + 1) + \mu_1(\gamma - 1)$$

$$- [(\gamma - 1)(4\lambda^2 - \mu_1^2) + (\gamma\mu_1 + 1)]\cos\lambda\pi$$

$$+ \mu_1(\gamma\mu_1 + 1)\cos 2\lambda\pi\}/(\lambda + 1)S(\lambda)$$

$$S(\lambda) = (\gamma\mu_1 + 1)^2 - 2\mu_1(\gamma - 1)(\gamma\mu_1 + 1)\cos\lambda\pi + (\gamma - 1)^2(\mu_1^2 - 4\lambda^2)$$

Antisymmetric Loading

The constant a_2 and c_2 are pure imaginary if λ is considered as real. Imposing boundary conditions gives the following characteristic equations.

$$\sin\lambda\pi = 0$$

and (5.22)

$$4\lambda^2(\gamma-1)(\mu_2+\gamma) + 2\mu_1(\gamma+\mu_2)(\gamma\mu_1+1)\cos\lambda\pi - \mu_1^2(\gamma-1)(\gamma+\mu_2) + (\gamma\mu_1+1)(\mu_2-\gamma\mu_1) = 0$$

These equations are identical with those for the symmetric loading.

All unknown constants are expressed in terms of $a_2 (= ib)$ in the form of

$$a_1 = if(\lambda)b$$
$$c_1 = ig(\lambda)b \qquad (5.23)$$
$$c_2 = ih(\lambda)b$$

where b is real if λ is considered as real and

$$f(\lambda) = (\mu_2+1)[(\gamma\mu_1+1) + (\gamma-1)(2\lambda-\mu_1)e^{-i\lambda\pi}]/S(\lambda)$$

$$g(\lambda) = -(\mu_2+1)[\lambda(\gamma\mu_1+1) + (\gamma-1)(\lambda+\mu_1)(2\lambda-\mu_1)e^{-i\lambda\pi} + \mu_1(\gamma\mu_1+1)e^{-2i\lambda\pi}]/(\lambda+1)S(\lambda)$$

$$h(\lambda) = (\lambda+e^{-i\lambda\pi})/(\lambda+1) - (\mu_2+1)\{2\lambda\gamma(\mu_1+1) - \mu_1(\gamma-1) + [(\gamma-1)(4\lambda^2-\mu_1^2) + (\gamma\mu_1+1)]e^{-i\lambda\pi} + \mu_1(\gamma\mu_1+1)e^{-2i\lambda\pi}\}/(\lambda+1)S(\lambda) \qquad (5.24)$$

$$S(\lambda) = (\gamma\mu_1+1)^2 - 2\mu_1(\gamma-1)(\gamma\mu_1+1)\cos\lambda\pi + (\gamma-1)^2(\mu_1^2-4\lambda^2)$$

The resulting displacement and stress couples are as follows.

In material 1:

$$w = -\mathrm{Re} \sum_{n=1}^{N} b_n r^{\lambda_n+1} [f_R \sin(\lambda_n - 1)\theta + f_I \cos(\lambda_n - 1)\theta + g_R \sin(\lambda_n + 1)\theta$$

$$+ g_I \cos(\lambda_n + 1)\theta]$$

$$M_x = D_1 \mathrm{Re} \sum_{n=1}^{N} \lambda_n b_n r^{\lambda_n - 1} \{2(1 + \nu_1)[f_R \sin(\lambda_n - 1)\theta + f_I \cos(\lambda_n - 1)\theta]$$

$$+ (1 - \nu_1)(\lambda_n - 1)[f_R \sin(\lambda_n - 3)\theta + f_I \cos(\lambda_n - 3)\theta]$$

$$+ (1 - \nu_1)(\lambda_n + 1)[g_R \sin(\lambda_n - 1)\theta + g_I \cos(\lambda_n - 1)\theta]\}$$

$$M_y = D_1 \mathrm{Re} \sum_{n=1}^{N} \lambda_n b_n r^{\lambda_n - 1} \{2(1 + \nu_1)[f_R \sin(\lambda_n - 1)\theta + f_I \cos(\lambda_n - 1)\theta]$$

$$- (1 - \nu_1)(\lambda_n - 1)[f_R \sin(\lambda_n - 3)\theta + f_I \cos(\lambda_n - 3)\theta]$$

$$- (1 - \nu_1)(\lambda_n + 1)[g_R \sin(\lambda_n - 1)\theta + g_I \cos(\lambda_n - 1)\theta]\}$$

$$M_{xy} = D_1(1 - \nu_1) \mathrm{Re} \sum_{n=1}^{N} \lambda_n b_n r^{\lambda_n - 1} \{(\lambda_n - 1)[f_R \cos(\lambda_n - 3)\theta$$

$$- f_I \sin(\lambda_n - 3)\theta] + (\lambda_n + 1)[g_R \cos(\lambda_n - 1)\theta - g_I \sin(\lambda_n - 1)\theta]\}$$

$$Q_x = 4D_1 \mathrm{Re} \sum_{n=1}^{N} b_n \lambda_n (\lambda_n - 1)[f_R \sin(\lambda_n - 2)\theta + f_I \cos(\lambda_n - 2)\theta]$$

$$Q_y = 4D_1 \mathrm{Re} \sum_{n=1}^{N} b_n \lambda_n (\lambda_n - 1)[f_R \cos(\lambda_n - 2)\theta - f_I \sin(\lambda_n - 2)\theta]$$

and in material 2

$$w = -\mathrm{Re} \sum_{n=1}^{N} b_n r^{\lambda_n+1} [\sin(\lambda_n - 1)\theta + h_R \sin(\lambda_n + 1)\theta]$$

$$M_x = D_2 \mathrm{Re} \sum_{n=1}^{N} b_n \lambda_n r^{\lambda_n - 1} \{2(1 + \nu_2)\sin(\lambda_n - 1)\theta$$

$$+ (1 - \nu_2)[(\lambda_n - 1)\sin(\lambda_n - 3)\theta + (\lambda_n + 1)h_R \sin(\lambda_n - 1)\theta]\}$$

$$M_y = D_2 \mathrm{Re} \sum_{n=1}^{N} b_n \lambda_n r^{\lambda_n - 1} \{2(1+\nu_2)\sin(\lambda_n - 1)\theta$$

$$- (1-\nu_2)[(\lambda_n - 1)\sin(\lambda_n - 3)\theta + (\lambda_n + 1)h_R \sin(\lambda_n - 1)\theta]\}$$

$$M_{xy} = D_2(1-\nu_2)\mathrm{Re} \sum_{n=1}^{N} b_n \lambda_n r^{\lambda_n - 1} [(\lambda_n - 1)\cos(\lambda_n - 3)\theta$$

$$+ (\lambda_n + 1)h_R \cos(\lambda_n - 1)\theta]$$

$$Q_x = 4D_2 \mathrm{Re} \sum_{n=1}^{N} b_n \lambda_n (\lambda_n - 1) r^{\lambda_n - 2} \sin(\lambda_n - 2)\theta$$

$$Q_y = 4D_2 \mathrm{Re} \sum_{n=1}^{N} b_n \lambda_n (\lambda_n - 1) r^{\lambda_n - 2} \cos(\lambda_n - 2)\theta \quad (5.25)$$

where

$$f_R(\lambda) = (\mu_2 + 1)[(\gamma\mu_1 + 1) + (\gamma - 1)(2\lambda - \mu_1)\cos\lambda\pi]/S(\lambda)$$

$$f_I(\lambda) = -(\mu_2 + 1)(\gamma - 1)(2\lambda - \mu_1)\sin\lambda\pi/S(\lambda)$$

$$g_R(\lambda) = -(\mu_2 + 1)[\lambda(\gamma\mu_1 + 1) + (\gamma - 1)(\lambda + \mu_1)(2\lambda - \mu_1)\cos\lambda\pi$$

$$+ \mu_1(\gamma\mu_1 + 1)\cos 2\lambda\pi]/(\lambda + 1)S(\lambda)$$

$$g_I(\lambda) = (\mu_2 + 1)[(\gamma - 1)(\lambda + \mu_1)(2\lambda - \mu_1)\sin\lambda\pi$$

$$+ \mu_1(\gamma\mu_1 + 1)\sin 2\lambda\pi]/(\lambda + 1)S(\lambda)$$

$$h_R(\lambda) = (\lambda + \cos\lambda\pi)/(\lambda + 1) - (\mu_2 + 1)\{2\lambda\gamma(\mu_1 + 1) - \mu_1(\gamma - 1)$$

$$+ [(\gamma - 1)(4\lambda^2 - \mu_1^2) + (\gamma\mu_1 + 1)]\cos\lambda\pi$$

$$+ \mu_1(\gamma\mu_1 + 1)\cos 2\lambda\pi\}/(\lambda + 1)S(\lambda)$$

$$S(\lambda) = (\gamma\mu_1 + 1)^2 - 2\mu_1(\gamma - 1)(\gamma\mu_1 + 1)\cos\lambda\pi + (\gamma - 1)^2(\mu_1^2 - 4\lambda^2)$$

5.4 Isotropic Plate with a Wedge-Shaped Notch

Consider the wedge-shaped notch shown in Figure 40. The origin of the coordinates is located at the tip of the notch and the notch surfaces are situated at $\theta = \pm\alpha$ in polar coordinates.

On the basis of the Poisson-Kirchhoff theory of thin plates and the complex variable approach, all field variables w, M_x, M_y, M_{xy}, Q_x and Q_y are expressed in terms of a set of analytic functions $\Phi(z)$ and $\chi(z)$, which are assumed as

$$\begin{aligned} \Phi(z) &= \sum_{n=1}^{N} a_n z^{\lambda_n} \\ \chi(z) &= \sum_{n=1}^{N} c_n z^{\lambda_n+1} \end{aligned} \tag{5.26}$$

Stress free conditions along the notch surfaces $\theta = \pm\alpha$ can be expressed in a single complex equation as

$$\kappa\Phi(z) + z\overline{\Phi'(z)} + \overline{\chi'(z)} = 0 \tag{5.27}$$

where $\kappa = -(3+\nu)/(1-\nu)$

ν is the Poisson's ratio.

Inserting Equation (5.26) into Equation (5.27), one obtains the following simultaneous equations.

$$\begin{aligned} &\kappa a e^{2i\lambda\alpha} + \bar{a}\lambda_n e^{2i\alpha} + \bar{c}(\lambda+1) = 0 \\ &\kappa a e^{-2i\lambda\alpha} + \bar{a}\lambda_n e^{-2i\alpha} + \bar{c}(\lambda+1) = 0 \end{aligned} \tag{5.28}$$

Eliminating $\bar{c}$ from the above equations gives the following characteristic equation,

$$\kappa a \sin 2\lambda\alpha + \bar{a}\lambda \sin 2\alpha = 0 \tag{5.29}$$

For a symmetric loading, a and c are real if λ is treated as real. The characteristic equation (5.29) yields

$$\kappa\sin 2\lambda\alpha + \lambda\sin 2\alpha = 0 \tag{5.30}$$

Putting a = b (b is real.) and substituting a = b into Equation (5.28) gives

$$c = -b(\kappa\cos 2\lambda\alpha + \lambda\cos 2\alpha)/(\lambda + 1) \tag{5.31}$$

The resulting displacements and stress couples are

$$w = \mathrm{Re}\sum_{n=1}^{N} b_n r^{\lambda_n+1}[\cos(\lambda_n - 1)\theta - \frac{1}{\lambda_n + 1}(\kappa\cos 2\lambda_n\alpha + \lambda_n\cos 2\alpha)\cos(\lambda_n + 1)\theta]$$

$$M_x = -D\mathrm{Re}\sum_{n=1}^{N} b_n\lambda_n r^{\lambda_n-1}[2(1+\nu)\cos(\lambda_n - 1)\theta + (1-\nu)\{(\lambda_n - 1)\cos(\lambda_n - 3)\theta - (\kappa\cos 2\lambda_n\alpha + \lambda_n\cos 2\alpha)\cos(\lambda_n - 1)\theta\}]$$

$$M_y = -D\mathrm{Re}\sum_{n=1}^{N} b_n\lambda_n r^{\lambda_n-1}[2(1+\nu)\cos(\lambda_n - 1)\theta - (1-\nu)\{(\lambda_n - 1)\cos(\lambda_n - 3)\theta - (\kappa\cos 2\lambda_n\alpha + \lambda_n\cos 2\alpha)\cos(\lambda_n - 1)\theta\}]$$

$$M_{xy} = D(1-\nu)\mathrm{Re}\sum_{n=1}^{N} b_n\lambda_n r^{\lambda_n-1}[(\lambda_n - 1)\sin(\lambda_n - 3)\theta - (\kappa\cos 2\lambda_n\alpha + \lambda_n\cos 2\alpha)\sin(\lambda_n - 1)\theta]$$

$$Q_x = -4D\mathrm{Re}\sum_{n=1}^{N} b_n\lambda_n(\lambda_n - 1)r^{\lambda_n-2}\cos(\lambda_n - 2)\theta$$

$$Q_y = 4D\mathrm{Re}\sum_{n=1}^{N} b_n\lambda_n(\lambda_n - 1)r^{\lambda_n-2}\sin(\lambda_n - 2)\theta \tag{5.32}$$

For an antisymmetric loading, a and c are pure imaginary if λ is considered as real. Putting a = ib (b is real.) and

substituting a = ib into Equation (5.28) gives

$$c = b(\kappa\cos 2\lambda\alpha - \lambda\cos 2\alpha)/(\lambda + 1) \tag{5.33}$$

The resulting displacement and stress fields are

$$w = -\mathrm{Re}\sum_{n=1}^{N} b_n r^{\lambda_n+1} [\sin(\lambda_n - 1)\theta$$

$$- \frac{1}{\lambda_n + 1}(\kappa\cos 2\lambda_n\alpha - \lambda_n\cos 2\alpha)\sin(\lambda_n + 1)\theta]$$

$$M_x = D\mathrm{Re}\sum_{n=1}^{N} b_n\lambda_n r^{\lambda_n-1} \{2(1+\nu)\sin(\lambda_n - 1)\theta$$

$$+ (1-\nu)[(\lambda_n - 1)\sin(\lambda_n - 3)\theta + (\kappa\cos 2\lambda_n\alpha$$

$$- \lambda_n\cos 2\alpha)\sin(\lambda_n - 1)\theta]\}$$

$$M_y = D\mathrm{Re}\sum_{n=1}^{N} b_n\lambda_n r^{\lambda_n-1} \{2(1+\nu)\sin(\lambda_n - 1)\theta$$

$$- (1-\nu)[(\lambda_n - 1)\sin(\lambda_n - 3)\theta + (\kappa\cos 2\lambda_n\alpha$$

$$- \lambda_n\cos 2\alpha)\sin(\lambda_n - 1)\theta]\}$$

$$M_{xy} = D(1-\nu)\mathrm{Re}\sum_{n=1}^{N} b_n\lambda_n r^{\lambda_n-1} [(\lambda_n - 1)\cos(\lambda_n - 3)\theta$$

$$+ (\kappa\cos 2\lambda_n\alpha - \lambda_n\cos 2\alpha)\cos(\lambda_n - 1)\theta]$$

$$Q_x = 4D\sum_{n=1}^{N} b_n\lambda_n(\lambda_n - 1) r^{\lambda_n-2} \sin(\lambda_n - 2)\theta$$

$$Q_y = 4D\sum_{n=1}^{N} b_n\lambda_n(\lambda_n - 1) r^{\lambda_n-2} \cos(\lambda_n - 2)\theta \tag{5.34}$$

5.5 Anisotropic Plate with a Through-the-Thickness Crack

Consider a thin plate made of an anisotropic material which possesses a plane of elastic symmetry parallel to the midplane of the plate [Figure 28]. In this case, the constitutive relations can be written in the following matrix form.

$$\underset{\sim}{\varepsilon} = \underset{\sim}{C}\underset{\sim}{\sigma} \tag{5.35}$$

where

$$\underset{\sim}{\varepsilon} = \{\varepsilon_x \ \varepsilon_y \ \varepsilon_z \ \gamma_{yz} \ \gamma_{zx} \ \gamma_{xy}\}$$

$$\underset{\sim}{\sigma} = \{\sigma_x \ \sigma_y \ \sigma_z \ \tau_{yz} \ \tau_{zx} \ \tau_{xy}\}$$

$$\underset{\sim}{C} = \begin{bmatrix} c_{11} & c_{12} & c_{13} & 0 & 0 & c_{16} \\ c_{12} & c_{22} & c_{23} & 0 & 0 & c_{26} \\ c_{13} & c_{23} & c_{33} & 0 & 0 & c_{36} \\ 0 & 0 & 0 & c_{44} & c_{45} & 0 \\ 0 & 0 & 0 & c_{45} & c_{55} & 0 \\ c_{16} & c_{26} & c_{36} & 0 & 0 & c_{66} \end{bmatrix}$$

The above elastic constants c_{11}, c_{12}, c_{13}, c_{22}, c_{23}, c_{33}, c_{44}, c_{45}, c_{55} and c_{66} can be expressed in terms of the usual engineering constants according to the following formulae:

$$\begin{aligned} c_{11} &= 1/E_x \ , \quad c_{12} = -\nu_{xy}/E_y = -\nu_{yx}/E_x \\ c_{13} &= -\nu_{xz}/E_z = -\nu_{zx}/E_x \ , \quad c_{22} = 1/E_y \\ c_{23} &= -\nu_{yz}/E_z = -\nu_{zy}/E_y \ , \quad c_{33} = 1/E_z \\ c_{44} &= 1/G_{yz} \ , \quad c_{55} = 1/G_{zx} \ , \quad c_{66} = 1/G_{xy} \end{aligned} \tag{5.36}$$

where E_x is the Young's modulus along the x-axis, etc. G_{xy} is the shear modulus in the x-y plane, etc. ν_{xy} is the

Poisson's ratio indicating the contraction along the x-axis during the expansion along the y-axis, etc.

Inverting the compliance matrix $\underset{\sim}{C}$, the Hooke's law can be rewritten in the following matrix form:

$$\underset{\sim}{\sigma} = \underset{\sim}{D}\underset{\sim}{\varepsilon} \tag{5.37}$$

where $\underset{\sim}{D}$ is the stiffness matrix written in the form of

$$\underset{\sim}{D} = \begin{bmatrix} d_{11} & d_{12} & d_{13} & 0 & 0 & d_{16} \\ d_{12} & d_{22} & d_{23} & 0 & 0 & d_{26} \\ d_{13} & d_{23} & d_{33} & 0 & 0 & d_{36} \\ 0 & 0 & 0 & d_{44} & d_{45} & 0 \\ 0 & 0 & 0 & d_{45} & d_{55} & 0 \\ d_{16} & d_{26} & d_{36} & 0 & 0 & d_{66} \end{bmatrix}$$

The bending moments, twisting moments and shear forces due to the transverse deflection w(x, y) can be expressed as:

$$\begin{aligned}
M_x &= -\frac{h^3}{12}(a_{11}\frac{\partial^2 w}{\partial x^2} + a_{12}\frac{\partial^2 w}{\partial y^2} + 2a_{16}\frac{\partial^2 w}{\partial x \partial y}) \\
M_y &= -\frac{h^3}{12}(a_{12}\frac{\partial^2 w}{\partial x^2} + a_{22}\frac{\partial^2 w}{\partial y^2} + 2a_{16}\frac{\partial^2 w}{\partial x \partial y}) \\
M_{xy} &= -\frac{h^3}{12}(a_{16}\frac{\partial^2 w}{\partial x^2} + a_{26}\frac{\partial^2 w}{\partial y^2} + 2a_{66}\frac{\partial^2 w}{\partial x \partial y}) \qquad (5.38) \\
Q_x &= -\frac{h^3}{12}[a_{11}\frac{\partial^3 w}{\partial x^3} + 3a_{16}\frac{\partial^3 w}{\partial x^2 \partial y} + (a_{12} + 2a_{66})\frac{\partial^3 w}{\partial x \partial y^2} + a_{26}\frac{\partial^3 w}{\partial y^3}] \\
Q_y &= -\frac{h^3}{12}[a_{16}\frac{\partial^3 w}{\partial x^3} + (a_{12} + 2a_{66})\frac{\partial^3 w}{\partial x^2 \partial y} + 3a_{26}\frac{\partial^3 w}{\partial x \partial y^2} + a_{22}\frac{\partial^3 w}{\partial y^3}]
\end{aligned}$$

where

$$a_{11} = (d_{11}d_{33} - d_{13}^2)/d_{33}\ ,\quad a_{12} = (d_{12}d_{33} - d_{13}d_{23})/d_{33}$$

$$a_{16} = (d_{16}d_{33} - d_{13}d_{36})/d_{33}\ ,\ a_{22} = (d_{22}d_{33} - d_{23}^2)/d_{33}$$

$$a_{26} = (d_{26}d_{33} - d_{23}d_{36})/d_{33}\ ,\ a_{66} = (d_{66}d_{33} - d_{36}^2)/d_{33}$$

The fundamental equation for the bending of thin anisotropic plates are

$$a_{11}\frac{\partial^4 w}{\partial x^4} + 4a_{16}\frac{\partial^4 w}{\partial x^3 \partial y} + 2(a_{12} + 2a_{66})\frac{\partial^4 w}{\partial x^2 \partial y^2} + 4a_{26}\frac{\partial^4 w}{\partial x \partial y^3} + a_{22}\frac{\partial^4 w}{\partial y^4} = 0 \tag{5.39}$$

The general solution of the above equation (5.39) depends on the roots of the following characteristic equation.

$$a_{22}s^4 + 4a_{26}s^3 + 2(a_{12} + 2a_{66})s^2 + 4a_{16}s + a_{11} = 0 \tag{5.40}$$

On the basis of energy considerations, it can be shown that the above characteristic equation has no real roots. These roots can be expressed in the form:

$$\begin{aligned} s_1 &= \alpha_1 + i\beta_1 \\ s_2 &= \alpha_2 + i\beta_2 \\ s_3 &= \alpha_1 - i\beta_1 = \bar{s}_1 \\ s_4 &= \alpha_2 - i\beta_2 = \bar{s}_2 \end{aligned} \tag{5.41}$$

where α_1, α_2, β_1 and β_2 are real constants and it is always possible to arrange that $\beta_1 > 0$ and $\beta_2 > 0$.

The general solution for Equation (5.39) can be expressed as:

$$w(x, y) = 2\mathrm{Re}[F_1(z_1) + F_2(z_2)] \tag{5.42}$$

where

$$z_1 = x + s_1 y = x + \alpha_1 y + i\beta_1 y$$
$$z_2 = x + s_2 y = x + \alpha_2 y + i\beta_2 y$$

Introducing $\Phi(z_1) = dF_1/dz_1$, $\Psi(z_2) = dF_2/dz_2$ and substituting the displacement function $w(x, y)$ into Equation (5.38) gives the general expression for moments and shear forces in terms of the two analytic functions $\Phi(z_1)$ and $\Psi(z_2)$ in the form:

$$M_x = -\frac{h^3}{6}\mathrm{Re}[p_1\Phi'(z_1) + q_1\Psi'(z_2)]$$

$$M_y = -\frac{h^3}{6}\mathrm{Re}[p_2\Phi'(z_1) + q_2\Psi'(z_2)]$$

$$M_{xy} = -\frac{h^3}{6}\mathrm{Re}[p_3\Phi'(z_1) + q_3\Psi'(z_2)] \tag{5.43}$$

$$Q_x = -\frac{h^3}{6}\mathrm{Re}[s_1p_4\Phi''(z_1) + s_2q_4\Psi''(z_2)]$$

$$Q_y = \frac{h^3}{6}\mathrm{Re}[p_4\Phi''(z_1) + q_4\Psi''(z_2)]$$

where

$$p_1 = a_{11} + a_{12}s_1^2 + 2a_{16}s_1$$
$$q_1 = a_{11} + a_{12}s_2^2 + 2a_{16}s_2$$
$$p_2 = a_{12} + a_{22}s_1^2 + 2a_{26}s_1$$
$$q_2 = a_{12} + a_{22}s_2^2 + 2a_{26}s_2$$
$$p_3 = a_{16} + a_{26}s_1^2 + 2a_{66}s_1$$
$$q_3 = a_{16} + a_{26}s_2^2 + 2a_{66}s_2$$
$$p_4 = a_{11}/s_1 + 3a_{16} + (a_{12} + 2a_{66})s_1 + a_{26}s_1^2$$

$$q_4 = a_{11}/s_2 + 3a_{16} + (a_{12} + 2a_{66})s_2 + a_{26}s_2^2$$

Introducing new variables ζ_1 and ζ_2 ($z_1 = \zeta_1^2$, $z_2 = \zeta_2^2$), $F_1(z_1)$ and $F_2(z_2)$ can be expressed as

$$\begin{aligned} F_1(z_1(\zeta_1)) &= \sum_{j=1}^{N} [(\beta_{2j+1} + i\beta_{2N+2j+1})\zeta_1^{2j+1} \\ &\qquad + (\beta_{2j+2} + i\beta_{2N+2j+2})\zeta_1^{2j+2}] \\ F_2(z_2(\zeta_2)) &= \sum_{j=1}^{N} [(\gamma_{2j+1} + i\gamma_{2N+2j+1})\zeta_2^{2j+1} \\ &\qquad + (\gamma_{2j+2} + i\gamma_{2N+2j+2})\zeta_2^{2j+2}] \end{aligned} \tag{5.44}$$

By applying the Kirchhoff stress free condition along the crack surface, all γ's can be expressed in terms of β's. Hence all the field variables can be expressed in terms of β's only as:

$$\begin{aligned} w = 2\sum_{j=1}^{N} \{&\beta_{2j+1}[\mathrm{Re}(\zeta_1^{2j+1}) + A\mathrm{Re}(\zeta_2^{2j+1}) + D\mathrm{Im}(\zeta_2^{2j+1})] \\ &+ \beta_{2j+2}[\mathrm{Re}(\zeta_1^{2j+2}) + C\mathrm{Re}(\zeta_2^{2j+2}) + B\mathrm{Im}(\zeta_2^{2j+2})] \\ &- \beta_{2N+2j+1}[\mathrm{Im}(\zeta_1^{2j+1}) - B\mathrm{Re}(\zeta_2^{2j+1}) + C\mathrm{Im}(\zeta_2^{2j+1})] \\ &- \beta_{2N+2j+2}[\mathrm{Im}(\zeta_1^{2j+2}) - D\mathrm{Re}(\zeta_2^{2j+2}) + A\mathrm{Im}(\zeta_2^{2j+2})]\} \end{aligned}$$

$$\begin{aligned} M_x = -\frac{h^3}{24}\sum_{j=1}^{N} \{&(2j+1)(2j-1)\beta_{2j+1}[\mathrm{Re}(p_1\zeta_1^{2j-3}) + A\mathrm{Re}(q_1\zeta_2^{2j-3}) \\ &+ D\mathrm{Im}(q_1\zeta_2^{2j-3})] + (2j+2)(2j)\beta_{2j+2}[\mathrm{Re}(p_1\zeta_1^{2j-2}) \\ &+ C\mathrm{Re}(q_1\zeta_2^{2j-2}) + B\mathrm{Im}(q_1\zeta_2^{2j-2})] \end{aligned}$$

$$- (2j+1)(2j-1)\beta_{2N+2j+1}[\mathrm{Im}(p_1\zeta_1^{2j-3}) - B\mathrm{Re}(q_1\zeta_2^{2j-3})$$

$$+ C\mathrm{Im}(q_1\zeta_2^{2j-3})] - (2j+2)(2j)\beta_{2N+2j+2}[\mathrm{Im}(p_1\zeta_1^{2j-2})$$

$$- D\mathrm{Re}(q_1\zeta_2^{2j-2}) + A\mathrm{Im}(q_1\zeta_2^{2j-2})]\}$$

$$M_y = -\frac{h^3}{24}\sum_{j=1}^{N}\{(2j+1)(2j-1)\beta_{2j+1}[\mathrm{Re}(p_2\zeta_1^{2j-3}) + A\mathrm{Re}(q_2\zeta_2^{2j-3})$$

$$+ D\mathrm{Im}(q_2\zeta_2^{2j-3})] + (2j+2)(2j)\beta_{2j+2}[\mathrm{Re}(p_2\zeta_1^{2j-2})$$

$$+ C\mathrm{Re}(q_2\zeta_2^{2j-2}) + B\mathrm{Im}(q_2\zeta_2^{2j-2})]$$

$$- (2j+1)(2j-1)\beta_{2N+2j+1}[\mathrm{Im}(p_2\zeta_2^{2j-3}) - B\mathrm{Re}(q_2\zeta_2^{2j-3})$$

$$+ C\mathrm{Im}(q_2\zeta_2^{2j-3})] - (2j+2)(2j)\beta_{2N+2j+2}[\mathrm{Im}(p_2\zeta_1^{2j-2})$$

$$- D\mathrm{Re}(q_2\zeta_2^{2j-2}) + A\mathrm{Im}(q_2\zeta_2^{2j-2})]\}$$

$$M_{xy} = -\frac{h^3}{24}\sum_{j=1}^{N}\{(2j+1)(2j-1)\beta_{2j+1}[\mathrm{Re}(p_3\zeta_1^{2j-3}) + A\mathrm{Re}(q_3\zeta_2^{2j-3})$$

$$+ D\mathrm{Im}(q_3\zeta_2^{2j-3})] + (2j+2)(2j)\beta_{2j+2}[\mathrm{Re}(p_3\zeta_1^{2j-2})$$

$$+ C\mathrm{Re}(q_3\zeta_2^{2j-2}) + B\mathrm{Im}(q_3\zeta_2^{2j-2})]$$

$$- (2j+1)(2j-1)\beta_{2N+2j+1}[\mathrm{Im}(p_3\zeta_1^{2j-3}) - B\mathrm{Re}(q_3\zeta_2^{2j-3})$$

$$+ C\mathrm{Im}(q_3\zeta_2^{2j-3})] - (2j+2)(2j)\beta_{2N+2j+2}[\mathrm{Im}(p_3\zeta_1^{2j-2})$$

$$- D\mathrm{Re}(q_3\zeta_2^{2j-2}) + A\mathrm{Im}(q_3\zeta_2^{2j-2})]\}$$

$$Q_x = -\frac{h^3}{48}\sum_{j=1}^{N}\{(2j+1)(2j-1)(2j-3)\beta_{2j+1}[\mathrm{Re}(s_1p_4\zeta_1^{2j-5})$$

$$+ A\mathrm{Re}(s_2q_4\zeta_2^{2j-5}) + D\mathrm{Im}(s_2q_4\zeta_2^{2j-5})]$$

$$+ (2j+2)(2j)(2j-2)\beta_{2j+2}[\mathrm{Re}(s_1p_4\zeta_1^{2j-4}) + C\mathrm{Re}(s_2q_4\zeta_2^{2j-4})$$

$$+ B\mathrm{Im}(s_2q_4\zeta_2^{2j-4})]$$

$$- (2j+1)(2j-1)(2j-3)\beta_{2N+2j+1}[\mathrm{Im}(s_1p_4\zeta_1^{2j-5})$$

$$- B\mathrm{Re}(s_2q_4\zeta_2^{2j-5}) + C\mathrm{Im}(s_2q_4\zeta_2^{2j-5})]$$

$$- (2j+2)(2j)(2j-2)\beta_{2N+2j+2}[\mathrm{Im}(s_1p_4\zeta_1^{2j-4}) - D\mathrm{Re}(s_2q_4\zeta_2^{2j-4})$$

$$+ A\mathrm{Im}(s_2q_4\zeta_2^{2j-4})]\}$$

$$Q_y = \frac{h^3}{48}\sum_{j=1}^{N}\{(2j+1)(2j-1)(2j-3)\beta_{2j+1}[\mathrm{Re}(p_4\zeta_1^{2j-5})$$

$$+ A\mathrm{Re}(q_4\zeta_2^{2j-5}) + D\mathrm{Im}(q_4\zeta_2^{2j-5})]$$

$$+ (2j+2)(2j)(2j-2)\beta_{2j+2}[\mathrm{Re}(p_4\zeta_1^{2j-4}) + C\mathrm{Re}(q_4\zeta_2^{2j-4})$$

$$+ B\mathrm{Im}(q_4\zeta_2^{2j-4})] - (2j+1)(2j-1)(2j-3)\beta_{2N+2j+1}[\mathrm{Im}(p_4\zeta_1^{2j-5})$$

$$- B\mathrm{Re}(q_4\zeta_2^{2j-5}) + C\mathrm{Im}(q_4\zeta_2^{2j-5})]$$

$$- (2j+2)(2j)(2j-2)\beta_{2N+2j+2}[\mathrm{Im}(p_4\zeta_1^{2j-4}) - D\mathrm{Re}(q_4\zeta_2^{2j-4})$$

$$+ A\mathrm{Im}(q_4\zeta_2^{2j-4})]\} \qquad (5.45)$$

where

$$A = (f_4g_1 - f_2g_3)/(f_2g_4 - f_4g_2)$$

$$B = (f_1f_4 - f_2f_3)/(f_2g_4 - f_4g_2)$$

$$C = (f_3g_2 - f_1g_4)/(f_2g_4 - f_4g_2)$$

$$D = (g_1g_4 - g_2g_3)/(f_2g_4 - f_4g_2)$$

$$f_1 = \mathrm{Re}(p_2)$$

$$g_1 = \mathrm{Im}(p_2)$$

$$f_2 = \mathrm{Re}(q_2)$$

$$g_2 = \mathrm{Im}(q_2)$$

$$f_3 = \mathrm{Re}(p_4 - p_3)$$

$$g_3 = \mathrm{Im}(p_4 - p_3)$$

$$f_4 = \mathrm{Re}(q_4 - q_3)$$

$$g_4 = \mathrm{Im}(q_4 - q_3)$$

REFERENCES

1. Gallagher, R.H., "Survey and Evaluation of the Finite Element Method in Fracture Mechanics Analysis", Proc. 1st. Int. Conf. on Structural Mech. in Reactor Technology, Berlin, Vol. 6, Part L, pp. 637-653, 1971.

2. Jeram, K. and Hellen, T.K., "Finite Element Techniques in Fracture Mechanics", Int. Conf. on Welding Research Related to Power Plants, Southampton, U.K., 1972.

3. Rowe, G.H., "Matrix Displacement Methods in Fracture Mechanics Analysis of Reactor Vessels", Nuclear Engng. & Design, 20, pp. 251-263, 1972.

4. Hilton, P.D. and Sih, G., "Application of Finite Element Method to the Calculation of Stress Intensity Factor", Methods of Analysis and Solutions of Crack Problems, Edited by G. Sih, Noodhoff, Groningen, The Netherlands, pp. 426-483, 1972.

5. Rice, J.R. and Tracey, D.M., "Computational Fracture Mechanics in Structural Mechanics", Edited by S. Fenves et al., Academic Press, pp. 585-623, 1973.

6. Oglesby, J.J. and Lomacky, O., "An Evaluation of Finite Element Methods for the Computation of Elastic Stress Intensity Factors", J. of Engng. for Industry, 95, pp. 177-183, 1973.

7. Pian, T.H.H., "Crack Elements", Proc. World Congress on Finite Element Methods in Structural Mechanics, Robinson & Associates, Verwood, Dorset, England, Vol. 1, pp. F1-F39, 1975.

8. Tong, P. and Pian, T.H.H., "On the Convergence of the Finite Element Method for Problems with Singularity", Int. J. Solids Structures, Vol. 9, pp. 313-321, 1973.

9. Chan, S.K., Tuba, I.S. and Wilson, W.K., "On the Finite Element Method in Linear Fracture Mechanics", Engng. Fracture Mechanics, Vol. 2, pp. 1-17, 1970.

10. Byskov, I., "The Calculation of Stress Intensity Factors Using the Finite Element Method with Cracked Elements", Int. J. of Fracture Mechanics, 6, No. 2, pp. 159-167, 1970.

11. Tracey, D.M., "Finite Elements for Determination of Crack Tip Elastic Stress Intensity Factors", Engng. Fract. Mech., 3, pp. 255-265, 1971.

12. Pian, T.H.H., Tong, P. and Luk, C.H., "Elastic Crack Analysis by a Finite Element Method", Proc. Third Conf. on Matrix Methods in Structural Mechanics, Wright-Patterson Air Force Base, AFFDL-TR-71-160, pp. 661-682, 1971.

13. Rao, A.K., Krishna Murty, A.V. and Raju, I.S., "Special Finite Elements for the Analysis of Stress Concentrations and Singularities", Proc. First Int. Conf. on Structural Mech. in Reactor Technology, Berlin, Vol. 6, Part M, pp. 391-408, 1971.

14. Rao, A.K., Raju, I.S. and Krishna Murty, A.V., "A Powerful Hybrid Method in Finite Element Analysis", Int. J. Numer. Method Engng., 3, pp. 389-403, 1971.

15. Blackburn, W.S., "Calculation of Stress Intensity Factors at Crack Tips Using Special Finite Elements", The Mathematics of Finite Elements and Applications, Academic Press, pp. 327-336, 1973.

16. Tong, P. and Lasry, S., "A Super-Element for Crack Analysis", Int. J. of Fract., 9, pp. 234-235, 1973.

17. Luk, C.H., "Assumed Stress Hybrid Finite Element Method for Fracture Mechanics and Elastic-Plastic Analysis", M.I.T., Dept. of Aeronautics and Astronautics, Ph.D. Thesis, 1973.

18. Tong, P. and Pian, T.H.H., "Application of Finite Element Method to Mixed-Mode Fracture", Presented at Society of Engng. Science, 10th Anniv. Meeting, North Carolina State Univ., Raleigh, N.C., 1973.

19. Tong, P., Pian, T.H.H. and Lasry, S., "A Hybrid-Element Approach to Crack Problems with Singularity", Int. J. Numer. Methods in Engng., Vol. 7, pp. 297-308, 1973.

20. Yamamoto, Y., Tokuda, H. and Sumi, Y., "Finite Element Treatment of Singularities of Boundary Value Problems and its Application of Stress Intensity Factors", Theory and Practice in Finite Element Structural Analysis, Edited by Y. Yamamoto and R.H. Gallagher, Univ. of Tokyo Press, pp. 75-90, 1973.

21. Yamamoto, Y., "Finite Element Approaches with the Aid of Analytical Solutions", Recent Advances in Matrix Method of Structural Analysis & Design, Edited by R.H. Gallagher, Y. Yamada and T.J. Oden, UAH Press, pp. 85-103, 1973.

22. Henshell, R.D. and Shaw, K.G., "Crack Tip Finite Elements are Unnecessary", Int. J. for Numer. Methods in Engng., Vol. 9, pp. 495-507, 1975.

23. Atluri, S.N., Kobayashi, A.S. and Nakagaki, M., "An Assumed Displacement Hybrid Finite Element Method for Fracture Mechanics", Int. J. of Fract., Vol. 11, pp. 257-271, 1975.

24. Atluri, S.N., Kobayshi, A.S. and Nakagaki, M., "Fracture Mechanics Application of an Assumed Displacement Hybrid Finite Element Procedure", AIAA J., Vol. 13, pp. 734-739, 1975.

25. Orringer, O. and Stalk, G., "A Hybrid Finite Element of Stress Analysis of Fastener Details", Engng. Fract. Mechanics, Vol. 8, pp. 719-729, 1976.

26. Bloom, J.M., "Determination of Stress Intensity Factors for Axisymmetric Crack Problems", Int. J. of Fract., 12, pp. 771-773, 1976.

27. Freese, C.E. and Tracey, D.M., "The Natural Isoparametric Triangle Versus Collapsed Quadrilateral for Elastic Crack Analysis", Int. J. of Fract., 12, pp. 767-770, 1976.

28. Orringer, O., Lin, K.Y., Stalk, G., Tong, P. and Mar, J., "K-Solutions with Assumed Stress Hybrid Elements", J. of the Structural Div., American Society of Civil Engineers, pp. 321-334, 1977.

29. Griffith, A.A., "The Phenomenon of Rupture and Flow in Solids", Phil. Trans. Royal Society, London, Series A, Vol. 221, pp. 163, 1920.

30. Williams, M.L., "On the Stress Distribution at the Base of a Stationary Crack", J. Appl. Mech., 24, pp. 109-114, 1957.

31. Irwin, G.R., "Analysis of Stresses and Strains Near the End of a Crack Traversing a Plate", J. Appl. Mech., 24, pp. 361-364, 1957.

32. Sneddon, I.N., "The Distribution of Stress in the Neighborhood of a Crack in an Elastic Solid", Proc. of the Royal Society, Series A, 187, pp. 229-260, 1946.

33. Paris, P.C. and Sih, G.C., "Stress Analysis of Cracks", Fracture Toughness Testing, ASTM. STP., Vol. 381, pp. 30-83, 1965.

34. Liebowitz, H. (Ed.), Fracture-An Advanced Treatise, Academic Press, New York, 1968.

35. Cartwright, D.J. and Rooke, D.P., "Stress Intensity Factors: A Review", Report No. ME/71/39, Dept. of Mech. Engng., Univ. of Southampton, 1971.

36. Sih, G.C. (Ed.), "Mechanics of Fracture Vol. 1 - Methods of Analysis and Solutions of Crack Problems, Noordhoof, 1973.

37. Kassir, M.K. and Sih, G.C. (Ed.), "Three-Dimensional Crack Problems", Mechanics of Fracture 2, Noordhoff, Leyden, The Netherlands, 1975.

38. Kassir, M.K. and Sih, G.C., "Three-Dimensional Stress Distribution Around an Elliptical Crack Under Arbitrary Loadings", J. of Appl. Mech., pp. 601-611, 1966.

39. Smith, F.W., Emery, A.F. and Kobayashi, A.S., "Stress Intensity Factors for Semi-Circular Cracks, Part 2 - Semi-Infinite Solid", J. of Appl. Mech., 89, pp. 953-959, 1967.

40. Smith, F.W. and Alavi, M.J., "Stress Intensity Factors for a Part-Circular Surface Flaw", Proc. of the 1st Int. Conf. on Pressure Vessel Technology, Delft, The Netherlands, 1969.

41. Ayres, D.J., "A Numerical Procedure for Calculating Stress and Deformation Near a Slit in a Three-Dimensional Elastic-Plastic Solid", J. of Engng. Fract. Mech., 2, pp. 87-106, 1970.

42. Smith, F.W. and Alavi, M.J., "Stress Intensity Factors for a Penny Shaped Crack in a Halfspace", J. of Engng. Fract. Mech., 3, pp. 241-254, 1971.

43. Emery, A.F. and Segedin, C.M., "The Evaluation of the Stress Intensity Factors for Cracks Subjected to Tension, Torsion and Flexure by an Efficient Numerical Technique", J. of Basic Engng., 94, Series D, pp. 387-393, 1972.

44. Gyekenyesi, J.P., Mendelson, A. and Kring, J., "Three-Dimensional Elastic Stress and Displacement Analysis of Tensile Fracture Specimens Containing Cracks", NASA TN D-7213, 1973.

45. Hartranft, R.J. and Sih, G.C., "Alternating Method Applied to Edge and Surface Crack Problems", Method of Analysis and Solutions of Crack Problems, Edited by G.C. Sih, pp. 179-238, Noordhoff, Leyden, 1973.

46. Cruse, T.A., "Application of the Boundary-Integral Equation Method to Three-Dimensional Stress Analysis", Computers & Structures, 3, pp. 509-527, 1973.

47. Cruse, T.A., "An Improved Boundary-Integral Equation Method for Three-Demensional Elastic Stress Analysis", Computers & Structures, 4, pp. 741-754, 1974.

48. Smith, F.W. and Sorensen, D.R., "The Semi-Elliptical Surface Crack - A Solution by the Alternating Method", Int. J. of Fract., 12, No. 1, pp. 47-57, 1976.

49. Parmerter, R.R., "Stress Intensity Factors for Three-Dimensional Problems", AFRPL-TR-76-30, 1976.

50. Cruse, T.A. and Meyers, G.J., "Three-Dimensional Fracture Mechanics Analysis", J. of the Structural Div., American Society of Civil Engineers, pp. 309-320, 1977.

51. Kanazawa, T., et al., "A Study of the C.O.D. Concept for Brittle Fracture Initiation", Proc. of the 2nd Int. Conf. on Fracture, Brighton, pp. 1-14, 1969.

52. Rice, J.R., "A Path Independent Integral and the Approximate Analysis of Strain Concentration by Notches and Cracks", J. of Appl. Mech., 35, pp. 379-386, 1968.

53. Levy, N., Marcal, P.V. and Rice, J.R., "Progress in Three-Dimensional Elastic-Plastic Stress Analysis for Fracture Mechanics", Nuclear Engng. & Design, 17, pp. 64-75, 1971.

54. Levy, N. and Marcal, P.V., "Three-Dimensional Elastic-Plastic Stress and Strain Analysis for Fracture Mechanics, Phase 2, Improved Modelling", HSST Technical Report No. 17, 1971.

55. Miyamoto, H., "Application of Finite Element Method to Fracture Mechanics", Proc. 1st Int. Conf. on Structural Mech. in Reactor Technology, Berlin, Vol. 6, Part L, pp. 535-566, 1971.

56. Miyamoto, H. and Miyoshi, T., "Analysis of Stress Intensity Factor for Surface-Flawed Tension Plate", High Speed Computing of Elastic Structures, Edited by B.F. de Veubeke, pp. 137-156, Univ. of Liege, 1971.

57. Miyamoto, H., Shiratori, S. and Miyoshi, T., "Analysis of Stress and Strain Distribution at Crack Tip by the Finite Element Method", Recent Advances in Matrix Methods of Structural Analysis and Design, Edited by R.H. Gallagher, Y. Yamamoto and J.T. Oden, UAH Press, pp. 629-701, 1971.

58. Tracey, D.M., "3-D Elastic Singularity Element for Evaluation of K Along an Arbitrary Crack Front", Int. J. of Fract., 9, pp. 340-343, 1973.

59. Tracey, D.M., "Finite Elements for Three-Dimensional Elastic Crack Analysis", J. Nuc. Engng. & Design, 26, pp. 282-290, 1974.

60. Yamamoto, Y. and Sumi, Y., "Stress Intensity Factors of a Twisted Round Bar with a Circumferential Crack", Int. J. of Fract., 10, pp. 269-270, 1974.

61. Parks, D.M., "A Stiffness Derivative Finite Element Technique for Determination of Crack Tip Stress Intensity Factors", Int. J. Fract., 10, pp. 487-502, 1974.

62. Bergan, P.G. and Aamodt, B., "Finite Element Analysis of Crack Propagation in Three-Dimensional Solids Under Cyclic Loading", Nuclear Engng. & Design, 29, pp. 180-188, 1974.

63. Barsoum, R.S., "Application of Quadratic Isoparametric Finite Elements in Linear Fracture Mechanics", Int. J. of Fract., 10, pp. 603-605, 1974.

64. Miyata, H. and Kusumoto, S., "A Method of Evaluation of Three-Dimensional Stress Intensity Factor Using the Finite Element Method", Paper Presented at the JSME-ASME Joint Western Conf. on Applied Mech., Honolulu, Hawaii, March 24-27, 1975.

65. Hellen, T.K., "On the Method of Virtual Crack Extensions", Int. J. Num. Meth. Engng., 9, pp. 187-207, 1975.

66. Atluri, S.N., Kathiresan, K. and Kobayashi, A.S., "Three-Dimensional Linear Fracture Mechanics Analysis by a Displacement Hybrid Finite Element Model", Paper No. L/3, 3rd Int. Conf. on Structural Mech. in Reactor Technology, London, Sept. 1-5, 1975.

67. Barsoum, R.S., "On the Use of Isoparametric Finite Elements in Linear Fracture Mechanics", Int. J. Num. Meth. Engng., 10, pp. 25-37, 1976.

68. Barsoum, R.S., "A Degenerate Solid Element for Linear Fracture Analysis of Plate Bending and General Shells", Int. J. Num. Meth. Engng., 10, pp. 551-564, 1976.

69. Bloom, J.M. and Van Fossen, D.B., "An Evaluation of the 20-Node Quadratic Isoparametric Singularity Brick Element", Int. J. of Fract., 12, pp. 161-163, 1976.

70. Yamamoto, Y. and Sumi, Y., "Stress Intensity Factors for Three-Dimensional Cracks", Presented at the 14th Int. Congress on Theoretical & Applied Mechanics, Delft, 1976.

71. Hibbit, H.D., "Some Properties of Singular Isoparametric Elements", Int. J. Num. Meth. Engng., 11, pp. 180-184, 1977.

72. Blackburn, W.S. and Hellen, T.K., "Calculation of Stress Intensity Factors in Three-Dimensions by Finite Element Methods", Int. J. for Num. Meth. in Engng., 11, pp. 211-229, 1977.

73. Hellen, T.K., "On Special Isoparametric Elements for Linear Fracture Mechanics", Int. J. for Num. Meth. in Engng., 11, pp.200-203, 1977.

74. Tracey, D.M., "Discussion of 'On the Use of Isoparametric Finite Elements in Linear Fracture Mechanics' by R.S. Barsoum", Int. J. for Num. Meth. in Engng., 11, pp. 401-402, 1977.

75. Raju, I.S. and Newman, J.C., "Three-Dimensional Finite Element Analysis of Finite Thickness Fracture Specimens", NASA TN D-8414, May 1977.

76. Raju, I.S. and Newman, J.C., "Improved Stress-Intensity Factors for Semi-Elliptical Surface Cracks in Finite-Thickness Plates", to be Presented at the 4th Int. Conf. on Structural Mech. in Reactor Technology, California, U.S.A., Aug. 15-19, 1977.

77. Zienkiewicz, O.C., <u>The Finite Element Method in Engineering Science</u>, McGraw-Hill, New York, 1971.

78. Desai, C.S. and Abel, J.F., <u>Introduction to the Finite Element Method--A Numerical Method for Engineering Analysis</u>, Van Nostrand, 1972.

79. Brebbia, C.A. and Connor, J.J., Fundamentals of Finite Element Techniques for Structural Engineers, Butterworth, London, 1973.

80. Robinson, J., Integrated Theory of Finite Element Methods, John Wiley, London, Chapter 11, 1973.

81. Cook, R.D., Concepts and Applications of Finite Element Analysis, John Wiley & Sons, 1974.

82. Tong, P. and Rossettos, J.N., Finite Element Method--Basic Technique and Implementation, MIT Press, 1977.

83. Washizu, K., Variational Methods in Elasticity and Plasticity, Pergamon Press, Oxford, 1968.

84. Pian, T.H.H., "Variational Formulation", MIT, Dept. of Aeronautics and Astronautics, 16.29 Class Notes, 1976,

85. Pian, T.H.H., "Derivation of Element Stiffness Matrices by Assumed Stress Distributions", AIAA J., pp. 1333-1336, 1964.

86. Pian, T.H.H., "Element Stiffness Matrices for Boundary Compatibility and for Prescribed Boundary Stresses", Proc. of the 1st Conf. on Matrix Methods in Structural Mech., AFFDL-TR-66-80, pp. 457-477, 1967.

87. Tong, P. and Pian, T.H.H., "A Variational Principle and the Convergence of a Finite-Element Method Based on Assumed Stress Distribution", Int. J. Solids Structures, 5, pp. 463-472, 1969.

88. Tong, P., "New Displacement Hybrid Finite Element Model for Solid Continua", Int. J. for Num. Meth. in Engng., 2, pp. 78-83, 1970.

89. Pian, T.H.H., "Hybrid Models", Numerical & Computer Meth. in Structural Mech., Edited by S.J. Fenves et al., Academic Press, pp. 59-78, 1973.

90. Tong, P., "A Hybrid Crack Element for Rectilinear Anisotropic Material", Int. J. for Num. Meth. in Engng., 11, pp. 377-403, 1977.

91. Apostal, M.C., Lee, G.C., Braun, F.W. and Jordan, S., "Anisotropic Hybrid Displacement Singularity Element", J. of the Structural Div., American Society of Civil Engineers, pp. 335-354, 1977.

92. Lin, K.Y., "Fracture of Filamentary Composite Materials", Ph.D. Thesis, Dept. of Aeronautic and Astronautics, M.I.T., 1977.

93. Henshell, R.D., "Differences between Isoparametric Assumptions and True Circles", Int. J. for Num. Meth. in Engng., 10, pp. 1193-1195, 1976.

94. Peterson, K., "Derivation of the Stiffness Matrix for Hexahedron Elements by the Assumed Stress Hybrid Method", S.M. Thesis, Dept. of Aeronautics and Astronautics, M.I.T., 1972.

95. Lee, S.W., "An Assumed Hybrid Finite Element for Three-Dimensional Elastic Structural Analysis", S.M. Thesis, Dept. of Aeronautics and Astronautics, M.I.T., 1974.

96. Bowie, O.L., "Rectangular Tensile Sheet with Symmetric Edge Cracks", J. of Appl. Mech., 31, pp. 208-212, 1964.

97. Bowie, O.L. and Neal, D.M., "Single Edge Crack in Rectangular Tensile Sheet", J. of Appl. Mech., 32, pp. 708-709, 1965.

98. Collins, W.D., "Some Axially Symmetric Stress Distributions in Elastic Solids Containing Penny Shape Cracks 1 --Cracks in an Infinite Solid and a Thick Plate", Proc. Roy. Soc., Section A, 266, pp. 359-386, 1962.

99. Ishida, M., "Method of Laurent Series Expansion for Internal Crack Problems, Method of Analysis and Solutions of Crack Problems, Edited by G.C. Sih, Noordhoff, Leyden, pp. 56-130, 1973.

100. Timoshenko, S. and Woinowsky, S., <u>Theory of Plates and Shells</u>, McGraw-Hill, New York, 1959.

101. Williams, M.L., "The Bending Stress Distribution at the Base of a Stationary Crack", J. of Appl. Mech., 28, pp. 78-83, 1961.

102. Sih, G.C., Paris, P.C. and Erdogan, F., "Crack-Tip Stress-Intensity Factors for Plane Extension and Plate Bending Problems", J. of Appl. Mech, 29, pp. 306-312, 1962.

103. Sih, G.C. and Rice, J.R., "The Bending of Plates of Dissimilar Materials with Cracks", J. of Appl. Mech., pp. 477-482, 1964.

104. Erdogan, F., Tuncel, O. and Paris, P.C., "An Experimental Investigation of the Crack Tip Stress Intensity Factors in Plate Under Cylindrical Bending", J. of Appl. Mech., 84, pp. 542-546, 1962.

105. Reissner, E., "The Effect of Transverse Shear Deformation on the Bending of Elastic Plates", J. of Appl. Mech., 67, A69-A77, 1945.

106. Knowles, J.K. and Wang, N.M., "On the Bending of an Elastic Plate Containing a Crack", J. of Math. & Phys., 39, pp. 223-236, 1960.

107. Hartranft, R.J. and Sih, G.C., "Effect of Plate Thickness on the Bending Stress Distribution Around Through Cracks", J. of Math. & Phys., 47, pp. 276-291, 1968.

108. Wang, N.M., "Twisting of an Elastic Plate Containing a Crack", Int. J. of Fract. Mech., 6, No. 4, pp. 367-378, 1970.

109. Wilson, W.K. and Thompson, D.G., "On the Finite Element Method for Calculating Stress Intensity Factors for Cracked Plates in Bending", Engng. Fract. Mech., 3, pp. pp. 97-102, 1971.

110. Moriya, K., "Hybrid-Element for the Analysis of Cracked Plates Under Bending", Term Project for Course 16.28, M.I.T., May 1976.

111. Rhee, H.C., Atluri, S.N., Moriya, K. and Pian, T.H.H., "Hybrid Finite Element Procedures for Analyzing Through Flaws in Plates in Bending", to be presented at the 4th Int. Conf. on Structural Mech. in Reactor Technology, San Francisco, California, Aug. 15-19, 1977.

112. Muskhelishvili, N.I., "Some Basic Problems of Mathematical Theory of Elasticity", Noordhoff, Groningen, Holland, 1953.

113. Savin, G.N., Stress Concentration Around Holes", Pergamon Press, 1961.

114. Bowie, O.L. and Neal, D.M., "A Modified Mapping-Collocation Technique for Accurate Calculation of Stress-Intensity Factors", Int. J. Fract. Mech., 6, pp. 199-206, 1970.

115. Bowie, O.L. and Freese, C.E., "Central Crack in Plane Orthotropic Rectangular Sheet", Int. J. of Fract. Mech., 8, pp. 49-58, 1972.

116. Bowie, O.L., "Solutions of Plate Crack Problems by Mapping Technique", Mechanics of Fracture Vol. 1-- Method of Analysis and Solutions of Crack Problems, Edited by G.C. Sih, Noordhoff, pp. 1-55, 1973.

117. Zak, A.R. and Williams, M.L., "Crack Point Stress Singularities at a Bi-Material Interface", J. of Appl. Mech., pp. 142-143, 1963.

118. Erdogan, F., "Stress Distribution in a Nonhomogeneous Elastic Plane with Cracks", J. of Appl. Mech., pp. 232-236, 1963.

119. Rice, J.R. and Sih, G.C., "Plane Problems of Cracks in Dissimilar Media", J. of Appl. Mech., pp. 418-423, 1965.

120. Kathiresan, K., "Three-Dimensional Elastic Fracture Mechanics Analysis by a Displacement Hybrid Finite Element Model", Ph.D. Thesis, School of Engineering Science and Mechanics, Georgia Institute of Technology, 1976.

121 Atluri, S.N. and Kathiresan, K., "On a 3-D "Singularity Element" for Computation of Combined Mode Stress singularities", Advances in Engineering Science, Vol. 1, NASA CP-2001, pp. 267-274, 1976.

Author(s) (Year of Publication) [Reference]	Type of Crack Front Element	Special Technique	Method of the Determination of the S.I.F.	Mode of Deformation	Numerical Example	Typical No. of D.O.F. & Accuracy	Typical CPU Time & Remarks
Levy & Marcal (1971) [53,54]	8-node assumed displacement hexahedron element	Special displacement interpolation function which leads to 1/r plastic strain singularity	Extrapolation from S.I.F. determined by stress values	Mode I	Semi-elliptical surface crack	4500 d.o.f.	15 min. for elastic sol. 10-12 min. for each load increment
Miyamoto & Miyoshi (1971) [56]	Conventional 6-node pentahedron element built up from 3 4-node tetrahedron elements	Two level substructuring	C.O.D.	Mode I	Semi-elliptical surface crack	2337 d.o.f. for 1st step, 1772 d.o.f. for 2nd step	1814 sec for 1st step, 1457 sec for 2nd step
Tracey (1973, 1974) [58,59]	Assumed displacement 6-node pentahedron special element	Special displacement interpolation function which contains $\sqrt{r}$ terms	C.O.D. @ the nodes closest to the crack front	Mode I, II	Compact tension specimen, Penny shape crack, Semi-cicular surface crack Quarter-circular corner crack	2000 d.o.f. 6%	

TABLE 1

SURVEY OF FINITE ELEMENT MODELS FOR 3-D CRACK ANALYSIS

Bergan & Aamodt (1974) [62]	Conventional 20-node iso-parametric hexahedron element	Three level sub-structuring	Strain energy release rate	Mode I	Semi-elliptical surface crack	3360 d.o.f. (360 d.o.f. after condensation)	$1\frac{1}{2}$ hr for condensation, 1.6 sec for finite element solution
Miyata & Kusumoto (1975) [64]	Conventional 4-node constant strain tetrahedron element	Multi level sub-structuring, Stress averaging technique	Calibration of the stress value	Mode I, II,III	Semi-elliptical surface	Several thousand d.o.f.	
Atluri, Kathiresan (1975, 1976),[66, 120,121]	*Hybrid disp.* 20-node brick element with 6 curved faces	*Special disp.* & traction assumption containing the dominant singular sol.	Direct computation	Mode I, II & III	Many examples; *through cracks* surface flaws; loadings: single and mixed mode	2670 d.o.f.	(20 min)
Barsoum (1976) [67]	Isoparametric 20-node collapsed pentahedron element, 20-node hexahedron element	Placing the mid-side nodes @ the quarter point	C.O.D. @ the nodes closest to the crack front	Mode I, II	Compact tension specimen	2634 d.o.f.	
Bloom (1976) [69]	Isoparametric 20-node hexahedron element	Placing the mid-side nodes @ the quarter point	C.O.D.	Mode I	Compact tension specimen	1200,3528 & 4965 d.o.f.	

TABLE 1 (CONTINUED)

Yamamoto & Sumi (1976) [70]	Conventional 8-node hexahedron element	Superposition of analytical & finite element sol.		Mode I, III	Twisted round bar with a circumferential crack, Compact tension specimen Slit crack in an infinite plate	2106 d.o.f., Computation should be performed (2m+1) times where m is the no. of finite element layers	
Raju & Newman (1977) [75,76]	Assumed displacement 8-node collapsed pentahedron singularity element & 8-node hexahedron $\sqrt{r}$ element	Similar to that of Tracey's	Extrapolating from the stress values @ several reference points near crack front.	Mode I	Center crack, double edge & single edge crack specimen, Compact tension specimen, Semi-elliptical surface crack	1875 d.o.f. for straight crack, 4317 d.o.f. for curved crack. 5% accur.	
Blackburn & Hellen (1977) [72]	Assumed displacement 15-node pentahedron singularity element	Similar to that of Tracey's	C.O.D., Method of virtual crack extensions	Mode I, III	Edge cracked plate, Embedded penny shaped crack, Semi-circular surface crack, Elliptical shaped crack, etc.	50~100 quadratic elements. 1~4% accur.	5 min. on IBM 370/165

TABLE 1 (CONCLUDED)

$$\{\sigma\} = \{\sigma_x, \sigma_y, \sigma_z, \tau_{yz}, \tau_{zx}, \tau_{xy}\} = [P]\{\beta_1, \beta_2, \beta_3, \beta_4, \cdots\cdots, \beta_{22}, \beta_{23}, \beta_{24}\}$$

where

$$[P] = \begin{bmatrix} 1 & 0 & 0 & 0 & 0 & 0 & y & z & x & yz & 0 & 0 & 0 & 0 & 0 & 0 & 0 & 0 & 0 & 0 & 0 & 0 & 0 & 0 \\ 0 & 1 & 0 & 0 & 0 & 0 & 0 & 0 & 0 & 0 & x & z & y & xz & 0 & 0 & 0 & 0 & 0 & 0 & 0 & 0 & 0 & 0 \\ 0 & 0 & 1 & 0 & 0 & 0 & 0 & 0 & 0 & 0 & 0 & 0 & 0 & 0 & x & y & z & xy & 0 & 0 & 0 & 0 & 0 & 0 \\ 0 & 0 & 0 & 1 & 0 & 0 & 0 & 0 & 0 & 0 & 0 & 0 & 0 & 0 & 0 & 0 & -y & 0 & z & -y & 0 & x & 0 & 0 \\ 0 & 0 & 0 & 0 & 1 & 0 & 0 & 0 & -z & 0 & 0 & 0 & 0 & 0 & 0 & 0 & 0 & 0 & 0 & x & -z & 0 & y & 0 \\ 0 & 0 & 0 & 0 & 0 & 1 & 0 & 0 & 0 & 0 & 0 & 0 & -x & 0 & 0 & 0 & 0 & 0 & -x & 0 & y & 0 & 0 & z \end{bmatrix}$$

TABLE 2

24β POLYNOMIAL BASIS STRESS ASSUMPTION FOR A TYPE B CRACK ELEMENT

$$\{T\} = \{T_x, T_y, T_z\} = [R]\{\beta_1, \beta_2, \beta_3, \beta_4, \cdots\cdots\cdots, \beta_{22}, \beta_{23}, \beta_{24}\}$$

where

$$[R] = \begin{bmatrix} 1 & 0 & 0 & 0 & n & m & ly & lz & lx-nz & lyz & 0 & 0 & -mx & 0 & 0 & 0 & 0 & 0 & -mx & nx & my-nz & 0 & ny & mz \\ 0 & m & 0 & n & 0 & 1 & 0 & 0 & o & 0 & mx & mz & -lx+my & mzx & 0 & 0 & -ny & 0 & -lx+nz & -ny & ly & nx & 0 & lz \\ 0 & 0 & n & m & 1 & 0 & 0 & 0 & -lz & 0 & 0 & 0 & 0 & 0 & nx & ny & -my+nz & nxy & mz & lx-my & -lz & 0 & mx & ly \end{bmatrix}$$

l,m,n; Direction cosine of surface normal

TABLE 3

SURFACE TRACTIONS RELATED TO 24β POLYNOMIAL BASIS STRESS ASSUMPTION FOR TYPE B CRACK ELEMENT

$$\{\sigma\} = \{\sigma_x, \sigma_y, \sigma_z, \tau_{yz}, \tau_{zx}, \tau_{xy}\} = [P]\{\beta_1, \beta_2, \beta_3, \cdots\cdots\cdots\cdots\cdots\cdots, \beta_{22}, \beta_{23}, \beta_{24}\}$$

where

$$[P] = \begin{bmatrix} 1 & 0 & 0 & y & z & x & 0 & 0 & 0 & 0 & 0 & 0 & xy & yz & zx & 0 \\ 0 & 1 & 0 & 0 & 0 & 0 & z & x & y & 0 & 0 & 0 & 0 & 0 & 0 & yz \\ 0 & 0 & 0 & 0 & 0 & 0 & 0 & 0 & 0 & 0 & 0 & 0 & 0 & 0 & 0 & 0 \\ 0 & 0 & 0 & 0 & 0 & 0 & 0 & 0 & -z & z & 0 & 0 & 0 & 0 & 0 & 0 \\ 0 & 0 & 0 & 0 & 0 & -z & 0 & 0 & 0 & 0 & z & 0 & -yz & 0 & 0 & 0 \\ 0 & 0 & 1 & 0 & 0 & 0 & 0 & 0 & 0 & -x & -y & z & 0 & 0 & -yz & -zx \end{bmatrix}$$

$$\begin{bmatrix} 0 & 0 & x^2 & x^2 & 0 & x^2y & 0 & x^2z \\ zx & xy & 0 & y^2 & y^2 & 0 & xy^2 & y^2z \\ 0 & 0 & z^2 & 0 & z^2 & yz^2 & z^2x & 0 \\ 0 & -zx & 0 & 0 & -2yz & 0 & -2xyz & 0 \\ 0 & 0 & -2zx & 0 & 0 & -2xyz & 0 & 0 \\ 0 & 0 & 0 & -2xy & 0 & 0 & 0 & -2xyz \end{bmatrix}$$

TABLE 4

24β POLYNOMIAL BASIS STRESS ASSUMPTION FOR A TYPE A CRACK ELEMENT

TABLE 5

SURFACE TRACTIONS RELATED TO 24β POLYNOMIAL

BASIS STRESS ASSUMPTION FOR TYPE A CRACK FRONT ELEMENT

$$\{T\} = \{T_x, T_y, T_z\} = [R]\{\beta_1, \beta_2, \beta_3, \beta_4, \beta_5, \cdots\cdots\cdots\cdots, \beta_{22}, \beta_{23}, \beta_{24}\}$$

where

$$[R] = \left[\begin{array}{ccccccccccccc} \ell & 0 & m & \ell y & \ell z & \ell x-nz & 0 & 0 & 0 & -mx & -my+nz & mz & \ell xy-nyz \\ 0 & m & \ell & 0 & 0 & 0 & mz & mx & my-nz & -\ell x+nz & -\ell y & \ell z & 0 \\ 0 & 0 & 0 & 0 & 0 & -\ell z & 0 & 0 & -mz & mz & \ell z & 0 & -\ell yz \end{array}\right.$$

$$\begin{array}{cccccccc} \ell yz & \ell zx-myz & -mzx & 0 & 0 & \ell x^2-2nzx & \ell x^2-2mxy & 0 \\ 0 & -\ell yz & -\ell zx+myz & mzx & mxy-nzx & 0 & -2\ell xy+my^2 & my^2-2nyz \\ 0 & 0 & 0 & 0 & -mzx & -2\ell zx+nz^2 & 0 & -2myz+nz^2 \end{array}$$

$$\left.\begin{array}{ccc} \ell x^2y-2nxyz & 0 & \ell x^2z-2mxyz \\ 0 & mxy^2-2nxyz & -2\ell xyz+my^2z \\ -2\ell xyz+nyz^2 & -2myz+nz^2x & 0 \end{array}\right]$$

$$\{\sigma\} = \{\sigma_x, \sigma_y, \sigma_z, \tau_{yz}, \tau_{zx}, \tau_{xy}\} = [P]\{\beta_1, \beta_2, \beta_3, \cdots\cdots\cdots, \beta_{43}, \beta_{44}, \beta_{45}\}$$

where

$$[P] = \begin{bmatrix} 1 & 0 & 0 & 0 & 0 & 0 & y & z & x & 0 & 0 & 0 & 0 & 0 & 0 \\ 0 & 1 & 0 & 0 & 0 & 0 & 0 & 0 & 0 & z & x & y & 0 & 0 & 0 \\ 0 & 0 & 1 & 0 & 0 & 0 & 0 & 0 & 0 & 0 & 0 & 0 & x & y & z \\ 0 & 0 & 0 & 1 & 0 & 0 & 0 & 0 & 0 & 0 & 0 & 0 & 0 & 0 & -y \\ 0 & 0 & 0 & 0 & 1 & 0 & 0 & 0 & -z & 0 & 0 & 0 & 0 & 0 & 0 \\ 0 & 0 & 0 & 0 & 0 & 1 & 0 & 0 & 0 & 0 & 0 & -x & 0 & 0 & 0 \end{bmatrix}$$

$$\begin{matrix} 0 & 0 & 0 & 0 & 0 & 0 & xy & yz & zx & 0 & 0 & 0 & 0 \\ 0 & 0 & 0 & 0 & 0 & 0 & 0 & 0 & 0 & xy & yz & zx & 0 \\ 0 & 0 & 0 & 0 & 0 & 0 & 0 & 0 & 0 & 0 & 0 & 0 & xy \\ 0 & 0 & x & z & -y & 0 & 0 & 0 & 0 & -zx & 0 & 0 & 0 \\ -z & 0 & 0 & 0 & x & y & -yz & 0 & 0 & 0 & 0 & 0 & 0 \\ y & z & 0 & -x & 0 & 0 & 0 & 0 & -yz & 0 & -zx & 0 & 0 \end{matrix}$$

TABLE 6

45β POLYNOMIAL BASIS STRESS ASSUMPTION FOR A TYPE B CRACK ELEMENT

$$
\begin{array}{ccccccccc}
0 & 0 & zx & xy & 0 & 0 & 0 & 0 & x^2 \\
0 & 0 & 0 & 0 & xy & yz & 0 & 0 & 0 \\
yz & zx & 0 & 0 & 0 & 0 & yz & zx & z^2 \\
0 & -xy & 0 & 0 & 0 & -z^2/2 & -y^2/2 & 0 & 0 \\
-xy & 0 & -z^2/2 & 0 & 0 & 0 & 0 & -x^2/2 & -2zx \\
0 & 0 & 0 & -y^2/2 & -x^2/2 & 0 & 0 & 0 & 0
\end{array}
$$

$$
\left.
\begin{array}{cccccccc}
x^2 & 0 & y^2 & z^2 & 0 & 0 & 0 & 0 \\
y^2 & y^2 & 0 & 0 & z^2 & x^2 & 0 & 0 \\
0 & z^2 & 0 & 0 & 0 & 0 & x^2 & y^2 \\
0 & -2yz & 0 & 0 & 0 & 0 & 0 & 0 \\
0 & 0 & 0 & 0 & 0 & 0 & 0 & 0 \\
-2xy & 0 & 0 & 0 & 0 & 0 & 0 & 0
\end{array}
\right]
$$

TABLE 6 (CONCLUDED)

TABLE 7

SURFACE TRACTIONS RELATED TO 45β POLYNOMIAL BASIS STRESS ASSUMPTION FOR TYPE B CRACK FRONT ELEMENT

$$\{T\} = \{T_x,\ T_y,\ T_z\} = [R]\{\beta_1,\ \beta_2,\ \beta_3,\ \beta_4,\ \beta_5, \cdots\cdots\cdots, \beta_{43},\ \beta_{44},\ \beta_{45}\}$$

where

$$[R] = \begin{bmatrix} \ell & 0 & 0 & 0 & n & m & \ell y & \ell z & \ell x-nz & 0 & 0 & -mx & 0 & 0 & 0 \\ 0 & m & 0 & n & 0 & \ell & 0 & 0 & 0 & mz & mx & -\ell x+my & 0 & 0 & -ny \\ 0 & 0 & n & m & \ell & 0 & 0 & 0 & -\ell z & 0 & 0 & 0 & nx & ny & -my+nz \end{bmatrix}$$

$$\begin{matrix} my-nz & mz & 0 & -mx & nx & ny & \ell xy-nyz & \ell yz & \ell zx-myz & 0 \\ \ell y & \ell z & nx & -\ell x+nz & -ny & 0 & 0 & 0 & -\ell yz & mxy-nzx \\ -\ell z & 0 & mx & mz & \ell x-my & \ell y & -\ell yz & 0 & 0 & -mzx \end{matrix}$$

$$\begin{matrix} -mzx & 0 & 0 & -nxy & 0 & \ell zx-nz^2/2 & \ell xy-my^2/2 & -mx^2/2 \\ -\ell zx+myz & mzx & 0 & 0 & -nxy & 0 & -\ell y^2/2 & -\ell x^2/2+mxy \\ 0 & 0 & nxy & -\ell xy+nyz & -mxy+nzx & -\ell z^2/2 & 0 & 0 \end{matrix}$$

TABLE 7 (CONCLUDED)

$$
\begin{matrix}
0 & 0 & -nx^2/2 & \ell x^2-2nzx & \ell x^2-2mxy & 0 & \ell y^2 & \ell z^2 \\
myz-nz^2/2 & -ny^2/2 & 0 & 0 & -2\ell xy+my^2 & my^2-2nyz & 0 & 0 \\
-mz^2/2 & -my^2/2+nyz & -\ell x^2/2+nzx & -2\ell zx+nz^2 & 0 & -2myz+nz^2 & 0 & 0
\end{matrix}
$$

$$
\left.\begin{matrix}
0 & 0 & 0 & 0 \\
mz^2 & mx^2 & 0 & 0 \\
0 & 0 & nx^2 & ny^2
\end{matrix}\right]
$$

AD-A069 748 MASSACHUSETTS INST OF TECH CAMBRIDGE AEROELASTIC AND--ETC F/G 20/11
HYBRID CRACK ELEMENTS FOR THREE-DIMENSIONAL SOLIDS AND PLATE BE--ETC(U)
SEP 77 K MORIYA F49620-77-C-0084

UNCLASSIFIED ASRL-TR-191-1 AFOSR-TR-79-0619 NL

3 OF 3
AD
A069748

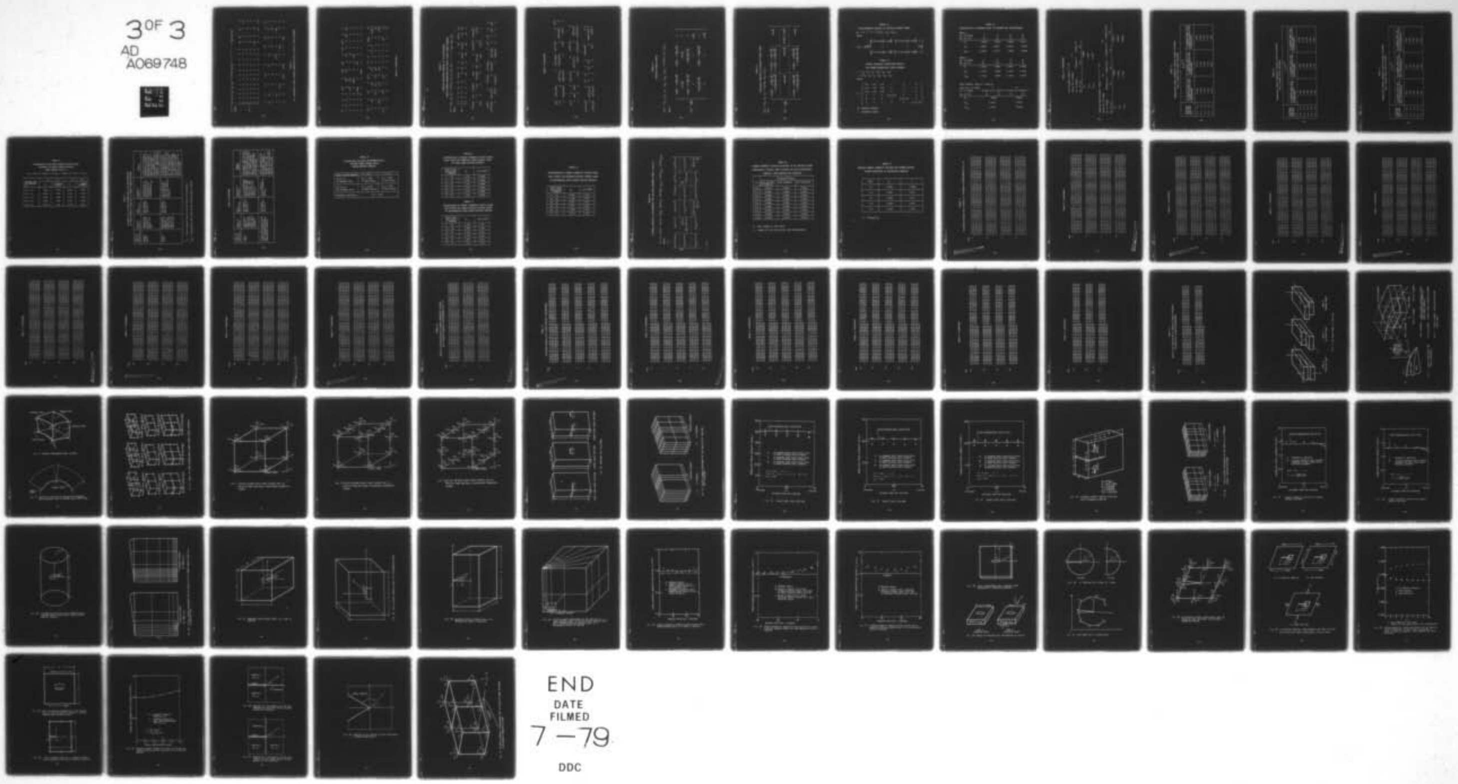

END
DATE
FILMED
7 -79
DDC

$$\{\sigma\} = \{\sigma_x, \sigma_y, \sigma_z, \tau_{yz}, \tau_{zx}, \tau_{xy}\} = [P]\{\beta_1, \beta_2, \beta_3, \ldots\ldots\ldots\ldots\ldots\ldots, \beta_{49}, \beta_{50}, \beta_{51}\}$$

where

$$[P] = \begin{bmatrix} 1 & 0 & 0 & y & z & x & 0 & 0 & 0 & 0 & 0 & 0 & xy & yz & zx & 0 \\ 0 & 1 & 0 & 0 & 0 & 0 & z & x & y & 0 & 0 & 0 & 0 & 0 & 0 & yz \\ 0 & 0 & 0 & 0 & 0 & 0 & 0 & 0 & 0 & 0 & 0 & 0 & 0 & 0 & 0 & 0 \\ 0 & 0 & 0 & 0 & 0 & 0 & 0 & 0 & -z & z & 0 & 0 & 0 & 0 & 0 & 0 \\ 0 & 0 & 0 & 0 & 0 & -z & 0 & 0 & 0 & 0 & z & 0 & -yz & 0 & 0 & 0 \\ 0 & 0 & 1 & 0 & 0 & 0 & 0 & 0 & 0 & -x & -y & z & 0 & 0 & -yz & -zx \end{bmatrix}$$

$$\begin{matrix} 0 & 0 & zx & xy & 0 & 0 & x^2 & x^2 & 0 & y^2 \\ zx & xy & 0 & 0 & xy & yz & 0 & y^2 & y^2 & 0 \\ 0 & 0 & 0 & 0 & 0 & 0 & z^2 & 0 & z^2 & 0 \\ 0 & -zx & 0 & 0 & 0 & -z^2/2 & 0 & 0 & -2yz & 0 \\ 0 & 0 & -z^2/2 & 0 & 0 & 0 & -2zx & 0 & 0 & 0 \\ 0 & 0 & 0 & -y^2/2 & -x^2/2 & 0 & 0 & -2xy & 0 & 0 \end{matrix}$$

TABLE 8

51β POLYNOMIAL BASIS STRESS ASSUMPTION FOR A TYPE A CRACK ELEMENT

z^2	0	0	0	x^2y	0	zx^2	xy^2	0	y^2z	yz^2	0	0
0	z^2	x^2	0	0	xy^2	y^2z	0	x^2y	0	0	zx^2	z^2x
0	0	0	0	yz^2	z^2x	0	0	0	0	0	0	0
0	0	0	0	0	$-2xyz$	0	0	$-zx^2$	0	0	0	0
0	0	0	0	$-2xyz$	0	0	$-y^2z$	0	0	0	0	0
0	0	0	z^2	0	0	$-2xyz$	0	0	0	0	0	0

z^2x	0	zx^2	0	$x^3/3$	0	y^3	z^3	0	0	$-2xyz$	0
0	yz^2	0	y^2z	0	$y^3/3$	0	0	z^3	x^3	0	$-2xyz$
0	0	$z^3/3$	$z^3/3$	z^2x	yz^2	0	0	0	0	0	0
0	$-z^3/3$	0	$-yz^2$	0	$-y^2z$	0	0	0	0	0	z^2x
$-z^3/3$	0	$-z^2x$	0	$-zx^2$	0	0	0	0	0	yz^2	0
0	0	0	0	0	0	0	0	0	0	0	0

TABLE 8 (CONCLUDED)

TABLE 9

SURFACE TRACTIONS RELATED TO 51 β POLYNOMIAL

BASIS STRESS ASSUMPTION FOR TYPE A CRACK FRONT ELEMENT

$$\{T\} = \{T_x, T_y, T_z\} = [R]\{\beta_1, \beta_2, \beta_3, \beta_4, \beta_5, \cdots\cdots\cdots\cdots, \beta_{49}, \beta_{50}, \beta_{51}\}$$

where

$$[R] = \left[\begin{array}{cccccccccccc} \ell & 0 & m & \ell y & \ell z & \ell x-nz & 0 & 0 & 0 & -mx & -my+nz & mz \\ 0 & m & \ell & 0 & 0 & 0 & mz & mx & my-nz & -\ell x+nz & -\ell y & \ell z \\ 0 & 0 & 0 & 0 & 0 & -\ell z & 0 & 0 & -mz & mz & \ell z & 0 \end{array}\right.$$

$$\begin{array}{cccccccc} \ell xy-nyz & \ell yz & \ell zx-myz & -mzx & 0 & 0 & \ell zx-nz^2/2 & \ell xy-my^2/2 \\ 0 & 0 & -\ell yz & -\ell zx+myz & mzx & mxy-nzx & 0 & -\ell y^2/2 \\ -\ell yz & 0 & 0 & 0 & 0 & -mzx & -\ell z^2/2 & 0 \end{array}$$

$$\begin{array}{ccccccccc} -mx^2/2 & 0 & \ell x^2-2nzx & \ell x^2-2mxy & 0 & \ell y^2 & \ell z^2 & 0 & 0 \\ -\ell x^2/2+mxy & myz-nz^2/2 & 0 & -2\ell xy+my^2 & my^2-2nyz & 0 & 0 & mz^2 & mx^2 \\ 0 & -mz^2/2 & -2\ell zx+nz^2 & 0 & -2myz+nz^2 & 0 & 0 & 0 & 0 \end{array}$$

TABLE 9 (CONCLUDED)

$$
\begin{array}{ccccccc}
mz^2 & \ell x^2y-2nxyz & 0 & \ell x^2z-2mxyz & \ell xy^2-ny^2z & 0 & \ell y^2z \\
\ell z^2 & 0 & mxy^2-2nxyz & -2\ell xyz+my^2z & 0 & mx^2y-nzx^2 & 0 \\
0 & -2\ell xyz+nyz^2 & -2mxyz+nz^2x & 0 & -\ell y^2z & -mzx^2 & 0
\end{array}
$$

$$
\begin{array}{ccccccc}
\ell yz^2 & 0 & 0 & \ell z^2x-nz^3/3 & 0 & \ell zx^2-nz^2x & 0 \\
0 & mzx^2 & mz^2x & 0 & myz^2-nz^3/3 & 0 & my^2z-nyz^2 \\
0 & 0 & 0 & -\ell z^3/3 & -mz^3/3 & -\ell z^2x+nz^3/3 & -myz^2+nz^3/3
\end{array}
$$

$$
\left.
\begin{array}{cccccccc}
\ell x^3/3-nzx^2 & 0 & \ell y^3 & \ell z^3 & 0 & 0 & -2\ell xyz+nyz^2 & 0 \\
0 & my^3/3-ny^2z & 0 & 0 & mz^3 & mx^3 & 0 & -2mxyz+nz^2x \\
-\ell zx^2+nz^2x & -my^2z+nyz^2 & 0 & 0 & 0 & 0 & \ell yz^2 & \ell mz^2x
\end{array}
\right]
$$

TABLE 10

SINGULAR STRESS MATRIX

$$\{\sigma_s\} = \{\sigma_{x_s}, \sigma_{y_s}, \sigma_{z_s}, \tau_{yz_s}, \tau_{zx_s}, \tau_{xy_s}\} = [P_s]\{K_I, K_{II}, K_{III}\}$$

where

$$[P_s] = \frac{1}{\sqrt{2\pi r}} \begin{bmatrix} \cos\frac{\theta}{2}(1 - \sin\frac{\theta}{2}\sin\frac{3\theta}{2}) & -\sin\frac{\theta}{2}(2 + \cos\frac{\theta}{2}\cos\frac{3\theta}{2}) & 0 \\ 2\nu\cos\frac{\theta}{2} & -2\nu\sin\frac{\theta}{2} & 0 \\ \cos\frac{\theta}{2}(1 + \sin\frac{\theta}{2}\sin\frac{3\theta}{2}) & \sin\frac{\theta}{2}\cos\frac{\theta}{2}\cos\frac{3\theta}{2} & 0 \\ 0 & 0 & \cos\frac{\theta}{2} \\ \sin\frac{\theta}{2}\cos\frac{\theta}{2}\cos\frac{3\theta}{2} & \cos\frac{\theta}{2}(1 - \sin\frac{\theta}{2}\sin\frac{3\theta}{2}) & 0 \\ 0 & 0 & -\sin\frac{\theta}{2} \end{bmatrix}$$

TABLE 11

TRACTIONS RELATED TO SINGULAR STRESS TERMS

$$\{T_s\} = \{T_x, T_y, T_z\} = [R_s]\{K_I, K_{II}, K_{III}\}$$

where

$$[R_s] = \frac{1}{\sqrt{2\pi r}} \left[\begin{array}{c|c|c} \ell\cos\frac{\theta}{2}(1 - \sin\frac{\theta}{2}\sin\frac{3\theta}{2}) + n\sin\frac{\theta}{2}\cos\frac{\theta}{2}\cos\frac{3\theta}{2} & -\ell\sin\frac{\theta}{2}(2 + \cos\frac{\theta}{2}\cos\frac{3\theta}{2}) + n\cos\frac{\theta}{2}(1 - \sin\frac{\theta}{2}\sin\frac{3\theta}{2}) & -m\sin\frac{\theta}{2} \\ \hline 2m\nu\cos\frac{\theta}{2} & -2m\nu\sin\frac{\theta}{2} & -\ell\sin\frac{\theta}{2} + n\cos\frac{\theta}{2} \\ \hline n\cos\frac{\theta}{2}(1 + \sin\frac{\theta}{2}\sin\frac{3\theta}{2}) + \ell\sin\frac{\theta}{2}\cos\frac{\theta}{2}\cos\frac{3\theta}{2} & \ell\cos\frac{\theta}{2}(1 - \sin\frac{\theta}{2}\sin\frac{3\theta}{2}) + n\sin\frac{\theta}{2}\cos\frac{\theta}{2}\cos\frac{3\theta}{2} & m\cos\frac{\theta}{2} \end{array} \right]$$

TABLE 12

DISPLACEMENTS RELATED TO SINGULAR STRESS TERMS

$\underset{\sim}{u}_s = \{u, v, w\} = [L_s]\{K_I, K_{II}, K_{III}\}$

where

$$[L_s] = \frac{1}{G}\left(\frac{2r}{\pi}\right)^{\frac{1}{2}}\begin{bmatrix} \frac{1}{8}\{(5-8\nu)\cos\frac{\theta}{2} - \cos\frac{3\theta}{2}\} & \frac{1}{8}\{(9-8\nu)\sin\frac{\theta}{2} + \sin\frac{3\theta}{2}\} & 0 \\ 0 & 0 & \sin\frac{\theta}{2} \\ \frac{1}{8}\{(7-8\nu)\sin\frac{\theta}{2} - \sin\frac{3\theta}{2}\} & \frac{1}{8}\{(-3+8\nu)\cos\frac{\theta}{2} - \cos\frac{3\theta}{2}\} & 0 \end{bmatrix}$$

TABLE 13

LINEAR ISOTROPIC COMPLIANCE MATRIX

FOR THREE-DIMENSIONAL CRACK ELEMENT

$\underset{\sim}{\varepsilon} = \{\varepsilon_x, \varepsilon_y, \varepsilon_z, \gamma_{yz}, \gamma_{zx}, \gamma_{xy}\}$

$= \underset{\sim}{C}\{\sigma_x, \sigma_y, \sigma_z, \tau_{yz}, \tau_{zx}, \tau_{xy}\}$

where

$$\underset{\sim}{C} = \begin{bmatrix} 1/E & -\nu/E & -\nu/E & 0 & 0 & 0 \\ -\nu/E & 1/E & -\nu/E & 0 & 0 & 0 \\ -\nu/E & -\nu/E & 1/E & 0 & 0 & 0 \\ 0 & 0 & 0 & 2(1+\nu)/E & 0 & 0 \\ 0 & 0 & 0 & 0 & 2(1+\nu)/E & 0 \\ 0 & 0 & 0 & 0 & 0 & 2(1+\nu)/E \end{bmatrix}$$

E; ELASTIC MODULUS

ν; POISSON'S RATIO

TABLE 14

EVALUATION OF DIFFERENT TYPES OF ELEMENT AND SUPERELEMENT

Type A

No. of Nodes	8	8	12	16
No. of β's	24	30	30	45
K_I	.94250	.94241	.98944	1.0031
K_{II}	1.0325	1.0287	1.0015	.97760
K_{III}	1.0574	1.0754	.99874	.99988

Type B

No. of Nodes	8	12	12	16
No. of β's	24	45	51	51
K_I	1.0126	.99841	1.0040	1.0040
K_{II}	1.0279	.99461	1.0012	1.0012
K_{III}	1.0019	.99896	1.0029	1.0029

Half Element (Type A + Type B)

Total No. of Nodes	12		20	
No. of Nodes	8(Type A)+8(Type B)		12(Type A)+12(Type B)	
No. of β's	24	24	30	45
K_I	.98245		.99608	
K_{II}	1.0136		.99647	
K_{III}	1.0257		.99886	

TABLE 14 (CONCLUDED)

Half Element (Type A' + B')

Total No. of Nodes	12	
No. of Nodes	8(Type A')	8(Type B')
No. of β's	24	24
K_I	.96286	
K_{II}	1.0497	
K_{III}	1.0257	

Complete Super Element (Type A + B + A' + B')

Total No. of Nodes	20		36	
No. of Nodes	8(Type A,A')	8(Type B,B')	12(Type A,A')	12(Type B,B')
No. of β's	24	24	30	45
K_I	.98025		.99312	
K_{II}	1.0290		.99619	
K_{III}	1.0257		.99886	

TABLE 15

NORMALIZED STRESS INTENSITY FACTORS ACROSS THICKNESS
FOR A SINGLE EDGE CRACK SPECIMEN

DISTANCE FROM THE MIDPLANE y/t	$K_I/\sigma a^{1/2}$		
	35 ELEMENT MESH WITH 12-NODE SINGULAR HALF SUPERELEMENT	85 ELEMENT MESH WITH 12-NODE SINGULAR HALF SUPERELEMENT	35 ELEMENT MESH WITH 20-NODE SINGULAR HALF SUPERELEMENT
0.0 ~ 0.2	4.668	5.133	4.898
0.2 ~ 0.4	4.658	5.122	4.880
0.4 ~ 0.6	4.632	5.092	4.852
0.6 ~ 0.8	4.603	5.053	4.747
0.8 ~ 1.0	4.520	4.592	4.584

TABLE 16

NORMALIZED STRESS INTENSITY FACTORS ACROSS THICKNESS
FOR A CENTER CRACK SPECIMEN

DISTANCE FROM THE MIDPLANE y/t	$K_I/\sigma a^{1/2}$		
	35 ELEMENT MESH WITH 12-NODE SINGULAR HALF SUPERELEMENT	85 ELEMENT MESH WITH 12-NODE SINGULAR HALF SUPERELEMENT	35 ELEMENT MESH WITH 20-NODE SINGULAR HALF SUPERELEMENT
0.0 ~ 0.2	1.853	2.098	2.138
0.2 ~ 0.4	1.852	2.096	2.135
0.4 ~ 0.6	1.849	2.092	2.130
0.6 ~ 0.8	1.846	2.086	2.097
0.8 ~ 1.0	1.841	2.074	2.089

TABLE 17

NORMALIZED STRESS INTENSITY FACTOR ACROSS THICKNESS
FOR A DOUBLE EDGE CRACK SPECIMEN

DISTANCE FROM THE MIDPLANE y/t	$K_I/\sigma a^{1/2}$		
	35 ELEMENT MESH SUB-DIVISION WITH 12-NODE HALF SUPERELEMENT	85 ELEMENT MESH SUB-DIVISION WITH 12-NODE HALF SUPERELEMENT	35 ELEMENT MESH SUB-DIVISION WITH 20-NODE HALF SUPERELEMENT
0.0 ~ 0.2	1.882	2.127	2.099
0.2 ~ 0.4	1.879	2.124	2.094
0.4 ~ 0.6	1.875	2.118	2.087
0.6 ~ 0.8	1.866	2.106	2.053
0.8 ~ 1.0	1.861	2.092	2.031

TABLE 18

DISTRIBUTION OF THE STRESS INTENSITY FACTOR ACROSS THICKNESS FOR COMPACT TENSION SPECIMEN (ASTM STANDARD E-399-72)

[$H = 0.6w$, $h = 0.275w$, $D = 0.25w$, $c = 0.25w$, $2t = 0.5w$, $\nu = 0.3$]

DISTANCE FROM THE MIDPLANE y/t	a/w = 3/8		a/w = 5/8	
	K_I	$K_I/\frac{T(2w+a)}{t(w-a)}$	K_I	$K_I/\frac{T(2w+a)}{t(w-a)}$
0.0 ~ 0.2	5.101	1.501	10.70	1.323
0.2 ~ 0.4	5.081	1.495	10.66	1.318
0.4 ~ 0.6	5.034	1.481	10.56	1.306
0.6 ~ 0.8	4.964	1.461	10.41	1.288
0.8 ~ 1.0	4.782	1.407	10.05	1.244

TABLE 19

COMPARISON OF 3-D FINITE ELEMENT MODELS FOR THE COMPUTATION OF STRESS INTENSITY FACTOR K_I OF A COMPACT TENSION SPECIMEN

Author(s) (Year of Publication)	Method of Analysis	Mesh Subdivision	Accuracy of Solution	Remarks
Yamamoto and Sumi (1976)	Superposition of analytical and finite element solution	480 elements 702 nodal pts. 2106 d.o.f.	Calculated K_c* is 6% above K_{2D}**, but with plane strain constraints, it coincides with K_{2D}	To solve on 3-D problem, computation of finite element solution should be performed (2m+1) times, where m is the number of finite element layers which subdivide the plate thickness. Application is limited to simple geometry.
Barsoum (1976)	Displacement method by isoparametric element with four mid-side nodes at the quarter points	150 elements 851 nodal pts. 2553 d.o.f.	K_c is within 2% of K_{2D}, which means up to 10% deviation from Yamamoto's solution	Stress intensity factor is calculated from the displacement solution for nodes closest to the crack tip. The element lacks the mode 3 singularity. The isoparametric element is a part of the element library of most general purpose programs, so its use is tractable.

*K_c: Stress intensity factor K_I at the center of the specimen.

**K_{2D}: 2-dimensional plane strain stress intensity factor solution.

TABLE 19 (CONCLUDED)

Author(s) (Year of Publication	Method of Analysis	Mesh Subdivision	Accuracy of Solution	Remarks Remarks
Tracey (1974)	Displacement model by wedge shape element with square root r displacement variation	522 elements 660 nodal pts. 1980 d.o.f.	K_c is 1% below K_{2D}, which means 9% deviation from Yamamoto's sol. With plane strain constraint, K_c is 6% below K_{2D}	The element lacks the constant strain and the rigid body motion modes and also lacks the mode 3 singularity. Stress intensity factor is inferred from the opening displacement of the crack face.
Present hybrid stress model including asymptotically exact stresses and boundary displacements assumption		85 elements 168 nodal pts. 504 d.o.f.	K_c is within 3% below of Yamamoto's solution	Stress intensity factors are directly computed. The element contains all singular modes. The accuracy is very high even when the very coarse mesh subdivision is used.

TABLE 20

CYLINDRICAL ROD WITH AXISYMMETRICALLY LOCATED PENNY SHAPED CRACK UNDER UNIFORM TENSION

Angle of One Sector	$\theta = 10^{\circ}$	$\theta = 5^{\circ}$
396 d.o.f. 52 Element Grid	$K_I = 1.583$ (1.20% Error)	$K_I = 1.556$ (2.87% Error)
810 d.o.f. 116 Element Grid	$K_I = 1.616$ (0.868% Error)	$K_I = 1.589$ (0.805% Error)
Benthem's Solution	$K_I = 1.602$	

TABLE 21

DISTRIBUTION OF STRESS INTENSITY FACTOR ALONG CRACK FRONT FOR EMBEDDED PENNY-SHAPED CRACK IN CUBE UNDER UNIFORM TENSION

Angle from the X-axis θ (degree)	K_I	$K_I/2\sigma\sqrt{a/\pi}$
0 ~ 15	1.578	0.9889
15 ~ 30	1.578	0.9889
30 ~ 45	1.578	0.9889
45 ~ 60	1.578	0.9889
60 ~ 75	1.578	0.9889
75 ~ 90	1.578	0.9889

TABLE 22

DISTRIBUTION OF STRESS INTENSITY FACTOR ALONG CRACK FRONT FOR SEMI-CIRCULAR SURFACE CRACK IN RECTANGULAR PRISM UNDER UNIFORM TENSION

Angle from the X-axis θ (degree)	K_I	$K_I/2\sigma\sqrt{a/\pi}$
0 ~ 15	1.820	1.141
15 ~ 30	1.698	1.064
30 ~ 45	1.652	1.035
45 ~ 60	1.629	1.021
60 ~ 75	1.618	1.013
75 ~ 90	1.613	1.011

TABLE 23

DISTRIBUTION OF STRESS INTENSITY FACTOR ALONG CRACK FRONT FOR QUARTER-CIRCULAR CORNER CRACK IN RECTANGULAR PRISM UNDER UNIFORM TENSION

Angle from the x-axis θ (degree)	K_I	$K_I/2\sigma\sqrt{a/\pi}$
0 ~ 15	1.813	1.136
15 ~ 30	1.708	1.070
30 ~ 45	1.677	1.051
45 ~ 60	1.677	1.051
60 ~ 75	1.708	1.070
75 ~ 90	1.813	1.136

TABLE 24

ASSUMED BOUNDARY DISPLACEMENTS FOR THE EDGE BETWEEN NODES p AND p+1

$$\underset{\sim}{u} = \{w,\ -\partial w/\partial x,\ -\partial w/\partial y\} = \underset{\sim}{L}\{w_{p},\ (\partial w/\partial x)_{p},\ (\partial w/\partial y)_{p},\ w_{p+1},\ (\partial w/\partial x)_{p+1},\ (\partial w/\partial y)_{p+1}\}$$

where

$$\underset{\sim}{L} = \left[\begin{array}{c|c|c|c|c|c}
(1-\xi)^2(1+2\xi) & \nu_y \ell\xi(1-\xi)^2 & -\nu_x \ell\xi(1-\xi)^2 & \xi^2(3-2\xi) & -\nu_y \ell\xi^2(1-\xi) & -\nu_x \ell\xi^2(1-\xi) \\
\hdashline
6\nu_y\xi(1-\xi)/\ell & \begin{array}{r} -\nu_x^2(1-\xi) \\ -\nu_y^2(1-\xi)(1-3\xi) \end{array} & -3\nu_x\nu_y\xi(1-\xi) & -6\nu_y\xi(1-\xi)/\ell & \begin{array}{r} -\nu_x^2\xi \\ +\ \nu_y^2\xi(2-3\xi) \end{array} & -3\nu_x\nu_y\xi(1-\xi) \\
\hdashline
-6\nu_x\xi(1-\xi)/\ell & -3\nu_x\nu_y\xi(1-\xi) & \begin{array}{r} -\nu_x^2(1-\xi)(1-3\xi) \\ -\ \nu_y^2(1-\xi) \end{array} & 6\nu_x\xi(1-\xi)/\ell & -3\nu_x\nu_y\xi(1-\xi) & \begin{array}{r} \nu_x^2\xi(2-3\xi) \\ -\ \nu_y^2\xi \end{array}
\end{array}\right]$$

$\xi = s/\ell$

TABLE 25

STRESS INTENSITY FACTOR SOLUTIONS OF AN INFINITE PLATE CONTAINING A FINITE CRACK SUBJECT TO PURE CYLINDRICAL BENDING, PURE BENDING AND TWISTING

ε/a	$K_{computed}/K_{exact}$		
	Pure Cylindrical Bending	Pure Bending	Pure Twisting
1/2	0.9897	0.9897	0.9902
1/3	0.9887	0.9887	0.9921
1/4	0.9883	0.9883	0.9929
1/5	0.9881	0.9881	0.9932
1/6	0.9880	0.9880	0.9935
1/7	0.9880	0.9880	0.9936
1/8	0.9879	0.9879	0.9937
1/9	0.9878	0.9879	0.9938
1/10	0.9878	0.9878	0.9939

a; Half Length of the Crack

ε; Length of the Crack within the Superelement

TABLE 26

BENDING STRESS INTENSITY FACTORS FOR CENTER CRACKED PLATES SUBJECTED TO CYLINDRICAL BENDING

2a/W	K_1	Y
0.1	2.669	0.9946
0.2	3.863	1.018
0.3	4.896	1.053
0.4	5.890	1.097
0.5	6.932	1.155

$Y = (h^2/6M_0a^{\frac{1}{2}})K_1$

TABLE 27

STIFFNESS MATRIX FOR 12-NODE 3-D UPPERHALF SUPERELEMENT (Fig. 41)

Row						
1	0.25272D+00	0.47413D-01	0.73224D-02	-0.33699D-01	0.94705D-01	-0.52311D-02
	-0.95316D-01	-0.14225D+00	-0.27948D-01	-0.10608D+00	0.25630D-01	-0.98161D-02
	0.20969D+00	0.17418D+00	0.27740D-01	-0.17420D+00	-0.18228D+00	0.11254D-02
	0.12975D+00	-0.68617D-02	0.96050D-02	-0.65819D-01	-0.14512D+00	0.41722D-02
	-0.31444D-01	0.10133D+00	-0.19174D-01	-0.16990D+00	0.46349D-01	-0.12720D-01
	0.19954D+00	-0.16848D+00	0.23224D-01	-0.11525D+00	0.15538D+00	0.17001D-02
2	0.47413D-01	0.64159D+00	-0.60915D-01	0.72806D-01	-0.87621D+00	0.60184D-01
	-0.29602D-01	0.11150D+01	-0.70130D-01	-0.20790D+00	-0.16578D+01	0.15586D+00
	0.24039D+00	0.10725D+01	-0.36703D-01	-0.12323D+00	-0.87959D+00	-0.82440D-02
	0.68617D-02	0.23138D+00	-0.61313D-01	-0.41631D-05	-0.14721D+00	-0.10038D+00
	0.59041D-01	0.42649D+00	0.75205D-01	-0.10302D-01	-0.19410D-01	0.50251D-01
	-0.34933D-01	0.12253D-01	-0.42699D-03	-0.20540D-01	0.80998D-01	-0.33918D-02
3	0.73224D-02	-0.60915D-01	0.31423D+00	-0.23211D-02	0.15782D+00	0.63094D-01
	-0.35661D-01	-0.16684D+00	-0.61562D-01	-0.15558D-01	0.32675D+00	-0.29286D+00
	0.39305D-01	-0.35979D+00	0.14906D+00	0.67306D-02	0.28468D+00	0.86176D-02
	0.96050D-02	0.61313D-01	0.10202D+00	-0.10575D-01	-0.76866D-01	-0.14994D-01
	-0.18697D-01	0.81265D-01	0.97575D-02	-0.62125D-02	-0.24589D+00	-0.23389D+00
	0.27741D-01	0.63047D-01	-0.32752D-01	-0.16795D-02	-0.64574D-01	-0.10720D-01
4	-0.33699D-01	0.72806D-01	-0.23211D-02	0.25137D+00	-0.24097D+00	-0.77187D-01
	0.86935D-02	0.20275D+00	-0.26118D-01	-0.11585D+00	-0.18334D+00	0.10115D+00
	-0.10436D-02	0.48773D-02	0.44415D-02	-0.17803D-03	-0.52666D-02	0.12518D-02
	-0.65819D-01	0.41631D-05	-0.10575D-01	0.71539D-01	0.13139D+00	-0.50891D-01
	0.34836D-01	-0.17625D+00	-0.44517D-02	-0.14924D+00	0.19273D+00	0.60882D-01
	-0.22906D-03	-0.27961D-02	0.29735D-02	-0.37639D-03	0.40758D-02	0.84288D-03

TABLE 27 (CONTINUED)

Row						
5	0.94705D-01	-0.87621D+00	0.15782D+00	-0.24097D+00	0.32869D+01	0.26576D+00
	-0.35700D-01	-0.38341D+01	-0.11575D+00	0.88216D-01	0.30012D+01	-0.17816D+00
	-0.36212D-02	0.70716D-02	0.56783D-02	0.11194D-02	-0.42590D-02	0.17414D-02
	0.14512D+00	-0.14721D+00	0.76866D-01	-0.13139D+00	-0.81931D+00	0.21789D+00
	-0.22029D+00	0.22960D+00	-0.24524D+00	0.30083D+00	-0.84735D+00	-0.18036D+00
	0.23110D-02	0.80858D-02	-0.50128D-02	-0.32522D-03	-0.44134D-02	-0.12367D-02
6	-0.52311D-02	0.60184D-01	0.63094D-01	-0.77187D-01	0.26576D+00	0.67080D+00
	-0.40718D-01	-0.15279D+00	-0.46625D+00	0.12303D+00	0.23332D-01	0.17418D-01
	-0.12284D-02	-0.52699D-02	-0.22575D-02	0.13503D-02	0.40969D-02	-0.13788D-03
	0.41722D-02	0.10038D+00	-0.14994D-01	-0.50891D-01	-0.21789D+00	0.66903D-01
	-0.74528D-01	0.26535D+00	-0.18662D+00	0.12168D+00	-0.34350D+00	-0.14730D+00
	-0.19847D-02	0.33374D-02	-0.89445D-03	0.15345D-02	-0.29912D-02	0.24183D-03
7	-0.95316D-01	-0.29602D-01	-0.35661D-01	0.86935D-02	-0.35700D-01	-0.40718D-01
	0.30055D+00	0.30155D-01	0.94332D-01	-0.23463D+00	-0.10859D+00	-0.18503D-01
	0.22187D-03	-0.11954D-02	-0.61739D-03	0.11422D-04	0.58020D-03	-0.12318D-03
	-0.31444D-01	-0.59041D-01	-0.18697D-01	0.34836D-01	0.22029D+00	-0.74528D-01
	0.14341D+00	-0.25242D+00	0.99258D-01	-0.12591D+00	0.23585D+00	-0.59889D-02
	-0.64039D-03	-0.10078D-02	0.93657D-03	0.22140D-03	0.68035D-03	0.30969D-03
8	-0.14225D+00	0.11150D+01	-0.16684D+00	0.20275D+00	-0.38341D+01	-0.15279D+00
	0.30155D-01	0.50347D+01	-0.34646D-02	-0.18869D+00	-0.38219D+01	0.22499D+00
	0.33197D-02	-0.39185D-02	-0.37105D-02	-0.13616D-02	0.18995D-02	-0.13161D-02
	-0.10133D+00	0.42649D+00	-0.81265D-01	0.17625D+00	0.22960D+00	-0.26535D+00
	0.25242D+00	0.61015D+00	0.28364D+00	-0.22970D+00	0.24516D+00	0.16039D+00
	-0.13395D-02	-0.79863D-02	0.46864D-02	-0.22693D-03	0.49119D-02	0.10229D-02

TABLE 27 (CONTINUED)

Row						
9	-0.27948D-01	-0.70130D-01	-0.61562D-01	-0.26118D-01	-0.11575D+00	-0.46625D+00
	0.94332D-01	-0.34646D-02	0.53720D+00	-0.40110D-01	0.43046D-01	-0.12032D+00
	0.45546D-03	0.31480D-02	0.12838D-02	-0.62877D-03	-0.20580D-02	0.86313D-04
	-0.19174D-01	-0.75205D-01	0.97575D-02	-0.44517D-02	0.24524D+00	-0.18662D+00
	0.99258D-01	-0.28364D+00	0.28208D+00	-0.76217D-01	0.25879D+00	0.53243D-02
	0.14709D-02	-0.53042D-03	-0.56252D-03	-0.87825D-03	0.56030D-03	-0.42798D-03
10	-0.10608D+00	-0.20790D+00	-0.15558D-01	-0.11585D+00	0.88216D-01	0.12303D+00
	-0.23463D+00	-0.18869D+00	-0.40110D-01	0.21476D+01	0.21538D+00	-0.36303D-01
	-0.14836D+01	-0.20740D+00	-0.35335D-01	0.48892D+00	0.37424D+00	-0.14919D-01
	-0.16990D+00	0.10302D-01	-0.62125D-02	-0.14924D+00	-0.30083D+00	0.12168D+00
	-0.12591D+00	0.22970D+00	-0.76217D-01	0.36153D+00	-0.17462D+00	-0.17182D-01
	-0.59045D+00	-0.27461D-01	0.62805D-02	-0.22375D-01	0.18904D+00	-0.91540D-02
11	0.25630D-01	-0.16578D+01	0.32675D+00	-0.18334D+00	0.30012D+01	0.23332D-01
	-0.10859D+00	-0.38219D+01	0.43046D-01	0.21538D+00	0.61819D+01	-0.52541D+00
	-0.69628D-01	-0.35873D+01	0.11836D+00	0.12075D+00	0.28774D+01	0.25349D-01
	-0.46349D-01	-0.19410D-01	0.24589D+00	-0.19273D+00	-0.84735D+00	0.34350D+00
	-0.23585D+00	0.24516D+00	-0.25879D+00	0.17462D+00	-0.21799D+01	-0.32002D+00
	0.75915D-01	0.10595D+01	-0.33045D-01	0.22420D+00	-0.12515D+01	0.11036D-01
12	-0.98161D-02	0.15586D+00	-0.29286D+00	0.10115D+00	-0.17816D+00	0.17418D-01
	-0.18563D-01	0.22499D+00	-0.12032D+00	-0.36303D-01	-0.52541D+00	0.78071D+00
	0.21317D-01	0.40311D+00	-0.26102D+00	-0.57694D-01	-0.33658D+00	-0.43238D-01
	-0.12720D-01	-0.50251D-01	-0.23389D+00	0.60882D-01	0.18036D+00	-0.14730D+00
	-0.59889D-02	-0.16039D+00	0.53243D-02	-0.17182D-01	0.32002D+00	0.39886D+00
	0.46165D-02	-0.24655D+00	-0.10028D+00	-0.29749D-01	0.21301D+00	-0.34100D-02

TABLE 27 (CONTINUED)

Row						
13	0.20969D+00	0.24039D+00	0.39305D-01	-0.10436D-02	-0.36212D-02	-0.12284D-02
	0.22187D-03	0.33197D-02	0.45546D-03	-0.14836D+01	-0.69628D-01	0.21317D-01
	0.15130D+01	0.33522D+00	-0.22522D-01	-0.52564D+00	-0.40856D+00	-0.19720D-01
	0.19954D+00	0.34933D-01	0.27741D-01	-0.22906D-03	-0.23110D-02	-0.19847D-02
	-0.64039D-03	0.13395D-02	0.14799D-02	-0.59045D+00	-0.75915D-01	0.46065D-02
	0.81809D+00	0.46970D-01	-0.38833D-01	-0.13897D+00	-0.10215D+00	-0.10616D-01
14	0.17418D+00	0.10725D+01	-0.35979D+00	0.48773D-02	0.70716D-02	-0.52699D-02
	-0.11954D-02	-0.39185D-02	0.31480D-02	-0.20740D+00	-0.35873D+01	0.40311D+00
	0.33522D+00	0.50419D+01	-0.34654D+00	-0.20966D+00	-0.38888D+01	-0.28713D-01
	0.16848D+00	0.12253D-01	-0.63047D-01	0.27961D-02	0.80858D-02	-0.33374D-02
	0.10078D-02	-0.79863D-02	0.53042D-03	0.27461D-01	0.10595D+01	0.24655D+00
	-0.46970D-01	-0.64885D+00	0.13528D+00	-0.24880D+00	0.93562D+00	0.18081D-01
15	0.27740D-01	-0.36703D-01	0.14906D+00	0.44415D-02	0.56783D-02	-0.22575D-02
	-0.61739D-03	-0.37105D-02	0.12838D-02	-0.35335D-01	0.11836D+00	-0.26102D+00
	-0.22522D-01	-0.34654D+00	0.31267D+00	0.26202D-01	0.26214D+00	0.15142D-01
	0.23224D-01	0.42699D-03	-0.32752D-01	0.29735D-02	0.50128D-02	-0.89445D-03
	0.93657D-03	-0.46864D-02	-0.56252D-03	0.62805D-02	0.33045D-01	-0.10028D+00
	-0.38833D-01	-0.13528D+00	-0.57452D-01	0.55093D-02	0.10227D+00	-0.22941D-01
16	-0.17420D+00	-0.12323D+00	0.67306D-02	-0.17803D-03	0.11194D-02	0.13503D-02
	0.11422D-04	-0.13616D-02	-0.62877D-03	0.48892D+00	0.12075D+00	-0.57694D-01
	-0.52564D+00	-0.20966D+00	0.26202D-01	0.42939D+00	0.31751D+00	0.32360D-01
	-0.11525D+00	0.20540D-01	-0.16795D-02	-0.37639D-03	0.32522D-03	0.15345D-02
	0.22140D-03	0.22693D-03	-0.87825D-03	-0.22375D-01	-0.22420D+00	-0.29749D-01
	-0.13897D+00	0.24880D+00	0.55093D-02	0.58448D-01	-0.15081D+00	0.16943D-01

TABLE 27 (CONTINUED)

Row						
17	-0.18228D+00	-0.87959D+00	0.28468D+00	-0.52666D-02	-0.42590D-02	0.40969D-02
	0.58020D-03	0.18995D-02	-0.20580D-02	0.37424D+00	0.28774D+01	-0.33658D+00
	-0.40856D+00	-0.38888D+01	0.26214D+00	0.31751D+00	0.33045D+01	0.36341D-01
	-0.15538D+00	0.80998D-01	0.64574D-01	-0.40758D-02	-0.44134D-02	0.29912D-02
	-0.68035D-03	0.49119D-02	-0.56030D-03	-0.18904D+00	-0.12515D+01	-0.21301D+00
	0.10215D+00	0.93562D+00	-0.10227D+00	0.15081D+00	-0.11768D+01	-0.35326D-03
18	0.11254D-02	-0.82440D-02	0.86176D-02	0.12518D-02	0.17414D-02	-0.13788D-03
	-0.12318D-03	-0.13161D-02	0.86313D-04	-0.14919D-01	0.25349D-01	-0.43238D-01
	-0.19720D-01	-0.28713D-01	0.15142D-01	0.32360D-01	0.36341D-01	0.39557D-01
	0.17001D-02	0.33918D-02	-0.10720D-01	0.84288D-03	0.12367D-02	0.24183D-03
	0.30969D-03	-0.10229D-02	-0.42798D-03	-0.91540D-02	-0.11036D-01	-0.34100D-02
	-0.10616D-01	-0.18081D-01	-0.22941D-01	0.16943D-01	0.35326D-03	0.17230D-01
19	0.12975D+00	0.68617D-02	0.96050D-02	-0.65819D-01	0.14512D+00	0.41722D-02
	-0.31444D-01	-0.10133D+00	-0.19174D-01	-0.16990D+00	-0.46349D-01	-0.12720D-01
	0.19954D+00	0.16848D+00	0.23224D-01	-0.11525D+00	-0.15538D+00	0.17001D-02
	0.25272D+00	-0.47413D-01	0.73224D-02	-0.33699D-01	-0.94705D-01	-0.52311D-02
	-0.95316D-01	0.14225D+00	-0.27948D-01	-0.10608D+00	-0.25630D-01	-0.98161D-02
	0.20969D+00	-0.17418D+00	0.27740D-01	-0.17420D+00	0.18228D+00	0.11254D-02
20	-0.68617D-02	0.23138D+00	0.61313D-01	0.41631D-05	-0.14721D+00	0.10038D+00
	-0.59041D-01	0.42649D+00	-0.75205D-01	0.10302D-01	-0.19410D-01	-0.50251D-01
	0.34933D-01	0.12253D-01	0.42699D-03	0.20540D-01	0.80998D-01	0.33918D-02
	-0.47413D-01	0.64159D+00	0.60915D-01	-0.72806D-01	-0.87621D+00	-0.60184D-01
	0.29602D-01	0.11150D+01	0.70130D-01	0.20790D+00	-0.16578D+01	-0.15586D+00
	-0.24039D+00	0.10725D+01	0.36703D-01	0.12323D+00	-0.87959D+00	0.82440D-02

TABLE 27 (CONTINUED)

Row						
21	0.96050D-02	-0.61313D-01	0.10202D+00	-0.10575D-01	0.76866D-01	-0.14994D-01
	-0.18697D-01	-0.81265D-01	0.97575D-02	-0.62125D-02	0.24599D+00	-0.23389D+00
	0.27741D-01	-0.63047D-01	-0.32752D-01	-0.16795D-02	0.64574D-01	-0.10720D-01
	0.73224D-02	0.60915D-01	0.31423D+00	-0.23211D-02	-0.15782D+00	0.63094D-01
	-0.35661D-01	0.16684D+00	-0.61562D-01	-0.15558D-01	-0.32675D+00	-0.29286D+00
	0.39305D-01	0.35979D+00	0.14906D+00	0.67306D-02	-0.28468D+00	0.86176D-02
22	-0.65819D-01	-0.41631D-05	-0.10575D-01	0.71539D-01	-0.13139D+00	-0.50891D-01
	0.34836D-01	0.17625D+00	-0.44517D-02	-0.14924D+00	-0.19273D+00	0.60882D-01
	-0.22906D-03	0.27961D-02	0.29735D-02	-0.37639D-03	-0.40758D-02	0.84288D-03
	-0.33699D-01	-0.72806D-01	-0.23211D-02	0.25137D+00	0.24097D+00	-0.77187D-01
	0.86935D-02	-0.20275D+00	-0.26118D-01	-0.11585D+00	0.18334D+00	0.10115D+00
	-0.10436D-02	-0.48773D-02	0.44415D-02	-0.17803D-03	0.52666D-02	0.12518D-02
23	-0.14512D+00	-0.14721D+00	-0.76866D-01	0.13139D+00	-0.81931D+00	-0.21789D+00
	0.22029D+00	0.22960D+00	0.24524D+00	-0.30083D+00	-0.84735D+00	0.18036D+00
	-0.23110D-02	0.80858D-02	0.50128D-02	0.32522D-03	-0.44134D-02	0.12367D-02
	-0.94705D-01	-0.87621D+00	-0.15782D+00	0.24097D+00	0.32869D+01	-0.26576D+00
	0.35700D-01	-0.38341D+01	0.11575D+00	-0.88216D-01	0.30012D+01	0.17816D+00
	0.36212D-02	0.70716D-02	-0.56783D-02	-0.11194D-02	-0.42590D-02	-0.17414D-02
24	0.41722D-02	-0.10038D+00	-0.14994D-01	-0.50891D-01	0.21789D+00	0.66903D-01
	-0.74528D-01	-0.26535D+00	-0.18662D+00	0.12168D+00	0.34350D+00	-0.14730D+00
	-0.19847D-02	-0.33374D-02	-0.89445D-03	0.15345D-02	0.29912D-02	0.24183D-03
	-0.52311D-02	-0.60184D-01	0.63094D-01	-0.77187D-01	-0.26576D+00	0.67080D+00
	-0.40718D-01	0.15279D+00	-0.46625D+00	0.12303D+00	-0.23332D-01	0.17418D-01
	-0.12284D-02	0.52699D-02	-0.22575D-02	0.13503D-02	-0.40969D-02	-0.13788D-03

TABLE 27 (CONTINUED)

Row						
25	-0.31444D-01	0.59041D-01	-0.18697D-01	0.34836D-01	-0.22029D+00	-0.74528D-01
	0.14341D+00	0.25242D+00	0.99258D-01	-0.12591D+00	-0.23585D+00	-0.59889D-02
	-0.64039D-03	0.10078D-02	0.93657D-03	0.22140D-03	-0.68035D-03	0.30969D-03
	-0.95316D-01	0.29602D-01	-0.35661D-01	0.86935D-02	0.35700D-01	-0.40718D-01
	0.30055D+00	-0.30155D-01	0.94332D-01	-0.23463D+00	0.10859D+00	-0.18503D-01
	0.22187D-03	0.11954D-02	-0.61739D-03	0.11422D-04	-0.58020D-03	-0.12318D-03
26	0.10133D+00	0.42649D+00	0.81265D-01	-0.17625D+00	0.22960D+00	0.26535D+00
	-0.25242D+00	0.61015D+00	-0.28364D+00	0.22970D+00	0.24516D+00	-0.16039D+00
	0.13395D-02	-0.79863D-02	-0.46864D-02	0.22693D-03	0.49119D-02	-0.10229D-02
	0.14225D+00	0.11150D+01	0.16684D+00	-0.20275D+00	-0.38341D+01	0.15279D+00
	-0.30155D-01	0.50347D+01	0.34646D-02	0.18869D+00	-0.38219D+01	-0.22499D+00
	-0.33197D-02	-0.39185D-02	0.37105D-02	0.13616D-02	0.18995D-02	0.13161D-02
27	-0.19174D-01	0.75205D-01	0.97575D-02	-0.44517D-02	-0.24524D+00	-0.18662D+00
	0.99258D-01	0.28364D+00	0.28208D+00	-0.76217D-01	-0.25879D+00	0.53243D-02
	0.14799D-02	0.53042D-03	-0.56252D-03	-0.87825D-03	-0.56030D-03	-0.42798D-03
	-0.27948D-01	0.70130D-01	-0.61562D-01	-0.26118D-01	0.11575D+00	-0.46625D+00
	0.94332D-01	0.34646D-02	0.53720D+00	-0.40110D-01	-0.43046D-01	-0.12032D+00
	0.45546D-03	-0.31480D-02	0.12838D-02	-0.62877D-03	0.20580D-02	0.86313D-04
28	-0.16990D+00	-0.10302D-01	-0.62125D-02	-0.14924D+00	0.30083D+00	0.12168D+00
	-0.12591D+00	-0.22970D+00	-0.76217D-01	0.36153D+00	0.17462D+00	-0.17182D-01
	-0.59045D+00	0.27461D-01	0.62805D-02	-0.22375D-01	-0.18904D+00	-0.91540D-02
	-0.10608D+00	0.20790D+00	-0.15558D-01	-0.11585D+00	-0.88216D-01	0.12303D+00
	-0.23463D+00	0.18869D+00	-0.40110D-01	0.21476D+01	-0.21538D+00	-0.36303D-01
	-0.14836D+01	0.20740D+00	-0.35335D-01	0.48892D+00	-0.37424D+00	-0.14919D-01

TABLE 27 (CONTINUED)

Row						
29	0.46349D-01	-0.19410D-01	-0.24589D+00	0.19273D+00	-0.84735D+00	-0.34350D+00
	0.23585D+00	0.24516D+00	0.25879D+00	-0.17462D+00	-0.21799D+01	0.32002D+00
	-0.75915D-01	0.10595D+01	0.33045D-01	-0.22420D+00	-0.12515D+01	-0.11036D-01
	-0.25630D-01	-0.16578D+01	-0.32675D+00	0.18334D+00	0.30012D+01	-0.23332D-01
	0.10859D+00	-0.38219D+01	-0.43046D-01	-0.21538D+00	0.61819D+01	0.52541D+00
	0.69628D-01	-0.35873D+01	-0.11836D+00	-0.12075D+00	0.28774D+01	-0.25349D-01
30	-0.12720D-01	0.50251D-01	-0.23389D+00	0.60882D-01	-0.18036D+00	-0.14730D+00
	-0.59889D-02	0.16039D+00	0.53243D-02	-0.17182D-01	-0.32002D+00	0.39886D+00
	0.46065D-02	0.24655D+00	-0.10028D+00	-0.29749D-01	-0.21301D+00	-0.34100D-02
	-0.98161D-02	-0.15586D+00	-0.29286D+00	0.10115D+00	0.17816D+00	0.17418D-01
	-0.18503D-01	-0.22499D+00	-0.12032D+00	-0.36303D-01	0.52541D+00	0.78071D+00
	0.21317D-01	-0.40311D+00	-0.26102D+00	-0.57694D-01	0.33658D+00	-0.43238D-01
31	0.19954D+00	-0.34933D-01	0.27741D-01	-0.22906D-03	0.23110D-02	-0.19847D-02
	-0.64039D-03	-0.13395D-02	0.14799D-02	-0.59045D+00	0.75915D-01	0.46065D-02
	0.81809D+00	-0.46970D-01	-0.38833D-01	-0.13897D+00	0.10215D+00	-0.10616D-01
	0.20969D+00	-0.24039D+00	0.39305D-01	-0.10436D-02	0.36212D-02	-0.12284D-02
	0.22187D-03	-0.33197D-02	0.45546D-03	-0.14836D+01	0.69628D-01	0.21317D-01
	0.15130D+01	-0.33522D+00	-0.22522D-01	-0.52564D+00	0.40856D+00	-0.19720D-01
32	-0.16848D+00	0.12253D-01	0.63047D-01	-0.27961D-02	0.80858D-02	0.33374D-02
	-0.10078D-02	-0.79863D-02	-0.53042D-03	-0.27461D-01	0.10595D+01	-0.24655D+00
	0.46970D-01	-0.64885D+00	-0.13528D+00	0.24880D+00	0.93562D+00	-0.18081D-01
	-0.17418D+00	0.10725D+01	0.35979D+00	-0.48773D-02	0.70716D-02	0.52699D-02
	0.11954D-02	-0.39185D-02	-0.31480D-02	0.20740D+00	-0.35873D+01	-0.40311D+00
	-0.33522D+00	0.50419D+01	0.34654D+00	0.20966D+00	-0.38888D+01	0.28713D-01

TABLE 27 (CONCLUDED)

Row						
33	0.23224D-01	-0.42699D-03	-0.32752D-01	0.29735D-02	-0.50128D-02	-0.89445D-03
	0.93657D-03	0.46864D-02	-0.56252D-03	0.62805D-02	-0.33045D-01	-0.10028D+00
	-0.38833D-01	0.13528D+00	-0.57452D-01	0.55093D-02	-0.10227D+00	-0.22941D-01
	0.27740D-01	0.36703D-01	0.14906D+00	0.44415D-02	-0.56783D-02	-0.22575D-02
	-0.61739D-03	0.37105D-02	0.12838D-02	-0.35335D-01	-0.11836D+00	-0.26102D+00
	-0.22522D-01	0.34654D+00	0.31267D+00	0.26202D-01	-0.26214D+00	0.15142D-01
34	-0.11525D+00	-0.20540D-01	-0.16795D-02	-0.37639D-03	-0.32522D-03	0.15345D-02
	0.22140D-03	-0.22693D-03	-0.87825D-03	-0.22375D-01	0.22420D+00	-0.29749D-01
	-0.13897D+00	-0.24880D+00	0.55093D-02	0.58448D-01	0.15081D+00	0.16943D-01
	-0.17420D+00	0.12323D+00	0.67306D-02	-0.17803D-03	-0.11194D-02	0.13503D-02
	0.11422D-04	0.13616D-02	-0.62877D-03	0.48892D+00	-0.12075D+00	-0.57694D-01
	-0.52564D+00	0.20966D+00	0.26202D-01	0.42939D+00	-0.31751D+00	0.32360D-01
35	0.15538D+00	0.80998D-01	-0.64574D-01	0.40758D-02	-0.44134D-02	-0.29912D-02
	0.68035D-03	0.49119D-02	0.56030D-03	0.18904D+00	-0.12515D+01	0.21301D+00
	-0.10215D+00	0.93562D+00	0.10227D+00	-0.15081D+00	-0.11768D+01	0.35326D-03
	0.18228D+00	-0.87959D+00	-0.28468D+00	0.52666D-02	-0.42590D-02	-0.40969D-02
	-0.58020D-03	0.18995D-02	0.20580D-02	-0.37424D+00	0.28774D+01	0.33658D+00
	0.40856D+00	-0.38888D+01	-0.26214D+00	-0.31751D+00	0.33045D+01	-0.36341D-01
36	0.17001D-02	-0.33918D-02	-0.10720D-01	0.84288D-03	-0.12367D-02	0.24183D-03
	0.30969D-03	0.10229D-02	-0.42798D-03	-0.91540D-02	0.11036D-01	-0.34100D-02
	-0.10616D-01	0.18081D-01	-0.22941D-01	0.16943D-01	-0.35326D-03	0.17230D-01
	0.11254D-02	0.82440D-02	0.86176D-02	0.12518D-02	-0.17414D-02	-0.13788D-03
	-0.12318D-03	0.13161D-02	0.86313D-04	-0.14919D-01	-0.25349D-01	-0.43238D-01
	-0.19720D-01	0.28713D-01	0.15142D-01	0.32360D-01	-0.36341D-01	0.39557D-01

TABLE 28

MATRIX FOR EVALUATION OF STRESS INTENSITY FACTORS

FOR 12-NODE UPPERHALF SUPERELEMENT (Fig. 41)

Row						
1	0.10579D+00	0.39151D-01	-0.41399D+00	-0.72741D-02	-0.37517D-01	-0.11262D+00
	-0.11525D-01	0.65242D-01	0.62764D-01	-0.97205D-01	-0.47770D+00	0.27582D+00
	0.15845D+00	0.46347D+00	0.18593D+00	-0.14824D+00	-0.39231D+00	0.21017D-02
	0.10579D+00	-0.39151D-01	-0.41399D+00	-0.72741D-02	0.37517D-01	-0.11262D+00
	-0.11525D-01	-0.65242D-01	0.62764D-01	-0.97205D-01	0.47770D+00	0.27582D+00
	0.15845D+00	-0.46347D+00	0.18593D+00	-0.14824D+00	0.39231D+00	0.21017D-02
2	-0.22922D+00	-0.80159D-02	0.99502D-01	-0.13302D+00	-0.42542D-01	-0.39519D-01
	-0.15034D-01	0.37451D-01	0.39754D-01	0.32965D+00	0.11716D+00	0.90625D-01
	0.69264D-01	-0.79259D-01	-0.13905D+00	-0.21639D-01	0.13751D+00	-0.51306D-01
	-0.22922D+00	0.80159D-02	0.99502D-01	-0.13302D+00	0.42542D-01	-0.39519D-01
	-0.15034D-01	-0.37451D-01	0.39754D-01	0.32965D+00	-0.11716D+00	0.90625D-01
	0.69264D-01	0.79259D-01	-0.13905D+00	-0.21639D-01	-0.13751D+00	-0.51306D-01
3	0.52595D-01	-0.27806D+00	-0.41178D+00	-0.31208D-01	-0.22729D+00	0.28979D-01
	0.33037D-01	0.17851D+00	-0.39251D-01	-0.13663D+00	0.45121D+00	0.34365D+00
	0.11378D+00	-0.29071D+00	-0.20505D+00	-0.27707D-01	0.16633D+00	-0.57119D-01
	-0.52595D-01	-0.27806D+00	0.41178D+00	0.31208D-01	-0.22729D+00	-0.28979D-01
	-0.33037D-01	0.17851D+00	0.39251D-01	0.13663D+00	0.45121D+00	-0.34365D+00
	-0.11378D+00	-0.29071D+00	0.20505D+00	0.27707D-01	0.16633D+00	0.57119D-01

TABLE 29

STIFFNESS MATRIX FOR 9-NODE BENDING SUPERELEMENT

Row						
1	0.60267E 00	0.17869E 00	-0.11393E 00	-0.33789E 00	-0.42398E-01	-0.13693E 00
	-0.10972E 00	0.49014E-01	-0.13082E 00	0.32804E-01	-0.60153E-02	-0.16412E-02
	-0.38389E-01	0.24814E-01	-0.10591E-01	0.28877E-01	-0.88688E-03	0.77536E-03
	-0.87385E-01	-0.88912E-02	0.34662E-01	0.82517E-02	-0.13231E-01	0.76328E-02
	-0.99228E-01	-0.30583E-01	-0.13699E-01			
2	0.17869E 00	0.12232E 00	-0.46666E-01	0.17612E-01	0.24655E-01	-0.22332E-02
	-0.13562E 00	0.30043E-01	-0.48199E-01	0.99556E-02	0.13280E-03	-0.14429E-02
	-0.17309E-01	0.87311E-02	-0.20274E-03	0.13619E-02	0.21728E-02	0.26160E-02
	-0.28255E-01	0.10651E-02	0.11052E-01	0.41450E-02	-0.33804E-02	0.29496E-02
	-0.30583E-01	-0.98772E-02	-0.31808E-02			
3	-0.11393E 00	-0.46666E-01	0.48443E-01	0.56562E-01	0.14176E-01	0.13545E-01
	0.42651E-01	-0.15704E-01	0.28563E-01	-0.59502E-02	0.36945E-02	0.10027E-02
	0.89592E-02	-0.65783E-02	0.19483E-02	-0.10444E-01	0.27011E-02	0.22286E-02
	0.10975E-01	0.42385E-02	-0.52332E-02	-0.25179E-02	0.22025E-02	0.84689E-03
	0.13700E-01	0.31810E-02	0.39066E-02			
4	-0.33789E 00	0.17613E-01	0.56562E-01	0.73369E 00	0.22512E 00	0.20375E 00
	-0.58275E 00	0.51088E-01	-0.24385E-01	0.12083E 00	-0.30004E-01	0.10601E-01
	0.59265E-01	-0.17915E-01	0.28327E-01	-0.46675E-01	0.60721E-02	0.70678E-02
	0.29340E-01	0.24784E-01	-0.68090E-02	0.15941E-01	0.56738E-02	-0.44642E-02
	0.82501E-02	0.41443E-02	0.25171E-02			
5	-0.42398E-01	0.24655E-01	0.14176E-01	0.22512E 00	0.12329E 00	0.59693E-01
	-0.19668E 00	0.31085E-02	-0.12335E-01	0.35242E-01	-0.76778E-02	-0.29993E-03
	-0.88594E-03	0.24672E-02	0.64104E-02	-0.51513E-02	0.98002E-03	0.12008E-02
	-0.76921E-02	0.34446E-02	0.47368E-02	0.56735E-02	-0.92718E-03	-0.52646E-03
	-0.13231E-01	-0.33804E-02	-0.22025E-02			

TABLE 29 (CONTINUED)

Row						
6	-0.13693E 00	-0.22332E-02	0.13545E-01	0.20375E 00	0.59693E-01	0.12168E 00
	-0.58288E-01	-0.28889E-02	0.19603E-01	0.77647E-02	0.23748E-02	-0.39502E-02
	0.18762E-02	0.17460E-03	0.52733E-02	-0.12028E-01	0.40880E-02	0.36690E-02
	-0.29731E-02	0.72495E-02	0.19988E-02	0.44640E-02	0.52643E-03	0.10929E-02
	-0.76326E-02	-0.29497E-02	0.84684E-03			
7	-0.10972E 00	-0.13562E 00	0.42652E-01	-0.58275E 00	-0.19668E 00	-0.58288E-01
	0.15522E 01	-0.59080E-02	0.39587E 00	-0.53031E 00	0.19379E 00	-0.48557E-01
	-0.26933E 00	0.18094E 00	0.58395E-01	0.46195E-01	0.20931E-02	-0.13442E-02
	-0.48266E-01	0.26158E-03	0.31166E-01	0.29339E-01	-0.76924E-02	0.29730E-02
	-0.87380E-01	-0.28253E-01	-0.10973E-01			
8	0.49014E-01	0.30043E-01	-0.15704E-01	0.51088E-01	0.31084E-02	-0.28888E-02
	-0.59081E-02	0.13037E 00	0.29515E-02	-0.12111E-01	-0.53571E-02	0.99025E-02
	-0.58337E-01	0.37083E-01	0.53116E-01	-0.39897E-01	0.42888E-02	0.64822E-02
	0.25944E-03	0.22293E-01	0.55514E-02	0.24787E-01	0.34453E-02	-0.72507E-02
	-0.88949E-02	0.10640E-02	-0.42392E-02			
9	-0.13082E 00	-0.48199E-01	0.28563E-01	-0.24385E-01	-0.12336E-01	0.19603E-01
	0.39587E 00	0.29516E-02	0.24527E 00	-0.20786E-01	0.13764E-01	0.20620E-01
	-0.18416E 00	0.63922E-01	0.27343E-01	0.23299E-01	-0.18150E-03	-0.10718E-02
	-0.31168E-01	-0.55514E-02	0.14667E-01	0.68097E-02	-0.47369E-02	0.19986E-02
	-0.34662E-01	-0.11052E-01	-0.52334E-02			
10	0.32804E-01	0.99557E-02	-0.59504E-02	0.12083E 00	0.35242E-01	0.77645E-02
	-0.53031E 00	-0.12111E-01	-0.20785E-01	0.72024E 00	-0.19792E 00	0.20596E 00
	-0.52943E 00	0.80355E-02	0.12627E-02	0.15747E 00	-0.11964E-01	-0.33652E-01
	0.46190E-01	-0.39899E-01	-0.23297E-01	-0.46673E-01	-0.51502E-02	0.12027E-01
	0.28873E-01	0.13601E-02	0.10442E-01			

TABLE 29 (CONTINUED)

Row						
11	-0.60152E-02	0.13276E-03	0.36946E-02	-0.30004E-01	-0.76777E-02	0.23748E-02
	0.19379E 00	-0.53571E-02	0.13764E-01	-0.19792E 00	0.12039E 00	-0.55587E-01
	0.44831E-01	0.24243E-01	0.13737E-01	-0.11964E-01	-0.49538E-02	-0.17100E-02
	0.20944E-02	0.42893E-02	0.18117E-03	0.60712E-02	0.97967E-03	-0.40877E-02
	-0.88476E-03	0.21735E-02	-0.27005E-02			
12	-0.16412E-02	-0.14430E-02	0.10027E-02	0.10601E-01	-0.29993E-03	-0.39502E-02
	-0.48557E-01	0.99025E-02	0.20620E-01	0.20596E 00	-0.55587E-01	0.12453E 00
	-0.19352E 00	0.11037E-01	-0.19994E-02	0.33652E-01	0.17101E-02	-0.49482E-02
	0.13440E-02	-0.64823E-02	-0.10718E-02	-0.70673E-02	-0.12006E-02	0.36689E-02
	-0.77659E-03	-0.26166E-02	0.22282E-02			
13	-0.38389E-01	-0.17309E-01	0.89590E-02	0.59265E-01	-0.88578E-03	0.18760E-02
	-0.26933E 00	-0.58337E-01	-0.18416E 00	-0.52943E 00	0.44830E-01	-0.19352E 00
	0.15558E 01	-0.39174E 00	0.31927E-06	-0.52944E 00	0.44832E-01	0.19352E 00
	-0.26931E 00	-0.58336E-01	0.18415E 00	0.59252E-01	-0.88996E-03	-0.18730E-02
	-0.38379E-01	-0.17304E-01	-0.89556E-02			
14	0.24814E-01	0.87311E-02	-0.65783E-02	-0.17915E-01	0.24673E-02	0.17471E-03
	0.18094E 00	0.37083E-01	0.63922E-01	0.80355E-02	0.24243E-01	0.11037E-01
	-0.39174E 00	0.24441E 00	-0.35137E-06	0.80387E-02	0.24243E-01	-0.11037E-01
	0.18093E 00	0.37083E-01	-0.63921E-01	-0.17908E-01	0.24693E-02	-0.17655E-03
	0.24809E-01	0.87295E-02	0.65769E-02			
15	-0.10591E-01	-0.20271E-03	0.19483E-02	0.28327E-01	0.64104E-02	0.52732E-02
	0.58394E-01	0.53116E-01	0.27343E-01	0.12628E-02	0.13738E-01	-0.19994E-02
	0.31927E-06	-0.35138E-06	0.11084E 00	-0.12618E-02	-0.13738E-01	-0.19996E-02
	-0.58397E-01	-0.53116E-01	0.27344E-01	-0.28328E-01	-0.64107E-02	0.52733E-02
	0.10591E-01	0.20288E-03	0.19483E-02			

TABLE 29 (CONTINUED)

Row						
16	0.28877E-01	0.13617E-02	-0.10444E-01	-0.46676E-01	-0.51516E-02	-0.12028E-01
	0.46195E-01	-0.39897E-01	0.23299E-01	0.15747E 00	-0.11963E-01	0.33652E-01
	-0.52943E 00	0.80388E-02	-0.12619E-02	0.72024E 00	-0.19792E 00	-0.20596E 00
	-0.53031E 00	-0.12110E-01	0.20788E-01	0.12082E 00	0.35241E-01	-0.77628E-02
	0.32810E-01	0.99573E-02	0.59516E-02			
17	-0.88671E-03	0.21728E-02	0.27011E-02	0.60723E-02	0.98009E-03	0.40879E-02
	0.20930E-02	0.42888E-02	-0.18149E-03	-0.11964E-01	-0.49538E-02	0.17101E-02
	0.44832E-01	0.24242E-01	-0.13738E-01	-0.19792E 00	0.12039E 00	0.55587E-01
	0.19379E 00	-0.53571E-02	-0.13765E-01	-0.30002E-01	-0.76769E-02	-0.23754E-02
	-0.60164E-02	0.13239E-03	-0.36949E-02			
18	0.77527E-03	0.26160E-02	0.22286E-02	0.70679E-02	0.12008E-02	0.36689E-02
	-0.13443E-02	0.64822E-02	-0.10718E-02	-0.33652E-01	-0.17100E-02	-0.49483E-02
	0.19352E 00	-0.11037E-01	-0.19995E-02	-0.20596E 00	0.55587E-01	0.12453E 00
	0.48559E-01	-0.99023E-02	0.20619E-01	-0.10601E-01	0.29996E-03	-0.39503E-02
	0.16402E-02	0.14428E-02	0.10024E-02			
19	-0.87385E-01	-0.28255E-01	0.10975E-01	0.29341E-01	-0.76918E-02	-0.29729E-02
	-0.48266E-01	0.25931E-03	-0.31168E-01	0.46189E-01	0.20945E-02	0.13440E-02
	-0.26931E 00	0.18093E 00	-0.58397E-01	-0.53031E 00	0.19379E 00	0.48559E-01
	0.15522E 01	-0.59105E-02	-0.39588E 00	-0.58273E 00	-0.19667E 00	0.58283E-01
	-0.10974E 00	-0.13563E 00	-0.42658E-01			
20	-0.88912E-02	0.10651E-02	0.42386E-02	0.24784E-01	0.34446E-02	0.72496E-02
	0.26180E-03	0.22293E-01	-0.55514E-02	-0.39899E-01	0.42893E-02	-0.64824E-02
	-0.58336E-01	0.37083E-01	-0.53116E-01	-0.12110E-01	-0.53571E-02	-0.99022E-02
	-0.59106E-02	0.13037E 00	-0.29508E-02	0.51092E-01	0.31096E-02	0.28874E-02
	0.49011E-01	0.30043E-01	0.15704E-01			

TABLE 29 (CONTINUED)

Row						
21	0.34662E-01	0.11052E-01	-0.52332E-02	-0.68093E-02	0.47370E-02	0.19987E-02
	0.31166E-01	0.55514E-02	0.14667E-01	-0.23297E-01	0.18112E-03	-0.10718E-02
	0.18415E 00	-0.63922E-01	0.27344E-01	0.20788E-01	-0.13765E-01	0.20619E-01
	-0.39588E 00	-0.29508E-02	0.24527E 00	0.24383E-01	0.12335E-01	0.19602E-01
	0.13083E 00	0.48202E-01	0.28565E-01			
22	0.82523E-02	0.41454E-02	-0.25180E-02	0.15941E-01	0.56737E-02	0.44638E-02
	0.29338E-01	0.24787E-01	0.68095E-02	-0.46673E-01	0.60710E-02	-0.70673E-02
	0.59253E-01	-0.17909E-01	-0.28328E-01	0.12082E 00	-0.30002E-01	-0.10601E-01
	-0.58273E 00	0.51092E-01	0.24384E-01	0.73367E 00	0.22512E 00	-0.20374E 00
	-0.33787E 00	0.17616E-01	-0.56557E-01			
23	-0.13231E-01	-0.33804E-02	0.22024E-02	0.56739E-02	-0.92718E-03	0.52642E-03
	-0.76928E-02	0.34454E-02	-0.47368E-02	-0.51501E-02	0.97961E-03	-0.12006E-02
	-0.89014F-03	0.24692F-02	-0.64106E-02	0.35241E-01	-0.76771E-02	0.29986E-03
	-0.19667E 00	0.31096E-02	0.12335E-01	0.22512E 00	0.12329E 00	-0.59691E-01
	-0.42394E-01	0.24656E-01	-0.14175E-01			
24	0.76329E-02	0.29497E-02	0.84686E-03	-0.44642E-02	-0.52654E-03	0.10929E-02
	0.29733E-02	-0.72506E-02	0.19987E-02	0.12028E-01	-0.40877E-02	0.36690E-02
	-0.18732E-02	-0.17643E-03	0.52733E-02	-0.77628E-02	-0.23754E-02	-0.39503E-02
	0.58283E-01	0.28874E-02	0.19602E-01	-0.20374E 00	-0.59691E-01	0.12168E 00
	0.13692E 00	0.22321E-02	0.13543E-01			

TABLE 29 (CONCLUDED)

Row						
25	-0.99228E-01	-0.30583E-01	0.13700E-01	0.82498E-02	-0.13231E-01	-0.76328E-02
	-0.87380E-01	-0.88948E-02	-0.34662E-01	0.28874E-01	-0.88490E-03	-0.77663E-03
	-0.38379E-01	0.24809E-01	0.10591E-01	0.32809E-01	-0.60165E-02	0.16401E-02
	-0.10974E 00	0.49011E-01	0.13083E 00	-0.33787E 00	-0.42393E-01	0.13692E 00
	0.60266E 00	0.17869E 00	0.11393E 00			
26	-0.30583E-01	-0.98772E-02	0.31810E-02	0.41440E-02	-0.33804E-02	-0.29496E-02
	-0.28253E-01	0.10639E-02	-0.11052E-01	0.13603E-02	0.21735E-02	-0.26166E-02
	-0.17304E-01	0.87296E-02	0.20291E-03	0.99573E-02	0.13242E-03	0.14426E-02
	-0.13563E 00	0.30043E-01	0.48202E-01	0.17615E-01	0.24656E-01	0.22321E-02
	0.17869E 00	0.12232E 00	0.46666E-01			
27	-0.13699E-01	-0.31808E-02	0.39066E-02	0.25171E-02	-0.22025E-02	0.84688E-03
	-0.10973E-01	-0.42392E-02	-0.52333E-02	0.10442E-01	-0.27005E-02	0.22282E-02
	-0.89557E-02	0.65769E-02	0.19483E-02	0.59515E-02	-0.36949E-02	0.10024E-02
	-0.42657E-01	0.15704E-01	0.28565E-01	-0.56557E-01	-0.14175E-01	0.13543E-01
	0.11393E 00	0.46666E-01	0.48442E-01			

TABLE 30

MATRIX FOR EVALUATION OF BENDING STRESS INTENSITY FACTORS FOR 9-NODE SUPERELEMENT

Row						
1	-0.93793E-01	-0.30052E-01	0.58450E-02	0.56850E-01	-0.13499E-03	0.52263E-02
	0.57644E-01	-0.35185E-02	-0.12453E-02	0.13052E-01	0.33134E-02	-0.29703E-02
	-0.67508E-01	0.28301E-01	0.45929E-07	0.13052E-01	0.33133E-02	0.29701E-02
	0.57649E-01	-0.35189E-02	0.12435E-02	0.56847E-01	-0.13514E-03	-0.52259E-02
	-0.93793E-01	-0.30053E-01	-0.58457E-02			
2	-0.26263E 00	-0.74729E-01	0.25911E-01	0.52402E-02	-0.26549E-01	-0.17627E-01
	-0.50905E-01	0.18747E-02	-0.24653E-01	0.37005E-01	-0.76636E-02	0.40534E-02
	0.64328E-06	-0.11214E-06	0.73108E-02	-0.37006E-01	0.76649E-02	0.40540E-02
	0.50907E-01	-0.18773E-02	-0.24653E-01	-0.52382E-02	0.26550E-01	-0.17628E-01
	0.26263E 00	0.74729E-01	0.25909E-01			

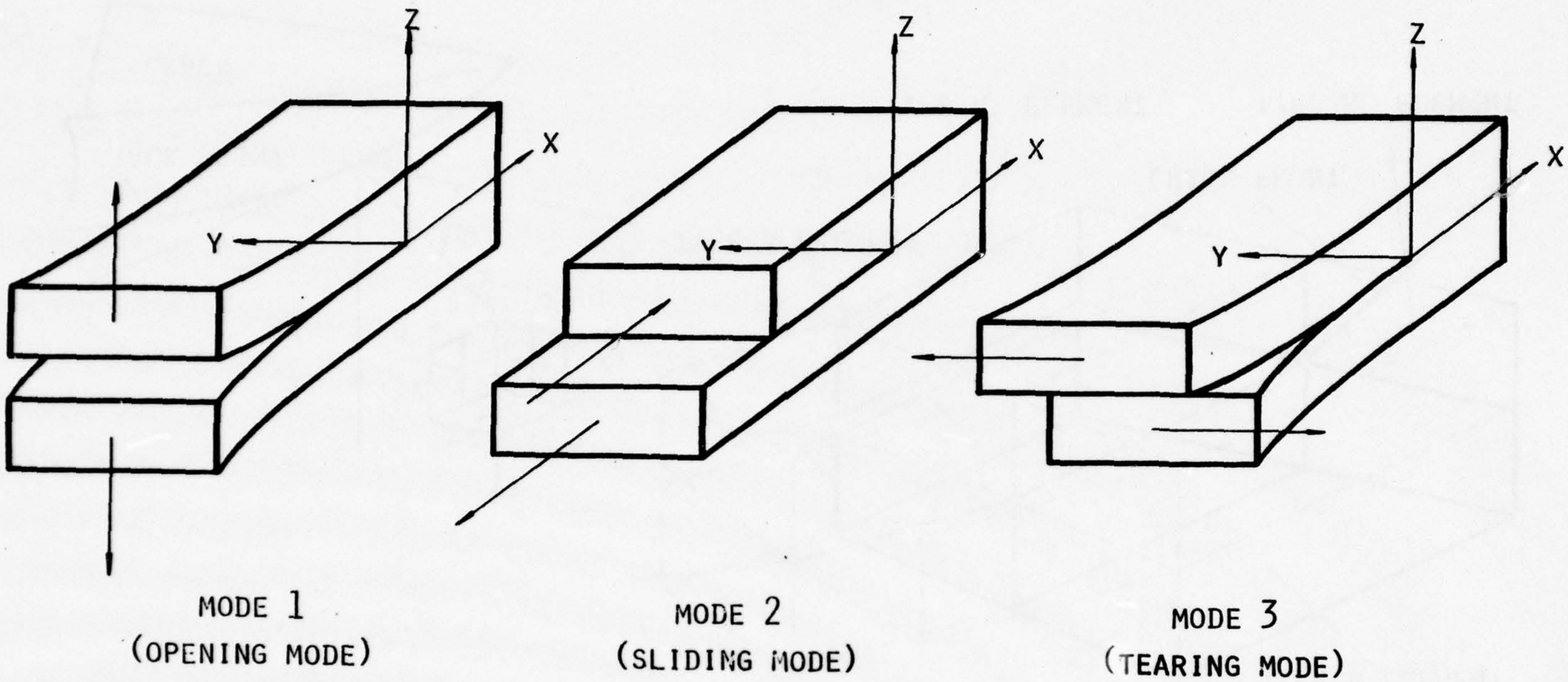

FIG. 1 THE THREE MODES OF FRACTURE

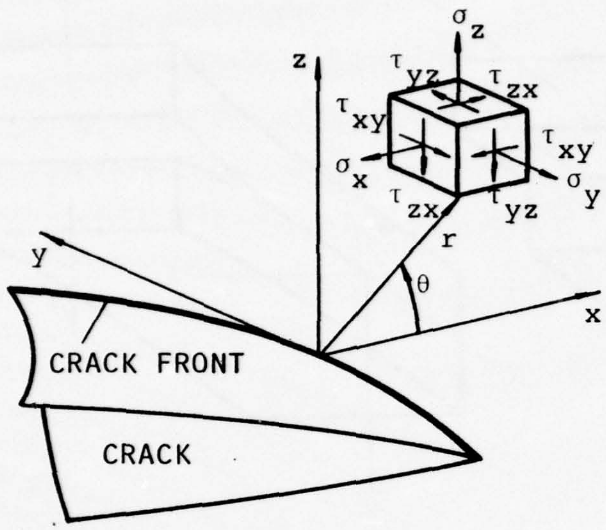

FIG. 2 LOCAL COORDINATES AND STRESS COMPONENTS

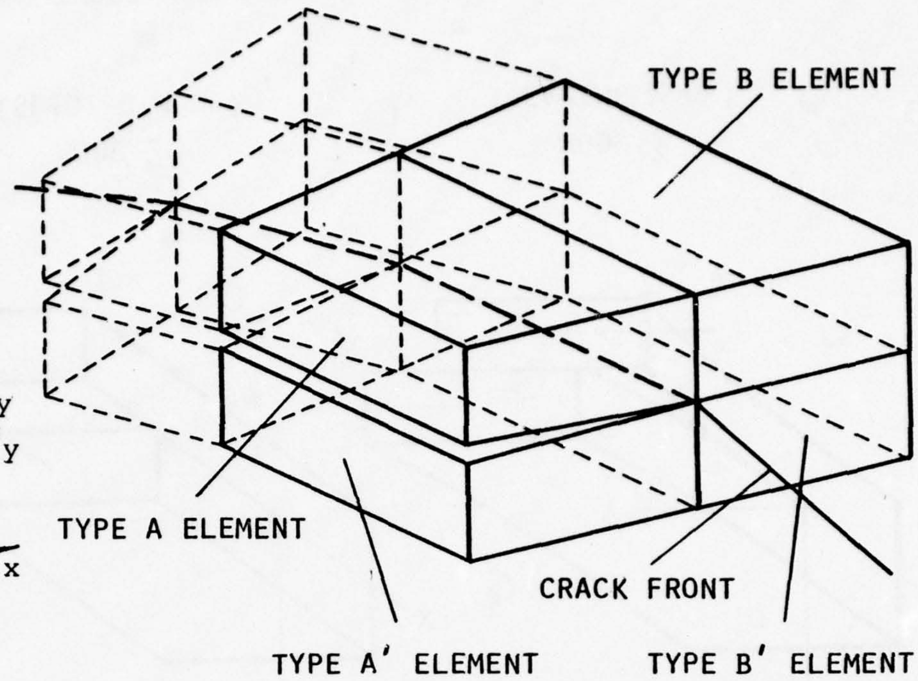

TYPE A ELEMENT: HYBRID STRESS SINGULAR ELEMENT WITH STRESS FREE CONDITION OVER CRACK SURFACE

TYPE B ELEMENT: HYBRID STRESS SINGULAR ELEMENT

FIG. 3 FINITE ELEMENT IDEALIZATION AROUND CRACK FRONT

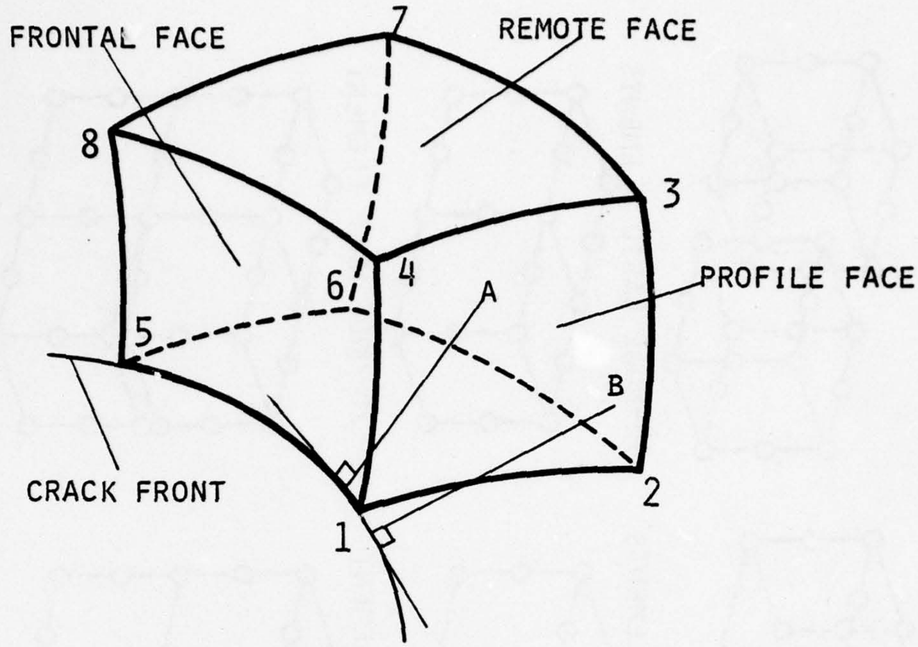

FIG. 4 GENERAL HEXAHEDRON CRACK ELEMENT

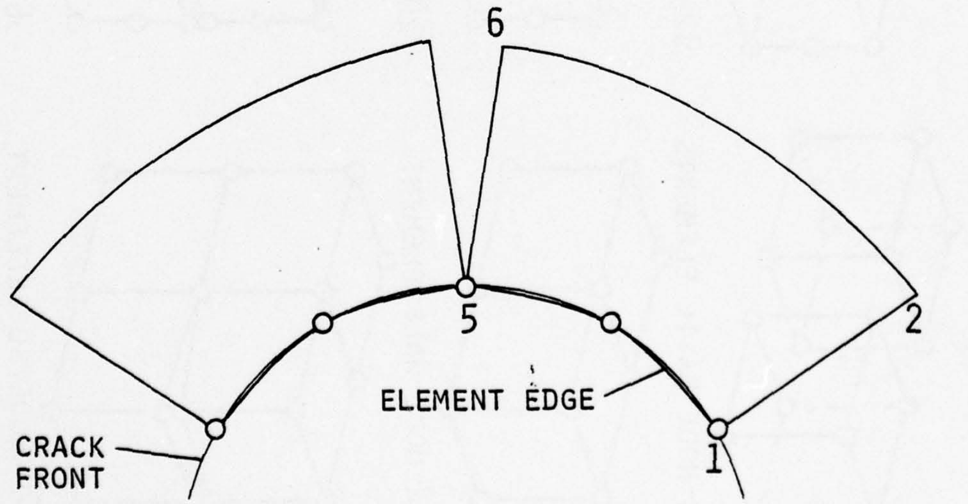

FIG. 5 GAPPING OR OVERLAPPING BETWEEN NEIGHBORING CRACK ELEMENTS WITH A CURVED CRACK FRONT EDGE

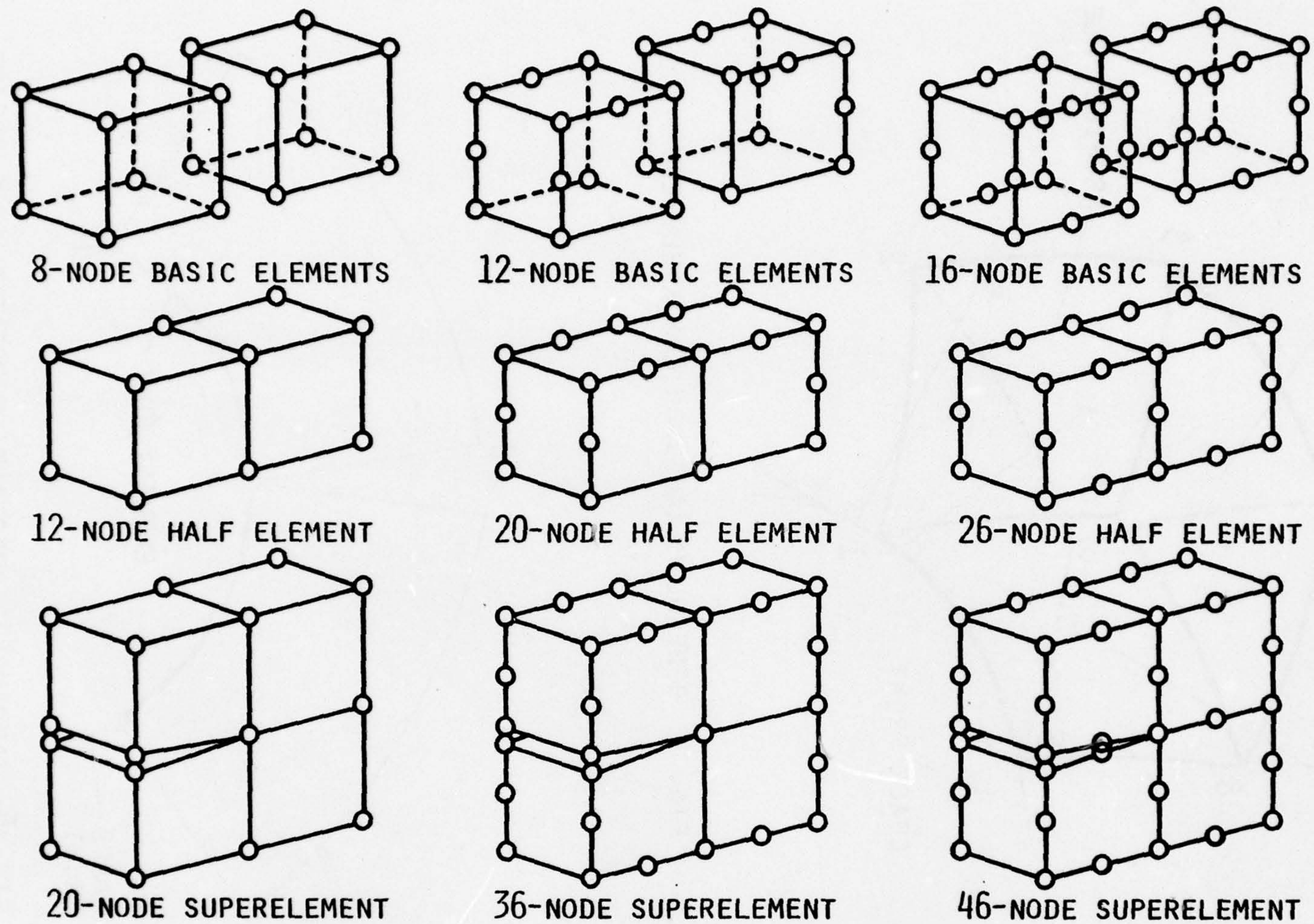

FIG. 6 FAMILY OF THREE-DIMENSIONAL HYBRID STRESS CRACK ELEMENTS

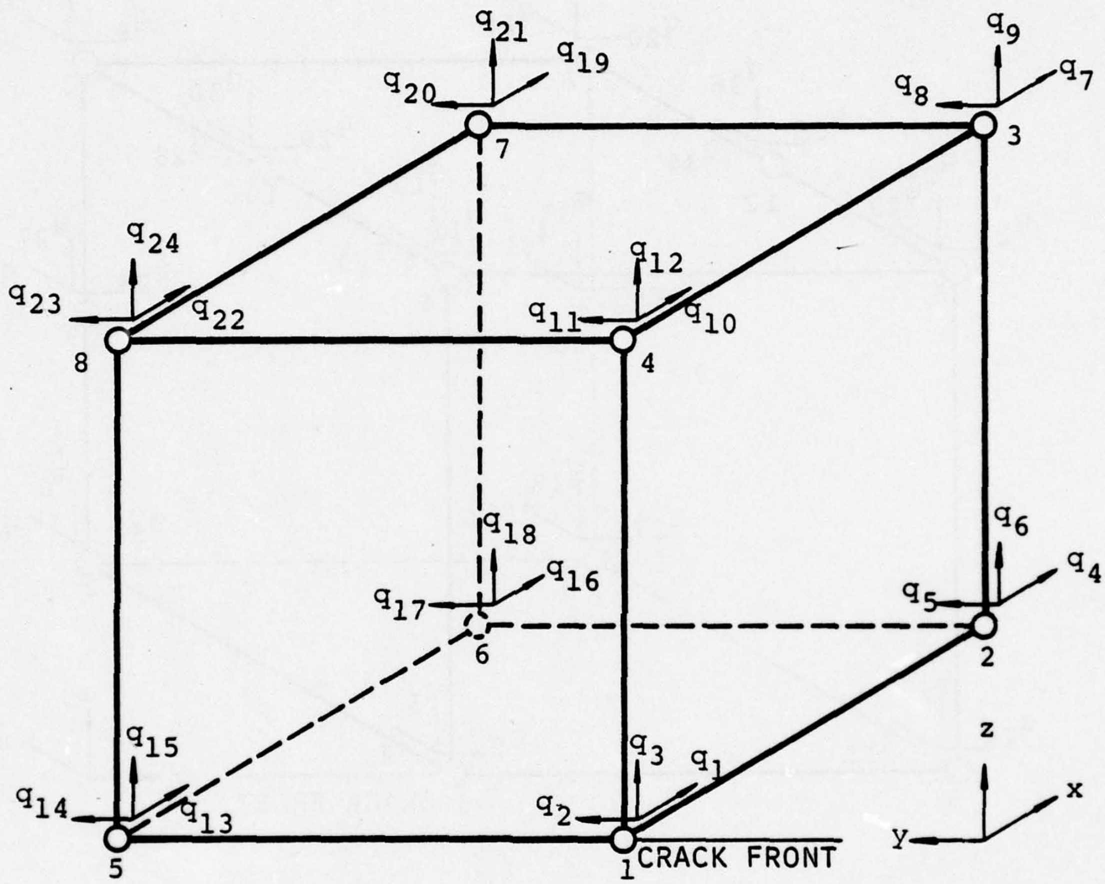

FIG. 7 TYPICAL 8-NODE CRACK FRONT ELEMENT AND ITS RELATIVE NODE AND NODAL DISPLACEMENT NUMBERING SCHEME

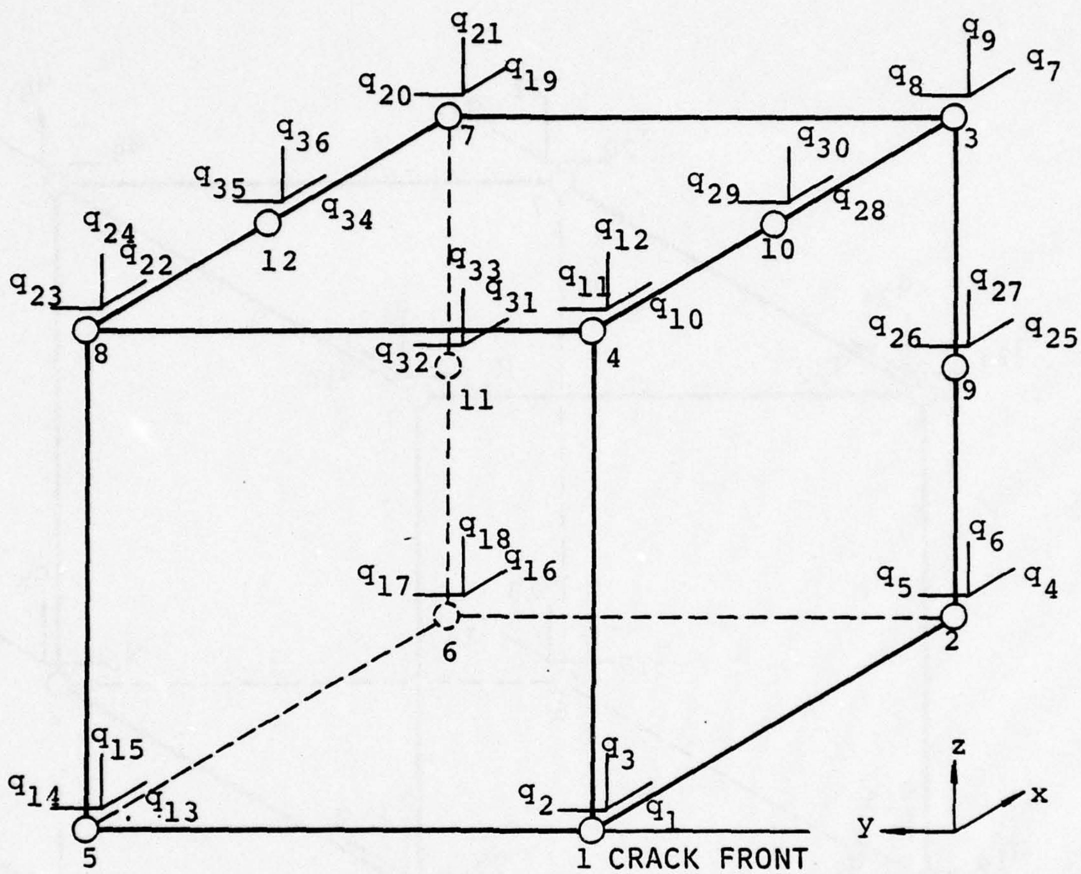

FIG. 8 TYPICAL 12-NODE CRACK FRONT ELEMENT AND ITS RELATIVE NODE AND NODAL DISPLACEMENT NUMBERING SCHEME

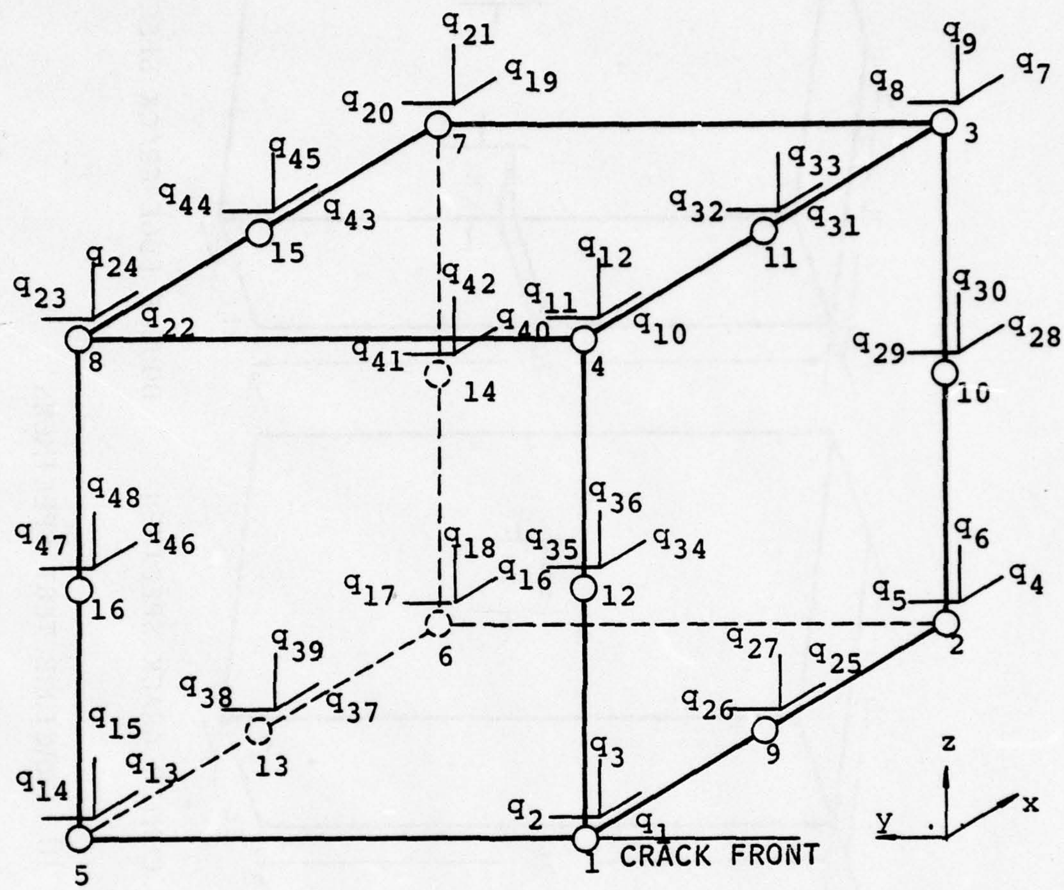

FIG. 9 TYPICAL 16-NODE CRACK FRONT ELEMENT AND ITS RELATIVE NODE AND NODAL DISPLACEMENT NUMBERING SCHEME

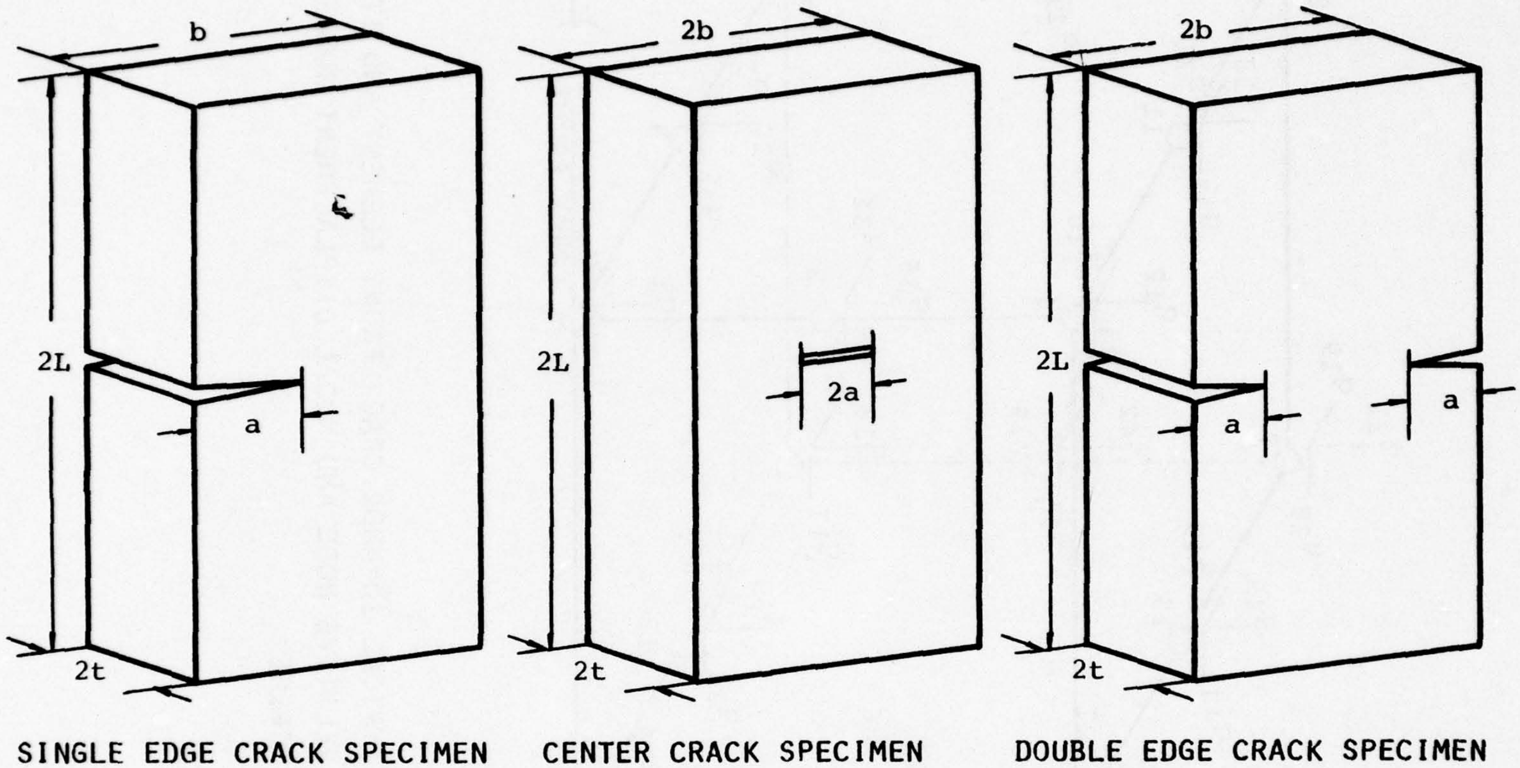

FIG. 10 FRACTURE TEST SPECIMENS

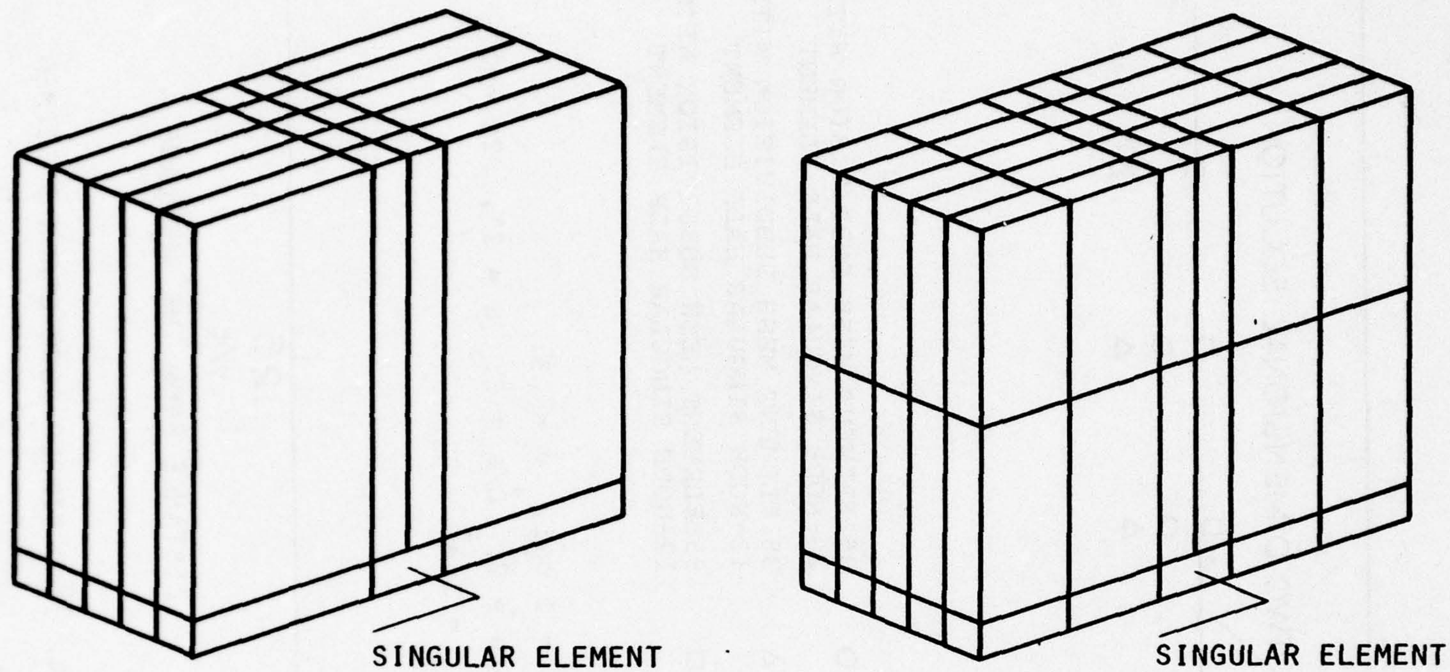

(1) 35 ELEMENTS (2) 85 ELEMENTS

FIG. 11 FINITE ELEMENT BREAKDOWN FOR THE ANALYSIS OF FRACTURE TEST SPECIMENS

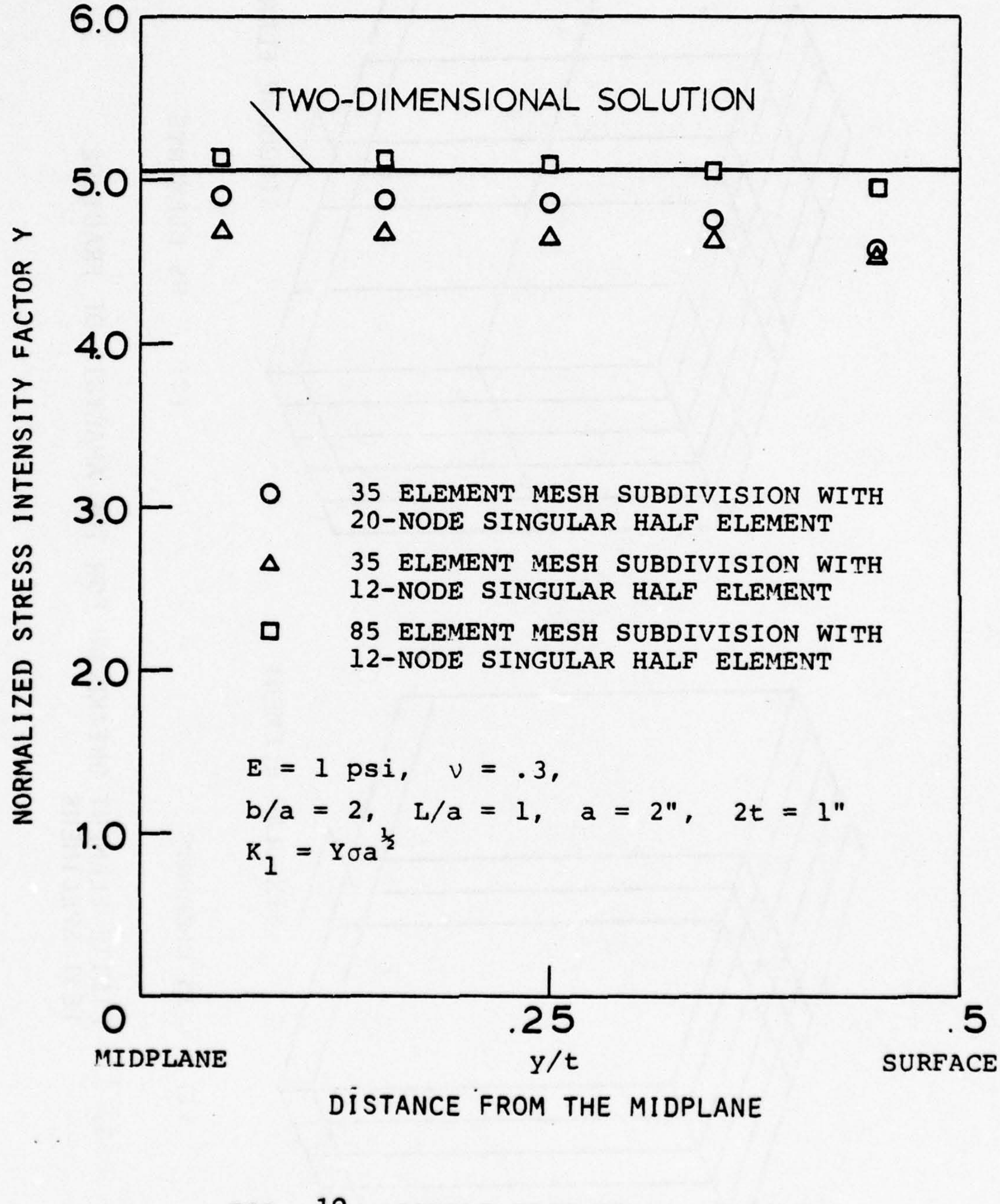

FIG. 12 SINGLE EDGE CRACK SPECIMEN

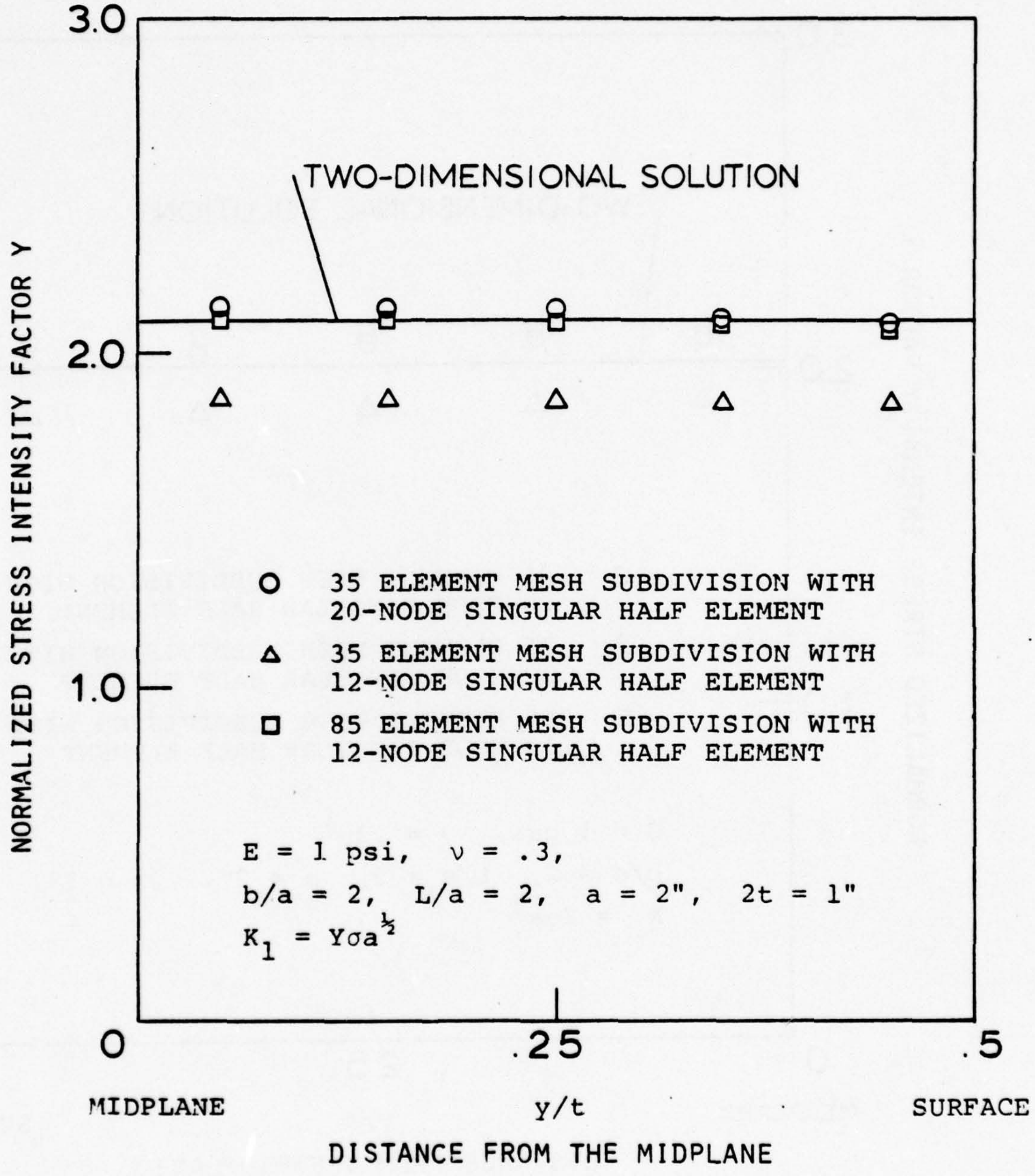

FIG. 13 CENTER CRACK SPECIMEN

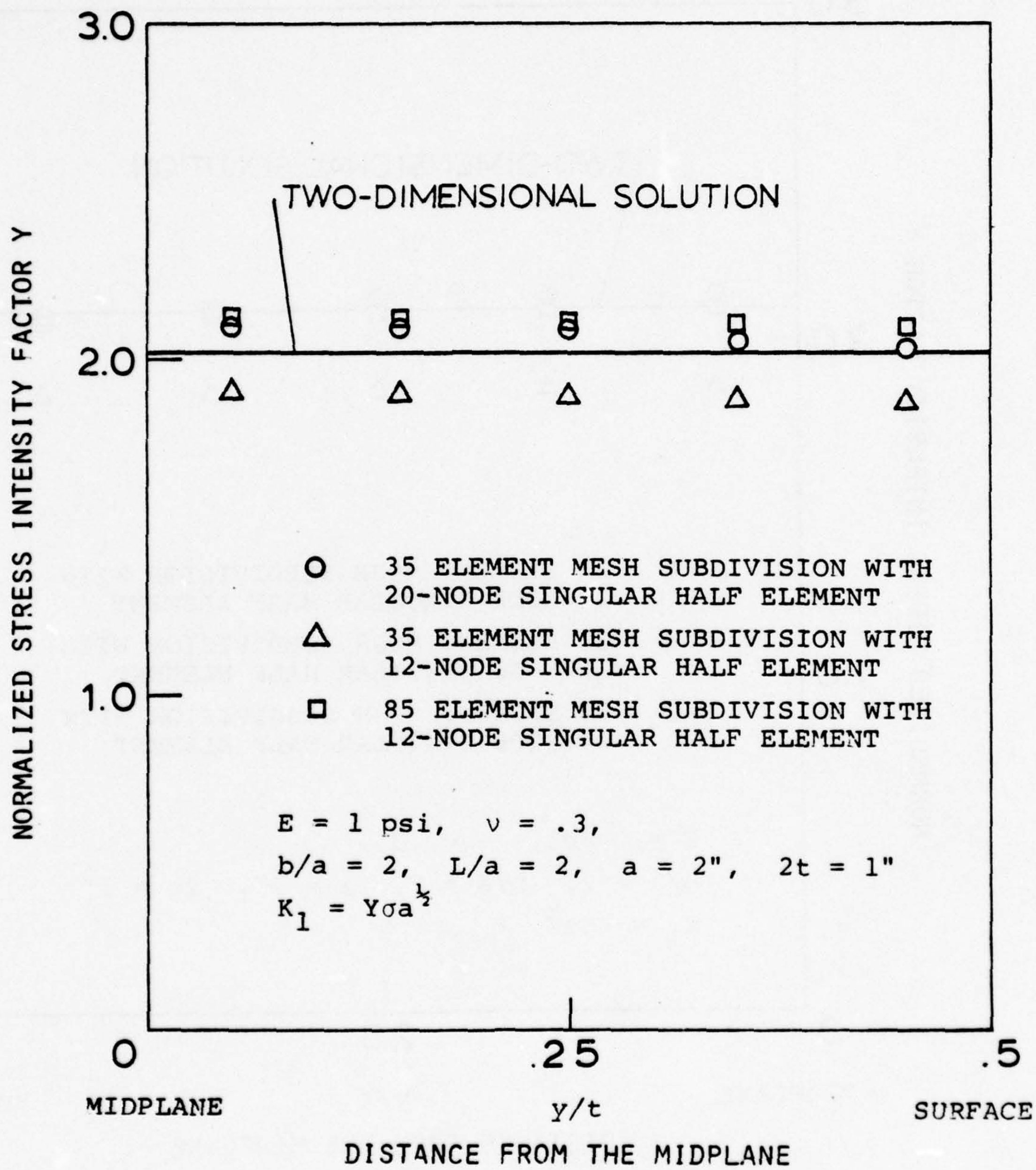

FIG. 14 DOUBLE EDGE CRACK SPECIMEN

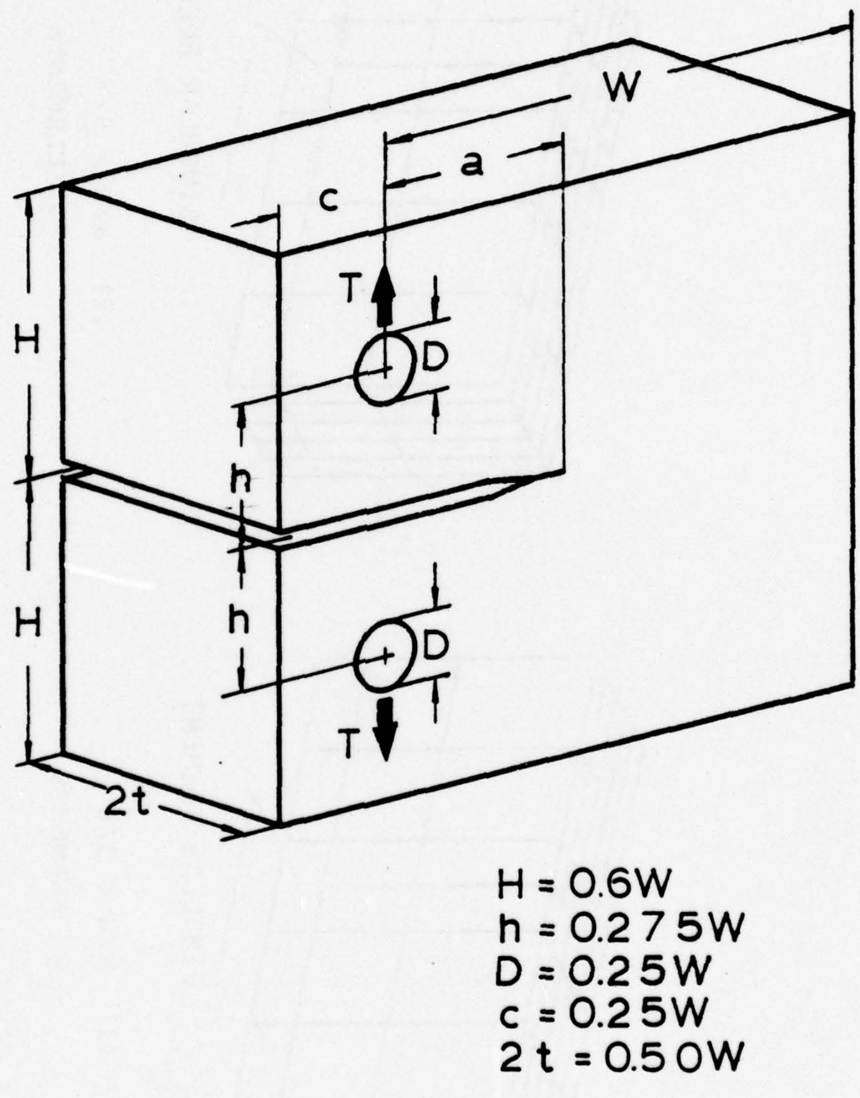

FIG. 15 STANDARD COMPACT TENSION SPECIMEN
(ASTM STANDARD E-399-72)

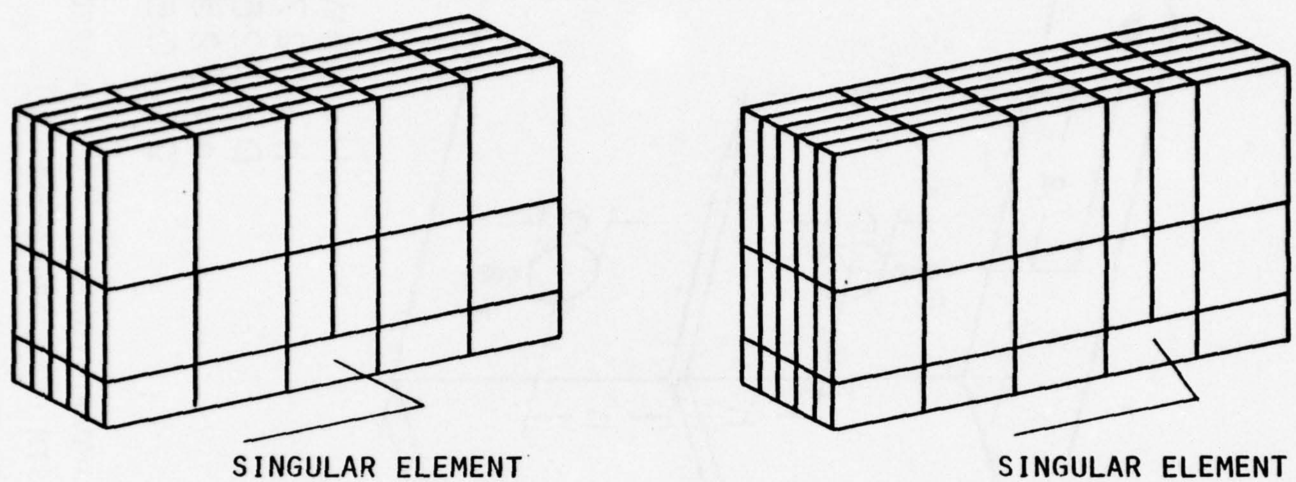

(1) a/W = 3/8
85 ELEMENTS

(2) a/W = 5/8
85 ELEMENTS

FIG. 16 FINITE ELEMENT BREAKDOWN FOR THE ANALYSIS OF STANDARD COMPACT TENSION SPECIMENS

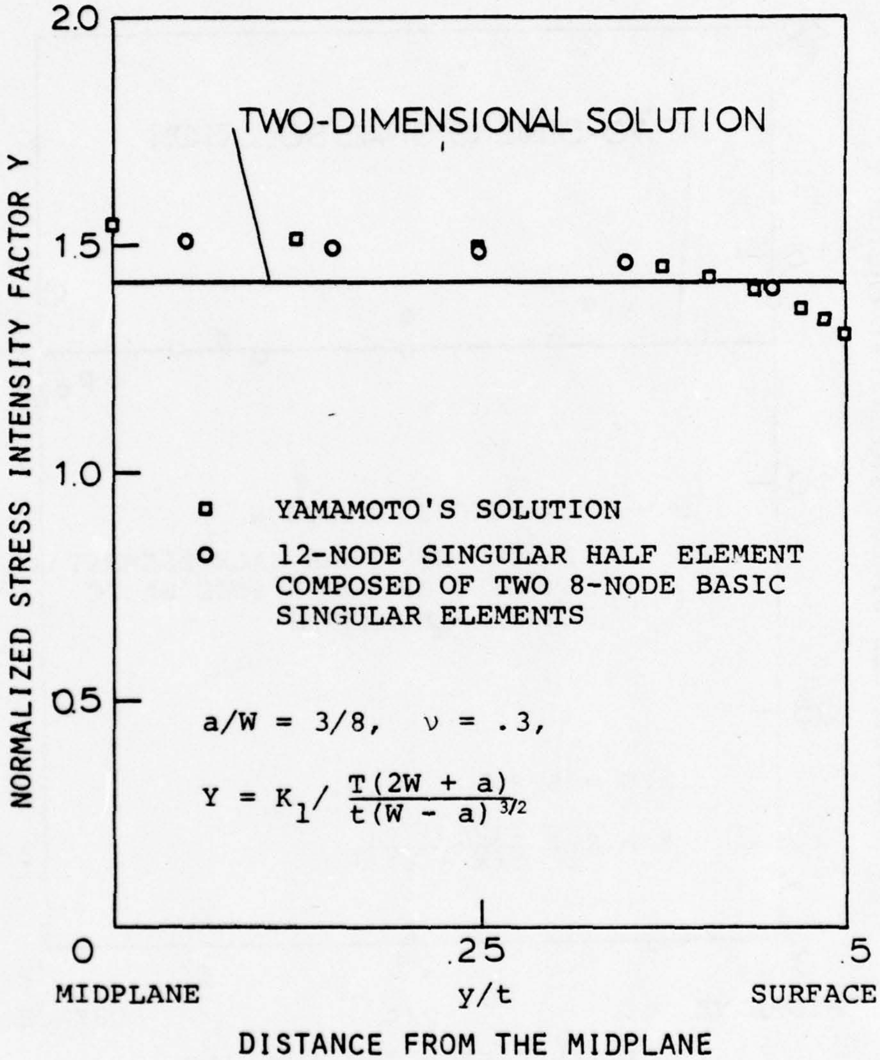

FIG. 17 STRESS INTENSITY FACTOR FOR COMPACT TENSION SPECIMEN

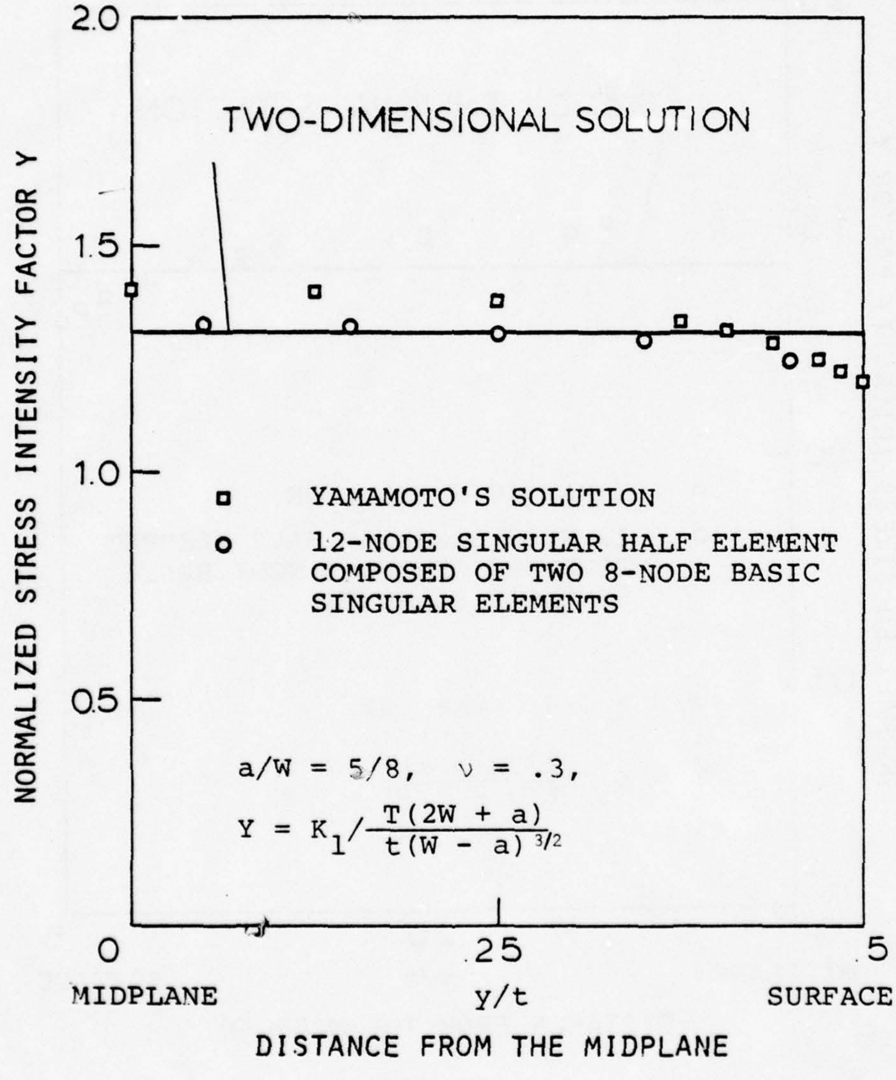

FIG. 18 STRESS INTENSITY FACTOR FOR COMPACT TENSION SPECIMEN

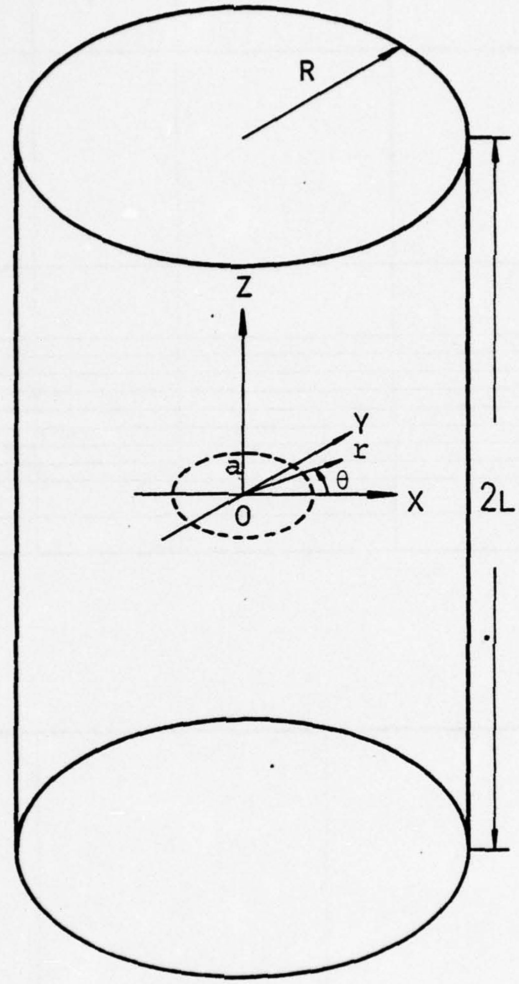

FIG. 19 CYLINDRICAL ROD WITH AN AXISYMMETRICALLY LOCATED PENNY-SHAPED CRACK UNDER UNIFORM TENSION LOADING

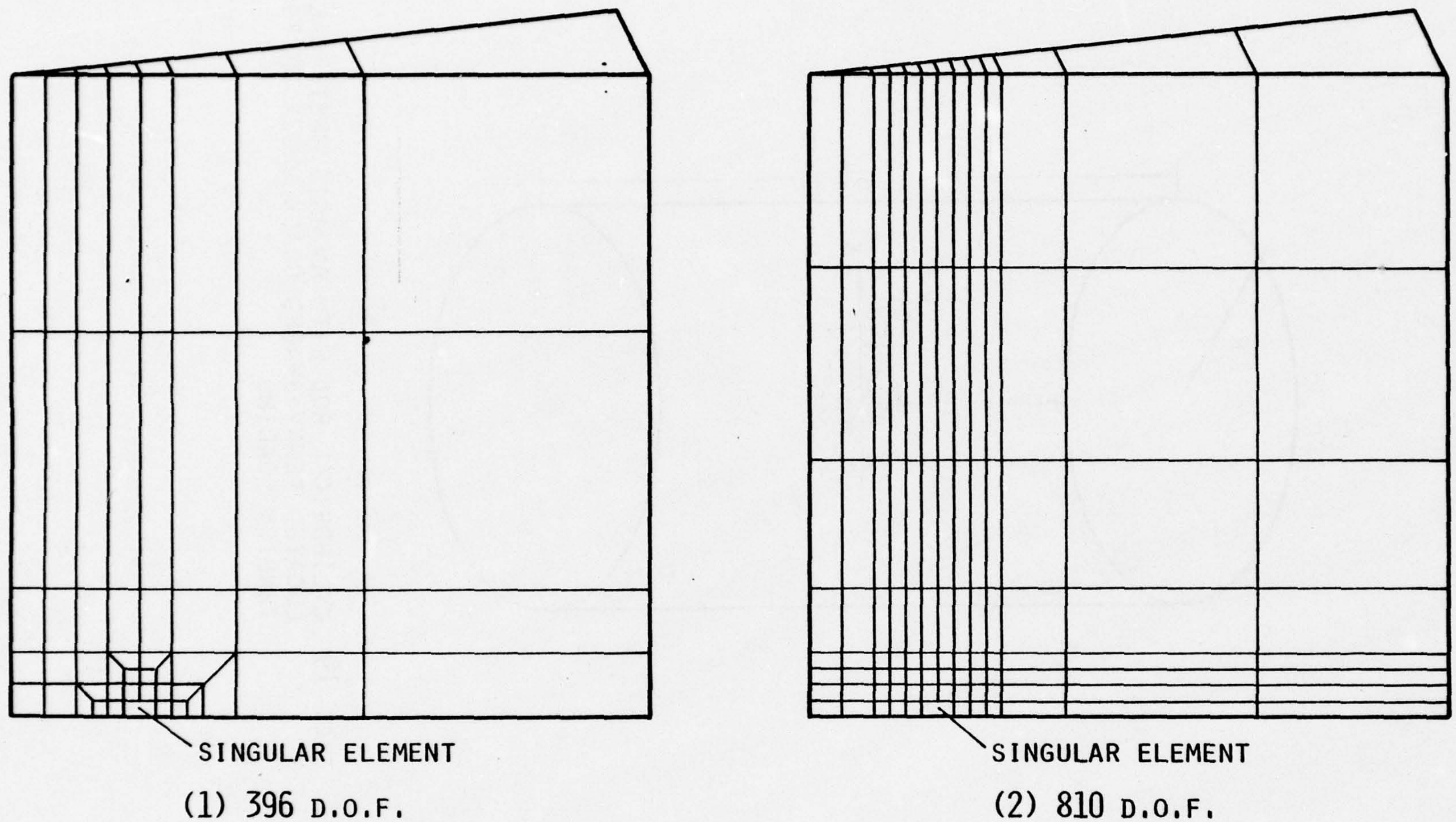

FIG. 20 FINITE ELEMENT BREAKDOWN FOR THE ANALYSIS OF A PENNY-SHAPED CRACK IN A CYLINDRICAL ROD

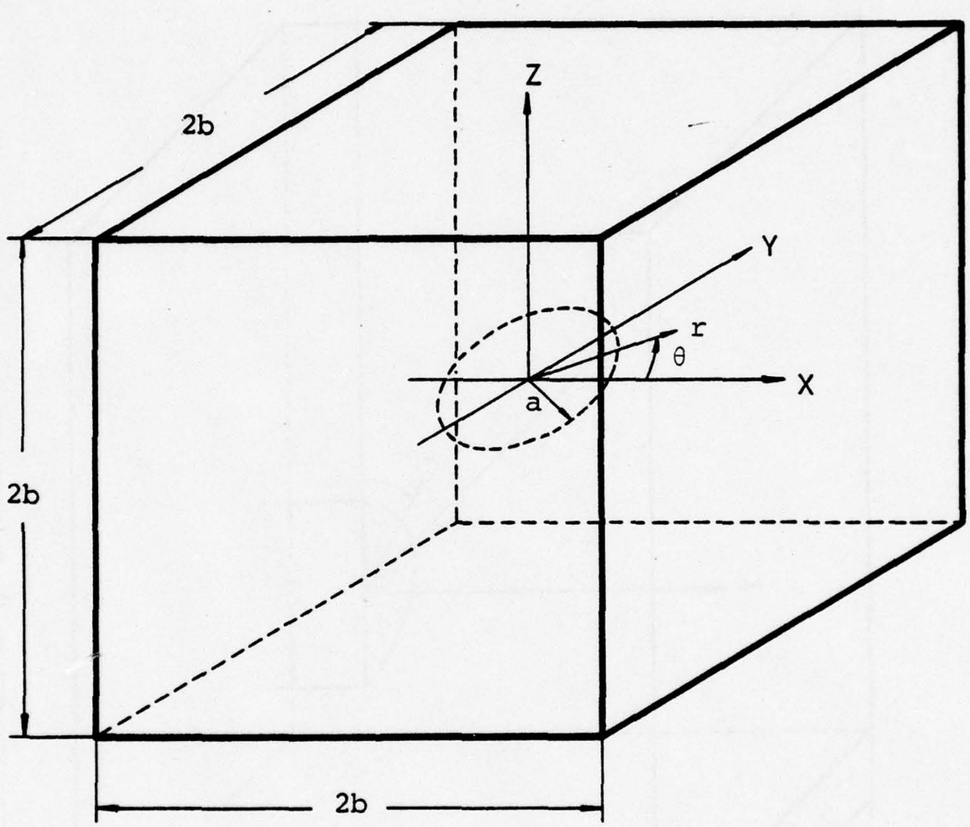

FIG. 21 EMBEDDED PENNY-SHAPED CRACK IN A CUBE IN TENSION

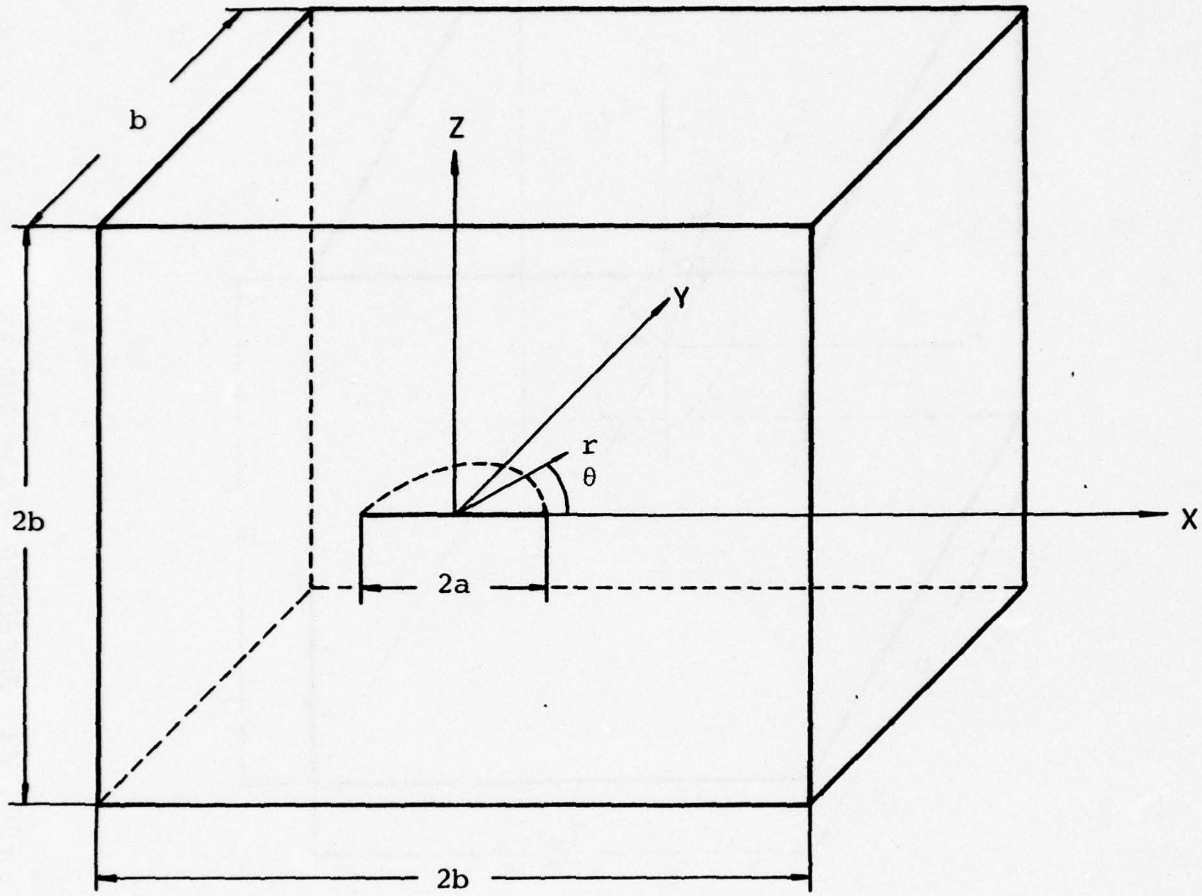

FIG. 22 SEMI-CIRCULAR SURFACE CRACK IN A RECTANGULAR PRISM

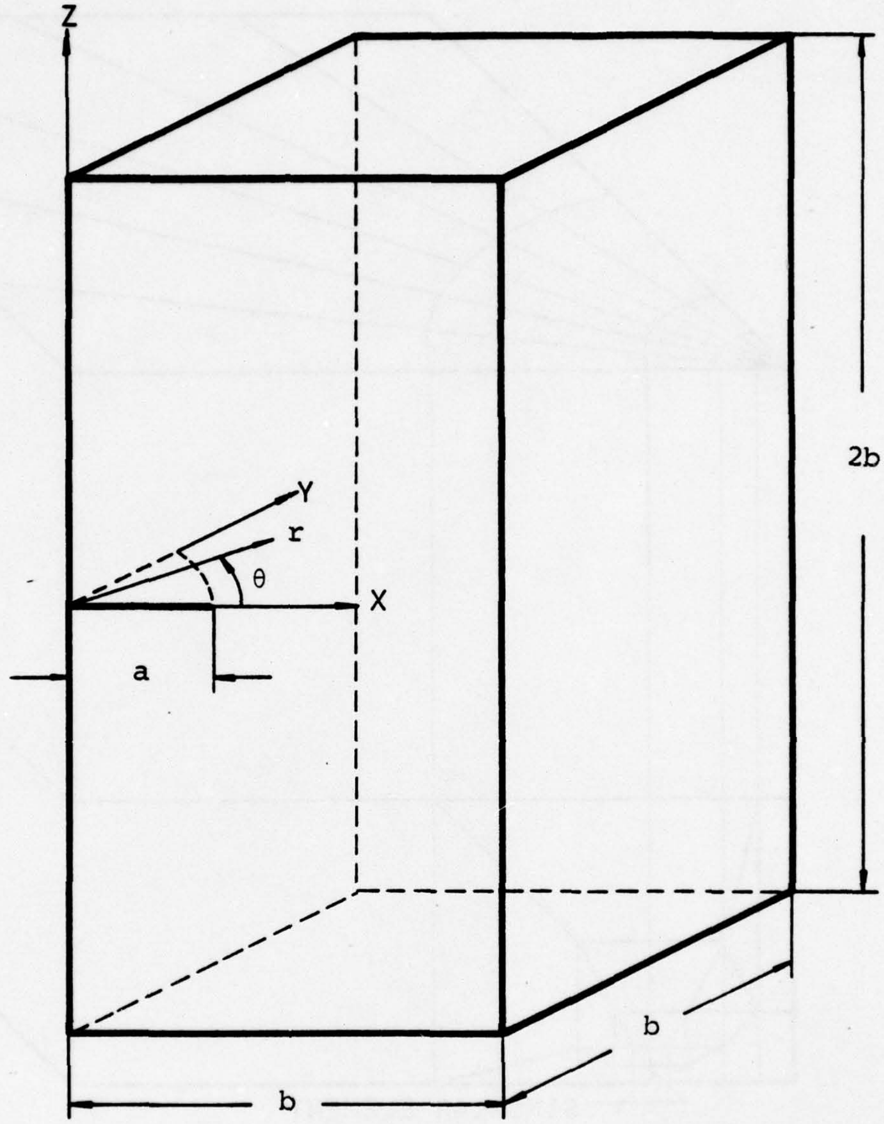

FIG. 23 QUARTER-CIRCULAR CORNER CRACK IN A RECTANGULAR PRISM IN TENSION

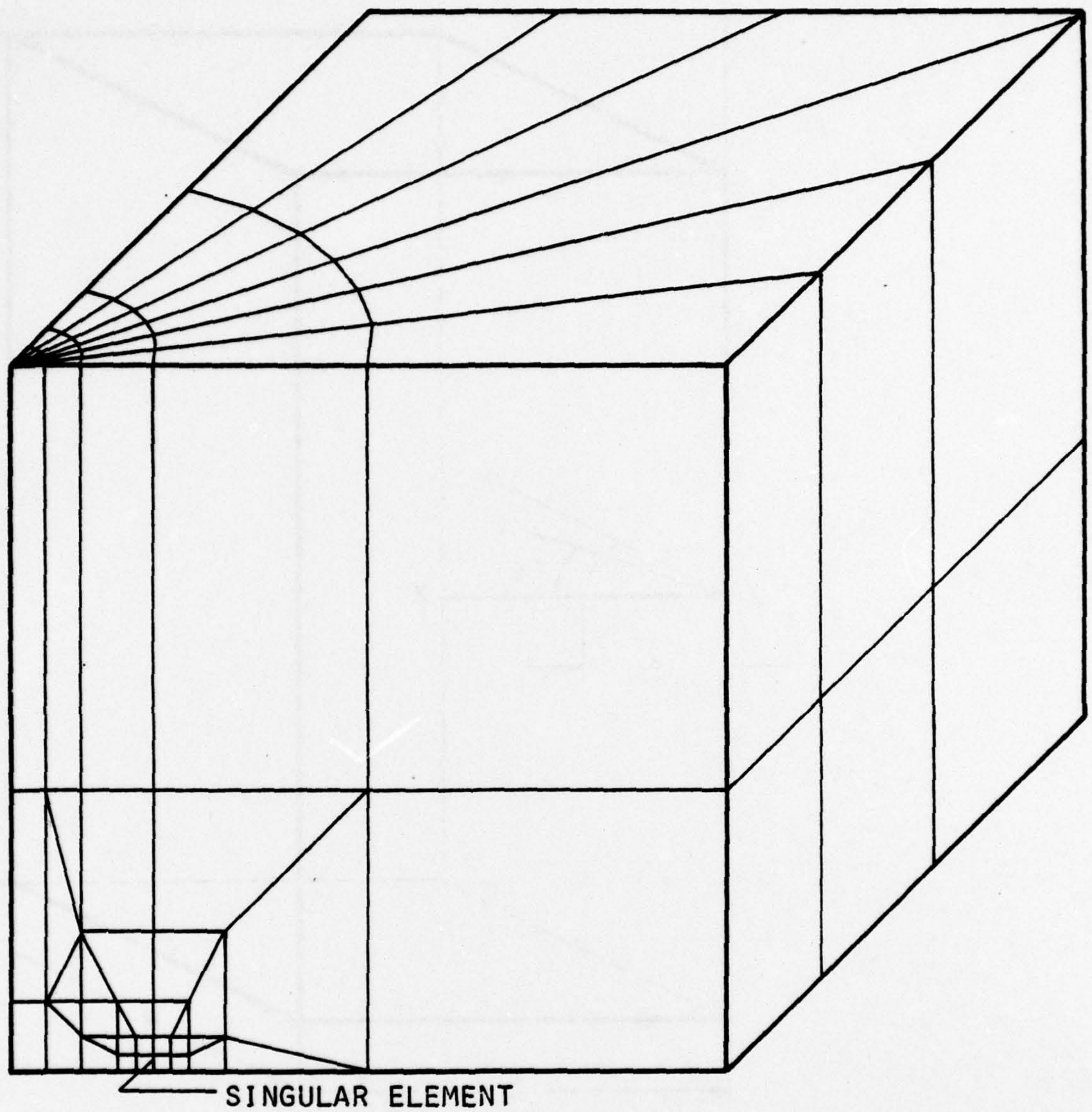

FIG. 24 FINITE ELEMENT BREAKDOWN FOR THE ANALYSIS OF A PENNY-SHAPED CRACK, A SEMI-CIRCULAR SURFACE CRACK AND A QUARTER-CIRCULAR CORNER CRACK IN A RECTANGULAR PRISM IN TENSION

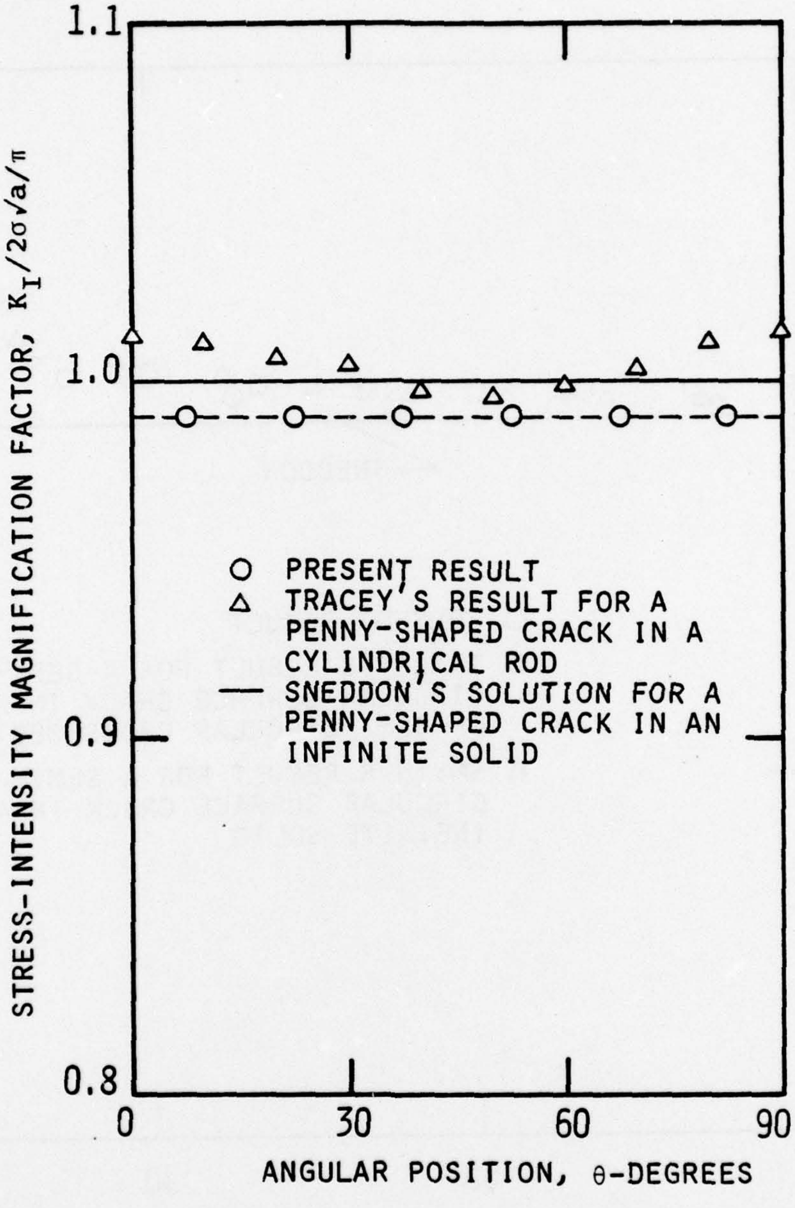

FIG. 25 STRESS-INTENSITY MAGNIFICATION FACTOR FOR A PENNY-SHAPED CRACK IN A CUBE IN TENSION

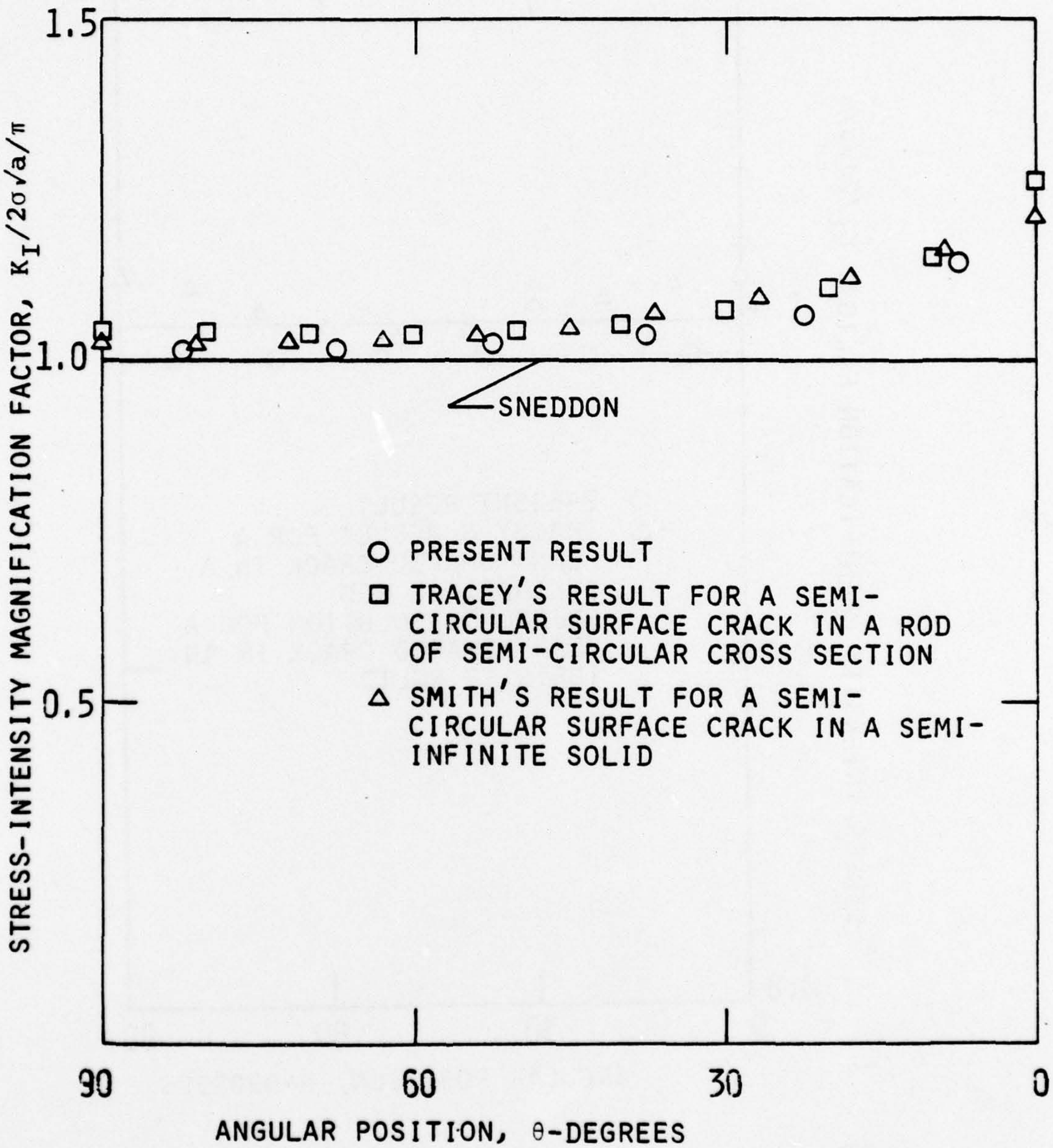

FIG. 26 STRESS-INTENSITY MAGNIFICATION FACTOR FOR A SEMI-CIRCULAR SURFACE CRACK IN A RECTANGULAR PRISM IN TENSION

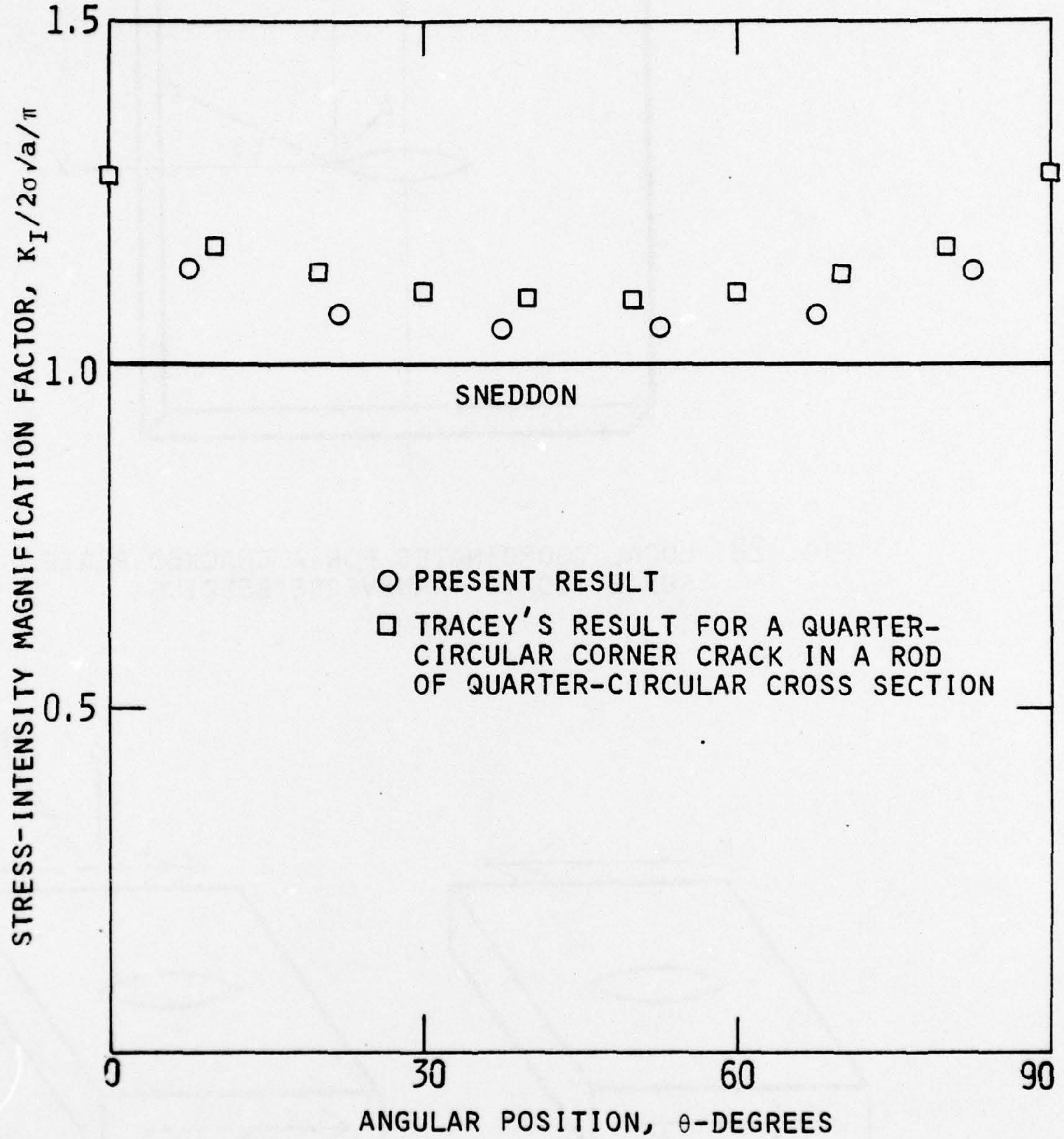

FIG. 27 STRESS-INTENSITY MAGNIFICATION FACTOR FOR A QUARTER-CIRCULAR CORNER CRACK IN A RECTANGULAR PRISM IN TENSION

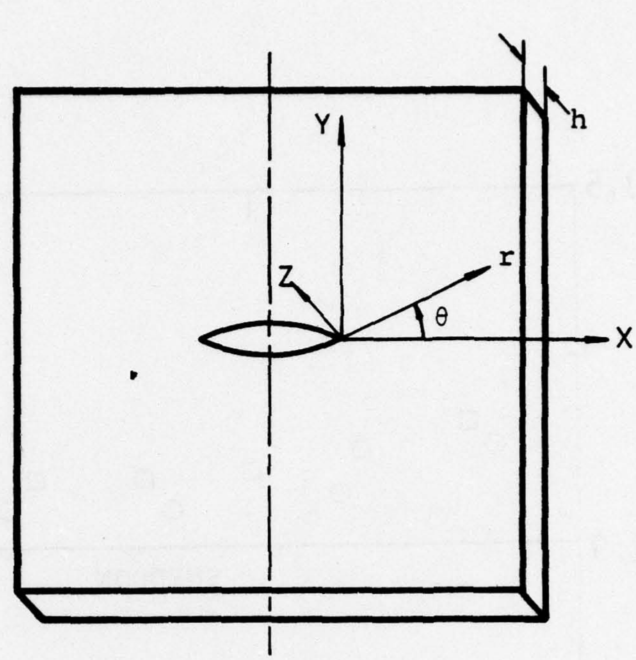

FIG. 28 LOCAL COORDINATES FOR A CRACKED PLATE SUBJECTED TO TRANSVERSE BENDING

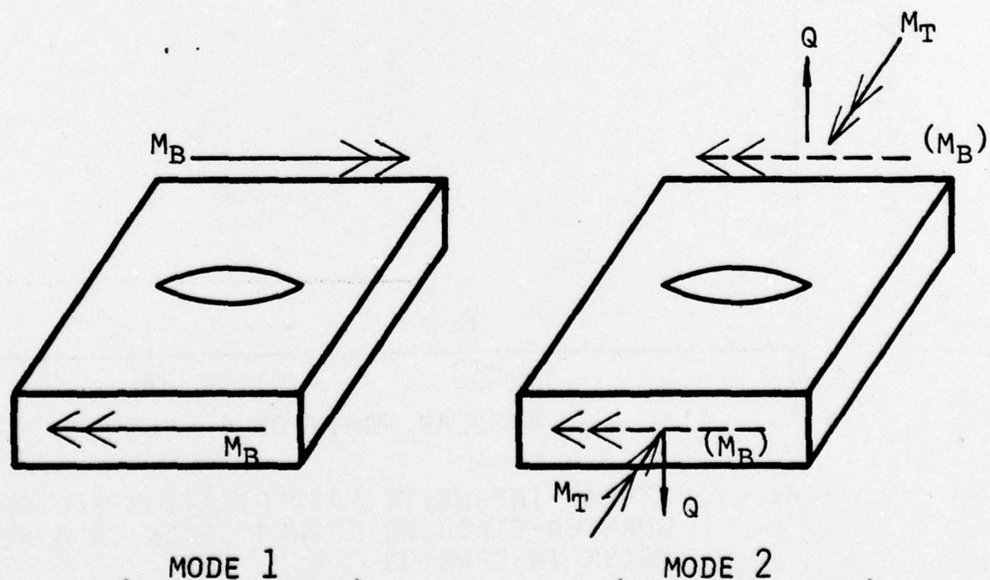

FIG. 29 MODES OF FRACTURE FOR THE BENDING OF PLATES

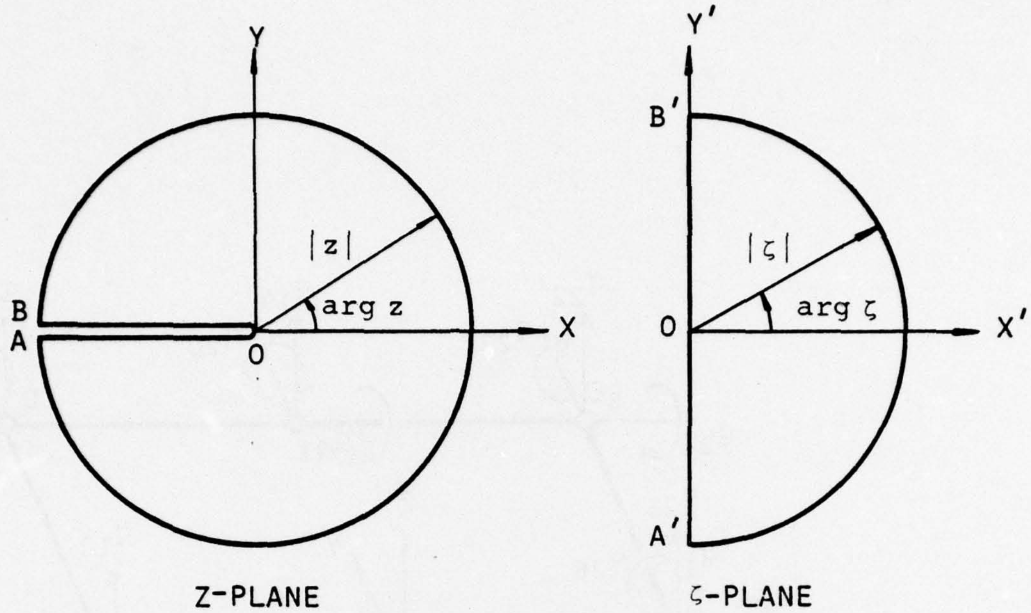

FIG. 30 $z=\zeta^2$ MAPPING OF Z PLANE TO ζ PLANE

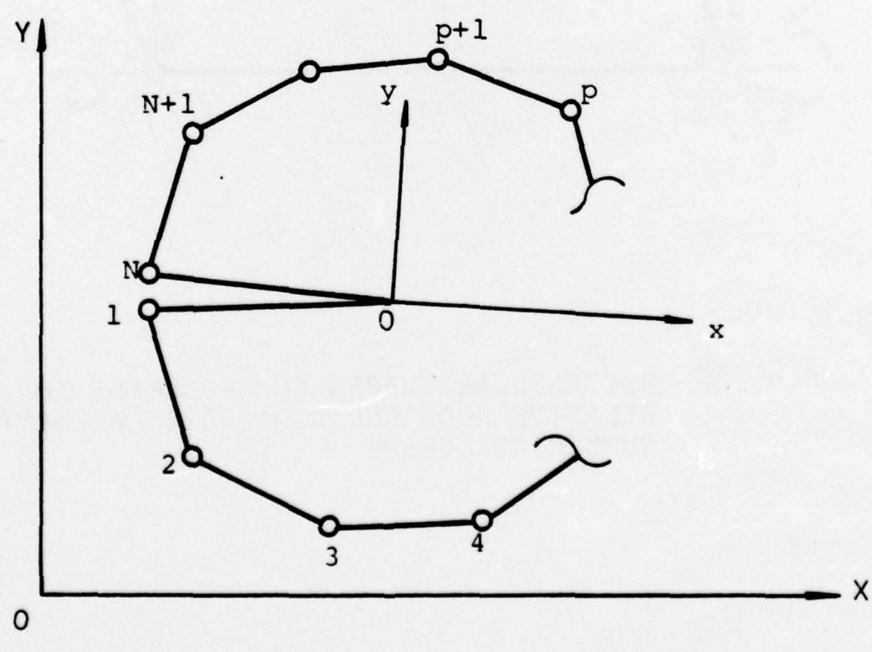

FIG. 31 CONFIGURATION OF SUPERELEMENT

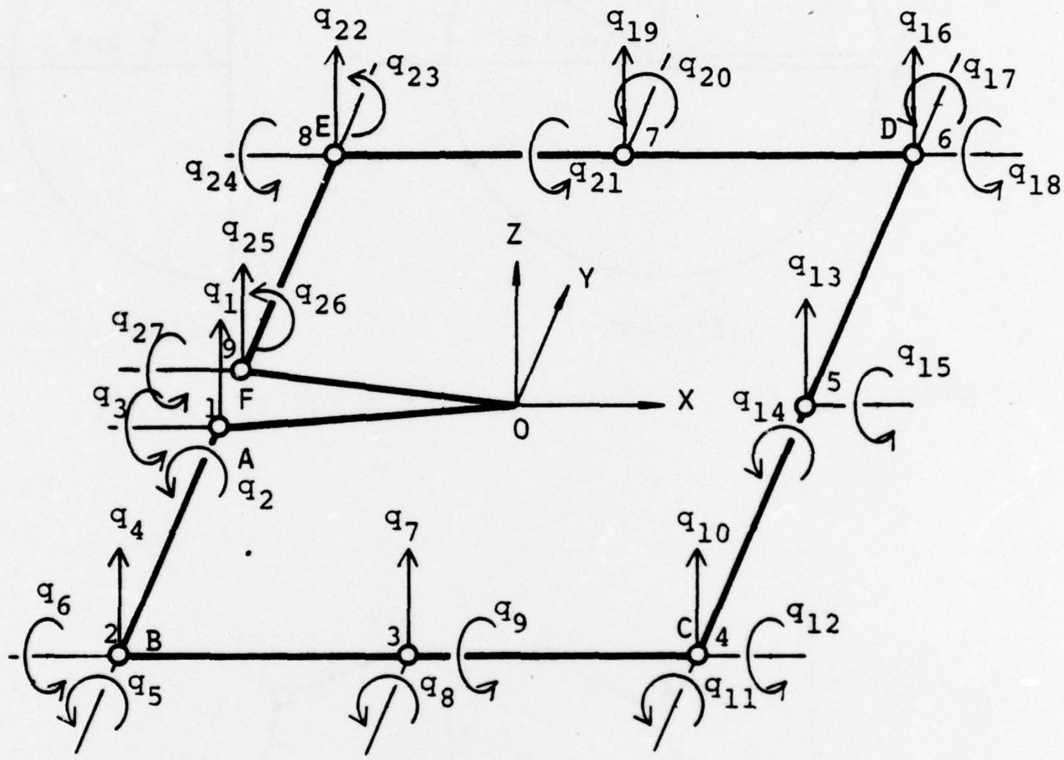

FIG. 32 RECTANGULAR SHAPED SUPERELEMENT AND ITS RELATIVE NODE AND NODAL DISPLACEMENT NUMBERING SCHEME

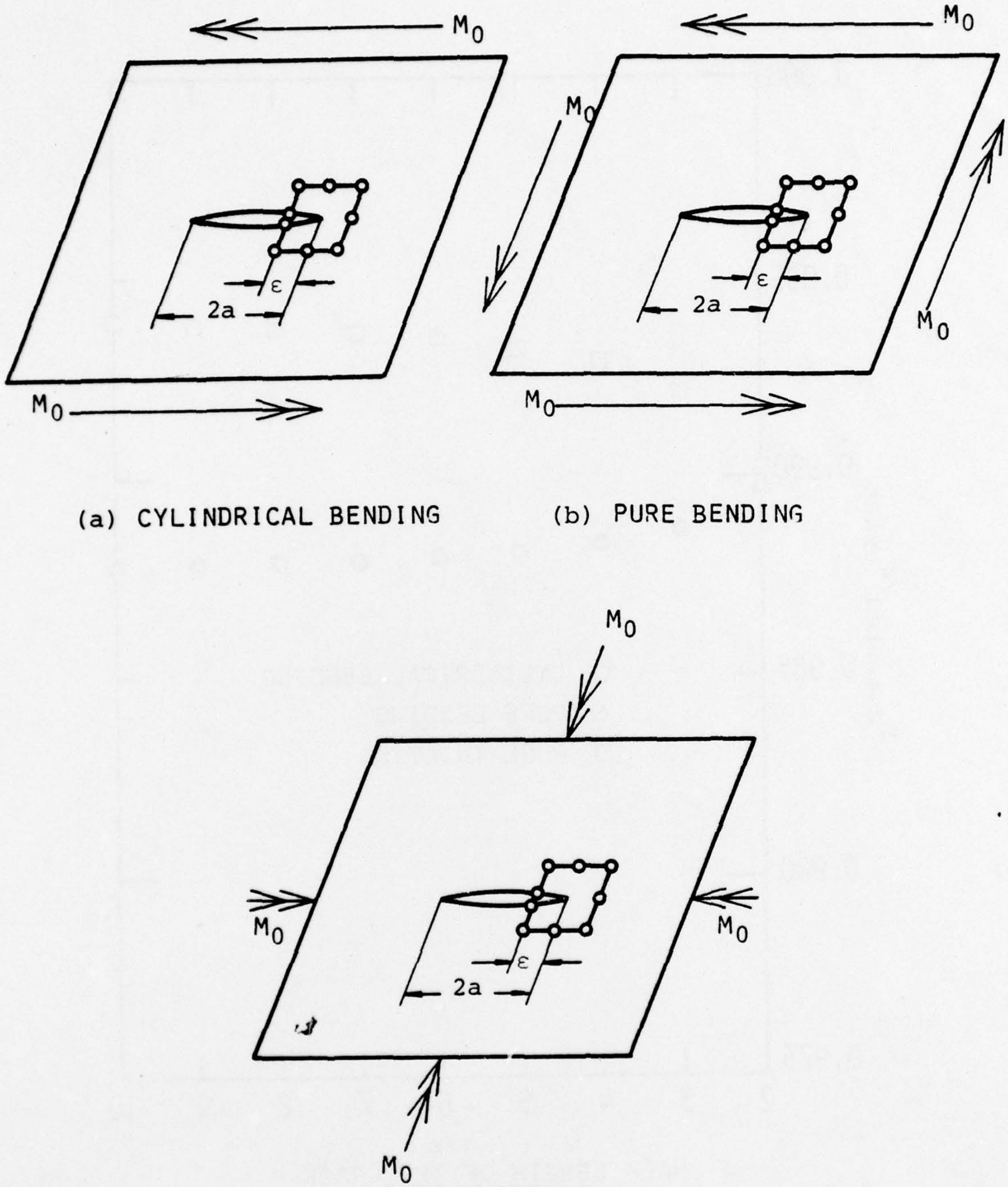

(a) CYLINDRICAL BENDING (b) PURE BENDING

(c) PURE TWISTING

FIG. 33 CYLINDRICAL BENDING, PURE BENDING AND PURE TWISTING OF AN INFINITE PLATE CONTAINING A FINITE CRACK

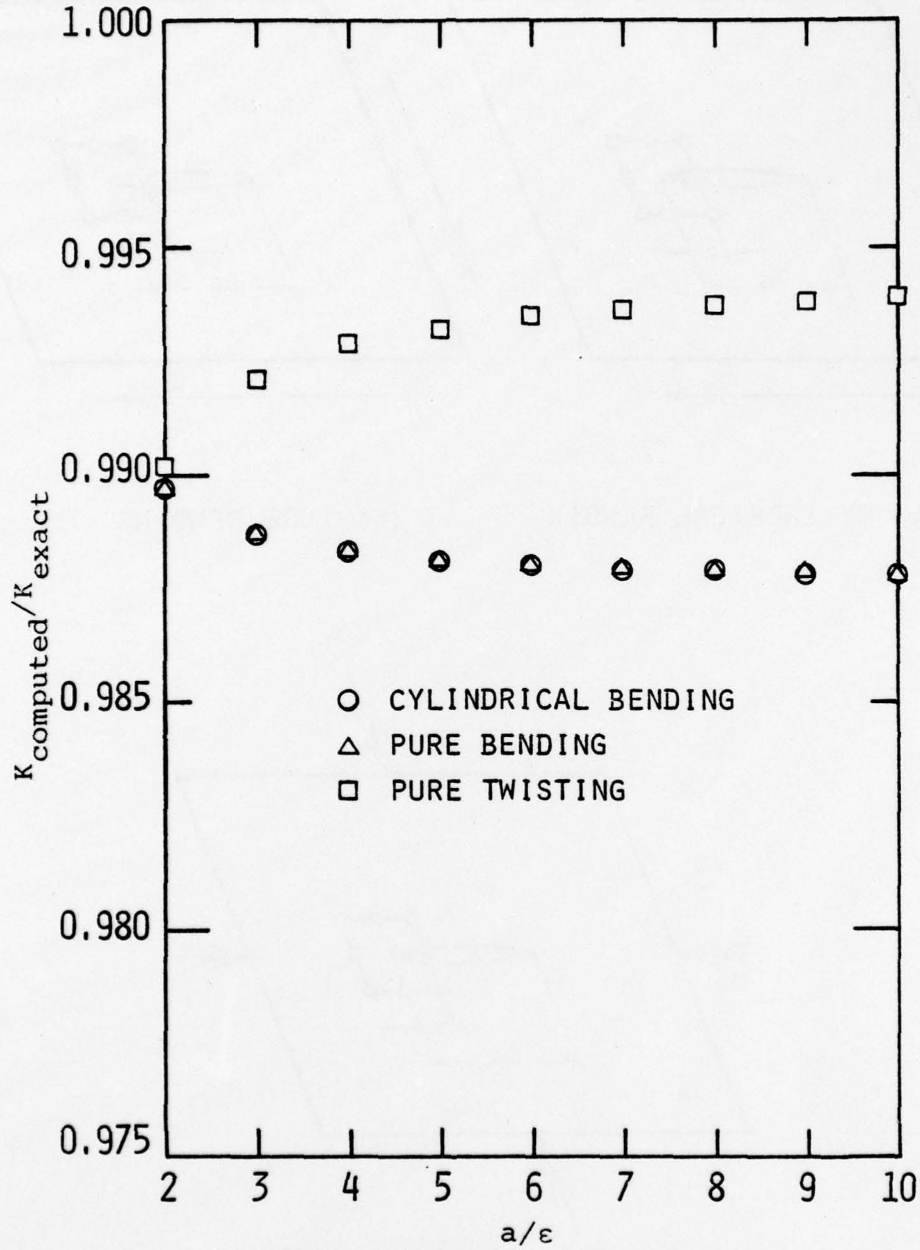

a HALF LENGTH OF THE CRACK
ε LENGTH OF THE CRACK WITHIN THE SUPERELEMENT

FIG. 34 STRESS-INTENSITY FACTOR SOLUTIONS FOR AN INFINITE PLATE CONTAINING A FINITE CRACK SUBJECTED TO PURE CYLINDRICAL BENDING, PURE BENDING AND PURE TWISTING

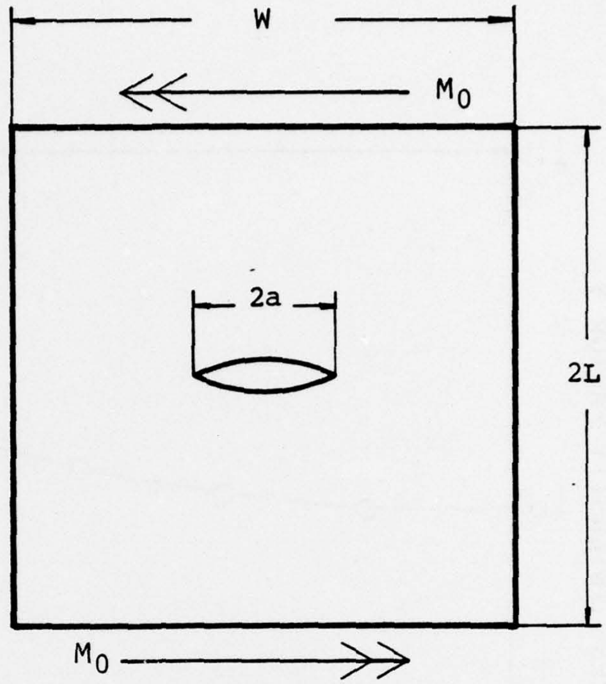

FIG. 35 PURE CYLINDRICAL BENDING OF A THIN PLATE WITH A FINITE WIDTH AND CENTRALLY LOCATED THROUGH-THE-THICKNESS CRACK

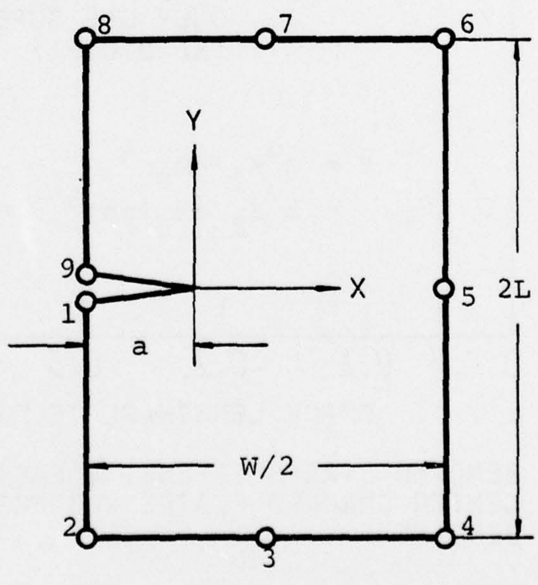

FIG. 36 FINITE ELEMENT MODEL FOR A CENTER-CRACKED PLATE SUBJECTED TO PURE CYLINDRICAL BENDING

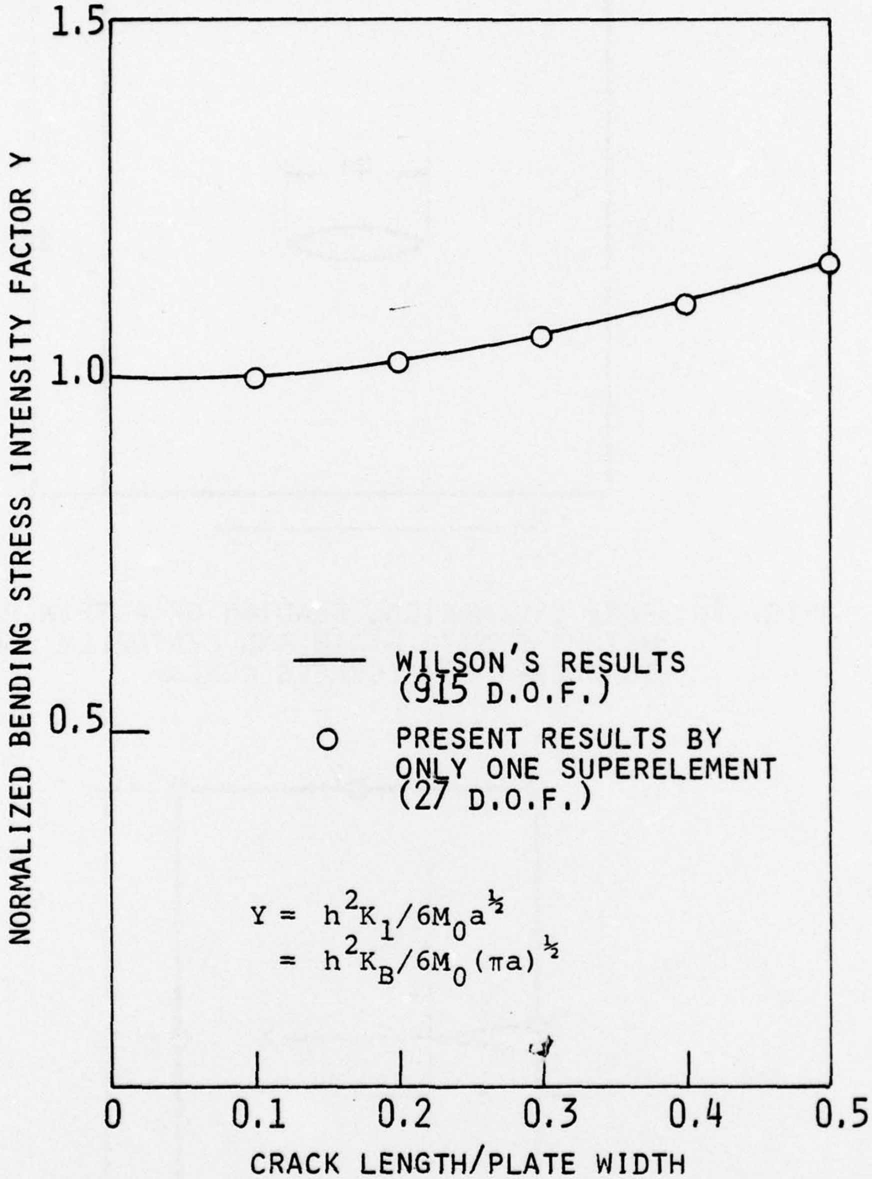

FIG. 37 BENDING STRESS INTENSITY FACTOR SOLUTIONS FOR CENTER CRACKED PLATES SUBJECTED TO CYLINDRICAL BENDING

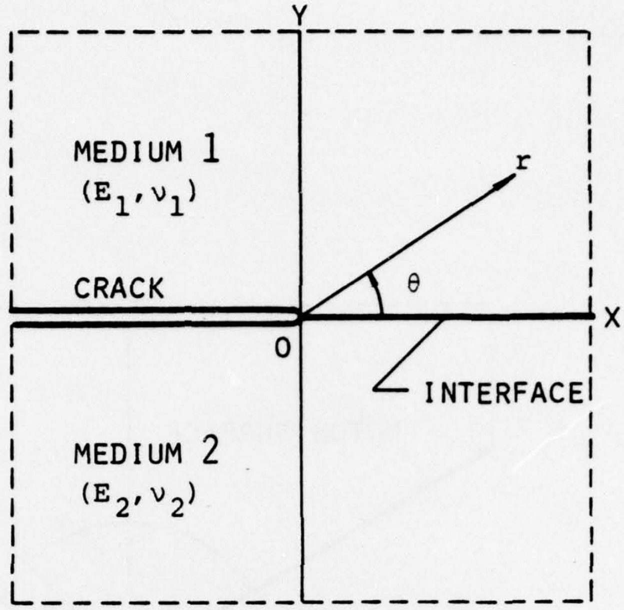

FIG. 38 BENDING OF A BI-MATERIAL PLATE WITH THROUGH-THE-THICKNESS CRACK LOCATED ALONG THE INTERFACE

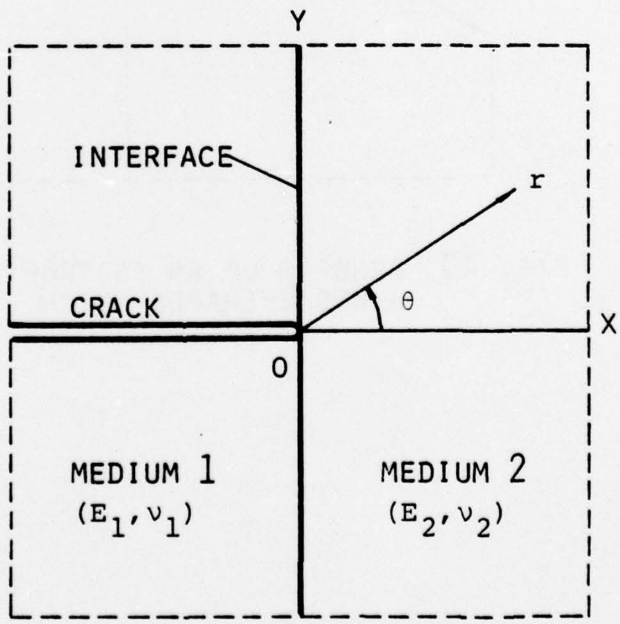

FIG. 39 BENDING OF A BI-MATERIAL PLATE WITH THROUGH-THE-THICKNESS CRACK LOCATED NORMAL TO THE INTERFACE

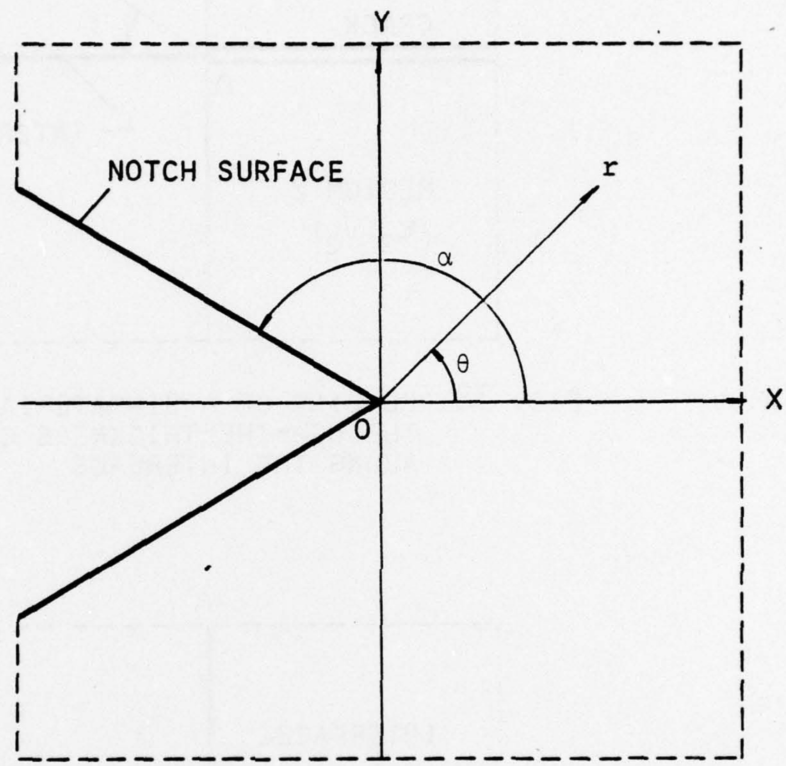

FIG. 40 BENDING OF AN ISOTROPIC PLATE CONTAINING A WEDGE-SHAPED NOTCH

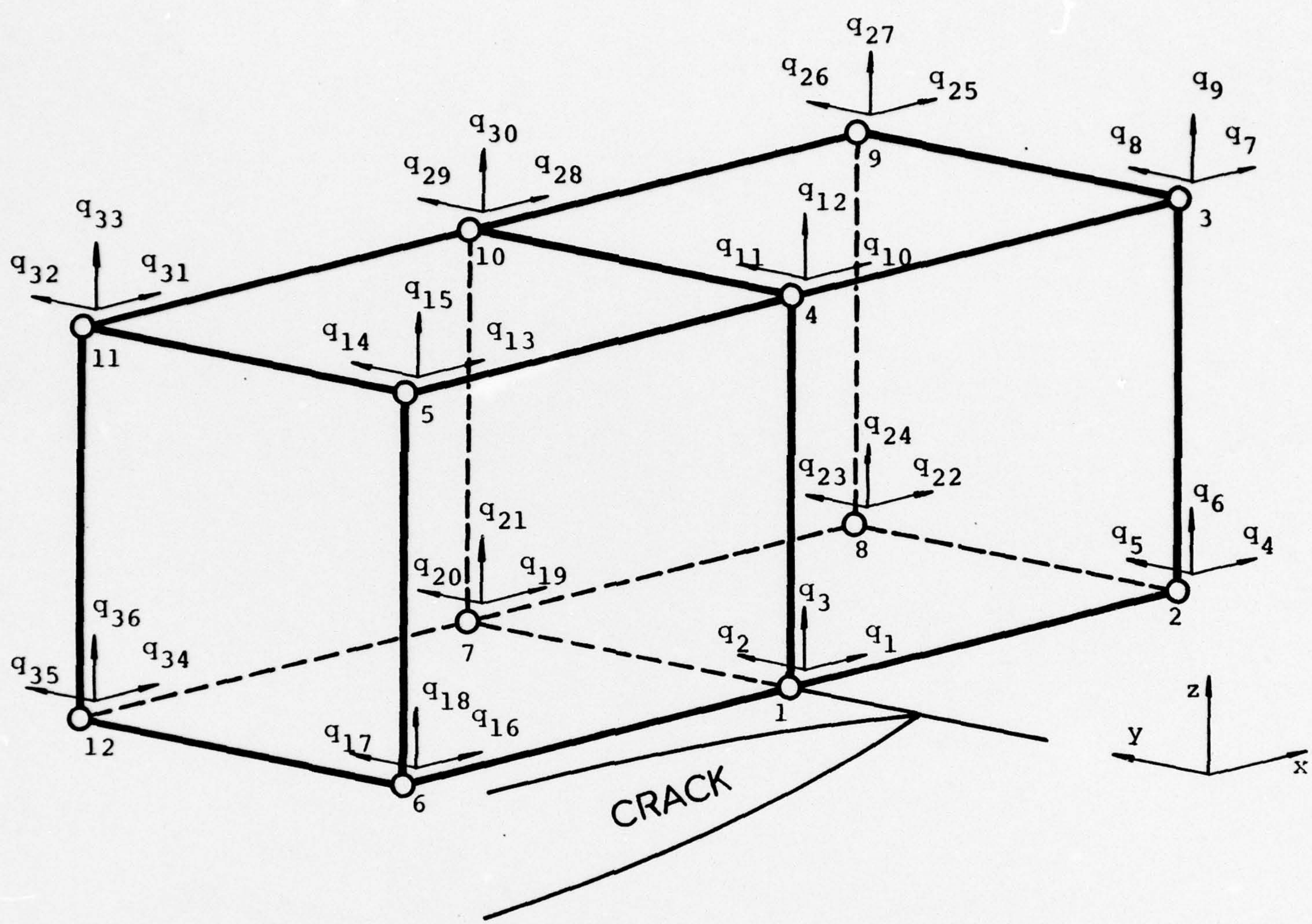

FIG. 41 12-NODE UPPERHALF SUPERELEMENT AND ITS RELATIVE NODE AND NODAL DISPLACEMENT NUMBERING SCHEME